

Institut für Prophylaxe und Epidemiologie der Kreislaufkrankheiten (IPEK)
Institut der Ludwig-Maximilians-Universität München



Dissertation

zum Erwerb des Doctor of Philosophy (Ph.D.)

an der Medizinischen Fakultät der

Ludwig-Maximilians-Universität zu München

**Pairing of Single Cell RNA Sequencing and Single Cell T Cell Receptor
Profiling Reveals Tolerance Breakdown of T Cells in Atherosclerosis**

vorgelegt von:

Zhihua Wang

aus:

Xinxiang, Henan, China

Jahr:

2022

Mit Genehmigung der Medizinischen Fakultät der
Ludwig-Maximilians-Universität zu München

First evaluator (1. TAC member): Prof. Dr. med. Andreas Habenicht

Second evaluator (2. TAC member): Prof. Dr. rer. nat. Changjun Yin

Third evaluator: Prof. Dr. Vigo Heissmeyer

Fourth evaluator: Prof. Dr. Gunnar Schotta

Dean: Prof. Dr. med. Thomas Gudermann

date of the defense:

21.11.2022

TABLE OF CONTENTS

CONTENTS

CONTENTS	I
ZUSAMMENFASSUNG.....	IV
ABSTRACT	VI
ABBREVIATIONS.....	VIII
1. INTRODUCTION	1
1.1. Atherosclerosis	1
1.2. T cells are involved in atherosclerosis progression.....	3
1.2.1. CD4 ⁺ T cells in atherosclerosis.....	3
1.2.2. CD8 ⁺ T cells in atherosclerosis.....	5
1.2.4. The balance of T helper (Th) 17/ regulatory (T _{reg}) cells and the plasticity of T _{reg} cells in atherosclerosis	7
1.3. T cell development.....	8
1.4. Immune tolerance to control T cell immune responses.....	10
1.4.1. Central tolerance	10
1.4.2. Peripheral tolerance	11
1.4.2.1. T cell intrinsic peripheral tolerance mechanisms.....	11
1.4.2.2. T _{reg} cell-mediated immune tolerance.....	14
1.4.2.3. Dendritic cell (DC)-mediated immune tolerance.....	15
1.5. Artery tertiary lymphoid organs (ATLOs) organize immune responses in aged apolipoprotein E-deficient (ApoE ^{-/-}) mice.....	16
1.5.1. T cell immune responses in ATLOs	17
1.5.2. B cell immune responses in ATLOs	18
1.6. Are there autoimmune B and/or T cell responses in atherosclerosis?	18
1.7. The T cell receptor (TCR) is an important target to search for autoantigen- specific T cells.....	20
1.8. Single cell RNA sequencing (scRNA-seq) as a tool to explore TCR repertoires and T cell immune responses in atherosclerosis.....	21
1.9. Aims of the project.....	24
2. MATERIALS AND METHODS.....	26
2.1. Mice	26
2.2. Solutions.....	26
2.3. Antibodies	27
2.4. Enzyme cocktail.....	27

TABLE OF CONTENTS

2.5. Equipment.....	28
2.6. R packages and other software	28
2.7. Methods.....	29
2.7.1. Plaque, ATLO and renal lymph node (RLN) collection and CD45 ⁺ cell isolation.....	29
2.7.2. Library preparation	30
2.7.3. Single cell sequencing data analysis	31
2.7.4. T cell clonal expansion and TCR repertoire analysis	34
2.7.5. Cell-cell interaction analysis	35
2.7.6. Gene set enrichment analysis (GSEA).....	36
2.7.7. Immunofluorescence staining.....	36
2.7.8. Integration analysis of human and mouse scRNA-seq data.....	36
2.7.9. Statistical analyses.....	38
3. RESULTS.....	39
3.1 Pre-processing of scRNA-seq and single cell TCR sequencing (scTCR-seq) analysis	39
3.2 Hyperlipidemia-associated differences in immune cells of blood between aged wild type (WT) and ApoE ^{-/-} mice.....	42
3.3 Transcriptome map of T cells in atherosclerotic plaques, ATLOs, ApoE ^{-/-} RLNs and WT RLNs.....	44
3.4 Transcriptome map of myeloid cells in atherosclerotic plaques, ATLOs, ApoE ^{-/-} RLNs and WT RLNs	49
3.5 Proportion of T cell subsets per total T cells in atherosclerotic plaques, ATLOs, ApoE ^{-/-} RLNs and WT RLNs	51
3.6 Proportion of myeloid cell subsets per total myeloid cells in atherosclerotic plaques, ATLOs, ApoE ^{-/-} RLNs and WT RLNs.....	53
3.7 The TCR repertoires across atherosclerotic plaques, ATLOs, ApoE ^{-/-} RLNs and WT RLNs suggest (auto)antigen-specific T cell immune responses in atherosclerosis.....	55
3.8 High-throughput paired scTCR(αβ)-seq indicates robust T cell clonal expansion in atherosclerosis.....	59
3.9 Plaque naïve T cells show a specific partially activated phenotype	66
3.10 Impaired immunosuppressive function of T _{reg} cells in atherosclerosis.....	69
3.11 Atypical gene expression profiles of CD4 and CD8 effector and memory T (T _{eff/mem}) cells in atherosclerosis	74
3.12 High expression of co-stimulatory and co-inhibitory molecules in myeloid cells in atherosclerosis	81
3.13 Cell-cell interactomes in atherosclerotic plaques, ATLOs, ApoE ^{-/-} RLNs and	

TABLE OF CONTENTS

WT RLNs.....	84
3.14 T cell adaptation in atherosclerotic plaques	87
3.15 Atherosclerotic plaques are home to interleukin (IL)-17-producing $\gamma\delta$ T cells..	89
3.16 Integrative analysis of murine and human plaques.....	92
3.16.1 scRNA-seq integration analysis reveals similar CD8 T cell tolerance dysfunction in human and mouse atherosclerotic plaques.....	92
3.16.2 Gene expression analysis reveals shared profiles of CD8 T _{eff/mem} cells in murine and human atherosclerotic plaques	95
3.16.3 Human and mouse scRNA-seq integration analysis indicates similar myeloid cell compositions in atherosclerotic plaques.....	97
3.16.4 Gene expression analysis reveals similarities of antigen-presenting cells (APCs) in murine versus human plaques.....	99
4. DISCUSSION.....	101
4.1. T _{reg} cell plasticity, tolerance and clonal expansion in atherosclerosis and caveats.....	102
4.2. CD4 and CD8 T _{eff/mem} cells tolerance and clonal expansion in atherosclerosis	104
4.3. T cell clonal expansion of major T cell subtypes indicate plaque antigen- specific T cell immune responses in atherosclerosis.....	106
4.4. Immune tolerance in cancer and autoimmune diseases.....	107
4.5. How can tolerance checkpoint dysfunction in autoimmune diseases be translated to develop new targets for atherosclerosis treatments?	108
4.6. Lessons from experimental mice for human atherosclerosis	109
4.7. Outlook	110
REFERENCES.....	111
APPENDIX	128
ACKNOWLEDGEMENTS	145
AFFIDAVIT	147
CONFIRMATION OF CONGRUENCY	148
LIST OF PUBLICATIONS.....	149

ZUSAMMENFASSUNG

Atherosklerotische Plaques entstehen in der inneren Schicht der Arterien und verursachen Herz- und Hirngefäßerkrankungen. T Zellen sind an Immunreaktionen beteiligt, die mit verschiedenen Formen von Herz-Kreislauf-Erkrankungen in Verbindung gebracht werden, und es hat sich gezeigt, dass bestimmte T Zell Subpopulationen das Fortschreiten der Atherosklerose regulieren können. Obwohl über proatherogene und antiatherogene Wirkungen von T-Zellen berichtet wurde, sind Toleranzkontrollpunkte zur Modulation der T Zell-medierten Immunreaktion bei fortgeschrittener Atherosklerose oder zur Beeinflussung der Krankheit nur ansatzweise erforscht. Hier haben wir eine Paarungsstrategie aus Einzelzell-RNA-Sequenzierung (scRNA-seq) und Einzelzell-T Zell Rezeptor-Sequenzierung (scTCR-seq) angewandt, um wichtige Toleranzkontrollpunkte in der murinen Atherosklerose zu untersuchen. Mit diesem Ansatz konnten wir die Immunantworten von T Zell Subtypen in Plaques, den tertiären lymphatischen Organen (ATLOs) der Arterien und den drainierenden Lymphknoten (LNs) der Aorta von gealterten Mäusen mit Apolipoprotein E-Mangel (ApoE^{-/-}) umfassend untersuchen. Als Kontrollen wurden zirkulierendes Blut und LN von alters- und geschlechtsgleichen Wildtyp (WT)-Mäusen verwendet. Zusätzlich zu 9 T-Zell-Untergruppen wurden 8 myeloische Zelluntergruppen definiert, um mögliche Interaktionen zwischen T-Zellen und myeloischen Zellen zu untersuchen. Unsere Daten zeigen, dass mehrere T-Zell- und myeloische Zell-Toleranzkontrollpunkte in atherosklerotischen Plaques - und in geringerem Ausmaß - in ATLOs, renalen LNs (RLNs) und der Zirkulation beeinträchtigt sind. In atherosklerotischen Plaques wurden fünf wichtige kompromittierte Immunkontrollpunkte beobachtet, darunter naive T Zellen, regulatorische T (T_{reg}) Zellen, CD4/CD8-Effektor- und Gedächtnis T Zellen (T_{eff/mem}) sowie Antigen-präsentierende Zellen (APCs), was sich in einer Verringerung der Anzahl naiver T-Zellen und T_{reg} Zellen, einer teilweisen Aktivierung naiver T-Zellen und einer deutlichen klonalen Expansion von CD4- und CD8-T_{eff/mem} Zellen und T_{reg}

ZUSAMMENFASSUNG

Zellen zeigte; atypische CD4- und CD8-T_{eff/mem} Zellen mit dysfunktionalen Toleranz-regulierenden Transkripten, die mit der Gewebsresidenz und der Aktivierung zusammenhängen; ein ausgeprägter Erschöpfungsphänotyp von CD4 und CD8 T_{eff/mem} Zellen; Verlust von Transkripten, die mit der immunsuppressiven Funktion von T_{reg} Zellen zusammenhängen; Umwandlung von T_{reg} Zellen in T Helfer (Th)17-ähnlichen Zellen; APC-vermittelte T Zell-Aktivierung; und durch die Plaque-Umgebung bedingte funktionsbezogene Gensignaturen von T Zellen. Darüber hinaus zeigte die scRNA-seq Integrationsanalyse, dass die Anzahl und die Transkriptprofile von CD8 T Zellen und bestimmten myeloischen Zelluntergruppen in atherosklerotischen Plaques bei Mäusen und Menschen ähnlich waren. Unsere Daten deuten darauf hin, dass eine Beeinträchtigung der Immuntoleranz zum Fortschreiten der Atherosklerose beiträgt und dass Atherosklerose mit der Bildung von autoimmunen T Zellen verbunden ist.

ABSTRACT

ABSTRACT

Atherosclerotic plaques arise in the inner layer of arteries causing cardio- and cerebral-vascular diseases. T cells have been implicated in immune responses associated with various forms of cardiovascular diseases and T cell subsets have been shown to regulate the progression of atherosclerosis. Although proatherogenic and antiatherogenic effects of T cells have been reported, tolerance checkpoints to modulate T cells in advanced atherosclerosis or affect the disease are poorly understood. Here, we adopted a pairing strategy of single cell RNA sequencing (scRNA-seq) and single cell T cell receptor sequencing (scTCR-seq) with the aim of studying key tolerance checkpoints in atherosclerosis. This approach allowed us to comprehensively investigate T cell subtype immune responses in plaques, artery tertiary lymphoid organs (ATLOs), aorta draining lymph nodes (LNs) of aged apolipoprotein E deficient (ApoE^{-/-}) mice. As controls, circulating blood and LNs of age- and sex-matched wild type (WT) mice were employed. In addition to 9 T cell subsets, 8 myeloid cell subsets were defined to examine potential interactions of T cells and myeloid cells. Our data reveal that multiple T cell and myeloid cell tolerance checkpoints are compromised in atherosclerotic plaques - and to a lesser extent - in ATLOs, renal LNs (RLNs) and the circulation. Five major compromised immune checkpoints were observed in atherosclerotic plaques, including those in naïve T cells, regulatory T (T_{reg}) cells, CD4/CD8 effector and memory T (T_{eff/mem}) cells and antigen-presenting cells (APCs) as revealed by contraction of the number of naïve T cells and T_{reg} cells; partial activation of naïve T cells; marked clonal expansion of CD4 and CD8 T_{eff/mem} cells and T_{reg} cells; atypical CD4 and CD8 T_{eff/mem} cells with dysfunctional tissue residency-related and activation-related transcripts; a distinct exhaustion phenotype of CD4 and CD8 T_{eff/mem} cells; loss of immunosuppressive function-related transcripts of T_{reg} cells; T_{reg} cell conversion to T helper (Th)17-like cells; APCs mediated T cell activation; and plaque environment-induced T cell function-related gene signatures. Moreover, scRNA-seq integration analysis showed

ABSTRACT

that the numbers and transcript profiles of CD8 T cells and distinct myeloid cell subsets were similar in murine and human atherosclerotic plaques. Our data strongly suggest that impairment of immune tolerance contributes to the progression of atherosclerosis and that atherosclerosis is associated with the generation of autoimmune T cells.

ABBREVIATIONS

ABBREVIATIONS

aa	Amino acid
APCs	Antigen-presenting cells
ApoB	Apolipoprotein B
ApoE	Apolipoprotein E
ATLO	Artery tertiary lymphoid organ
cDC	Classical dendritic cell
cDNA	Complementary DNA
CDR	Complementarity determining region
CTLA4	Cytotoxic T lymphocyte-associated protein 4
cT _{reg}	Central regulatory T cells
CVD	Cardiovascular disease
DCs	Dendritic cells
DEGs	Differentially expressed genes
EDTA	Ethylenediaminetetraacetic
T _{eff/mem}	Effector and memory T cell
eT _{reg}	Effector regulatory T cells
FACS	Fluorescence activated cell sorting
FC	Fold change
Foxp3	Forkhead box P3
GSEA	Gene set enrichment analysis
HFD	High fat diet
IFN- γ	Interferon γ
IL	Interleukin
LDL	Low density lipoprotein
Ldlr	Low density lipoprotein receptor
LN	Lymph node
Lyve1 ⁺ res-like M Φ	Lyve1 ⁺ resident-like macrophage
MHC	Major histocompatibility complex
Mo/M Φ	Monocyte/macrophage
mRNA	Messenger RNA
mTECs	Medullary thymic epithelial cells
NF- κ B	Nuclear factor kappa-light-chain-enhancer of activated B cells
NKT	Natural killer T cells
oxLDL	Oxidized low density lipoprotein

ABBREVIATIONS

PBS	Phosphate buffered saline
PCA	Principal component analysis
PCs	Principal components
PD1	Programmed cell death 1
pDC	Plasmacytoid dendritic cell
QC	Quality control
RLN	Renal lymph node
ROR γ T	Retinoid-related orphan receptor γ T
RT	Room temperature
scRNA-seq	Single cell RNA sequencing
scTCR-seq	Single cell TCR sequencing
SLOs	Secondary lymphoid organs
SMCs	Smooth muscle cells
SNN	Shared nearest neighbor
T _{cm}	Central memory T cells
TCR	T cell receptor
T _{em}	Effector memory T cells
T _{fh}	Follicular T helper cells
TGF- β	Transforming growth factor beta
Th	T helper
TLO	Tertiary lymphoid organs
TNF- α	Tumor necrosis factor α
TRBV	T cell receptor β chain V family
T _{reg}	Regulatory T cells
Trem2 ^{high} M Φ	Trem2 ^{high} macrophage
TRM	Tissue resident memory T cells
tSNE	T-distributed stochastic neighbor embedding
UMI	Unique molecular identifier
V(D)J	Variable diversity joining region
VISTA	V-type immunoglobulin domain-containing suppressor of T cell activation
WT	Wild type
$\gamma\delta$ T	Gamma delta T cells

1. INTRODUCTION

1.1. Atherosclerosis

Cardiovascular diseases (CVD) including coronary artery disease, peripheral artery disease, and cerebral artery disease are the major cause of mortality worldwide. Atherosclerosis constitutes the major pathology of CVD [1]. As a chronic disease, the progression of atherosclerosis can be divided into several stages including of the initial fatty streaks, fibrous plaques, and complicated lesions. Atherosclerotic plaques are located in the inner layer (in short the intima) of medium and large arteries. The rupture of plaque lesions causes the formation of blood clots (thrombi) leading acutely to occlusion of the artery with downstream tissue ischemia and infarcts. Unhealthy lifestyles and diseases including diabetes mellitus, obesity, smoking, hypertension, sedentary lifestyle, and hyperlipidemia are major risk factors for atherosclerosis. Formation of low-density lipoprotein (LDL) deposits in the subendothelial space of the arterial wall is considered as the initial process of atherogenesis [2]. Some LDL particles residing in the arterial wall will undergo oxidation resulting in oxidized LDL (oxLDL) particles that are hypothesized to promote the development of atherosclerosis [3](**Fig. 1.1**). Leukocyte adhesion molecules expressed on activated endothelial cells are assumed to recruit monocytes and T cells into the sub-endothelium (**Fig. 1.1**). Monocytes differentiate into macrophages and convert to foam cells by engulfing oxLDL in plaque lesions (**Fig. 1.1**). Peripheral naïve T cells will activate and differentiate into effector T cells after encountering antigens in LNs and disease sites. CD4⁺ T cells can differentiate into different cell types including Th₁, Th₂, Th₁₇, and T_{reg} cells [4]. Each of these T cell subsets is believed to play distinct roles during the development of atherosclerosis by a series of activities including secretion of multiple cytokines with sometimes opposing roles: interferon γ (IFN- γ) and tumor necrosis factor α (TNF- α) display proatherogenic effect; interleukin (IL)-10 shows antiatherogenic role in atherosclerosis; the effect of IL-4 and IL-17 is still controversial [4]. Likewise, CD8⁺ T

INTRODUCTION

cells secrete granzyme B, perforin, IFN- γ and TNF upon activation to exacerbate plaque instability. While CD8⁺ T_{reg} cells have been reported to limit the progression of atherosclerosis by targeting APCs and suppressing polarization of pathogenic CD4⁺ T cells [4]. During atherogenesis, media smooth muscle cells (SMCs) migrate into the intima and produce extracellular matrix molecules, which form the fibrous cap to protect atherosclerosis plaques from rupture (**Fig. 1.1**). The accumulation of the lipid and dead cells in some lesions promotes the formation of necrotic cores of plaques, which are considered to represent an important precipitating factor for unstable plaque formation, rupture and infarcts [5] (**Fig. 1.1**). Plaques with less SMCs but abundant macrophages have been termed as vulnerable/unstable plaques with a tendency to rupture and initiate formation of a thrombus. Several hypotheses have been proposed for atherosclerosis development including the response to injury hypothesis and the altered lipoprotein hypothesis [6]. The discovery of T cells, macrophages, and dendritic cells (DCs) in atherosclerotic plaques led to the hypothesis that atherosclerosis is a chronically unresolvable inflammatory disease with an adaptive T cell-related immune response [7] (**Fig. 1.1**). This hypothesis is currently the focus of atherosclerosis research at an international scale. Various clinical trials have been performed to modulate the immune response in atherosclerosis, but it remains to be determined whether such general approaches will lead to tangible treatments. The dilemma of antigen-independent treatment strategies and global interference approaches lies in the plasticity of the systemic regulation of the immune response and the unpredictable nature of these concepts regarding cancer, immunosuppression, infectious diseases versus atherosclerosis outcomes [8]. Our concept presented in this thesis has therefore been to initiate studies to identify atherosclerosis-specific autoantigens and the search for autoimmune T cells [9, 10].

INTRODUCTION

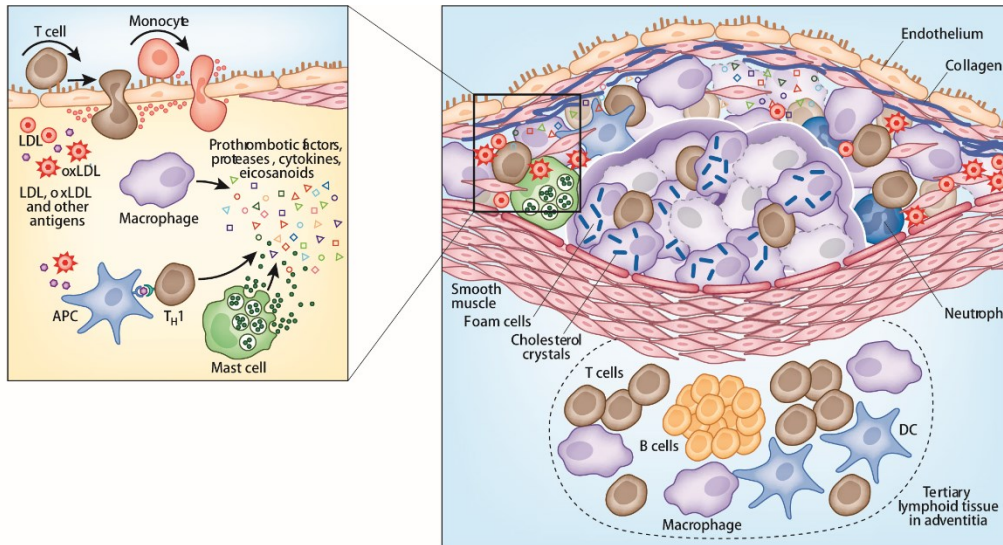


Fig. 1.1 Immune responses contribute to the development and stability of atherosclerotic plaques (adopted from Hansson, G. K. et al [3]). Atherosclerotic plaques are characterized by complex inflammatory infiltration that accumulates in the arterial wall including lipid deposits, immune cells and SMCs. The immune responses that control plaque formation, plaque growth and plaque stability involve both innate and adaptive immune responses. Moreover, tertiary lymphoid organs (TLOs) generated in the adventitia of plaque-burdened artery segments may be involved in atherosclerosis.

1.2. T cells are involved in atherosclerosis progression

1.2.1. CD4⁺ T cells in atherosclerosis

T cells play important roles in the progression of atherosclerosis, with different subsets displaying different and even opposite functions. CD4⁺ T cells are the dominant T cells in all phases of lesion development [11]. The main CD4⁺ T cell subsets are Th₁, Th₂, Th₁₇, and T_{reg} cells [12]. The presence of IL-12 and IL-18 gives rise to Th₁ polarization and promotes Th₁-mediated immune responses [13]. IL-12 activates T cells to express T-box, which will result in secreting the pro-inflammatory cytokines IFN- γ and TNF- α . IFN- γ promotes vascular cell adhesion molecule expression in endothelial cells and further promotes the development of atherosclerosis. It also contributes to plaque vulnerability by accelerating macrophage apoptosis and extracellular matrix breakdown [14]. Moreover, intraperitoneally administered IFN- γ in ApoE^{-/-} mice significantly increases lesion size [15]. Conversely, IFN- γ receptor knockout mice show a substantial reduction in

INTRODUCTION

lesion size [16, 17]. TNF- α is a central mediator of inflammation. It activates downstream events by binding to tumor necrosis factor receptor 1 or tumor necrosis factor receptor 2 [18], mediating the expression of adhesion molecules on endothelial cells [19], and triggering apoptosis signaling [20] and T cell proliferation [21]. TNF- α and ApoE double knockout mice show a 50% reduction of lesion size [22]. As prominent factors for Th₁ development, IL-12 and IL-18 both accelerate atherosclerosis lesion formation in ApoE^{-/-} mice [23, 24]. Blocking Th₁ polarization protect the mice as shown by treatment with pentoxifylline, a known Th₁ differentiation inhibitor [25]. These data indicate an atherogenic role of Th₁ cells in atherosclerosis, but the role of Th₂ cells in atherosclerosis remains controversial [26]. Differentiation of Th₁₇ cells require the presence of several cytokines including IL-6, transforming growth factor beta (TGF- β), and IL-1 β . Th₁₇ cells express retinoic acid-related orphan receptor γ T (ROR γ T) and secrete cytokines including IL-17A, IL-22, and IL-17F. IL-17A is the key cytokine secreted by Th₁₇ cells. Studies documented IL-17A contributes to autoimmune diseases such as rheumatoid arthritis and inflammatory bowel disease [27, 28]. IL-17A expressing T cells have been observed in the aorta of ApoE^{-/-} mice on chow diet or on Western diet, while blocking IL-17A in ApoE^{-/-} mice led to reduction of the plaque burden on a Western diet suggesting a proatherogenic role of IL-17A in atherosclerosis [29]. However, some ApoE and IL-17/IL-17A double-deficient mice show different results making it difficult to define the impact of Th₁₇ cells in atherosclerosis [30-32]. Therefore, the proatherogenic versus the antiatherogenic effect of Th₁₇ cells in atherosclerosis needs further studies [26]. T_{reg} cells as the major immunosuppressive population of the T helper cell family that have been identified to play an atheroprotective role in atherosclerosis [33, 34]. T_{reg} cells highly express the forkhead box P3 (Foxp3) transcriptional factor involved in T_{reg} cell development and their immunosuppressive functions. To maintain its phenotype and function, T_{reg} cells also co-express cytotoxic T lymphocyte-associated protein 4 (CTLA4), CD25, but lack expression of CD127 [4]. T_{reg} cells can be classified into two populations based on their origin. T_{reg} cells which survive following selection in the thymus migrate to the circulation are called natural T_{reg} cells. T_{reg}

INTRODUCTION

cells that are generated in the periphery from circulating naïve CD4 T cells are termed induced T_{reg} cells [35]. Studies documented there are three conserved non-coding DNA sequences of T_{reg} cells modulate their function and stability. The non-coding DNA sequences region 2, which was thought to represent the key region to regulate Foxp3 expression and account for the plasticity of T_{reg} cells in inflammatory diseases, is demethylated in natural T_{reg} cells, while it is methylated in induced T_{reg} cells [36, 37]. Clinical study also demonstrated that T_{reg} cells are both significantly decreased in number and functionally compromised in acute coronary syndrome patients compared to patients with stable angina due to coronary heart disease and normal controls. Their study also revealed that the messenger RNA (mRNA) and protein level of Foxp3 in purified T_{reg} cells were both reduced in acute coronary syndrome patients [38]. IL-10, the main immunosuppressive cytokine secreted by T_{reg} cells, also showed a dramatic decline in patients with vulnerable coronary plaques [39]. T_{reg} cells regulate peripheral tolerance checkpoints, which will be discussed below as we will outline the plasticity of T_{reg} cells in other disease conditions.

1.2.2. CD8⁺ T cells in atherosclerosis

CD8⁺ T cells are observed in all stages of atherosclerotic plaque lesions. Antigen-experienced cytotoxic CD8⁺ memory T cells were found to be dominant in human plaques. Its percentage of total T cells showed a significant increase in human plaque lesions when compared to peripheral blood, while CD4⁺ T cells did not change [40]. Complete knock out of CD8⁺ T cells in ApoE^{-/-} mice showed a less important role of CD8⁺ T cells on preventing atherosclerosis development: the extent of atherosclerosis in total aortic area and aortic root were similar in ApoE^{-/-}/CD8^{-/-} vs ApoE^{-/-} mice both at 18 weeks and at 1 year of age whereas the absence of CD4⁺ T cells induced an increase of lesion sizes throughout the descending thoracic and abdominal aorta segments. However, this complete knock out strategy was thought to bring about compensatory effects on the immune system, as a significant increase of CD8 T cells in ApoE^{-/-}/CD4^{-/-} mice was observed when compared to ApoE^{-/-} mice

INTRODUCTION

[41]. Targeting CD8 α or CD8 β by monoclonal antibody treatment to deplete CD8 $^+$ T cells showed that CD8 $^+$ T cells promote vulnerable atherosclerotic plaque formation via perforin- and granzyme B-mediated apoptosis of macrophages, smooth muscle cells, and endothelial cells and in turn induce the formation of necrotic cores [42]. Interestingly, the study demonstrated expression of a non-self-microbial antigen on vascular smooth cells triggered strong CD8 $^+$ T cells activation and further promoted atherosclerotic lesion formation in ApoE $^{-/-}$ mice fed with Western diet. While hypercholesterolemia induced by ApoE deficiency and Western diet in ApoE $^{-/-}$ mice only bring about a mild type of vascular inflammation with less CD8 $^+$ T cell infiltration, these data indicate mutual interactions of hypercholesterolemia with the immune system in atherosclerosis progression [43]. CD8 $^+$ T $_{reg}$ cells were also reported in atherosclerosis by regulating follicular T helper (T $_{fh}$) cells [44].

1.2.3. Gamma delta ($\gamma\delta$) T cells in atherosclerosis

Different from the $\alpha\beta$ T cells, the T cell receptor (TCR) of $\gamma\delta$ T cells is composed by γ and δ chains. It accounts for a minor population (~3-5%) of total T cells in the human blood. $\gamma\delta$ T cells recognize antigens without the presentation by major histocompatibility complex (MHC) molecules expressed on APCs [45]. However, a recent study demonstrated it could recognize phosphorylated prenylated metabolites and lipids presented by a cluster of differentiation 1 molecules [46]. $\gamma\delta$ T cells were found to be significantly increased in human atherosclerotic plaques, and they are already highly enriched in the early stages of plaque lesions [47, 48]. However, the effect of $\gamma\delta$ T cells in atherosclerosis is still elusive. TCR δ -deficient mice revealed that there was no difference in aortic lesion area, cholesterol and lipoprotein fractions, and several plasma cytokine concentrations between TCR δ $^{-/-}$ ApoE $^{-/-}$ and ApoE $^{-/-}$ mice [45]. Another study observed a reduction of lipid accumulation in the early stage in atherosclerotic intima [49]. $\gamma\delta$ T cells are also the source of IL-17 *in vivo* as IL-17 $^+$ CD3 $^+$ T cells were $\gamma\delta$ T cells in the aorta [29].

INTRODUCTION

1.2.4. The balance of Th₁₇/T_{reg} cells and the plasticity of T_{reg} cells in atherosclerosis

Th₁₇ cells are considered to represent a subset of CD4⁺ T cells with the capacity of producing IL-17. Th₁₇ cell transdifferentiation from CD4⁺ T cells is regulated by ROR γ t (transcribed by gene RAR-related orphan receptor C, *Rorc* in brief) [50]. Although studies have studied Th₁₇ cells and IL-17 in atherosclerosis, it is still too early to define their exact roles in atherogenesis [51]. A skewed relation between T_{reg} and Th₁₇ cells was observed in chronic inflammatory and autoimmune diseases [51-60]. A clinical study has shown that patients with severe coronary atherosclerosis have increased CD4⁺IL-17⁺ cells concomitant with a decrease of T_{reg} cells and CD4⁺IL-10⁺ T cells resulting in a decline of T_{reg}/Th₁₇ ratios in patients with severe coronary atherosclerosis compared to controls [52]. Importantly, IL-17-producing T_{reg} cells are less effective in suppressing the activation of naïve T cells [53]. The phenomenon of T_{reg} cells with reduced Foxp3 expression but a phenotype resembling Th₁₇ cells (termed as exT_{reg} cells or Th₁₇-like T_{reg} cells) has been observed in many diseases, like autoimmune arthritis [54], periodontitis [55], diabetes [56] by using Foxp3 T_{reg} cells lineage tracking mice. exT_{reg} cells were found to accumulate at the disease sites and played different roles in different diseases. exT_{reg} cells were considered as potent bone-damaging cells in arthritis, and exacerbated diabetes, but promoted protection against oral bacteria in periodontitis. These studies should be taken as evidence that the role of exT_{reg} cells in atherosclerosis requires further work. Moreover, the immunosuppressive activity of exT_{reg} cells also vary in different studies including defective suppression [54, 56-59] or no change in their immunosuppression activity [60, 61]. And more recently, by using tetramers and scRNA-seq assays, Klaus group identified apolipoprotein B (ApoB) peptide-specific autoreactive T_{reg} cells in human and murine studies [62-64]. Both studies showed conversion of T_{reg} cells to effector/memory-like phenotype Th₁₇ cells, and adoptive transfer these ApoB-specific T_{reg} cells did not show obvious atheroprotective effects [62-64].

INTRODUCTION

1.3. T cell development

T cell precursors originate from hematopoietic stem cells in the bone marrow and further develop and differentiate in the thymus, the central lymphoid organ for immature precursor T cell maturation. In the thymus, precursor T cells will undergo β -selection, positive selection, negative selection, and variable diversity joining region (V(D)J) arrangement to generate mature T cells with unique TCRs (**Fig. 1.2**). After precursor T cells migrate into the thymus, they first home in the outer regions of the thymic cortex and undergo four double negative stages. The expression of recombination activating gene 1 and recombination activating gene 2 promotes β chain rearrangement at the double negative 3 stage, at which β -selection occurs resulting in precursor T cell development into $\alpha\beta$ T cells. A non-arranging pre-TCR α chain can also be produced to generate pre-TCRs. The pre-TCR $\alpha\beta$ associates with the CD3 complex both contribute to the signaling cascade for T cell maturation. During TCR β chain rearrangement, the germline DNA begins with joining one of diversity segment of β chain ($D\beta$) to one of joining segment of β chain ($J\beta$), then it is followed with variable segment ($V\beta$) joining to the $DJ\beta$ recombination segment. The redundant sequences of rearranged DNA are spliced during transcription, leading to complete TCR β chain with V, D, J and constant domains (C). Then, double negative T cells convert into $CD4^+CD8^+$ double-positive cells followed with TCR α chain rearrangement resulting in the formation of paired TCR $\alpha\beta$ chains [65, 66]. This random recombination process of α and β chains generate numerous T cells with diverse TCRs thereby contributing to the diversity of TCR repertoire of our body. The binding strength of TCR with self-peptide/MHC complex determines the fate of each double-positive T cell. 90% of T cells fail to bind to the peptide-MHC complex. Instead, they will undergo apoptosis via a process termed death by neglect [67]. T cells which bind to the peptide- MHC-I/II presented by cortical epithelial cells with an appropriate modest affinity lead to their maturation and turn to CD4 or CD8 single positive T cells [67]. Positive selection ensures that the TCR recognizes the MHC complex and enables it to respond to antigens. Thus, formation of the TCR-peptide-MHC complex is a basic principle to initiate T cell-dependent adaptive immune

INTRODUCTION

response in peripheral tissues. After single positive T cell commitment, negative selection is continuously carried out in the medulla of the thymus where T cells interact with self-peptide-MHC complexes presented by medullary thymic epithelial cells (mTECs) and medullary DCs. A fraction of T cells with appropriate affinity thresholds will differentiate into T_{reg} cells by clonal diversion. More details about negative selection and clonal diversion will be discussed below. T cells which survive positive and negative selection will emigrate to peripheral tissues and these cells are capable of being activated by specific antigens. However, some TCRs which bind to self-antigens after negative selection still exist in the thymus. If these autoreactive T cells migrate to the periphery, they could potentially trigger detrimental auto-immune responses. Several mechanisms to remove autoreactive T cells and restrain these cells activation in the periphery will be discussed below.

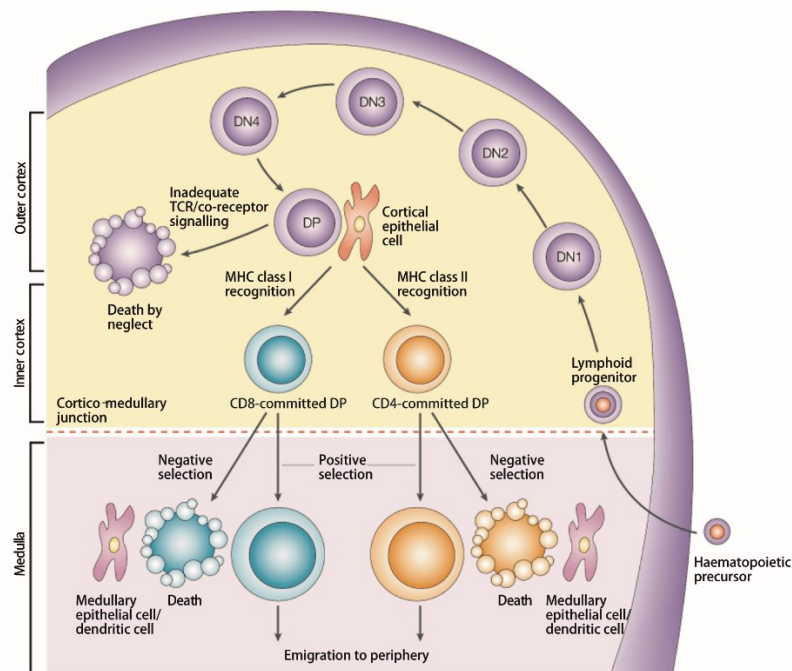


Fig. 1.2 Overview of T cell development in the thymus (adopted from Germain RN [68]). T cell precursors generate in the bone marrow and migrate to the thymus to mature. During maturation, precursor T cells will go through several stages to develop into mature naïve T cells with paired TCR $\alpha\beta$ chains, including β -selection, TCR recombination, positive selection, and negative selection. β -selection in the double-negative 3 stage promotes precursor T cell development into $\alpha\beta$ T cells. TCR recombination of $\alpha\beta$ chains produces a large T cell pool with diverse TCRs resulting in the large diversity of TCR repertoire of each individual. The strength of binding affinity between TCR and peptide-MHC complex determines the fate of double positive T cells. T cells which are not capable of

INTRODUCTION

recognizing peptide-MHC complexes presented by cortical thymic epithelial cells will be deleted via death by neglect. A modest binding strength promotes double positive T cells survival and development into single positive T cells. Single positive T cells which have very strong affinities with self-peptide-MHC complexes presented by mTECs or DCs will undergo apoptosis during negative selection. Mature T cells will egress to the periphery ready to engage their naïve TCR to exogenous and endogenous (auto)antigens.

1.4. Immune tolerance to control T cell immune responses

1.4.1. Central tolerance

Central tolerance mechanisms in the thymus are crucial to remove autoreactive T cells and suppress autoimmune responses in diseases. Various mechanisms have been identified to mediate T cell central tolerance including clonal deletion, clonal diversion (agonist selection), TCR re-editing and anergy [69]. Clonal deletion is defined as T cells with very high-affinity binding of their TCRs to self-peptide-MHC complexes on the surface of APCs resulting in deletion through apoptosis. mTECs express transcription factor autoimmune regulator to promote tissue-specific self-antigen expression on mTECs. Loss of function mutations of the autoimmune regulator gene in humans results in autoimmune disease polyendocrinopathy-candidiasis-ectodermal dystrophy, which manifests itself as autoimmune endocrine and nonendocrine disorders including chronic mucocutaneous candidiasis and chronic hypoparathyroidism [70]. The deficiency of gene autoimmune regulator shows multiple autoimmune polyendocrinopathy-candidiasis-ectodermal dystrophy-like features in mice with inflammatory cell infiltration in multiple organs and the production of autoantibodies [71]. mTECs as APCs in the thymus play a crucial role in presenting tissue-specific self-antigens to thymocytes [72, 73]. DCs are also implicated in antigen presentation in the thymus. Thymic DCs present soluble antigens to thymocytes [74] and peripheral migratory DCs have also been reported to participate in transporting antigens to the thymus to regulate thymic tolerance [75, 76]. It has been assumed that the fate of T cells during negative selection depends on the binding affinity of immature T cells to the peptide-MHC complex on mTECs [67]. T cells that have a very high or too strong affinity to self-antigens will be

INTRODUCTION

eliminated whereas a moderate affinity will ensure T cells maturation and survival [77]. However, the affinity theory to exclusively define T cell fates does not explain the entirety of tolerance mechanisms in the thymus. Studies showed that - under certain conditions - a strong TCR signal can lead to the development of T_{reg} cells. This process has been termed as clonal diversion (also called agonist selection) [78]. A higher affinity is required for CD4 single positive T cells transdifferentiate into T_{reg} cells. Experiments using Nur77 green fluorescent protein reporter mice in which green fluorescent protein expression levels reflect the extent of TCR activation but not inflammatory stimulation, illustrated that T_{reg} cells acquire higher levels of green fluorescent protein than conventional non-T_{reg} cells during development [79]. Recognizing the self-antigen is thought to be indispensable for T_{reg} cell development in the thymus [78]. As the influenza hemagglutinin-specific autoreactive T cells in influenza hemagglutinin transgenic mice were found to differentiate into CD4⁺CD25⁺ T_{reg} cells deletion [80]. Although central tolerance in the thymus can eliminate most self-reactive T cells, many autoreactive T cells still escape to the periphery. In the periphery, multiple peripheral tolerance mechanisms become available to remove or suppress self-activated T cells when activated by the self-antigens including antigens that are generated and displayed during chronic infection and inflammation [69].

1.4.2. Peripheral tolerance

1.4.2.1. T cell intrinsic peripheral tolerance mechanisms

Naïve T cells, i.e. T cells that have never encountered peripheral antigens, will migrate to LNs and other tissues ready to encounter antigens there for the first time in their life cycle [81, 82]. During this encounter, the cells undergo activation and differentiation into effector memory cells (T_{em}) cells. The journey of naïve T cell differentiation into T_{em} cells is controlled by multifaceted intrinsic tolerance checkpoints to keep T cell-mediated immunity at an appropriate level to meet the specific requirements for multiple types of immune responses [83]. Quiescence and ignorance are two initial key mechanisms of peripheral tolerance to keep naïve T cells in a state of low responsiveness to peripheral antigens (**Fig. 1.3**). Quiescence

INTRODUCTION

relates to the G₀ stage of their cell cycle which is associated with a small cell size, low metabolic activity, and low responsiveness to antigen. Many transcription factors and genes have been reported to regulate quiescence of T cells. B cell translocation gene anti-proliferation factor 1/2 (*Btg1/Btg2*) are genes mainly expressed during the G₀ phase of cell cycle. BTG1/BTG2 knockout leads to T cell proliferation and a low threshold to activation by antigen stimulation [84]. Moreover, *Klf2* (Lung Krüppel-like factor) is a transcription factor, which suppresses cell growth and participates in maintaining T cell quiescence by inhibiting the c-Myc-dependent pathway [85]. The expression of *Klf2* was reported to be regulated by forkhead box O1 (*Foxo1*) and runt-related transcription factor 1 (*Runx1*). Accordingly, FOXO1 deletion results in spontaneous T cell activation, proliferation and triggers autoimmune responses in *Foxo1*-deficient mice [86]. The role of *Runx1* was also demonstrated as RUNX1 deficiency leads to spontaneous CD4 T cell activation, cytokine production and autoimmune reactions [87]. Recently, V-type immunoglobulin domain-containing suppressor of T cell activation (VISTA) has been shown as a major regulator of naïve CD4 T cell quiescence by affecting many downstream quiescence-related transcription factors such as *Btg1*, *Btg2*, *Klf2* and Forkhead Box P1 (*Foxp1*). Genetic deletion of VISTA resulted in significant reduction of the naïve T cell population and a concomitant increase of a memory-like activated T cell phenotype [88]. The phenomenon of autoreactive T cells unable to respond to antigens is called T cell ignorance but its underlying mechanisms remain to be fully understood [83].

Dysfunctional co-stimulatory molecules trigger anergy of T cells during T cell priming thereby preventing harmful T cell responses ahead of their activation (**Fig. 1.3**). Anergic T cells show low levels of IL-2 secretion, which results in impaired PI3K (phosphoinositide 3-kinases)/AKT (protein kinase B)-mTOR (mammalian target of rapamycin) pathway activation [83]. Moreover, the defective RAS (rat sarcoma viral oncogene)-MAPK (mitogen-activated protein kinase) pathway in anergic T cells is thought to promote NFAT1 (nuclear factor of activated T cells) signaling, which in turn aggravates T cell anergy [83]. Ubiquitin ligases were also observed to be enriched in anergic T cells by regulating several pathways associated with anergy

INTRODUCTION

[89]. Diminished anergy of T cells after adoptive transfer into lymphopenic mice were observed raising the possibility that long-term antigen stimulation is crucial for anergy maintenance [90]. The interaction of CD28-CD80/86 between APCs and T cells provide the co-stimulatory signal for T cell activation. CTLA4 on T_{reg} cells has a highly competitive affinity with CD80/CD86 on APCs resulting in anergy of T cells [91]. Also, production of adenosine catalyzed by CD39 and CD73 on T_{reg} cells were observed to induce T cell anergy [92].

T cell exhaustion is another key mechanism to limit T cell immune responses (**Fig. 1.3**). The phenotype of T cell exhaustion was initially described in chronic viral infection. Co-inhibitory markers are highly expressed in exhausted T cells, like programmed cell death 1 (PD1, encoded by gene *Pdcd1*), lymphocyte activation gene 3 (LAG3, encoded by gene *Lag3*), T cell immunoreceptor with Ig and ITAM domains (TIGIT, encoded by gene *Tigit*), T cell immunoglobulin domain and mucin domain-containing protein 3 (TIM3, encoded by *Havcr2*) and CTLA4, which compromise TCR signaling activation. Targeting co-inhibitory markers on the exhausted T cells by immune checkpoint inhibitors in cancer patients remains a milestone for some cancer treatments [93]. T cells with exhausted phenotypes have also been reported in chronic inflammation and autoimmune diseases [94]. Exhausted T cell profiles have been reported in human atherosclerotic plaques, with high levels of exhaustion-related genes relative to their blood counterparts, such as *Eomes*, *Pdcd1* and *Lag3* [95]. Pd1 deficiency in low density lipoprotein receptor-deficient (*Ldlr*^{-/-}) mice have large plaque burdens accompanied with increased immune cell infiltration and activation [96]. *Ldlr*^{-/-} mice treatment with anti-PD1 antibody reproduced the data vs the genetic knockout mice. The activation of PD1 signaling promotes phosphorylation of intracellular ITIM (tyrosine-based inhibitory motif) and ITSM (tyrosine-based switch motif), which in turn recruit tyrosine phosphatases. These tyrosine phosphatases will dephosphorylate the main modulator in the TCR signaling pathway and co-stimulatory signaling pathway including PI3K and RAS resulting in attenuated T cell activation [97]. Other co-inhibitory molecules, like CTLA4 and TIGIT share similar mechanisms to suppress T

INTRODUCTION

cell activation [98].

T cell senescence can be described as cells with poorly replicative capacity after extensive TCR stimulation during aging (**Fig. 1.3**). Different from exhausted T cells, senescent T cells show a senescence-associated secretory phenotype producing high levels of proinflammatory cytokines. Recent studies also showed that senescent T cells play critical role in immune responses [99]. Apart from the above T cell intrinsic mechanisms of T cell tolerance, T_{reg} cells and APCs are involved in extrinsic T cell tolerance as described below.

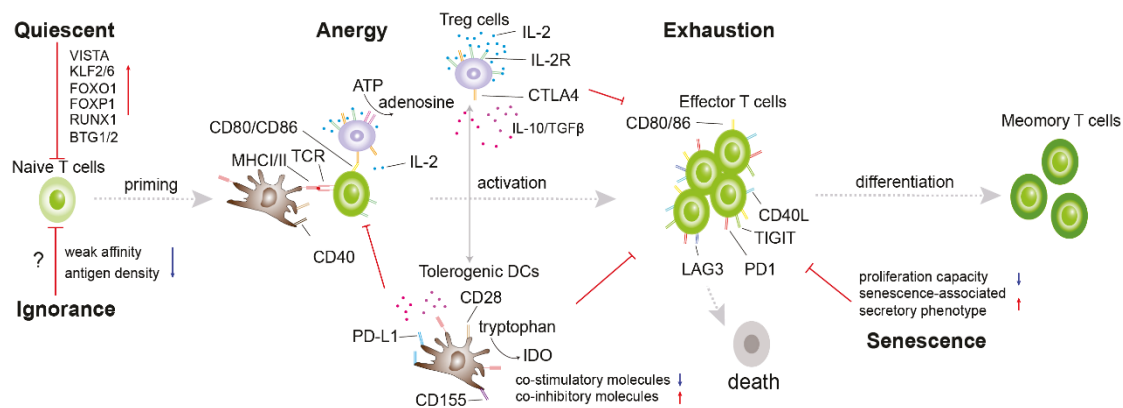


Fig. 1.3 T cell intrinsic and extrinsic mechanisms to induce T cell tolerance (modified from EITanbouly, M.A. et al. [83]). T cell immune responses are regulated by multiple molecules. They can be divided into T cell intrinsic and T cell extrinsic mechanisms. Quiescence-related gene expression profiles lead to naïve T cells locked in the G₀ phase of the cell cycle with low metabolic activity and low responsiveness to activation. The weak binding affinity and low antigen levels are thought to be the main mechanism to cause naïve T cell ignorance after antigen stimulation. At the T cell priming stage, lack of the second co-stimulatory signaling promote T cell anergy. Tolerogenic DCs with low co-stimulatory molecule expression but a high co-inhibitory molecule level result in the anergic state of T cells. T_{reg} cells also participate in T cell anergy by competitive binding the co-stimulatory ligand in APCs and deprivation of IL-2, which both involve T cell activation. When T cells activated by antigens, robust T cell immune responses are restrained by T cell exhaustion and T cell senescence. The interaction of exhaustion-related molecules with their ligands on APCs trigger T cell exhaustion. Immune responses can also be controlled by T cell senescence.

1.4.2.2. T_{reg} cell-mediated immune tolerance

Foxp3⁺ T_{reg} cells are viewed as the main population to maintain peripheral tolerance to restrain activation of self-reactive T cells in the periphery (**Fig. 1.3**). They operate through several mechanisms including CTLA4-dependent suppression and release

INTRODUCTION

of IL-10 and TGF- β [100]. As a potent negative regulator of immunologic self-tolerance, CTLA4 has been reported to be expressed in thymus derived and induced Foxp3⁺ T_{reg} cells to mediate immunosuppressive function in the periphery. In humans, highly suppressive Foxp3^{high}CD25^{high}CD4⁺ T cells selectively express CTLA4 [101-103]. CTLA4-deficient mice suffer from fatal multiorgan inflammation [104]. *In vivo* blockade of CTLA4 leads to autoimmunity and inflammatory bowel disease [102, 105]. Specifically, deficiency of CTLA4 in Foxp3⁺ T_{reg} cells elicits spontaneous development of systemic lymphoproliferation and T cell-mediated autoimmune disease. The immunosuppressive effect of CTLA4 may be mediated by affecting DCs to activate other T cells. Meanwhile, the impact of T_{reg} cells on DC activation and peripheral CD8 T cell tolerance depends on CTLA4 [106]. Apart from CTLA4 mediated competitive binding to co-stimulatory molecule ligands on APCs, T_{reg} cells can also suppress T cell activation by transendocytosis of co-stimulatory ligands from APCs by CTLA4 [107]. Furthermore, the interaction of T_{reg} cells with DCs has been illustrated to induce the generation of tolerogenic DCs by depleting co-stimulatory ligands from DCs and secreting the inhibitory cytokines IL-10 and TGF- β [108], but other reports have indicated that IL-10 production by T_{reg} cells is not essential for restraining systemic autoimmunity but contribute to suppressing local inflammation [109, 110].

1.4.2.3. DC-mediated immune tolerance

As a main population of APCs, DCs play a critical role to prime T cells and regulate the T cell immunity. Immature DCs patrol peripheral tissues, where they encounter and engulf membrane-bound or soluble antigens. These antigens are degraded and presented to the cell surface with MHC molecules to activate T cells [111]. The pattern-recognition receptors including Toll-like receptors and nucleotide-binding oligomerization domain-like receptors to sense inflammation are also important for maturation of DCs [112, 113], which in turn enhance proinflammatory cytokines, co-stimulatory molecules and MHC-II expression to promote activation of naïve T cells [114]. Tolerogenic DCs constitute a subpopulation of DCs, which can effectively take

INTRODUCTION

up antigens but have low levels of MHC-II and co-stimulatory molecules, lack the ability of antigen processing, presentation, and T cell priming [114, 115] (**Fig. 1.3**). Many immunosuppressive factors such as IL-10 and TGF- β and pharmacological components like rapamycin and dexamethasone can induce the generation of tolerogenic DCs [116]. Tolerogenic DCs have been reported to induce immune tolerance in the periphery by several mechanisms including to induce T cell anergy (CD80/86-CTLA4 interaction, PD-L1-PD1 interaction, inducible T cell costimulator (ICOS for short)-ICOS-L interaction) and clonal deletion (Fas cell surface death receptor ligand- (FasL in brief) Fas interaction, tumor necrosis factor-related apoptosis-inducing ligand or Apo 2 ligand- (TRAIL in brief) tumor necrosis factor superfamily interaction, indoleamine 2,3-dioxygenase production), induction of T_{reg} cells (PD1-PD-L1 interaction, CD80/86-CTLA4 interaction, ICOS-ICOS-L interaction, immunoglobulin-like transcript 3/4 expression) and producing immunosuppressive cytokines (IL-10, TGF- β , IL-27, IL-35) [115]. The cross-presentation property of DCs allows the exogenous antigens to be presented to CD8⁺ T cells. Cross-presenting DCs also restrain the immune response of autoreactive CD8⁺ T cells [117]. Relative to the traditional peptide vaccination approach, targeting antigens which induce antigen-specific tolerogenic DCs may be a promising method for clinical therapy. Research has demonstrated that using anti-DEC205 (endocytic receptor)-mediated targeting self-peptide proteolipid protein to DCs alleviated the autoimmune symptoms of PLP-induced experimental autoimmune encephalomyelitis in SJL mice by inducing T cell anergy and generating immunosuppressive T cells [118].

1.5. ATLOs organize immune responses in aged ApoE^{-/-} mice

Chronic non-resolving inflammatory diseases are often associated with unbalanced pro-inflammatory and anti-inflammatory lymphocytes, which lead to tissue damage and injury. TLOs emerge in tissues in response to chronic non-resolving inflammation such as chronic infection, autoimmune disease, and graft rejection. In

INTRODUCTION

recent years, our group reported that a tertiary lymphoid tissue, named artery TLO (ATLO), arises in the adventitia of aorta segments that are burdened with atherosclerotic plaques during aging of ApoE^{-/-} mice [119, 120]. Advanced stages of ATLOs contain separated T and B cell areas and activated germinal centers in B cell follicles, clusters of plasma cells, several subsets of myeloid cells. ATLOs also contain structures known to promote immune cell trafficking and subsequent immune responses including functional conduit meshworks, newly formed high endothelial venules, blood vessels, and aberrant lymph vessels. Their formation in mice is preferentially located in the abdominal aorta adventitia, but they can also develop in other parts of the arterial tree of mice and humans including coronary arteries [120]. Transcript atlases of plaques, ATLOs, and secondary lymph organs (SLOs) constructed by laser capture microdissection-based mRNA expression analysis showed both T cell- and B cell-specific genes are highly expressed in ATLOs. Multiple gene ontology terms covering broad aspects of immunology including proliferation, differentiation and activation are all highly enriched in ATLOs of aged ApoE^{-/-} mice when compared with WT mice. These data indicate that adaptive immune response in atherosclerosis appears to be regulated locally rather than systemically [120-122].

1.5.1. T cell immune responses in ATLOs

ATLOs resemble SLOs in many ways including structural components and cellularity though its gene expression differs considerably [121-124]. Its strong lymphocyte signature indicates ongoing lymphocyte activation pathways. FACS analyses of T cell subsets in ATLOs showed that ATLOs harbor large numbers of CD4⁺, CD8⁺ and T_{reg} cells. Further, T_{em} and central memory T cells (T_{cm}), which serve as immunosurveillance-regulating cells in peripheral tissues [125, 126], dominate in ATLOs when compared to SLOs. CD4⁺ T_{em} cells yielded a 27-fold ratio vs naïve cells and T_{reg} cells with T_{em} phenotype showed an 86-fold ratio vs naïve T_{reg} cells [121]. These data indicate that ATLO CD4⁺ and CD8⁺ T_{em} cells are the major lymphocyte populations involved in initiating inflammatory immune responses in the

INTRODUCTION

atherosclerotic arterial wall. The T_{em} phenotype of T_{reg} cells may limit inflammatory immune responses, which may contribute to the immune response balance of atherosclerosis. T cell tissue tropism was also studied by performing a series of adoptive transfer experiments and detecting the tissue homing regulators in T cells including CD103, CD69 and PD-1. The results demonstrated that numerous ATLO $CD4^+$, $CD8^+$ and T_{reg} cells express CD103, CD69 and PD-1. ATLOs have a large capacity to recruit naïve T cells into the arterial wall adventitia and a high capacity to generate T_{em} cells. Moreover, ATLOs can also convert naïve $CD4^+$ T cells into induced T_{reg} cells. These data suggest that not only do ATLOs act as a reservoir for immune cells, but they also organize T cell immune responses that potentially contribute to disease pathogenesis [121].

1.5.2. B cell immune responses in ATLOs

Although B cells appear to be scarce in atherosclerotic plaques, B cells in ATLOs are abundant. B cells are present in T cell areas but also form separate B cell follicles in ATLO stages II and III. Importantly, germinal centers with follicular DCs can also be detected in ATLOs and they are signature cells of advanced stage III ATLOs. B cell-related aorta transcriptomes demonstrated large B cell-related gene signatures which functionally associated with recruitment of B cells into ATLOs and the formation of ATLO germinal centers [122]. Gene signatures of mice with different ages showed differentially B cell-related transcript expression profiles during atherosclerosis progression. Similar changes could not be observed in WT or ApoE^{-/-} LNs.

1.6. Are there autoimmune B and/or T cell responses in atherosclerosis?

Atherosclerosis cannot yet be defined as a prototypic bona fide autoimmune disease because studies have not yet shown the major *Witebsky criteria* that are recognized to define autoimmune diseases such as Basedow disease and myasthenia gravis [127]. These criteria require isolation of a pathogenic autoantigen or a B cell receptor with exclusive specificity to an autoantigen or transfer of the autoimmune T cells or

INTRODUCTION

autoantibody to other individuals resulting in the appropriate disease. Similar to this unresolved problem in atherosclerosis, although many autoimmune antibodies and self-specific T cells have been identified in multiple sclerosis, they may not cause disease [128-131]. Thus, the direct evidence to meet the criteria in multiple sclerosis, rheumatoid arthritis, and type I diabetes has not yet been achieved [132, 133]. In line with the hypothesis that autoantigens may be generated during atherosclerosis progression, however, many efforts have been made to obtain evidence to support it. oxLDL is being considered by some investigators as the major autoantigen in atherosclerosis. Unexpectedly, however, an important study showed oligoclonal expansion of TRBV31⁺ (T cell receptor β chain V family 31) T cells after oxLDL immunization and that these TCRs recognize native human LDL and ApoB100 rather than oxLDL in human ApoB100 transgenic mice [134]. More importantly, blocking TRBV31⁺ T cells by inducing anti-TRBV31 antibodies with peptide of TRBV31 complementarity determining region (CDR) 2 significantly decreased atherosclerosis lesion size by 65% [134]. However, the strategy of vaccination atherosclerosis prone mice with oxLDL in search of autoantigens induces a strong T/B cells immune responses that may not simulate the actual immune responses in atherosclerosis. Therefore, other studies took another strategy by interrogating ApoB100 peptides by generating a polypeptide library covering the complete sequence of ApoB100. The candidate peptides were screened by recognizing plasma antibodies in patients with coronary heart disease and controls [135, 136] or had a high binding affinity with MHC molecules [63, 137]. Then, the authors immunized mice with these peptides to confirm their proatherogenic or atheroprotective effects on atherosclerosis [136-138]. Their data confirmed that ApoB100 peptides immunization could trigger T cell immune responses and regulate plaque progression which may be atherogenic or antiatherogenic [136-138].

For the reasons above, to identify T cell autoantigens in atherosclerosis is still a major challenge as the previous approaches have a principal and conceptual problem: All of them pursue a biased approach by limiting their scope to the prejudgment that the autoantigens should derive from lipoproteins, i.e. either native

INTRODUCTION

LDL or oxLDL [63, 134-138]. After carefully considering the weaknesses of previous approaches, we decided to use an unbiased approach using technologies developed during the past several years (see below).

1.7. The TCR is an important target to search for autoantigen-specific T cells

As a major part of adaptive immunity to protect from foreign antigens, the proliferation, differentiation, and activation of (antigen-specific) T cells require interaction of MHC-I/II and antigenic peptide epitopes with its specific cognate TCR. TCRs are heterodimers with most T cells expressing an α chain and a β chain while $\gamma\delta$ T cells express γ chain and δ chains. The TCR α gene locus contains a V gene segment, a J gene segment, and a C gene segment, whereas the TCR β gene locus has an additional D segment (**Fig. 1.4A**). T cells develop and mature in the thymus as outlined above (**1.3. T cell development**). During maturation, the TCR α/β chains go through VJ /VDJ recombination events and add or delete nucleotides at the junctions between gene segments (**Fig. 1.4B**), which results in the diversity of theoretically $>10^{15}$ individual T cell clones comprising the unique TCR repertoire of an individual [139]. TCR α and β chains possess three hypervariable regions termed CDRs, including CDR1, CDR2 and CDR3. Among these regions, CDR3 is the most hypervariable region, and it is responsible for recognizing antigen peptides while CDR1 and CDR2 also contribute to binding of the TCR to MHC molecules. The CDR3 region of the β chain was thought to exert a dominant role in recognizing peptides [140]. Diseases can affect the TCR repertoires by inducing antigen-driven differential clonotype proliferation after encounter with disease-related antigens [141]. Therefore, analyses of TCR repertoires in distinct diseases can help to gain a better understanding of the immune system under distinct conditions and the progression of diseases, in particular those with unknown antigenic triggers [142, 143]. Scientists have discussed that the library of peptides that can bind to the MHC molecules may be larger than the total TCR diversity indicating cross-reactivity of single T cells to several peptide presented by MHC molecules [144, 145]. T cell

INTRODUCTION

cross-reactivity enables the immune system to cover more foreign antigens with fewer TCRs and makes it more difficult for foreign antigens to escape immune surveillance [145]. However, the property of T cell cross-reactivity also increases the possibility to react to self-peptides, which may bring about a risk to develop detrimental autoimmune diseases. TCRs that recognize distinct peptides with structural similarity has been reported in several studies [145-147].

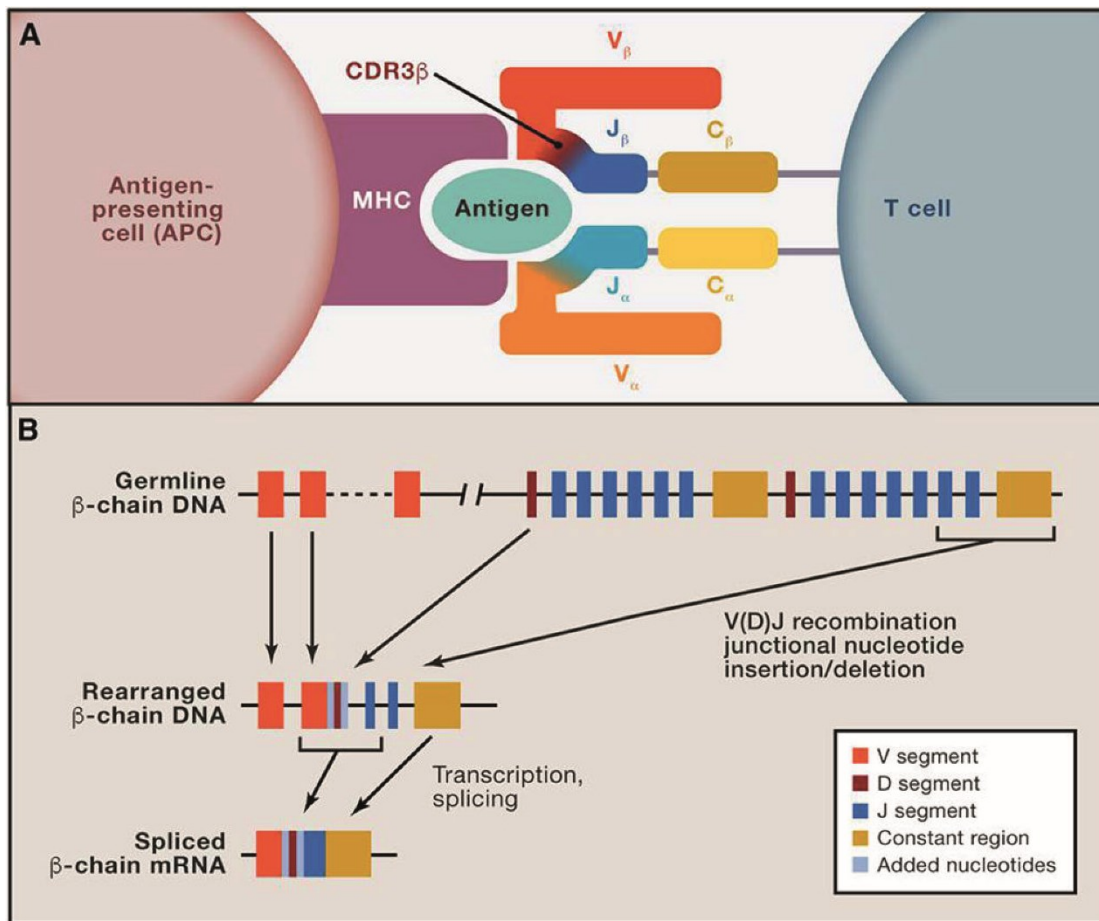


Fig. 1.4 TCR structure and TCR arrangement (cited from Liu. et al. [148]). A. Any given TCR recognizing a peptide/MHC complex is the first requirement for antigen-specific T cell activation. The CDR3 region of each TCR play dominant roles in antigen recognition. **B.** V(D)J recombination and transcriptional processing of a TCR- β subunit chain.

1.8. scRNA-seq as a tool to explore TCR repertoires and T cell immune responses in atherosclerosis

High throughput next-generation sequencing technology has significantly promoted the research in genomics, transcriptomics and epigenomics. However, it was limited

INTRODUCTION

to decipher the differences at the single cell level. Single cell sequencing technology, which was first reported in 2009, has become a powerful tool to explore the gene expression profile of individual cells, uncover complex and rare cell populations and track the trajectories of cell development [149, 150]. Several groups have applied the single cell sequencing technology in atherosclerosis. Holger Winkels and his colleagues detected 11 principal leukocyte clusters in the aorta of *Ldlr*^{-/-} and *ApoE*^{-/-} mice. The associated protein-based mass cytometry method showed a high correlation with the single cell sequencing transcriptionally defined cell clusters. Their results also indicated the variance of the cell percentages among different mouse strains and dietary conditions [151]. At the same time, Cochain et al. explored the landscape and heterogeneity of myeloid cells in the diseased aorta [152]. They identified several dendritic cell and macrophage subsets and their phenotypes. Among the macrophage populations, TREM2^{hi} (triggered receptor expressed on myeloid cells 2) macrophages were identified, which also had been reported in neurodegenerative diseases and obesity [153, 154]. Moreover, Fernandez et al. used CITE-seq, i.e. a single cell sequencing method with antibodies to gain quantitative and qualitative information of cell surface proteins, to study the immune cell populations in blood and human atherosclerotic plaques. They found that CD8⁺ T cells were enriched in plaques compared to blood. Importantly, different immune cell gene expression profiles were observed between blood and plaque indicating tissue-specific activation and differentiation pathways. More importantly, they discovered that CD69⁺CCR5⁺PD1^{int}CD127⁻CD8⁺ T cell numbers correlated with TCR clonality in human plaques suggesting that T cell clonal expansion takes place in plaques [40]. Recently, Chowdhury et al. applied the scRNA-seq to interrogate the T cell immune responses in different stages of human coronary plaques. They found that clonal expansion of T cells was more prominent in CD8 memory T cells and TCRs from these T cells were found to cross-react to viral and self-antigens [155]. TCR analyses have been used to understand the underlying mechanisms of protective vs pathogenic T cell responses in many autoimmune diseases. These studies helped to identify disease-specific autoantigens, such as in type 1 diabetes (i.e. insulin,

INTRODUCTION

glutamic acid decarboxylase 65 [156], zinc transporter-8 [157], chromogranin A [157]), multiple sclerosis (i.e. myelin basic protein, proteolipid protein, myelin-associated glycoprotein [158]), psoriasis (i.e. ADAMTSL5, cathelicidin) and rheumatoid arthritis (i.e. anti-citrullinated protein antibodies, N-acetylglucosamine-6-sulfatase and filamin A) [159-161]. To analyze the TCR repertoire, previous studies used CDR3 spectratyping, a technology that uses capillary electrophoresis to analyze the CDR3 fragment only by the degree of skewing and oligoclonality. However, this method provided rather limited information and cannot provide the exact sequences of clones [162]. 5' rapid amplification of cDNA ends (5'RACE) and multiplex PCR of single cell cloning provide opportunities to identify the paired $\alpha\beta$ chains of autoreactive T/B cells at the single cell level to understand the relationship of immune reactions and disease [163-165], but the method is not efficient and labor-intensive. The advances of bulk next generation sequencing have dramatically improved the technology to provide numerous types of information on the TCR repertoire in a very short time in large numbers of cells. Nevertheless, it is also limited because we cannot get the paired $\alpha\beta$ chains information and correlate this information with the transcriptome at the single cell level. scRNA-seq not only defines transcriptomes of T and B lymphocytes or any other cells, but it can also establish the paired TCRs or B cell receptors of that identical cell. For these reasons, we chose a pairing approach of scRNA-seq and scTCR-seq to investigate tolerance mechanisms in atherosclerosis. It allows us to comprehensively define the T lymphocyte landscape and identify the TCR repertoires at the diseased tissues simultaneously at the single cell level. The 10x Genomics technology employs a gel bead-in-emulsion partition method to obtain single cell compartments. In appropriate cell loading numbers, most gel bead-in-emulsions contain one cell, one cell-specific barcode and the components for reverse transcription reaction. For 5' end gene expression and TCR V(D)J sequencing, the poly(dT) reverse transcription primer was used to obtain the complementary DNA (cDNA). Upon reaching the 5' end of the RNA template, reverse transcriptase adds several additional nucleotides (deoxycytidine) to the 3' end of the newly formed first-strand cDNA. The additional

INTRODUCTION

deoxycytidine serves as a template switching oligonucleotide binding site when the unique template oligonucleotide (having riboguanosines at its 3' end) specifically binds to the deoxycytidine sequence. The template switch oligo primer consists of a barcode, a unique molecular identifier (UMI) and a template switch oligo. The template switch reaction will make sure template strands switch from the cellular RNA to the unique template switching oligonucleotide, which contains a cell barcode for distinguishing cells and UMI for calculating mRNA copy numbers. TCR enrichment is also required to amplify cDNA of the full length of TCR with primers of constant regions of α , β chains and a universal forward primer. By integrating the TCR repertoire and gene expression profile, Huang et al. studied the differences between conventional CD8⁺ T cells, mucosal-associated invariant T cells and invariant natural killer T cells (NKT), in response to *Mycobacterium tuberculosis* [166].

1.9. Aims of the project

As a chronic inflammatory disease, complex T cell responses have been documented to be implicated in all stages of atherosclerosis. During long-lasting inflammation, new/autoantigens may be generated, processed, and presented by APCs to T cells, which results in the antigen-specific T cell immune responses. T cells escape central and peripheral tolerance and specifically recognize new/auto antigens could lead to T cell clonal expansion. T cell immune responses in diseases are controlled by several T cell immune tolerance checkpoints. Although many exciting results have been acquired in atherosclerosis, there are many critical questions are still needed to be addressed, i.e. (i) whether atherosclerosis is driven by aberrant chronic inflammation without antigen-specific T cells engaging or whether the antigen-specific T cell immune responses significantly regulate the progression of atherosclerosis; (ii) the immune tolerance in atherosclerosis remains to be understood; (iii) the differences of T cell immune responses carried out in ATLOs, SLOs and the circulation when compared to atherosclerotic plaques?

INTRODUCTION

Meanwhile, previous studies were limited to single cell types or cytokines limiting the depth of understanding of the overall blueprint of immune responses in atherosclerosis. At the core of our studies is the question whether atherosclerosis is associated and affected by autoimmune T cells. These issues are of central importance to understand the pathogenesis of atherosclerosis and the answers will determine future strategies for developing new therapeutics to treat atherosclerosis. For the present work we aim to make a first step to define atherosclerosis as a bona fide autoimmune T cell disease. To figure out these questions, a combination of gene transcriptome and TCR sequencing at single cell level are applied in our study to establish the T cell landscape in plaque lesions, ATLOs, SLOs and the peripheral circulation of aged WT and ApoE^{-/-} mice.

2. MATERIALS AND METHODS

2.1. Mice

Male ApoE^{-/-} mice on the C57BL/6 background were bred and housed in the specific pathogen-free animal facility of Munich University with a 12 h light/dark cycle. Mice used in this project were more than 78 weeks old, fed on a normal chow diet and without external interferences during the experiments. Male C57BL/6 mice (wild-type, WT mice) raised under the same conditions were used as the control group. The animal procedures were approved by the Regierung Oberbayern according to the guidelines of the local Animal Use and Care Committee and the National Animal Welfare Laws.

2.2. Solutions

Table 2.1 List of standard solutions and buffers

Solution	Composition	Storage
Phosphate buffered saline (PBS) (10x stock solution)	80 g NaCl, 2 g KCl, 27 g Na ₂ HPO ₄ ·7H ₂ O, 2.4 g KH ₂ PO ₄ into 800 ml ddH ₂ O, then, adjust the pH to 7.4, add ddH ₂ O to 1000 ml	Room temperature (RT)
PBS (1x)	Dilute the 10x PBS into 1x with ddH ₂ O	RT
Ethylenediaminetetraacetic acid (EDTA) solution (50 mM stock solution)	18.61 mg Na ₂ EDTA in 1 L ddH ₂ O, pH 7.3	RT
EDTA buffer (5 mM)	Dilute the 50 mM EDTA stock solution into 5 mM with ddH ₂ O	RT
Ammonium-chloride-potassium lysis buffer	0.15 mM NH ₄ Cl, 1 mM KHCO ₃ , 0.1 mM Na ₂ EDTA, adjust to pH 7.3	RT
FACS buffer	PBS with 2% fetal calf serum	Freshly prepared and kept on ice

MATERIALS AND METHODS

4% paraformaldehyde	Dissolve 40 g paraformaldehyde in PBS (1000 ml final), pH 7.2-7.4	4° C
---------------------	---	------

2.3. Antibodies

Table 2.2 List of antibodies for FACS sorting

Antibody	Clone	Format	Dilution	Company
FVD	/	V500	1:1000	eBioscience
CD45	30-F11	Perce-cy5.5	1:200	BD biosciences

Table 2.3 List of primary antibodies for immunofluorescence staining

Antibody	Clone	Host	Dilution	Company
CD3e	145-2C11	hamster	1:100	BD PharMingen
ER-TR7	T-2109	rat	1:100	BMA Biomedicals

Table 2.4 List of secondary antibodies for immunofluorescence staining

Antibody	Host	Against	Clone	Format	Dilution	Company
SMA	mouse	mouse	1A4	Cy3	1:400	Sigma-Aldrich
/	donkey	rat	/	Cy5	1:200	dianova
/	goat	hamster	/	A488	1:200	dianova
/	/	/	/	DAPI	1:500	eBioscience

2.4. Enzyme cocktail

The enzyme cocktail stock solution was prepared according to our previous experiment [167]. The concentration of each component was shown as follows:

Components	Final concentration	Company
Collagenase type I	400 U/ml	Sigma-Aldrich
Collagenase type XI	120 U/ml	Sigma-Aldrich
DNase I	60 U/ml	Sigma-Aldrich
Hyaluronidase	60 U/ml	Sigma-Aldrich
HEPES	20 mM	Sigma-Aldrich
Dulbecco's PBS	1x	Gibco

The enzyme digestion stock solution was kept at -20° C. Dulbecco's PBS was used to dilute the enzyme solution at a 1:5 ratio, then kept on ice for the subsequent

MATERIALS AND METHODS

digestion.

2.5. Equipment

Table 2.5 List of equipment

Equipment	Type	company
General Stereo microscope	S8 APO	Leica
Incubator shaker	Innova 4230	New Brunswick Scientific
Centrifuge	Megafuge 40R	Thermo Scientific
FACS sorter	BD FACSAria™ III	BD Bioscience
Automated cell counter	TC20™	Bio-rad
10x genomics Chromium controller	/	10x genomics
Sequencer	NextSeq 500	Illumina
Computer	Linux system, minimum with 8+ cores, 64GB RAM	DELL
Computer	windows system, 64-bit operating system	Lenovo

2.6. R packages and other software

- R (version 4.0.3, <https://www.r-project.org/>).
- RStudio (version 3.6.0, <https://rstudio.com/>).
- Cell Ranger (version 3.1.0, <https://www.10xgenomics.com/>. Note: run in Linux system).
- Seurat package (version 3.0).
- clusterProfiler package (version 3.12.0).
- Phyllentropy package (version 0.4.0).
- edgeR package (version 3.26.8).
- vegan package (version 2.5-6).
- circlize package (version 0.4.11).

MATERIALS AND METHODS

- ggplot2 (version 3.3.3).
- biomaRt (version 2.46.0).
- msigdb (version 7.2.1).
- dplyr (version 1.0.2).
- fifer (version 1.1).
- PMCMRplus (version 1.9.3).
- tidyr (version 1.1.2).
- CellPhoneDB (version 2.0, Note: run in Python under Linux system).
- UCell (version 1.1.0).
- Metascape (<https://metascape.org/gp/index.html#/main/step1>).

2.7. Methods

2.7.1. Plaque, ATLO and RLN collection and CD45⁺ cell isolation

Mice were euthanized by intraperitoneal injection of ketamine hydrochloride (Medistar) and xylazine hydrochloride (Pharma partner). After anesthesia, the mouse was placed in the supine position and fixed on the foam plate. Mouse was sprayed with 75% ethanol on the abdominal fur. Blood was collected by cardiac puncture using a 1 ml syringe. The blood samples were mixed with 5 ml 5 mM EDTA gently to avoid blood coagulation. Perfusion was performed from the left ventricle with 10 ml 5 mM EDTA buffer, 20 ml PBS and 20 ml FACS buffer, respectively, to remove the residual blood from the circulation. After removing other tissues, the adipose tissue surrounding the RLNs was carefully removed and the RLNs were collected under a light microscope. The method to collect the plaques and ATLOs was described in previous studies by our group [167, 168]. In short, adipose tissue and LNs close to the aorta were carefully removed. The whole aorta including ascending aorta, aortic arch and descending aorta was collected in a cell culture dish with pre-cooled FACS buffer. The aorta was cut in the longitudinal direction and the plaques were carefully collected using curved forceps under a light microscope. The remaining aorta was collected and regarded as ATLOs. 3 aged ApoE^{-/-} mice and 3 aged WT mice were used to collect RLNs and for ApoE^{-/-} mice ATLOs and plaques. Samples were pooled

MATERIALS AND METHODS

for each genotype mouse group for further preparation of single cell suspensions. Blood samples were pooled from 5 ApoE^{-/-} mice and 5 WT mice, respectively.

The method to prepare single cell suspensions for single cell sequencing and to construct the libraries have been fully described in our publication [168]. The pre-processing steps were conducted according to different sample properties. Blood samples were first centrifuged at 4° C 400 X g for 5 mins and the supernatant was discarded, then 8 ml ammonium-chloride-potassium lysis buffer was added to lysate the red blood cells at RT for 8 mins. ATLO and plaque samples were cut into small pieces and digested with enzyme cocktail (400 U/ml collagenase type I, 10 U/ml collagenase type XI, 60 U/ml hyaluronidase, 60 U/ml DNase I, and 20 mM HEPES in Dulbecco's PBS) for 40 mins at 37° C with slow shaking. The digested cell suspensions were filtered through a 100 µm strainer and rinsed with 5 ml pre-cooled FACS buffer. RLNs were cut into small pieces and mashed on the 100 µm strainer with the plunger of 5 ml syringe, then rinsed with 5 ml pre-cooled FACS buffer. Following two times centrifugation and resuspension, cells of each tissue were stained with fixable viability dye (FVD V500, 1:1000) in PBS at 4° C for 20 mins. After two times washing, cells were stained with CD45 (Percp-cy5.5, 1:200) and incubated at 4° C for 25 mins. Cells were used to sort the CD45⁺ live cells with FACS sorter (BD FACSAria™ III) after twice washing.

2.7.2. Library preparation

The single cell suspensions of CD45⁺ live cells were first used to calculate cell density and the rate of the live cells by an automated cell counter (Bio-rad). The corresponding aliquots of the cell suspension were used to generate gel beads-in-emulsions using the 10x Genomics Chromium controller. Following reverse transcription and cDNA amplification, 5' gene expression libraries and (or) TCR V(D)J library preparations for each sample were performed strictly following the protocol of corresponding kits. Libraries were sequenced with the NextSeq 500 or NovaSeq 6000 platforms (Illumina). Sequencing was performed in an asymmetrical manner: read 1 was adjusted to 26 bp, read 2 to 98 bp and the index 1 to 8 bp. TCR

MATERIALS AND METHODS

libraries together with 1% PHiX control library spike-in were sequenced in a symmetrical manner (150+150 bp pair-end).

2.7.3. Single cell sequencing data analysis

The sequencing raw base call files were demultiplexed to fastq files by running 'cellranger mkfastq' command with Cell Ranger (version 3.1.0) on the Linux system computer (Intel(R) Xeon(R) E5-1650 v3 processor, cores: 6, threads: 12) (**Fig. 2.1**). For the 5' gene expression sequencing data, reads were aligned to mouse mm10 reference transcriptome using STAR aligner in the 'cellranger count' command. For the V(D)J libraries, reads were aligned to the GRCm38-3.1.0 reference transcriptome using the 'cellranger vdj' command to perform sequence assembly and paired clonotype calling in Cell Ranger. The output raw barcodes, features, and matrix files after running Cell Ranger were loaded into RStudio (version 3.6.0) and processed with the Seurat (version 3.0) package according to published reports [151, 152].

Cells with less than 200 genes and genes detected in less than 3 cells were removed. Low quality and doublet cells were filtered out by limiting the percentage of mitochondrial genes and the number of detected genes of each cell, respectively. For blood samples, we removed cells with > 3000 detected genes and > 10% of mitochondrial genes (**Fig. 2.1**). For RLN, ATLO and plaque samples, we filtered out cells containing > 8% mitochondrial genes and cells with > 4000 genes in RLNs and ATLOs, but > 5000 in plaques (**Fig. 2.1**). After filtering, data were normalized, and log transformed to remove the confounding of different sequence depths (**Fig. 2.1**). Then, 2000 highly variable genes among cells, which exhibit high cell-to-cell variation, were used to perform principal component analysis (**Fig. 2.1**). Following data integration for integrating analysis, data were scaled to get rid of the effect of highly expressed genes. Principal component analysis was used for dimension reduction. Principal component analysis is an algorithm that generalizes the 2000 highly variable genes into several features (namely principal components, PCs), which represent the combination of information from the variable gene sets. For cell

MATERIALS AND METHODS

clustering and visualization, different values were used to cluster cells in different samples. In blood samples, the top 20 significant PCs were used for t-distribution stochastic neighbor embedding (tSNE) visualization and the top 20 significant PCs were used to construct shared nearest neighbor (SNN) graphs. Cells were identified using the SNN graph with a resolution at 0.5. For RLNs, ATLOs and plaques, the top 10 significant PCs were used for tSNE visualization and top 10 significant PCs were used to construct SNN graphs. Cells were clustered with a resolution at 1. Cell clusters were defined based on each specific markers, such as *Cd3e* for T cells, *Cd19*, *Cd79a* for B cells, *Cd68*, *Flt3*, and *Itgam* for myeloid cells. For the downstream re-clustering analyses of T and myeloid cells, we extracted T and myeloid cell clusters, separately. For T cell analysis, we used the top 15 PCs to construct SNN graphs. Cells were clustered with a resolution at 0.7, and the top 11 PCs were used to visualize tSNE plots. For myeloid cell analyses, the top 10 PCs were used to construct SNN graphs. Cells were clustered with a resolution at 0.5, and the top 10 PCs were used to visualize tSNE plots (**Fig. 2.1**). Differentially expressed genes (DEGs) were calculated by 'FindMarkers' or 'FindAllMarkers' function in Seurat, genes with fold change (FC) > 0.25 and adjusted $p < 0.05$ were considered as significant DEGs. Significant DEGs of each cluster were used to conduct pathway analysis by using the on-line website: metascape (<http://metascape.org/gp/index.html#/main/step1>) with default setting [169].

MATERIALS AND METHODS

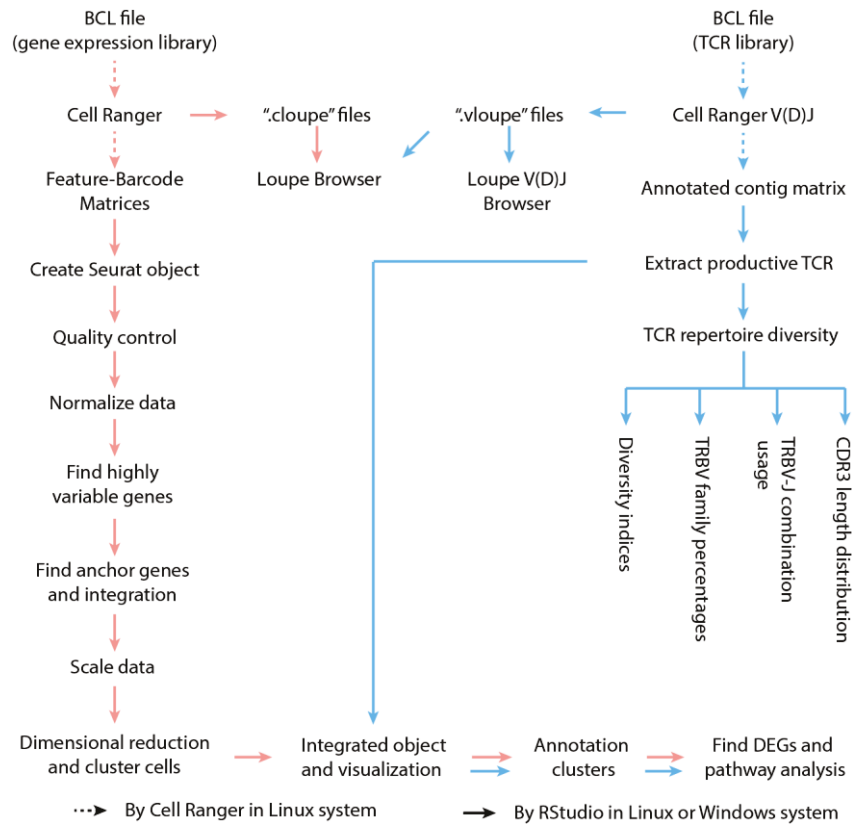


Fig. 2.1 Basic workflow for integrated analyses of scRNA-seq and scTCR-seq data. The pink arrows represent the scRNA-seq analysis workflow. The light blue arrows designate the process of scTCR-seq analysis.

For plaque-inducible gene expression analyses, cells with identical TCRs but located in two or three tissues were used for analyses. With these criteria, 81 CD8 T_{eff/mem} cells were included, including 28 CD8 T_{eff/mem} cells in plaques, 27 CD8 T_{eff/mem} cells in ATLOs, and 26 CD8 T_{eff/mem} cells in RLNs of aged ApoE^{-/-} mice. DEGs between cells in plaques and cells in ATLOs/RLNs were identified by Wilcoxon rank sum test in the Seurat package.

The antigen presentation module score of each myeloid cell in different clusters was calculated by the ‘AddModuleScore_UCell’ function in UCell (version 1.1.0). The genes used to calculate the antigen presentation score have been used to analyze the antigen presentation function of DCs as described [170]. To calculate the expression of co-inhibitory molecules in myeloid cells, we also took the myeloid cell percentages into consideration, which reflect the contribution of myeloid cells in each tissue to induce T cell immune tolerance. First, the average expression of each gene

MATERIALS AND METHODS

in each tissue was calculated, then multiplied by the corresponding coefficient of each tissue (WT RLNs: 4.63, ApoE^{-/-} RLNs: 4.33, ATLOs: 24.42, plaques: 61.82), which correlate to their richness in each tissue.

2.7.4. T cell clonal expansion and TCR repertoire analysis

Single cell TCR data were extracted from the outputs after running single cell 5' V(D)J library sequencing data with the Cell Ranger 'cellranger vdj' pipeline (**Fig. 2.1**). The reconstructed TCR contigs were selected by limiting to productive TCR α and β chains and cell barcode match to a unique cell barcode in 5' gene expression sequencing data. Clonally expanded T cells were considered as at least two cells have identical V family and CDR3 region of paired $\alpha\beta$ chains. Cells without detected TCRs were considered as TCR non-detected T cells. Cells with unique paired $\alpha\beta$ chains or with single α or β chains were categorized as non-expanded T cells. The productive TCR information was integrated into the metadata of 5' gene expression sequencing Seurat object by the unique cell barcode between these two libraries (**Fig. 2.1**). Productive TCRs with cell barcodes filtered out in the quality control (QC) steps of 5' gene expression sequencing analysis were also removed. TRBV family percentages were calculated as: count of each individual TRBV family / the total count of TRBV families \times 100% (**Fig. 2.1**). The percentage of each CDR3 length was calculated as: frequency of each CDR3 length / the total frequency of all CDR3 length \times 100% (**Fig. 2.1**). The cosine similarity of CDR3 aa regions between two tissues was calculated by the lsa (Latent semantic analysis, version v0.63-1) package, and only the cells with paired $\alpha\beta$ chains were used for analyses. TRBV-J combination usage and the CDR3 overlap were plotted with the Circlize package based on the percentage of each TRB VJ family and the number of each CDR3 clone, respectively (**Fig. 2.1**). To compare the TCR diversity of each sample, only the cells with paired $\alpha\beta$ chains were included in the analyses (**Fig. 2.1**). In consideration of the different sample depths, resampling can eliminate different sample depth-induced errors. Therefore, all sample depths were reduced to 95% of the one with the lowest read counts for calculating TCR repertoire diversity. Plaques contain the

MATERIALS AND METHODS

lowest read counts in our study. All the sample sizes were randomly reduced to 161 cells with paired $\alpha\beta$ chains. Then the Shannon entropy, Gini index and inverse Simpson diversity index were calculated by phylentrophy (version 0.4.0, function: $H(x)$), edgeR (version 3.26.8, function: $\text{gini}(x)$) and vegan (version 2.5-6, function: $\text{diversity}(x, \text{"invsimpson"})$) packages, respectively. To get more valid data, the randomly down-sample processes were repeated 1000 times.

2.7.5. Cell-cell interaction analysis

Cell-cell interaction was performed with CellPhoneDB (version 2.0), a python package as reported [171]. The mouse genes were first converted into human genes by the 'getLDS()' function in biomaRt (version 2.46.3) package. Genes could not convert to human genes were excluded for downstream analyses. The count data (gene expression) and meta data (cell type) were used for interaction analyses. These analyses were performed in Linux system computer. The number of iterations were set as 1000 for statistical analysis, other parameters were used the default values. Successfully running will get four files: means.csv, significant means.csv, pvalues.csv and deconvoluted.csv. The "means.csv" file contains mean values for each ligand-receptor interaction. The "deconvoluted.csv" file gives additional information for each of the interacting partners. The "significant means.csv" and "pvalues.csv" files are used to explore significant interactions. The ligand-receptor interaction with a p value more than 0.05 was filtered and not used. The interaction events of each T cell or myeloid cell cluster were also summarized. The igraph package (version 1.2.6) was then used to display the network interactions among different cell clusters of each tissue. In the network plot of each tissue, the different color represents different cell type. The size of the circle designates the magnitude of interaction events of each cell type, and the thickness of ribbons which connect two different cell types indicate the interaction events between these two cell types.

The enrichment interaction of each cell type was also presented by using ggplot2 package (version 3.3.3) to show the detailed interacting pairs among different cell types. Only the significant means were used for plotting. To get a better readable

MATERIALS AND METHODS

graph quality, p values less than 1×10^{-5} were all set as 1×10^{-5} . In the interacting map, the dot size represents the p value and the dot color represents the mean value of each ligand-receptor interaction.

2.7.6. Gene set enrichment analysis (GSEA)

Gene pathway analyses, like Gene Ontology and Kyoto Encyclopedia of Genes and Genomes analysis, were performed by applying the significant DEGs. These approaches omit the functions of genes with small expression differences but have important biological functions in a set of related genes. GSEA has been developed for addressing this disadvantage [172]. The differences of genes calculated by Seurat were selected for GSEA analysis. The symbol gene names were transformed into Entrez gene IDs. Then avg_logFC values and Entrez gene IDs were used for analyses by clusterProfiler (version 3.12.0) package [173]. The different gene sets (hallmark gene sets, curated gene sets and Gene Ontology gene sets) of MSigDb (molecular signatures database) were used for enrichment analysis.

2.7.7. Immunofluorescence staining

Aorta taken from aged ApoE^{-/-} mice (more than 78 weeks) were embedded with Tissue-Tek® OCT cryo embedding compound (Sakura Finetek) on dry ice. Tissue blocks were cut at a thickness of 10 μ m with a Leica CM3050 S cryostat, the sections were kept at -20° C until staining. For immunofluorescence staining, the slides were dried on a 37° C hot plate for 1 min and dried in the air for 30 mins. Slides were then immersed in PBS for 10 mins and blocked with blocking buffer (normal donkey/goat serum was diluted by PBS and the final concentration was 5%) at RT for 1 h. Primary antibodies were prepared with blocking buffer and incubated slides at RT for overnight. After that, secondary antibodies and DAPI were incubated at RT for 1 h. Then slides were mounted with Fluoromount G mounting medium. The expressions of targeted proteins were checked by confocal microscope.

2.7.8. Integration analysis of human and mouse scRNA-seq data

Published human and mouse atherosclerotic plaque scRNA-seq data were

MATERIALS AND METHODS

downloaded from Gene Expression Omnibus (GSE131776, GSE131778, GSE155512, GSE155513). The human atherosclerotic plaques are obtained from carotid arteries (GSE155512) and coronary arteries (GSE131778), respectively. The mouse scRNA-seq data are both obtained from SMC-lineage tracking mice. The mice in the published studies had an ApoE or Ldlr deficiency background and fed with a high fat diet (HFD) for 8-26 weeks. Whole aortas were collected to prepare single cell pellets. Low-quality cells were removed according to filtering criteria of each study [174, 175]. The human genes were converted to mouse genes by using the biomaRt package (version 2.40.5) and the multi-matched converted genes were filtered out.

To perform the integration analysis, Seurat object of each study was first set up. Immune cells were then extracted based on immune cell markers. Re-clustering was performed in each study to distinguish T cells and myeloid cells from total immune cells. For the re-clustering analyses, the first 20 PCs were used for tSNE visualization. 20 PCs were used as input to construct SNN graph. Clusters were identified in these four published datasets by using the SNN graph with a resolution parameter of 1.2. Next, T cell and myeloid cell populations extracted from each dataset will be integrated, separately. For T cell and myeloid cell integration analyses, the top 20 PCs were used to construct the SNN graph and top 20 PCs were used for visualization. Resolution values were set to 1 to cluster cells, respectively. Cells with multiple immune cell lineage markers were regarded as doublets and were removed. Then, we reran these steps with a lower dimension and resolution values (11, 11, 1.2 and 12, 12, 0.6) for T cell and myeloid cell clustering, respectively. The subclusters were named based on corresponding canonical T cell and myeloid cell markers. Each cluster percentage was calculated and samples with a low number of total T cells (GSE131776 and patient 4 in GSE131778) were not presented in the column figures.

Due to the specific study design in mice of GSE131776 and GSE155513, in which cells were sorted based on SMC-derived or not. In these studies, monocyte-derived macrophage and SMC-derived macrophage were separated into two samples, and

MATERIALS AND METHODS

their respective percentages could not be compared to the total macrophages in plaques. Therefore, we only included the human study and our mouse study in the data presentation. To compare the gene expression similarities between murine plaque T cells and human plaque T cells, the correlation of different T cells between murine and human plaques were calculated. The top 50 DEGs of each five major phenotypes in our own data were first selected and genes expressed in both mouse and human studies were kept, which results in 197 unique genes. Then, the average expression of five major T cell phenotypes were calculated by using the 'AverageExpression' function in Seurat. As a negative control, the total myeloid cells of each tissue were also included for analysis. Spearman correlations were calculated among different T cell phenotypes and species after $\log_2(1 + \text{average expression})$ transformation of average expression values [176]. The pheatmap package (version 1.0.12) was used to generate correlation heatmaps among different samples.

2.7.9. Statistical analyses

The Shapiro-Wilk test was first used to assess the data distribution ('shapiro.test' function in R). Data that did not follow normal distribution were analyzed by the non-parametric method. Comparisons between two groups were performed by Wilcoxon rank sum test ('wilcox.test' function in R). Comparisons in multiple groups were made by using Kruskal–Wallis rank sum test ('kruskal.test' function in R). Dunn's non-parametric all-pairs comparison test was used to calculate the differences between each of two groups ('kwAllPairsDunnTest' function in PMCMRplus package). For categorical data, differences were compared using chi-square test between two groups ('chisq.test' function in R). Chi-square post hoc test was used to compare differences in multiple groups ('chisq.post.hoc' function in fifer package). P values were adjusted by Benjamini Hochberg correction.

3. RESULTS

3.1 Pre-processing of scRNA-seq and scTCR-seq analysis

scRNA-seq was employed to simultaneously obtain the transcriptomic profile and TCR from each individual T cell. Aged ApoE^{-/-} mice form advanced atherosclerotic plaques and ATLOs allowing us to simultaneously study T cell immune responses in plaques, ATLOs, aorta-draining lymph nodes (that is RLNs in our study), and the circulation. To construct the T cell atlas and TCR repertoire, we collected total live CD45⁺ leukocytes of plaques, ATLOs and RLNs from three aged ApoE^{-/-} mice (more than 78 weeks). As controls, total live CD45⁺ leukocytes of RLNs from three aged C57BL/6 mice (more than 78 weeks) were also collected and blood immune cells were also examined. The droplet-based single cell technology (Chromium platform, 10x Genomics) allows to obtain the transcriptome of 1,000 – 10,000 single cells per sample. To obtain both the transcriptome and TCR sequences from a single cell, the 5' gene expression library and TCR V(D)J library were constructed simultaneously and sequenced separately by next generation sequencing (**Fig. 3.1**). Data were combined and analyzed to evaluate the change of tolerance checkpoints in atherosclerosis. Five checkpoints are defined as follows: checkpoint 1: maintenance of quiescence of naïve T cells; checkpoint 2: promotion of T_{eff/mem} cell-related transcripts; checkpoint 3: preservation of immunosuppression of T_{reg} cells; checkpoint 4: APC interaction to mediate T cell activation or suppression; checkpoint 5: tissue homeostasis to control T cell function.

RESULTS

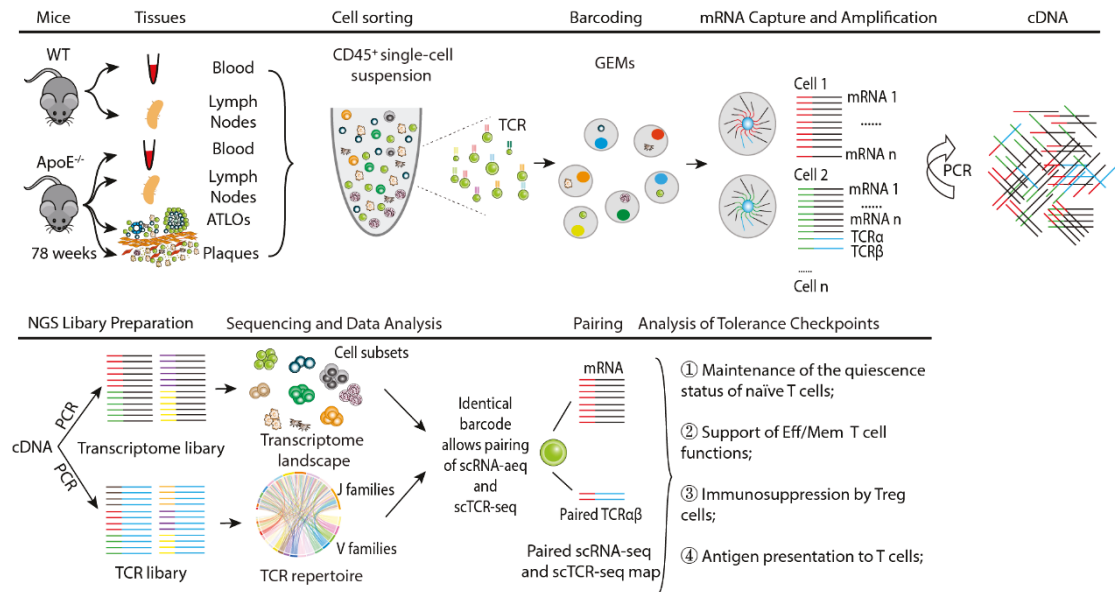


Fig. 3.1 Schematic of the single cell sequencing workflow to identify the transcriptome of immune cells and TCR repertoires. Plaques, ATLOs, RLNs and blood were collected and pooled from three mice per tissue, total live CD45⁺ leukocytes were sorted by flow cytometry. 10x Chromium platform was used to capture the single cell droplet. The 5' gene expression library and TCR V(D)J library were constructed. mRNAs in each single cell were barcoded by unique cell barcode and UMIs, which used to identify the origin and quantify the copy of mRNA molecules. Then the libraries were sequenced and analyzed. The T cell transcriptome and TCR repertoire were combined by using the identical cell barcodes.

To ensure the accuracy of our scRNA-seq data, histological staining was performed to confirm the reliability of our method to separate plaque lesions and ATLOs from the diseased aorta. The results showed that the separated plaque lesions had intact structures and defined edges, while the adventitia closely adhered to the media of remaining aorta (**Fig. 3.2**). Immunofluorescence staining also showed a defined border of plaque lesion with media and scattered T cells in the adventitia (yellow arrows in **Fig. 3.2**). Both results indicated that we were able to separate the atherosclerotic plaques from diseased aorta.

RESULTS

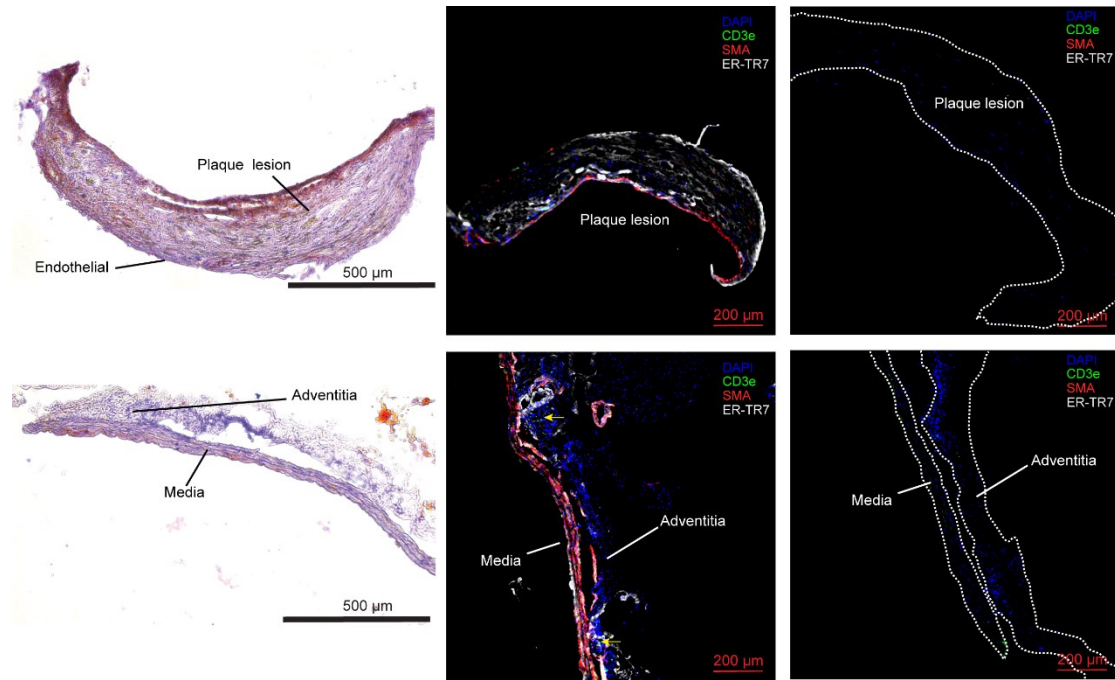


Fig. 3.2 Isolated atherosclerotic plaque (upper panel) from the diseased aorta and the remaining media with adventitia are shown in lower panel. Left panel: tissue sections are stained with Oil red O for lipid (red) and hematoxylin for nuclei (blue). Middle panel: tissue sections are stained with DAPI (blue, nuclei), anti-CD3e (green, T cells), anti-SMA (red, SMCs) and anti-ER-TR7 (white, fibroblast). The yellow arrows represent the CD3e⁺ T cells in the adventitia. Right panel: negative control.

Technical limitations, i.e., dead cells (high levels of mitochondrial mRNA), cell debris (small amount of total mRNA per cell), and duplicate cells (high amount of total mRNA per cell) cannot be avoided during sample preparation. Therefore, data pre-processing QC analysis to remove the low-quality cells and cell duplicates in each sample were conducted by Seurat R package (see below QC criteria in **Fig. 3.3**).

RESULTS

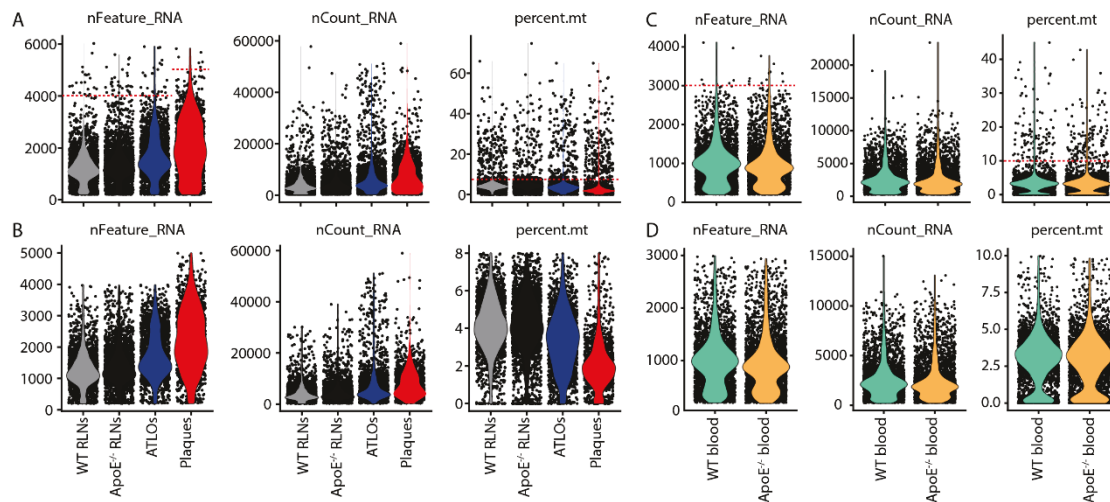


Fig. 3.3 Violin plots to show the QC criteria to remove the low-quality and duplicated leukocytes of each sample. The characterizes of total number of mRNAs detected per cell (nFeature_RNA), total number of reads detected per cell (nCount_RNA) and mitochondrial gene percentage per cell (percent.mt) before (**A, C**) and after (**B, D**) QC in WT RLNs, ApoE^{-/-} RLNs, ATLOs, plaques samples and WT blood, ApoE^{-/-} blood, respectively. By droplet-based single cell transcriptome, each mRNA carries a unique UMI, and each single cell carries a unique cell barcode. Combining the UMI and cell barcodes, we determined the number of cells, and the expression level of each gene. Cells with < 200 of nFeature_RNA were removed. Cells with > 4000 of nFeature_RNA and > 10% of mitochondrial genes were filtered in ATLOs and RLNs. Cells in plaques were filtered with > 5000 of nFeature_RNA and > 10% of mitochondrial transcripts. The red dashed lines indicate the threshold for different QC parameters.

3.2 Hyperlipidemia-associated differences in immune cells of blood between aged WT and ApoE^{-/-} mice

To uncover the immune responses in atherosclerosis, the immune cell landscape was constructed and the cell composition and gene expressions of different immune cells in the circulation were compared. 3361 leukocytes from WT mice peripheral blood and 3770 leukocytes from ApoE^{-/-} mice peripheral blood were obtained (**Fig. 3.4A**). Total immune cells were separated into five clusters by using cell specific markers, i.e., B cells (*Cd19*, *Cd79a*, *Ms4a1*), T cells (*Cd3e*, *Cd4*, *Cd8a*), monocytes/DCs (*Cd68*, *Ly6c2*, *Lyz2*, *S100a4*, *Cd74*, *Flt3*), neutrophils (*S100a8*, *S100a9*, *Malat1*, *Il1b*, *Tyrobp*, *Ccl6*, *Ftl1*) [177] and NK cells (*Klrb1c*) (**Fig. 3.4B**).

RESULTS

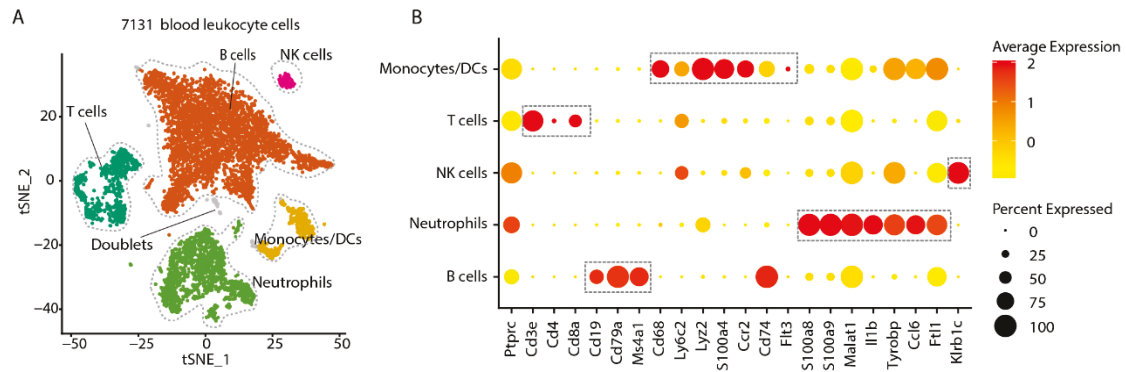


Fig. 3.4 Pooled immune cell map of WT and ApoE^{-/-} mice peripheral blood. A. tSNE plot to show five clusters of blood leukocytes analyzed by scRNA-seq. **B.** Five blood immune cell populations including T cells, B cells, monocytes/DCs, NK cells and neutrophils were defined according to their cell-specific markers.

WT and ApoE^{-/-} blood comprised all five immune cell clusters. ApoE^{-/-} mice blood showed major similarity as cell percentages when compared to WT blood (**Fig. 3.5A**). B cells constitute the majority of leukocytes in peripheral blood (61.2% in aged WT blood and 51.9% in aged ApoE^{-/-} blood). This observation is similar to our previous reports in aged WT and ApoE^{-/-} mice using flow cytometry analysis [122], in which we reported ~53% B cells (CD19⁺ cells/CD45⁺ cells) in WT blood, and ~43% B cells in aged ApoE^{-/-} blood, and there are no statistical differences in B cell percentages between WT blood versus ApoE^{-/-} blood. The difference in the percentage of B cells between our current data and previous data may be caused by different methods used to identify B cells. The FACS method relies on several cellular markers to name cells, whereas scRNA-seq groups cells with similar genes expression into clusters by using algorithms that depends on highly variable genes of transcriptomes. To explore whether hyperlipidemia and/or atherosclerosis causes changes in the transcriptomes in peripheral blood immune cells, the DEGs of different immune cells, including the sub-clusters of T cells and myeloid cells between WT and ApoE^{-/-} blood were compared (the sub-clustered tSNE plots of T cells and myeloid cells are not shown). However, only few DEGs were detected, and similar gene expression profiles of different immune cell populations between WT and ApoE^{-/-} mice peripheral blood were observed (**Fig. 3.5B and C**, the DEGs were listed in the **appendix table 1**). Moreover, these DEGs were not reported to

RESULTS

modulate T cell immune tolerance. These results are consistent with our previous report, which revealed robust age-associated changes in inflammation and immune responses in WT and ApoE^{-/-} mice blood that are independent of hyperlipidemia or atherosclerosis [121]. These data point to the argument that atherosclerosis-specific immune response is not mirrored in blood leukocytes.

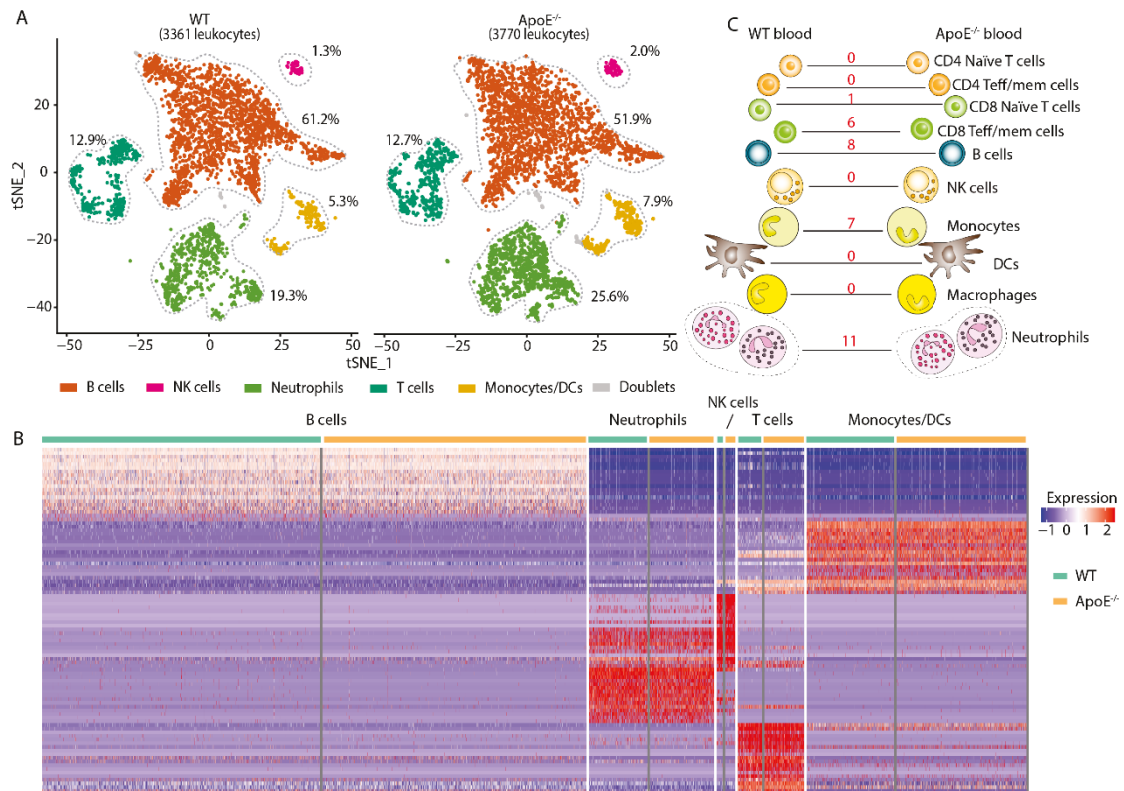


Fig. 3.5 The immune cell composition and transcription differences between WT and ApoE^{-/-} mice blood. **A.** tSNE plot to display the immune cell clusters of WT and ApoE^{-/-} mice, separately. **B.** Schematic diagram to show the number of DEGs of different immune cell clusters between WT and ApoE^{-/-} mice. **C.** Heatmap shows the top 20 DEGs of each immune cell cluster in peripheral blood of WT and ApoE^{-/-} mice (the DEGs were listed in the appendix table 1).

3.3 Transcriptome map of T cells in atherosclerotic plaques, ATLOs, ApoE^{-/-} RLNs and WT RLNs

After QC pre-processing, 3379 T cells were extracted from the total 8992 CD45⁺ leukocytes for further sub-clustering analysis (**Fig. 3.6A**). T cell lineage-, phenotype- and function-specific markers were used to define subsets of T cells: *Cd4* as a marker of helper T cells; *Cd8a* and *Gzmb* for cytotoxic T cells; *Foxp3* for T_{reg} cells; *Ccr7*, a chemokine receptor and *Sell*, a cell surface marker that are both highly

RESULTS

expressed in naïve T cells; CD44 is a marker of T cell activation, the combination of *Sell* (CD62L), *Cd44* and *Ccr7* are widely used to discriminate naïve, T_{cm} and T_{em} cells; killer cell lectin-like receptor subfamily B member 1C (*Klrb1c*) for natural killer T cells; TCR gamma constant region 1 (*Tcrγ-c1*) and TCR delta constant region (*Trdc*) for γδ T cells. Thus, we named 9 T cell subsets as follows: cluster 1, effector T_{reg} cells (eT_{reg}, Cd4⁺Foxp3⁺Cd44⁺*Sell*⁻*Ccr7*^{low}); cluster 2, CD4 T_{em} (CD4 effector memory T cells, Cd4⁺Foxp3⁻Cd44⁺*Sell*⁻*Ccr7*^{low}); cluster 3, CD8 T_{em} (CD8 effector memory T cells, Cd8a⁺Cd44⁺*Sell*⁻*Ccr7*^{low}Gzmb^{high}); cluster 4, CD8 naïve T cells (Cd8a⁺Cd44⁻*Sell*⁺*Ccr7*^{high}); cluster 5, CD8 T_{cm} (CD8 central memory T cells, Cd8a⁺Cd44⁺*Sell*⁺*Ccr7*^{int}); cluster 6, NKT/CD8 T_{cm} (Cd8a⁺Cd44⁺*Sell*⁺*Ccr7*^{int}*Klrb1c*⁺); cluster 7, CD4 naïve T cells (Cd4⁺Cd44⁻*Sell*⁺*Ccr7*^{high}); cluster 8, central T_{reg} cells (cT_{reg}, Cd4⁺Foxp3⁺CD44⁻*Sell*⁺*Ccr7*^{low}); cluster 9, γδ T cells (Cd4⁻Cd8a⁻*Tcrγ-C1*⁺*Trdc*⁺) (**Fig. 3.6B**). Cells in cluster 10 had very low nFeature_RNA and nCount_RNA values, which were considered as low-quality cells that escape from the QC analysis [178]. Cells of cluster 11 showed highly expressed B cell specific markers (*Cd19*, *Cd79a*, *Mas4a1*, data not shown), showing they are mixed T and B cells, indicating the doublet cells. Since the parallel gene expression between short-lived effector T cells (T_{eff}) and long-lived T_{em} cells, T_{eff} cells may also be present in CD4 and CD8 T_{em} cells in our study. Thus, cells of cluster 10 and cluster 11 were excluded from our downstream analysis. Finally, 3262 T cells with well-defined phenotypes were used for further analysis.

RESULTS

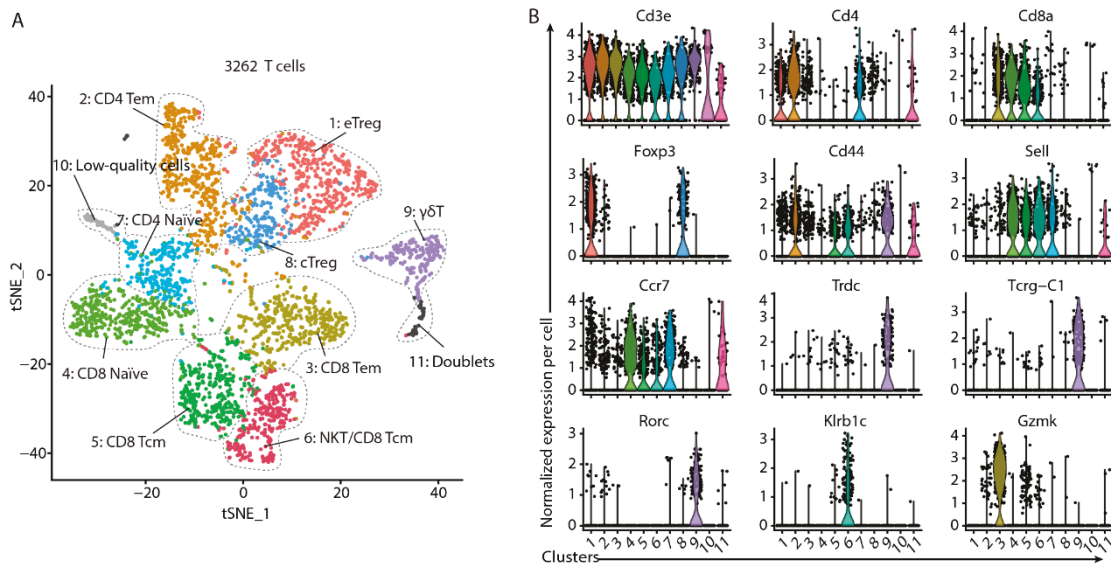


Fig. 3.6 The landscape of T cells in plaques, ATLOs, *ApoE*^{-/-} RLNs and WT RLNs. **A.** 3262 T cells were grouped into 11 sub-clusters in tSNE plot based on top 2000 highly variable genes. **B.** Violin plot to show the markers used to define each T cell cluster.

The heatmap was used to show the top 10 DEGs of each T cell cluster (**Fig. 3.7, appendix table 2**). Cell-specific genes were detected by enrichment signatures in different clusters. eT_{reg} showed a high expression of *Foxp3*, *Ikzf2* (encoding Helios), *Ctla4*, *Cd83*, *Ccr8*, *Trnfsf4* and *Trnfsf9* [179-181]. *Foxp3*, *Ikzf2*, *Izumo1r* were found to be expressed in cT_{reg} cells. Besides the CD8 specific cytotoxicity genes *Gzmk* expressed in CD8 T_{em} and *Gzmm* in CD8 T_{cm}, inflammation-related genes *Ccl5*, *Nkg7* and *Ccl4* were also observed to be significantly enriched in CD8 T_{em} cells and T cell exhaustion-related gene *Eomes* was observed to be highly expressed in CD8 T_{em} cells. CD8 T_{cm} cells revealed high expression levels of *Ccl5*, *Nkg7*, *Ctsw* and killer cell lectin like receptor *Klrd1*, *Klrk1*, *Klrc1* were enriched in CD8 T_{cm} cells. NKT/CD8 T_{cm} cells strongly expressed *Klrb1c*, *Klre1*, *Klrk1*, *Klrc1*, and *Nfkbiz*. $\gamma\delta$ chain-specific genes *Tcrγ-C1*, *Trdc* and *Tmem176b*, *Tmem176a*, *Cd163l1*, *Blk*, which are reported to be highly expressed in $\gamma\delta$ T cells were all exclusively expressed in $\gamma\delta$ T cells [182]. CD4 and CD8 naïve T cells had significant expression of *Igfbp4*, *Lef1*, *Ccr7*, *Tcf7*, and *Sell*, which indicate the naïve phenotype of T cells.

RESULTS

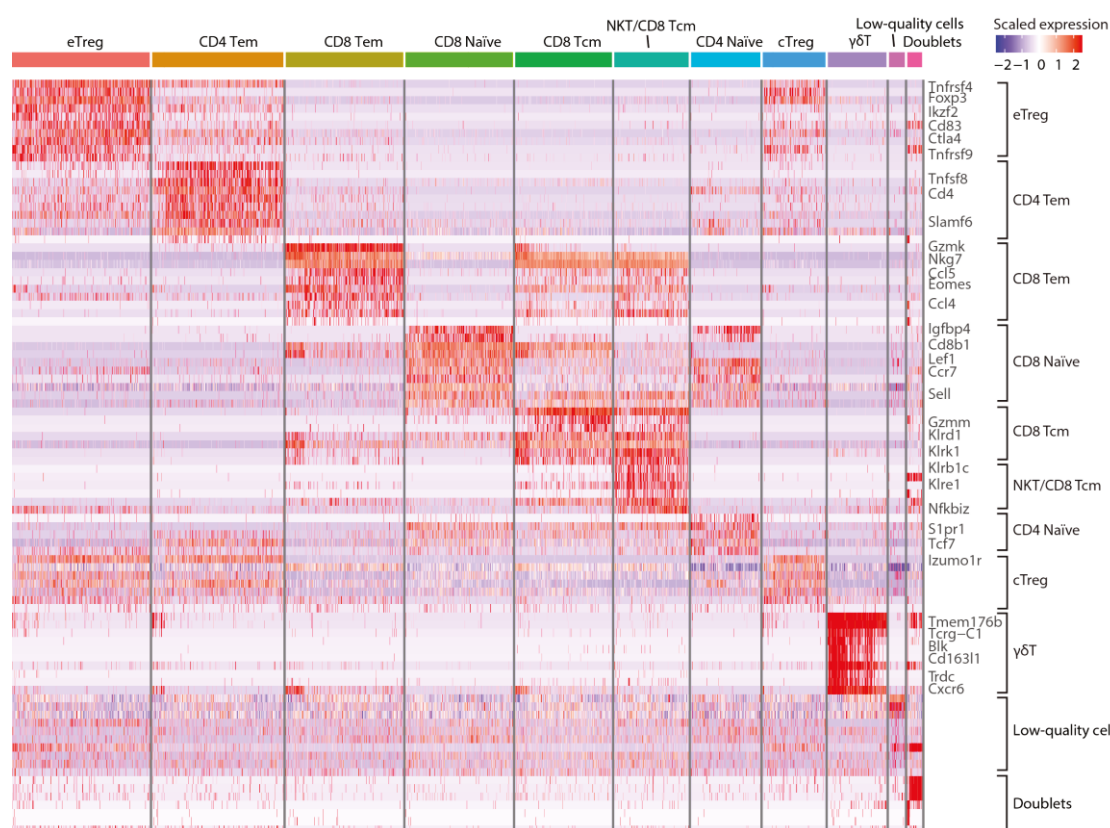


Fig. 3.7 Heatmap to show the top 10 DEGs of each cluster. The width of each cell type correlates with their cell percentage. The color indicates the gene expression level. The red color indicates transcripts highly expressed; the blue indicates genes expressed in cells at low level. Only the representative genes for each cluster are shown.

To further validate our data, pathway enrichment analyses were performed by using DEGs of each T cell cluster. Metascape, an online pathway enrichment tool [169], was used to explore the biological functions of each T cell cluster. To take several T cell clusters as examples, eT_{reg} cells were found to be enriched in transcripts mediating negative regulation of leukocyte activation (**Fig. 3.8A**), which is closely related to the immunosuppressive function of T_{reg} cells. I-kappaB kinase/NF-kappaB signaling and TNF-alpha nuclear factor kappa-light-chain-enhancer of activated B cells (NF-kB) signaling pathway were observed to be enriched in eT_{reg} cells (**Fig. 3.8A**), which are known to play important role in the development of eT_{reg} cells and the maintenance of their immunosuppressive functions [183]. Pathways associated with cell biosynthesis like SRP-dependent cotranslational protein targeting to membrane ribosome assembly, parvulin-associated pre-rRNP complex, and mRNA

RESULTS

processing were significantly enriched in CD8 naïve T cells (**Fig. 3.8B**). The immunoregulatory interactions between a lymphoid and a non-lymphoid cell, T cell activation, and adaptive immune response were found to be enriched in CD8 T_{em} cells (**Fig. 3.8C**). The pathway enrichment analyses further confirmed the phenotype and function of each cluster.

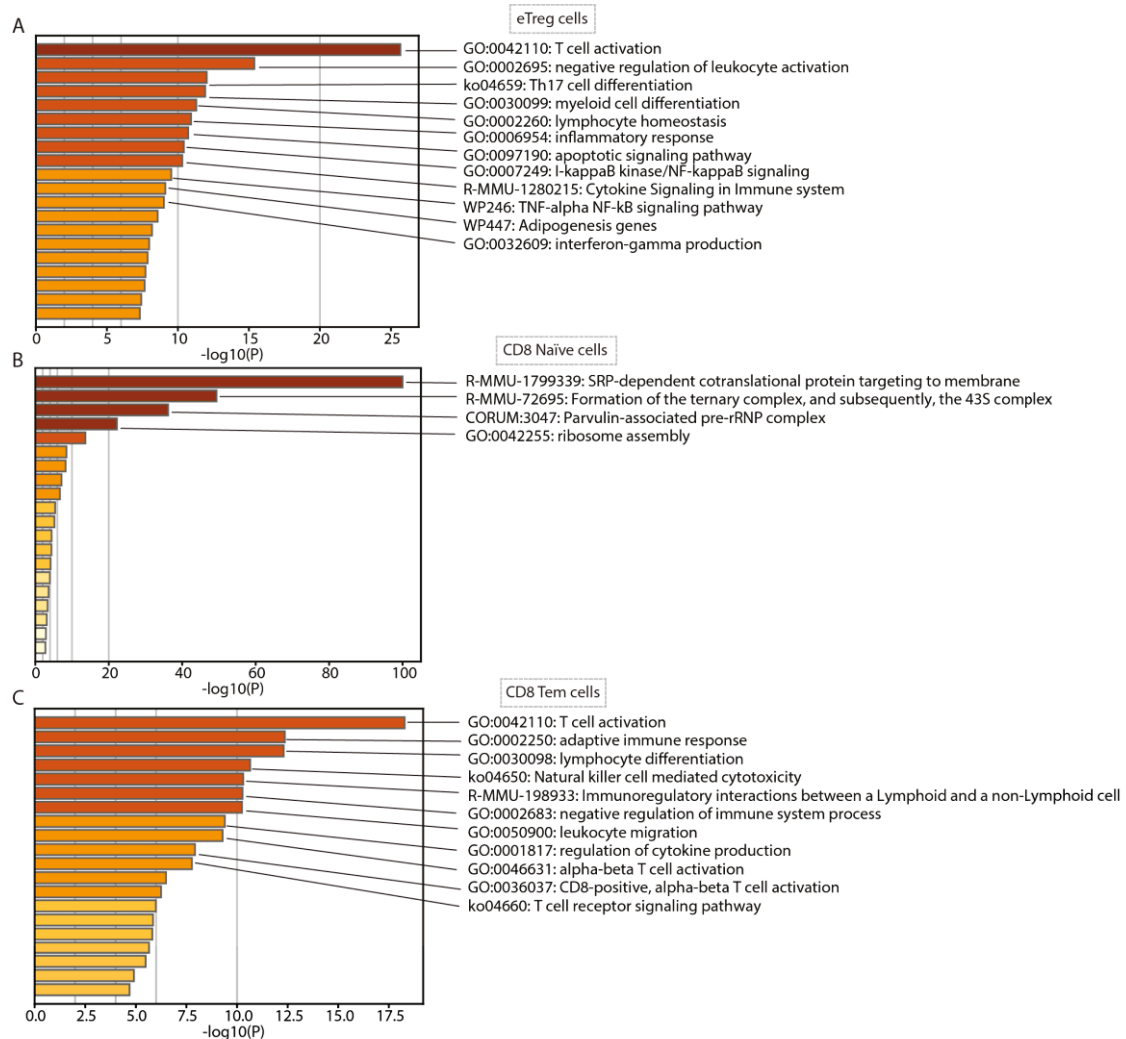


Fig. 3.8 Pathway enrichment to analysis T cell clusters. A. eT_{reg} cells; **B.** CD8 naïve T cells; **C.** CD8 T_{em} cells. DEGs of each cluster were used to perform metaspice pathway enrichment analyses.

Using scRNA-seq, a T cell atlas in atherosclerotic plaques and ATLOs, and SLOs was constructed, which facilitates our understanding of T cell immune responses in atherosclerosis. Total T cells were separated into 9 clusters based on the expression of their top 2000 genes per cell. These T cell subsets all have been reported in mouse models or human patients [95]. Next, transcriptome differences between

RESULTS

different cell types or different tissues were determined.

3.4 Transcriptome map of myeloid cells in atherosclerotic plaques, ATLOs, ApoE^{-/-} RLNs and WT RLNs

Myeloid cells not only participate in the innate immune responses, but as the major APCs, they also play a vital role in regulating adaptive T cell immune responses [184]. To investigate the effect of myeloid cells on T cells in atherosclerosis, the myeloid cell populations in WT RLNs, ApoE^{-/-} RLNs, ATLOs, and plaques were analyzed. Myeloid cells were separated into 8 clusters, including 4 DC populations: CD11b⁺ classical DC (cDC), CD8a⁺ cDC, CD11c⁻ DC, plasmacytoid DC (pDC); 3 macrophage populations: Lyve1⁺ resident-like macrophage (Lyve1⁺ res-like MΦ), Trem2^{high} macrophages (Trem2^{high} MΦ), monocyte/macrophages (Mo/MΦ), and 1 neutrophil population according to lineage-specific markers which have been used in myeloid cell scRNA-seq studies of atherosclerosis by others [152] (**Fig. 3.9A and B, appendix table 3**). Macrophage clusters highly express *Adgre1* (encoding F4/80), *Csf1r*, *Fcgr1*, *Cd74* and *Cd68* (**Fig. 3.9B**). Trem2^{high} MΦ showed a gene signature containing highly expressed *Trem2*, *Cd9*, *Spp1*, *Ctsd*, *Ctsz* and *Hvcn1* (**Fig. 3.9B**). Lyve1⁺ res-like MΦs displayed a resident-like macrophage (*Lyve1*, *F13a1*) and M2-like (*Folr2*, *Cbr2*, and *Mrc1*) phenotype and also expressed high levels of chemokines genes (*Ccl24* and *Ccl9*) (**Fig. 3.9B**). Mo/MΦ cluster in our data had high gene expressions of *Ace*, *Plac8*, *Chil3*, *Ly6c2*, and *Ccr2* as reported [185] (**Fig. 3.9B**). DCs were identified by high expression levels of *Cd68*, *Cd74*, *H2-Eb1*, and *Flt3*, of which, *Flt3* is a key regulator for DC development [186] (**Fig. 3.9B**). DCs can be subdivided into cDCs and pDCs. pDCs can be distinguished from cDCs by their highly expressed genes *Siglech* and *Bst2* (**Fig. 3.9B**). cDCs can be divided into several subclusters including CD8a⁺ cDCs (*Cd8a*⁺*Xcr1*⁺) and CD11b⁺ cDCs (*Cd11b*⁺) (**Fig. 3.9B**). A population of DCs, which didn't express pDC- or cDC-specific markers were observed that we named CD11c⁻ DCs characterized by higher expression of *Ccr7* and *Fscn1* (**Fig. 3.9B**). The neutrophil population had a higher expression of

RESULTS

genes such as *S100a8*, *S100a9*, *Malat1*, *Ii1b*, *Tyrobp*, *Ccl6*, and *Ftl1*, which has been documented in a neutrophil scRNA-seq study [177].

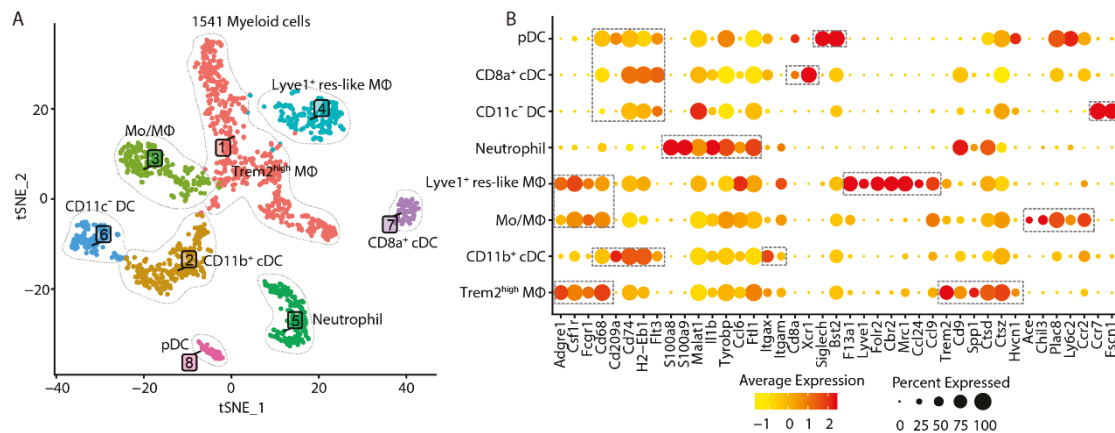


Fig. 3.9 Landscape of myeloid cells in plaques, ATLOs, and RLNs. A. 4 dendritic cell (DC) subsets, 3 macrophage subsets, and 1 granulocyte subset are shown in tSNE plot. **B.** Cluster-specific genes to distinguish myeloid cell subsets. Dot color represents the gene expression level. Dot size means the gene expression percentage.

Next, the DEGs of CD11c⁻ DCs were analyzed to explore their potential effects on atherosclerosis. CD11c⁻ DCs were characterized by high expression of *Ccr7*, *Fscn1*, *Ii15ra*, and *Ii4i1*, which have been reported to be highly expressed in migratory DCs [187](**Fig. 3.10A**). Migratory DCs are thought to migrate from non-lymphoid tissues to lymphoid organs. The migration capacity of migratory DCs promote transportation of antigens from the diseased sites to lymphoid tissues and activate antigen-specific T cells in the lymphoid organs [188, 189]. Various migratory DCs have been reported in lung, intestine, brain and skin [190]. The chemokine receptor CCR7 has been documented as the key mediator to regulate the movement of migratory DCs in steady-state and inflammatory conditions [191]. Deficiency of CCR7 results in the absence of migratory DCs in draining LNs [191]. The actin bundling protein FASCIN, encoded by *Fscn1*, has also been demonstrated to mediate the migration of DCs [192]. Pathway enrichment analyses were next performed by using the DEGs of CD11c⁻ DCs versus other DCs. CD11c⁻ DCs were significantly enriched in transcripts encoding components of the NF- κ B signaling pathway, antigen processing and presentation, and cytokine signaling in the immune system (**Fig. 3.10B**). Deleting

RESULTS

IKK β , the activator of the NF- κ B pathway restrains the accumulation of migratory DCs in LNs and the conversion of T_{reg} cells, indicating that the NF- κ B pathway plays a vital role in regulating migratory DCs to maintain immune tolerance [187]. These results indicate the migratory profile of CD11c⁻ DCs in our data, which supports the possibility that plaque migratory DCs transport plaque-specific autoantigens to lymphoid organs and then initiate T cell immune responses there. The migratory DCs in atherosclerosis have not been fully characterized. To further elucidate the functional effects of migratory DCs in atherosclerosis may provide new prospective to understand atherosclerosis specific T cell responses.

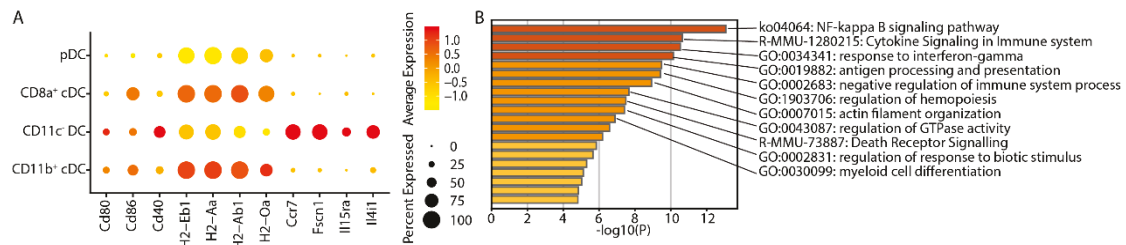


Fig. 3.10 The migratory profile of CD11c⁻ DCs. **A.** Dotplot to present the gene expression level of migratory DC-related genes in pDC, CD8a⁺ cDC, CD11c⁻ DC and CD11b⁺ cDC. Dot color represents the gene expression level. Dot size means the gene expression percentage. **B.** Pathway enrichment to analyze the phenotype and function related pathways associated with CD11c⁻ DCs.

3.5 Proportion of T cell subsets per total T cells in atherosclerotic plaques, ATLOs, ApoE^{-/-} RLNs and WT RLNs

To explore the proportion of T cell subsets among these tissues, the percentage of T cell subsets per total T cells in each tissue was determined. All T cell subsets were detected in each tissue. Using FACS, our previous studies had examined the percentage of total CD8 and CD4 T cells in RLNs of aged WT and ApoE^{-/-} mice showing that there were no substantial differences in the percentage of CD8 T cells (~43% vs ~38%), Foxp3-CD4 Th cells (~33% vs ~32.4%) and T_{reg} cells (~18% and ~20%) in RLNs of WT mice when compared to ApoE^{-/-} mice [121]. Our present study showed that WT RLNs and ApoE^{-/-} RLNs had similar percentages of CD8 T cells (49.6% vs 43.2%), Foxp3-CD4 Th cells (23.1% vs 26.0%), and T_{reg} cells (23.6% vs 29.2%). Two different methods showed similar results.

RESULTS

In the current work, scRNA-seq data showed highly significant changes in tissues: WT RLNs contained high numbers of CD4/CD8 naïve T cells, CD4/CD8 T_{cm}, NKT/CD8 T_{cm}, CD4 T_{em}, and T_{reg} cells and less of $\gamma\delta$ T cells and CD8 T_{em} cells (**Fig. 3.11B**). Compared to WT RLNs, ApoE^{-/-} RLNs and ATLOs showed contraction of CD4/CD8 naïve T cells ($p < 0.001$), NKT/CD8 T_{cm} ($p < 0.01$ for ApoE^{-/-} RLNs) and eT_{reg} cells, while CD4 T_{em} ($p < 0.05$ for ApoE^{-/-} RLNs and $p < 0.01$ for ATLOs) and CD8 T_{em} ($p < 0.001$) were increased (**Fig. 3.11B**). A significant increase of $\gamma\delta$ T cells was also observed in ATLOs relative to WT RLNs ($p < 0.001$) (**Fig. 3.11B**). In addition, plaques showed even more pronounced differences from WT RLNs, manifested by reduction of CD4/CD8 naïve T cells ($p < 0.001$) and T_{reg} cells ($p < 0.01$ for cT_{reg} cells and $p < 0.001$ for eT_{reg} cells), and accumulation of CD4/CD8 memory T cells ($p < 0.01$ for CD4 T_{em}, CD8 T_{cm} and $p < 0.001$ for CD8 T_{em}, NKT/CD8 T_{cm}) and $\gamma\delta$ T cells ($p < 0.001$) (**Fig. 3.11B**). Our present study is the first to compare the proportion of T cell subsets in plaques, ATLOs and aorta draining LNs in aged mice at the single cell level. The T cell landscape reveals tissue-specific T cell subsets in atherosclerosis of aged ApoE^{-/-} mice. Plaques predispose to less naïve T cells and T_{reg} cells but increased CD8 T_{cm} and T_{em} cells, which indicates the activation and proliferation (or recruitment) of cytotoxic T lymphocytes into plaque lesions. These differences lead us to examine whether the imbalance of anti- and proatherogenic lymphocytes contributes to the immune tolerance breakdown in atherosclerotic plaques.

RESULTS

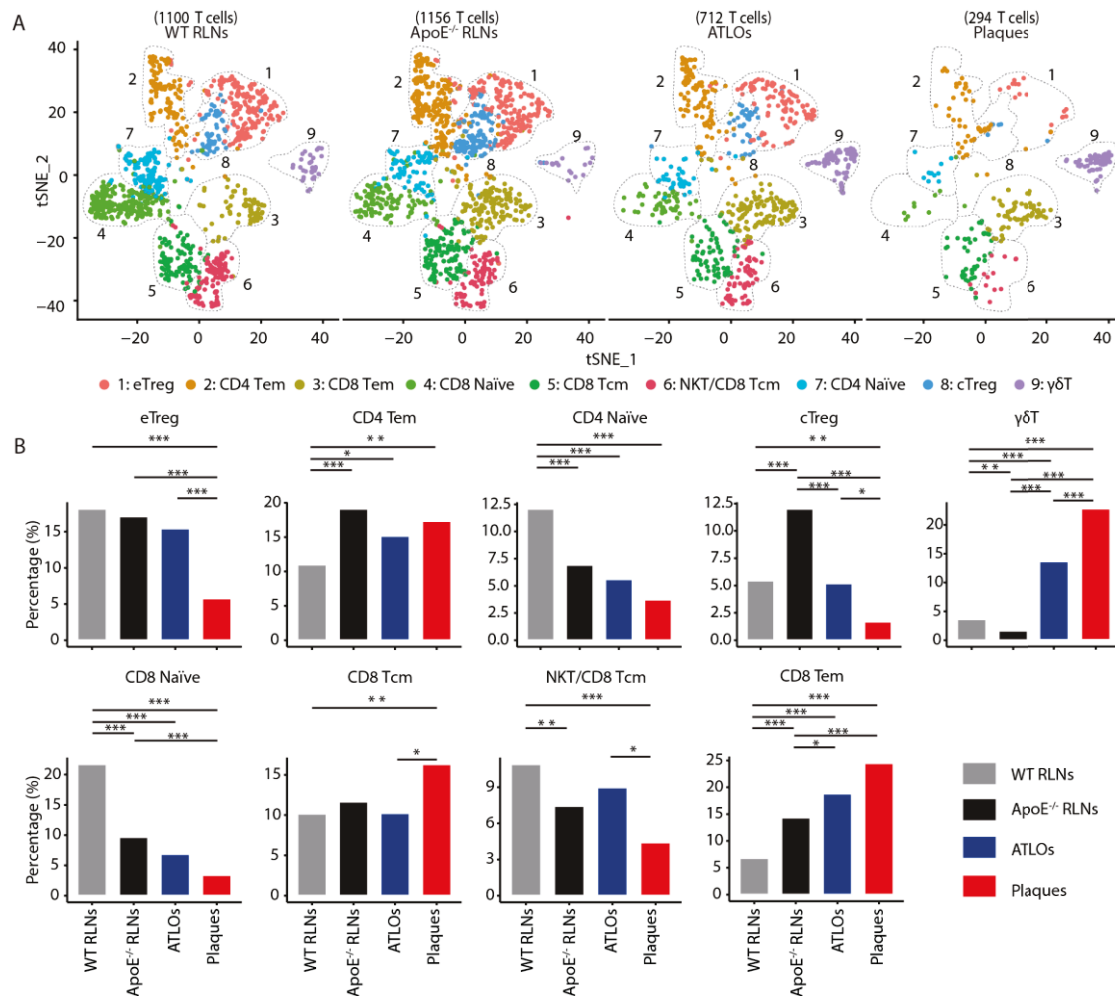


Fig. 3.11 The composition of T cell subsets in each tissue. **A.** Distribution of T cell subsets in tSNE plots of WT RLNs, ApoE^{-/-} RLNs, ATLOs, and plaques. **B.** The percentage of CD4 and CD8 Naïve T cells, effector and central regulatory T cells (eT_{reg} and cT_{reg}), CD4 T_{em} cells, CD8 T_{em}, CD8 T_{cm}, NKT/CD8 T_{cm} cells, and γδ T cells in different tissues. T_{em}: effector memory T cells; T_{cm}: central memory T cells; NKT: natural killer T cells; T_{reg}: regulatory T cells; γδ T: gamma delta T cell. The comparison of T cell proportions in different tissues were performed by chi-square test, and the differences between each two tissues were tested by chi-square post hoc test. The p values were adjusted by Benjamini-Hochberg method. * indicates $p < 0.05$, ** indicates $p < 0.01$, *** indicates $p < 0.001$.

3.6 Proportion of myeloid cell subsets per total myeloid cells in atherosclerotic plaques, ATLOs, ApoE^{-/-} RLNs and WT RLNs

Myeloid cells are the predominant leukocyte population in plaques (61.82%), significantly higher than their counterparts in ATLOs (24.42%), ApoE^{-/-} RLNs (4.33%) and WT RLNs (4.63%), suggesting an important role of myeloid cells on

RESULTS

atherosclerosis-specific immune responses including those of T cells (**Fig. 3.12A**). The composition of different myeloid cell subsets showed dramatic differences in tissues (**Fig. 3.12A**). DCs were found to be the major population of myeloid cells in the WT and ApoE^{-/-} RLNs, whereas macrophages dominated myeloid cells in ATLOs and plaques, accounting for 60.76% and 68.37% of myeloid cells, respectively (**Fig. 3.12B**). The migratory and tolerogenic CD11c⁻ DCs were the dominate population in WT RLNs and declined in ApoE^{-/-} mice ($p < 0.05$ for ApoE^{-/-} RLNs and $p < 0.001$ for ATLOs and plaques). ATLOs and plaques had even fewer CD11c⁻ DCs than ApoE^{-/-} RLNs (the tolerogenic profile of CD11c⁻ DCs will be discussed in result 3.12) (**Fig. 3.12C**). While inflammatory CD11b⁺ cDCs accounted for 21.1% of total DCs in WT RLNs, its percentage showed an increase in ApoE^{-/-} RLNs (32.4%), ATLOs (52.9%) and plaques (66.7%). CD11b⁺ cDCs were also the major DCs in ATLOs and plaques (**Fig. 3.12C**). CD8a⁺ cDCs and pDCs, which were reported to be involved in antigen presentation and IFN production respectively [117], showed similar percentage in WT RLNs, ApoE^{-/-} RLNs and ATLOs but plaques showed a significant decrease when compared to WT RLNs ($p = 0.002$ for pDCs and $p < 0.001$ for CD8a⁺ cDCs) (**Fig. 3.12C**). Lyve1⁺ res-like MΦs were the main macrophages in WT RLNs (48.0%) as reported in atherosclerosis [152] (**Fig. 3.12D**). It accounted for about 18.9% and 29.2% of macrophages in ApoE^{-/-} RLN and ATLO, respectively. A reduction of Lyve1⁺ res-like MΦs in plaques were also observed, accounting for 12.4% of plaques macrophages. Different from WT RLNs, the Trem2^{high} MΦs, which are thought to be involved in lipid metabolism, lesion calcification and resembling phenotypes of foam cells in plaque lesions [152], were the largest macrophage population in ApoE^{-/-} RLNs ($p < 0.05$), ATLOs ($p < 0.001$) and plaques ($p < 0.001$) (**Fig. 3.12D**). Only a few neutrophils were detected in WT RLNs and ApoE^{-/-} RLNs, its percentages were found higher in ATLOs ($p < 0.01$) and plaques ($p < 0.01$), about 4-7 times than RLNs.

RESULTS

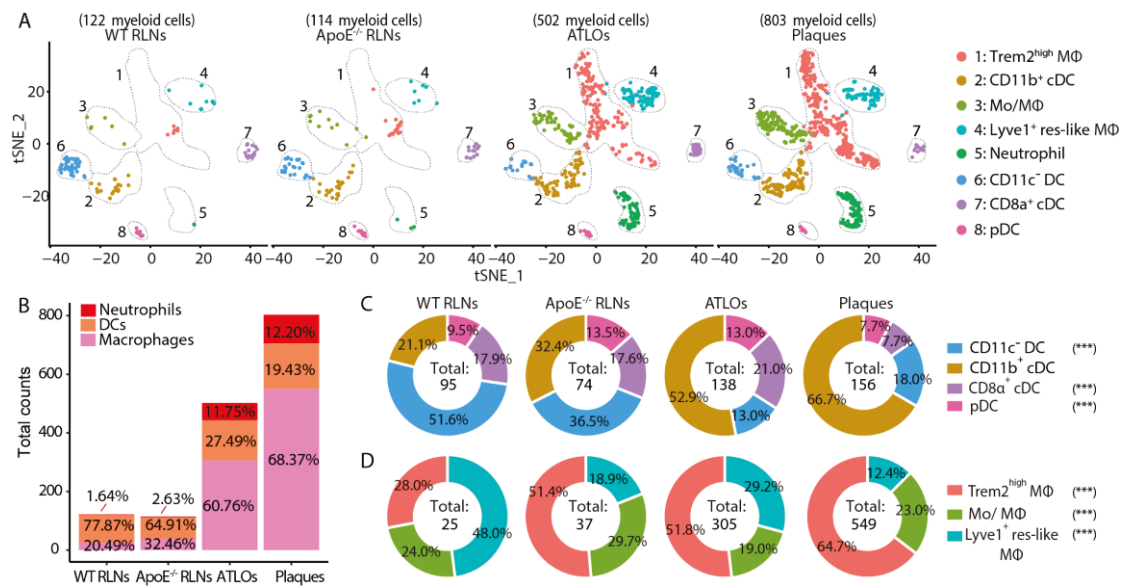


Fig. 3.12 Percentages of myeloid cells in plaques, ATLOs, and RLNs. **A.** Distribution of myeloid cell subsets in tSNE plots of WT RLNs, ApoE^{-/-} RLNs, ATLOs, and plaques. **B.** Bar plot of total cell numbers and percentages of macrophages, DCs, and Neutrophils. The Y axis indicates the cell numbers of macrophage, DCs and neutrophils in each tissue. The number in each column means the percentage of macrophages, DCs and neutrophils in myeloid cells of each tissue. Circular plot to present the percentage of DC (**C**) and macrophage (**D**) subsets in each tissue. The number in the inner circle indicates cell numbers of DCs or macrophage in each tissue. The comparison of myeloid cell proportions in different tissues were performed by chi-square test (represented by asterisks in parentheses), and the differences between each two tissues were tested by chi-square post hoc test (differences were not shown in the figure). The p values were adjusted by Benjamini-Hochberg method. * indicates $p < 0.05$, ** indicates $p < 0.01$, *** indicates $p < 0.001$.

3.7 The TCR repertoires across atherosclerotic plaques, ATLOs, ApoE^{-/-} RLNs and WT RLNs suggest (auto)antigen-specific T cell immune responses in atherosclerosis

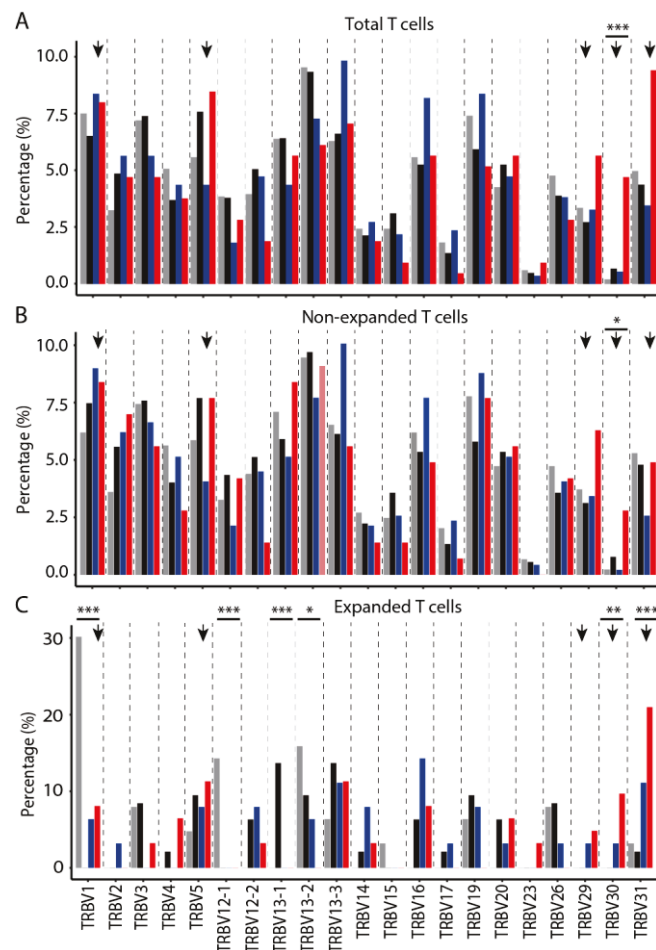
TCRs are generated by recombination of different V, D, J families and random deletion and insertion of nucleotides at the junctions between gene segments. The recognition of TCRs with peptide-MHC complexes is crucial for the maintenance of central tolerance and peripheral tolerance, which determines the composition of individual TCR repertoires. Disease-induced tolerance breakdown can greatly shape the TCR repertoire [142, 143]. We aimed to get insight into the possible disease-associated TCR repertoire diversity in atherosclerosis. The parameters to reflect the TCR repertoire were analyzed, such as TCR β V family usage, CDR3 length

RESULTS

distribution and TCR β chain V and J gene combination usage. To explore the diversity of TCR repertoire in atherosclerosis, the TCR of each cell was constructed. Among the total 3262 T cells, 2757 TCR α chain or TCR β chain sequences (84.5% of total T cells) and 2061 paired-TCR α/β chains (63.2% of total T cells) were obtained. The frequency of TCR β chain V region in different tissues were then examined. WT RLNs and ApoE^{-/-} RLNs showed similar TCR β subfamilies usage in total T cells and non-expanded T cells (**Fig. 3.13A and B**). The top three fractions in total T cells of WT RLNs were TRBV13-2 (9.88% of total TRBV families in WT RLNs), TRBV1 (7.78%), and TRBV19 (7.68%). The top 3 families in ApoE^{-/-} RLNs were TRBV13-2 (9.68%), TRBV5 (7.86%), and TRBV3 (7.66%). The top 3 families in ATLOs were TRBV13-3 (10.19%), TRBV1 (8.68%), and TRBV19 (8.68%). However, the top 3 families in plaques were TRBV31 (9.76%), TRBV5 (8.78%), and TRBV1 (8.29%) (**Fig. 3.13A**). Although WT RLNs, ApoE^{-/-} RLNs and ATLOs differed from each other in the usage of top TRBV families, the difference of total 21 TRBV family percentage among them were small (majority were less than 2%, $p > 0.05$) (**Fig. 3.13A**). However, TRBV31 was 1.9 to 2.7-fold higher in plaques than in other tissues, even though no statistically significant difference was found in these tissues ($p = 0.06$) (**Fig. 3.13A**). Although TRBV30 was not the top 10 highly used TRBV families in plaques, plaque TRBV30 was 7-23 times higher when compared to other tissues ($p < 0.001$) (**Fig. 3.13A**). The TRBV frequency in the expanded and non-expanded T cells were also compared. The proportion of TRBV families in non-expanded T cells of WT RLNs, ApoE^{-/-} RLNs, ATLOs and plaques were similar to their percentage in total T cells, with the exception of TRBV30 ($p = 0.027$) (**Fig. 3.13B**). Interestingly, apparent changes were observed in expanded T cells. The proportions of TRBV1 ($p < 0.001$), TRBV12-1 ($p < 0.001$), TRBV13-1 ($p < 0.001$), TRBV13-2 ($p = 0.04$), TRBV30 ($p = 0.007$) and TRBV31 ($p < 0.001$) were found to be significantly different across tissues (**Fig. 3.13C**). WT RLNs showed enrichment in TRBV1, TRBV12-1, TRBV13-2 (**Fig. 3.13C**), ApoE^{-/-} RLNs were enriched in TRBV13-1 (**Fig. 3.13C**). No significant enrichment of TRBV families were found in ATLOs compared to other tissues. Plaques were found to be enriched in TRBV30 and TRBV31 (**Fig. 3.13C**).

RESULTS

TRBV31 made around 4.9% in plaques non-expanded T cells and displayed similar percentage to TRBV31 of non-expanded T cells in other tissue. Whereas TRBV31 accounting for 21% of expanded T cells in plaques and its percentage was about 7-10 times higher than in RLNs (**Fig. 3.13B and C**). These data suggest that the specific increase of TRBV31 in plaques in expanded T cells may be caused by antigen-dependent T cell clonal expansion. Interestingly, ApoB100-specific T cells has been reported to express TRBV31 [134]. Depletion of TRBV31⁺ T cells by immunizing *Ldlr^{-/-}* mice with peptide of the TRBV31 CDR2 region resulted in significant reduction of atherosclerotic plaques in aortic arch and aortic root. Further studies are needed to fully understand the antigen specificity and their functions of TRBV31⁺ CD8 T cells on atherosclerosis identified in our study. What's more, the enrichment of TRBV30 in plaque-expanded T cells (**Fig. 3.13B and C**) raises the possibility that the TRBV30-expanded T cells may also contribute to the antigen-specific T cell clonal expansion in plaques.



RESULTS

Fig. 3.13 Distribution of TCR β V families (TRBV) of total T cells (A), clonally non-expanded (B) and clonally expanded (C) T cells in plaques, ATLOs, RLNs (cells with paired TCR $\alpha\beta$ chains or single α/β chain were both included). Clonally expanded T cells were identified as having at least two cells with identical V family and CDR3 region amino acid sequences of α and β chain. The comparison of TRBV family proportions in total T cells, expanded T cells and non-expanded T cells of different tissues were performed by the chi-square test, and the differences between two tissues were tested by chi-square post hoc test. The p values were adjusted by Benjamini-Hochberg method. * indicates $p < 0.05$, ** indicates $p < 0.01$, *** indicates $p < 0.001$.

CDR3 is the most variable region of the TCR, which plays a predominant role in antigen recognition, the CDR3 length was used to monitor T cell immune responses toward different antigens, and it was used to evaluate the diversity of TCR repertoire [193]. CDR3 amino acid (aa) length of TCR α chains showed a Gaussian-like distribution with a peak at 14 aa in different tissues (**Fig. 3.14A**). Expanded T cells in WT RLNs had a peak at 14 aa. Expanded T cells in ApoE^{-/-} RLNs and ATLOs showed a similar distribution and had an enrichment at 14 aa (**Fig. 3.14A**). However, plaques showed a preferential distribution from 12-14 aa (**Fig. 3.14A**). Similarly, β chains of total T cells in RLNs, ATLOs and plaques also displayed a normal distribution (**Fig. 3.14B**). β chains of total T cells in WT RLNs showed an enrichment in 13 aa (**Fig. 3.14B**). β chains of total T cells in ApoE^{-/-} RLNs, ATLOs and plaques displayed a peak at 14 aa (**Fig. 3.14B**). CDR3 length of expanded T cells in WT RLNs showed a higher enrichment in 13 aa, while its counterpart in ApoE^{-/-} RLNs and ATLOs displayed an enrichment in 14 aa (**Fig. 3.14B**). CDR3 length of expanded T cells in plaques had a peak at 15 aa (**Fig. 3.16B**).

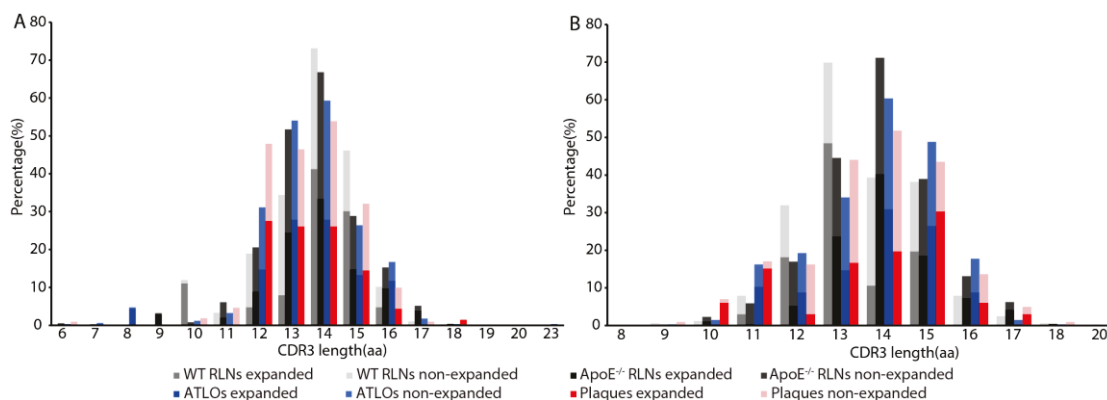


Fig. 3.14 The CDR3 amino acid (aa) length distribution of T cell α (A) and β (B) chains in

RESULTS

plaques, ATLOs and RLNs (only cells with paired TCR $\alpha\beta$ chains were included). Each color represents expanded or non-expanded T cells among different tissues, the light color indicates non-expanded T cells, and the deep color indicates expanded T cells.

V and J regions of TCRs are the main domains of CDR3s and they contribute to the diversity of TCRs. Distinct patterns of TRBV-J combination may suggest disease-specific antigen-induced T cell immune responses [194]. Therefore, the TRBV-J combination usage in different tissues were analyzed. From the combination circular plot, numerous TRBV-J combinations in each tissue were observed, which represents an intensive diversity of TCR β chains. No pronounced TRBV-J combination usage was found in RLNs (Fig. 3.15). while a slight increase of TRBV16-TRBJ2-7 were observed in ATLOs (Fig. 3.15). Intriguingly, plaques had a significant and obvious preference for TRBV31-TRBJ1-1 and TRBV5-TRBJ2-7 when compared to RLNs and ATLOs (Fig. 3.17). Taken together, these results imply skewed TRBV-J combinations in atherosclerosis, particularly in plaques that may be induced by T cell activation and expansion through recognizing disease-associated (auto)antigens.

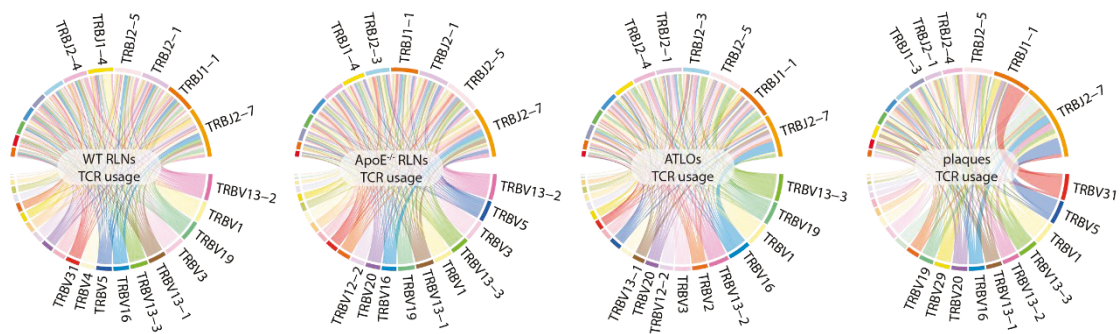


Fig. 3.15 Circular plots show the TCR β V families and TCR β J families combination usages of T cells among four tissues (cells with paired TCR $\alpha\beta$ chains or single $\alpha\beta$ chain were both included). Top 10 highly expressed TRBV families and top 6 highly expressed TRBJ families are listed in the outer layer of each circle. Each color represents one family. The size of color represents the percentage of each family. The total percentage of TRBV and TRBJ families in each figure was 100%. The link between TRBV and TRBJ means the combination usage.

3.8 High-throughput paired scTCR($\alpha\beta$)-seq indicates robust T cell clonal expansion in atherosclerosis

Diversity of TRBV usage, CDR3 length distribution and combined TRB V-J usage is

RESULTS

tissue-dependent in ApoE^{-/-} mice suggesting the potential of T cell clonal expansion in atherosclerosis, particularly in atherosclerotic plaques. Changing in TCR repertoire or preferred usage of certain TCR β chains during atherosclerosis has been reported in several studies previously [40, 143, 195, 196]. To further investigate the association between clonal expansion of different T cell subsets and antigen-specific T cell immune responses in atherosclerosis, scTCR-seq data was paired with scRNA-seq data at the single cell level. Clonally expanded T cells were defined as having at least two cells with identical V family and CDR3 region nucleic acid sequence of α and β chains. When the frequency of expanded T cells of each tissue was examined, clonally expanded T cells accounted for 5.44% of total TCR-detected T cells in WT RLNs. Compared to WT RLNs, a significant increase of clonal expansion T cells was observed in ApoE^{-/-} RLNs ($p < 0.01$) and ATLOs ($p < 0.001$), which contained 8.98% and 11.6% clonally expanded T cells, respectively (**Fig. 3.13A**). Furthermore, clonally expanded T cells accounted for 29.0% in atherosclerotic plaques, showing a dramatic increase when compared to WT RLNs, ApoE^{-/-} RLNs, and ATLOs ($p < 0.001$) (**Fig. 3.13A**). Low percentages of T cells with undetectable TCR α or TCR β chains were observed in each tissue due to either the technical limitations or T cells carrying $\gamma\delta$ TCR chains, because the general 10x V(D)J sequencing kit does not contain the primers to clone TCR γ and δ chains [197]. The higher percentages of un-detectable TCR α or β chains were observed in ATLOs (23.60%) and plaques (27.21%) when compared to WT RLNs (11.46%) and ApoE^{-/-} RLNs (11.33%) in total T cells. This observation is consistent with the higher percentages of $\gamma\delta$ T cells observed in ATLOs and plaques (**Fig. 3.11B**).

To understand the clonality of antigen-driven T cells in different tissues, the TCR diversity (negatively correlated with clonality) was quantified in all tissues. After adjustment of sample depth by reducing sample depth to the same level [198], the Shannon entropy, Gini indices and inverse Simpson diversity indices were calculated in the four tissues. The Shannon entropy quantifies the uncertainty of predicting the characteristics of a random sample from the whole dataset. A larger value of Shannon entropy indicates a higher diversity of sample [199]. The Gini index was

RESULTS

proposed and used to evaluate the income inequality in economy [200], a lower Gini index reflects a higher TCR diversity. The Simpson diversity index measures the possibility of two samples taken randomly from dataset with the same characteristics, a lower Simpson index reflect higher TCR diversity [201]. Inverse Simpson index is calculated by $1/\lambda$ (λ represents Simpson index). All the three indices have been widely used to measure the TCR diversity [201]. TCR diversities of four different tissues were then compared. WT RLNs had a small Gini index (0.03 ± 0.01), and large values of inverse Simpson index (150.93 ± 7.13) and Shannon entropy (7.26 ± 0.03) (Fig. 3.16B, C and D), indicating WT RLNs had a high TCR diversity and low TCR expansion. When compared to WT RLNs, ApoE^{-/-} RLNs showed a minor decrease of Gini index (0.02 ± 0.01 , $p < 0.001$), and a minor increase of inverse Simpson index (154.40 ± 4.33 , $p < 0.001$) and Shannon entropy (7.27 ± 0.03 , $p < 0.001$) values (Fig. 3.16B, C and D). ATLOs also showed a slight increase of the Gini index (0.05 ± 0.01 , $p < 0.001$), and a slight decrease of the inverse Simpson index (144.95 ± 5.99 , $p < 0.001$) and Shannon entropy (7.22 ± 0.04 , $p < 0.001$) when compared to WT RLNs (Fig. 3.16B, C and D). These data indicate a slight reduction of TCR diversity and increase of T cell expansion in ATLOs. More interestingly, atherosclerotic plaques had the highest Gini index (0.23 ± 0.01 , $p < 0.001$) and the lowest Shannon entropy (6.61 ± 0.03 , $p < 0.001$) and inverse Simpson index (64.7 ± 3.13 , $p < 0.001$) when compared to other tissues, suggesting the lowest TCR diversity and the highest T cell expansion of atherosclerotic plaques (Fig. 3.16B, C and D).

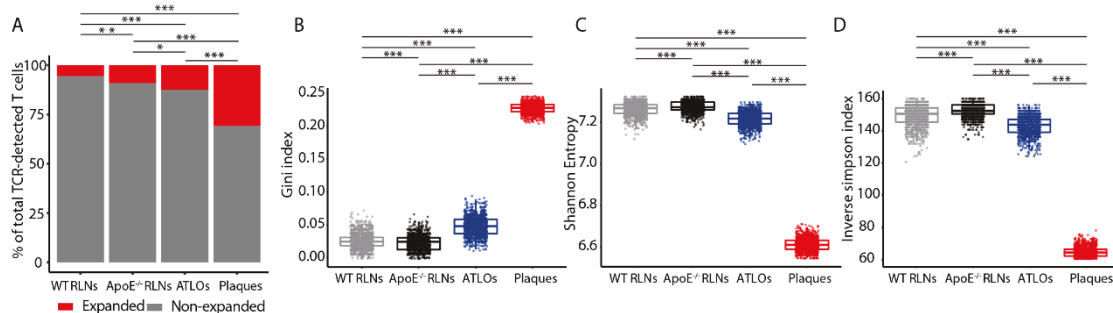


Fig. 3.16 T cell clonal expansion and TCR diversity among four tissues. A. Bar plot display the proportions of clonal expanded (red), and non-expanded T cells (grey) in different tissues. Cells without detectable TCR α or TCR β chains or $\gamma\delta$ T cells were excluded. The comparison of expanded

RESULTS

and non-expanded T cell composition between two tissues were performed by chi-square post hoc test, p values were adjusted by Benjamini Hochberg method. * designates $p < 0.05$, ** designates $p < 0.01$, *** designates $p < 0.001$. The Gini index (**B**), Shannon entropy (**C**), and inverse Simpson diversity index (**D**) were used to evaluate the TCR repertoire diversity of each tissue. Values are presented by boxplots with overlaid dotplots. The samples of each tissue were randomly down-sampled to the same level and repeated for 1000 times. For each index, each dot represents one-time repetition. The boxplot shows the 25th percentile, median, 75th percentile values. Shapiro-Wilk test was first used to evaluate the data distribution of each group. Data that did not follow normal distribution will be analyzed using the Kruskal–Wallis test with Dunn's non-parametric all-pairs comparison test. The p values were adjusted by Bonferroni method. *** designates $p < 0.0001$.

By pairing TCR sequence data and gene expression profiles at the single cell level, the 9 T cell clusters were further grouped into five major groups based on T cell biological functions including antigen-experienced CD4 $T_{\text{eff/mem}}$ cells (group I, CD4 T_{em} cells), T cells with regulatory functions (group II, eT_{reg} and cT_{reg}); antigen-experienced CD8 $T_{\text{eff/mem}}$ cells (group III, CD8 T_{em} , CD8 T_{cm} and NKT/CD8 T_{cm}); antigen-inexperienced naïve T cells (group IV, CD4 naïve and CD8 naïve T cells), and MHC-independent antigen recognition of $\gamma\delta$ T cells (group V: $\gamma\delta$ T cells) (**Fig. 3.17A**). A variable distribution of expanded T cells was observed between WT and ApoE^{-/-} mice (**Fig. 3.17B**). The clonally expanded T cells were found to be limited to CD4 $T_{\text{eff/mem}}$ and CD8 $T_{\text{eff/mem}}$ cells (group I and III) (**Fig. 3.17B and C**). A lack of clonally expanded T cells in naïve and $\gamma\delta$ T cells (group IV and V) in all tissue were observed, as expected, suggesting the high quality of our data set (**Fig. 3.17B and C**). Of note, there are minor differences of CD4 $T_{\text{eff/mem}}$ clonally expanded T cells in four tissues ($p > 0.05$) (**Fig. 3.17C**). Major differences were observed in CD8 $T_{\text{eff/mem}}$ cells in all tissues ($p < 0.001$) (**Fig. 3.17C**). WT RLNs showed 5.9% expanded T cells in CD8 $T_{\text{eff/mem}}$ cells. ApoE^{-/-} RLNs and ATLOs showed significant increases of expanded T cells in CD8 $T_{\text{eff/mem}}$ cells ($p < 0.001$), accounting for 16.0% and 17.3% of expanded T cells in CD8 $T_{\text{eff/mem}}$ cells, respectively (**Fig. 3.17C**). A further increase of clonally expanded T cells was found in CD8 $T_{\text{eff/mem}}$ cells of plaques (37.6%), which showed significant differences compared to RLNs ($p < 0.001$) and ATLOs ($p < 0.001$) (**Fig. 3.17C**). Moreover, the higher percentage of expanded CD8 $T_{\text{eff/mem}}$ cells

RESULTS

associated with the highest percentage of CD8 T cells in plaques (45.2% of total T cells) when compared to WT RLNs/ApoE^{-/-} RLNs/ATLOs (27.9%/33.5%/38.1% of total T cells, respectively), indicating that CD8 T cell clonal expansion contributes to the enrichment of CD8 T cells in plaques. WT RLNs T_{reg} cells showed 9.6% of clonal expansion, in contrast, ApoE^{-/-} RLNs and ATLOs showed lower expanded T_{reg} cells, 3.3% ($p < 0.01$) and 1.4% ($p < 0.01$), respectively (**Fig. 3.17C**). Plaque T_{reg} cells showed 13.6% clonally expanded cells, and it was significant higher when compared to ATLO T_{reg} cells ($p < 0.05$) (**Fig. 3.17C**). Taken together, our data showed extensive clonal expansion of CD8 T_{eff/mem} cells in different tissues, which suggests tissue-specific impaired T cell immune tolerance in atherosclerosis.

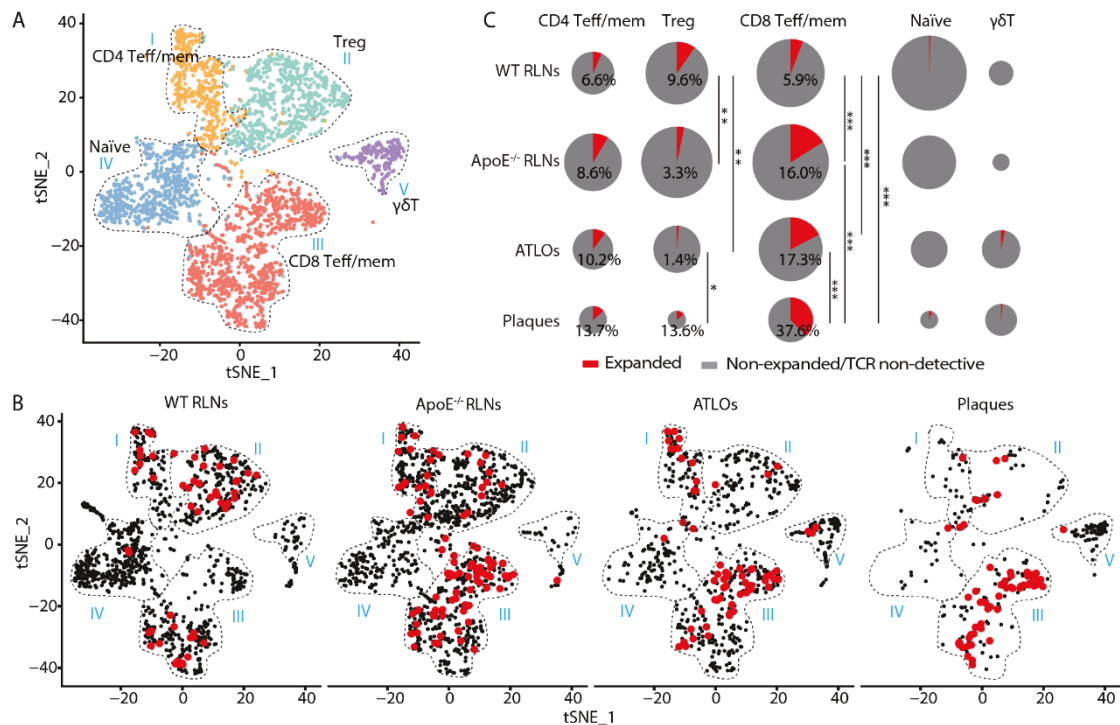


Fig. 3.17 Clonally expanded T cells with paired-TCR α/β distribution in WT RLNs, ApoE^{-/-} RLNs, ATLOs, and plaques. A. tSNE shows a total of 3262 T cells that were grouped into five major groups according to their gene expressions and functions including CD4 T_{eff/mem} cells (group I; CD4 T_{em}), T_{reg} cells (group II; cT_{reg} and eT_{reg} cells), CD8 T_{eff/mem} cells (group III; CD8 T_{em}, CD8 T_{cm} and NKT/CD8 T_{cm} cells), naïve T cells (group IV; CD4 naïve and CD8 naïve T cells), and $\gamma\delta$ T cells (group V; $\gamma\delta$ T); **B.** Distribution of clonally expanded T cells in tSNE plot. The clonally expanded T cells are highlighted and bolded in red. **C.** Pie chart shows percentages of clonally expanded versus non-expanded T cells in different groups in different tissues. The size of circle represents the cell numbers within each tissue. Each circle represents 100%, red color represents the percentage of clonally expanded T cells

RESULTS

within each group. The comparisons of expanded and non-expanded T cell composition between each two tissues in each T cell group were performed by chi-square post hoc test, p values were adjusted by Benjamini Hochberg method. * designates $p < 0.05$, ** designates $p < 0.01$, *** designates $p < 0.001$.

To assess the association of tissue-specific T cell clonal expansion in different tissues, common CDR3 regions between different tissues in expanded or non-expanded T cells were visualized (**Fig. 3.18**). Results showed that (i) plaques-, ATLOs- and ApoE^{-/-} RLNs-CD8 expanded T cells shared a large number of CDR3 regions, especially in plaques (64.2% and 56.0% for α and β chain) and ATLOs (61.7% and 57.4% for α and β chain) (**Fig. 3.18A upper panel**); (ii) the expanded CDR3 aa sequences of CD4 and CD8 T cells were not shared between WT and ApoE^{-/-} mice (**Fig. 3.18A upper panel**); (iii) the number of shared expanded CDR3 aa sequences in plaques-, ATLOs-, and ApoE^{-/-} RLNs-CD8 T cells were significantly higher when compared to CD4 T cells from the same tissues (**Fig. 3.18A upper panel**); (iv) apart from plaques which had a higher percentage of shared CDR3 in non-expanded T cells (32.8% and 38.5% for α and β chain of CD8 non-expanded T cells; 15.8% for α chain of CD4 non-expanded T cells) than other tissues, the majority of non-expanded CDR3 aa sequences showed a tissue-specific distribution (**Fig. 3.18A lower panel**); (v) only a small number of non-expanded CDR3 aa sequences were shared by WT with other tissues in ApoE^{-/-} mice (11.7% and 0.6% for α and β chain of CD8 T cells in WT mice, respectively; 10.4% and 2.9% for α and β chain of CD4 T cells in WT mice, respectively) (**Fig. 3.18A lower panel**). Considering all CDR3 amino acid sequences and their frequencies among tissues, the cosine similarities between two tissues were calculated, which indicated the overall similarity of CDR3 in the two tissues. The results found that for the single α chain or β chain or paired $\alpha\beta$ TCRs, WT RLNs had a very low similarity to all other tissues, while ApoE^{-/-} RLNs had a relatively higher similarity to ATLOs. Plaques showed similarity to ApoE^{-/-} RLNs and ATLOs, but their similarity was less than that between ApoE^{-/-} RLNs and ATLOs (**Fig. 3.18B**). When taken together, all these results imply that the expanded CD8 T cells in ApoE^{-/-} mice (RLNs, ATLOs, and

RESULTS

plaques) are likely to be triggered by hyperlipidemia-related (auto)antigens.

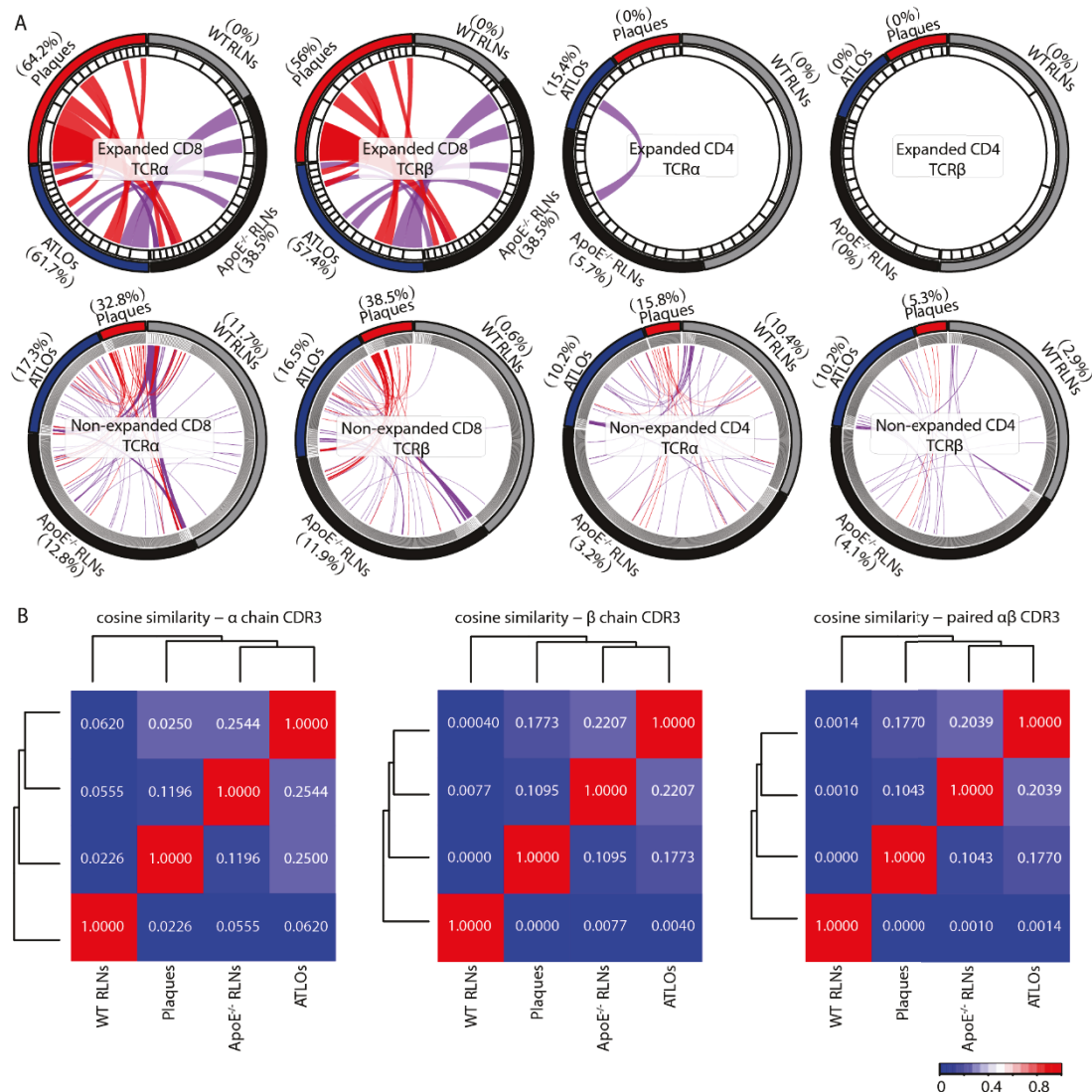


Fig. 3.18 The similarity of CDR3 region among tissues. A. Circular plot shows the shared CDR3 regions among four tissues (for the expanded T cells, only the cells with paired TCR αβ chains were included; for the non-expanded T cells, cells with TCR single chain or paired chains were both included). In the outer circle, each color represents different tissue. The column size of the inner circle represents the cell numbers of each clonotype. The link between two tissues represents shared CDR3, the red link underlines the shared CDR3 region between plaques and other tissues. The number in the parentheses represents the percentage of shared CDR3 in each tissue in different populations. **B.** Heatmap represents the cosine similarity between two tissues. Cosine similarity was calculated by R package lsa (Latent semantic analysis, version: v0.63-1). The cosine similarity value 1 means that the two samples have complete similarity, the value 0 means two samples are totally different.

The TCR repertoire diversity of different tissues from various aspects were evaluated

RESULTS

in our current study. All data support the conclusion that there is a significant clonal expansion of T cells in atherosclerosis, which is particularly pronounced in atherosclerotic plaques. The significant TRBV frequency, TRBV-J combination usage and CDR3 common usage among tissues all point to our hypothesis that compromised peripheral tolerance induces specific CD8 and CD4 T cell clonal expansion in atherosclerosis providing critical information for the next step in investigating atherosclerotic antigen-specific T cell immune responses.

3.9 Plaque naïve T cells show a specific partially activated phenotype

Naïve T cells as the reservoir for immune defense are kept at a quiescent state to prevent potential self-attack during normal physiological immune system homeostasis. We therefore aimed to investigate signs of tolerance breakdown within the naïve T cell pool in atherosclerosis. For this purpose, the DEGs of CD4 and CD8 naïve T cells were compared between ApoE^{-/-} RLNs, ATLOs, plaques and their counterpart in WT RLNs. There were several significantly upregulated DEGs in CD4 naïve T cells of ApoE^{-/-} RLNs (*mt-Atp8*, *S100a6*, *Ly6a*, *Ifi2712a*, *Nme2*, *AW112010*) and ATLOs (*Igkv3-2*, *Sec24b*) when compared to CD4 naïve T cells in WT RLNs. Among them, *S100a6* and *AW112010* were reported to be present in activated T cells [202]. Many upregulated genes associated with T cell function were detected in plaque CD4 naïve T cells compared with CD4 naïve T cells in WT RLNs, i.e. TCR V(D)J recombination (*Rag1*, *Dntt*, *Lig4*) [203, 204], T cell activation and differentiation (*S100a6*, *Ctla2a*, *Ctstl*, *Ccl27a*, *P2rx1* [205], *Ly6d* [206], *Rorc*, *Il17re*, *Gzma*), T cell migration (*Ccr2*, *Ccr9*, *Ccr4*), and cellular component morphogenesis (*Tubb2b*, *Anxa2*). This data suggested that CD4 naïve T cells in atherosclerotic plaques are partially activated (**Fig. 3.19A**). Likewise, upregulated DEGs were detected in ApoE^{-/-} RLNs (*mt-Atp8*, *Rpl27*, *Igkv17-121*, *Ifi2712a*, *Fbxo17*, *Uba52*, *Ly6a*, *Malat1*, *Irgc1*, *Nme2*, *Igkc*) and ATLOs (*Igkv3-2*, *Igkv1-99*, *Irgc1*, *Plaur*, *Vps37b*, *Igkc*, *Junb*, *Slc38a2*, *H3f3b*) CD8 naïve T cells against their counterparts in WT RLNs. Among these genes, *Junb* was demonstrated regulating T cell function

RESULTS

[207]. In contrast to CD8 naïve T cells in WT RLNs, several genes were upregulated in the plaque CD8 naïve T cell pool were observed to be associated with CD8 T cell functions after infection (*S100a6*, *S100a4*, *Cd44*, *Pdcd1*, *Myo1f*) [208], and genes to regulate T cell morphogenesis (*Tube1*, *Zmym4*) and TCR V(D)J recombination (*Lig4*) (Fig. 3.19B). Moreover, *Ccl5* was highly expressed in plaque CD8 naïve T cells, while the *Igfbp4*, which had been observed to be highly expressed in naïve T cells [209], showed an attenuated expression both in plaque CD4 and CD8 naïve T cells (Fig. 3.19A and B). To confirm our findings, GSEA analysis was performed. This data illustrated a significant enrichment score in T cell activation and differentiation of plaque CD4 naïve T cells (Fig. 3.19C and D). All these data point to a partially activated phenotype of CD4 naïve T cells in atherosclerotic plaques indicating the initial stages of tolerance breakdown by the checkpoint regulating quiescence. A few DEGs between blood CD4 and CD8 naïve T cells of WT mice and ApoE^{-/-} mice (Fig. 3.5C), the DEGs are listed in the appendix table 1).

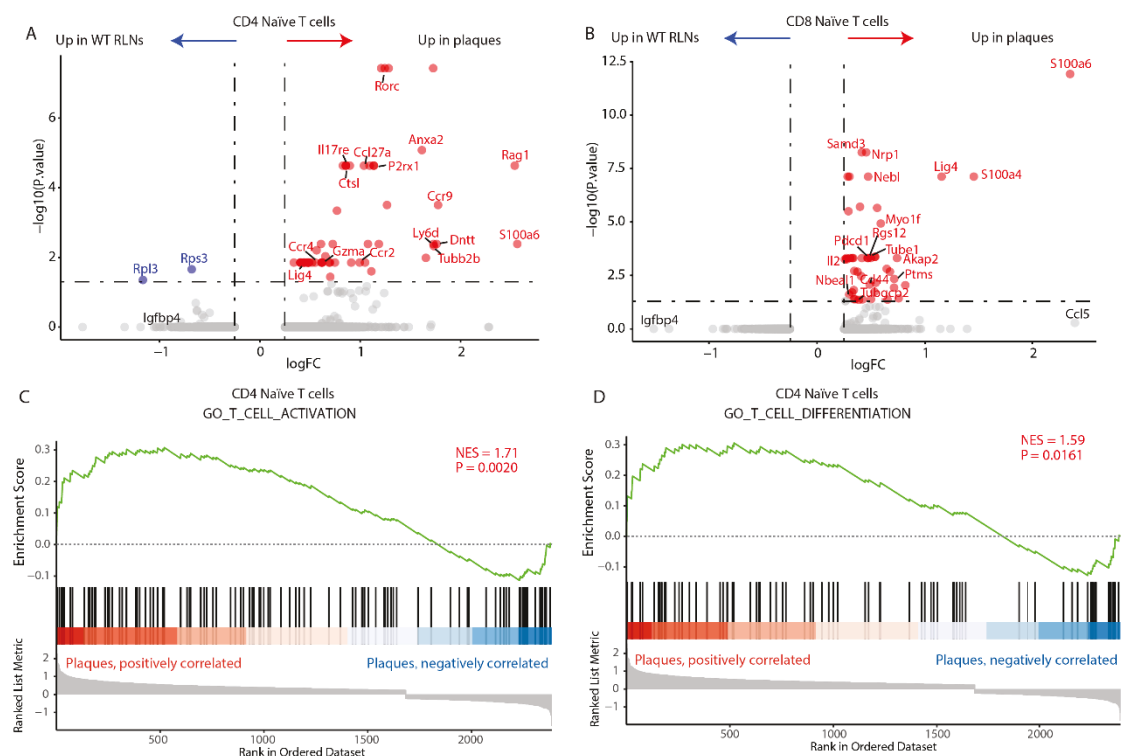


Fig. 3.19 Plaques naïve T cells acquire activated phenotype. Volcano plot to display the DEGs of CD4 (A) and CD8 (B) naïve T cells of plaques against WT RLNs. GSEA analysis illustrates the enriched pathways of T cell activation (C) and differentiation (D) in CD4 naïve T cells in atherosclerosis plaques in relative to WT RLNs. NES: normalized enrichment score; logFC: log

RESULTS

transformed fold change.

The expression of genes regulating quiescence of naïve T cells were then explored. Studies have demonstrated that VISTA (encoded by the *Vsir* gene) is a functionally relevant gene to maintain quiescence of the CD4 naïve T cell pool by inducing downstream gene expression of *Klf2*, *Btg1*, and *Foxp1*. The deficiency of *Vsir* causes CD4 naïve T cells development into memory-like activated T cells [88]. Plaque CD4 naïve T cells displayed a slight decrease of *Vsir* expression together with downstream genes like *Ccr7*, *Btg1*, *Foxp1* and *Foxo1* compared to their CD4 naïve T cells in WT RLNs. Moreover, *Tcf7*, *Bcl2*, *Ifngr1* that direct memory T cell activity and *Cd247*, *Fos*, *Lat*, *Cd4*, *Myc*, *Pdcd1*, *Ctla4*, *Cd6*, *Cd2*, *Lck* that modulate TCR signaling were upregulated in plaque CD4 naïve T cells versus WT RLNs CD4 naïve T cells (**Fig. 3.20A**). Although mechanisms that mediate quiescence of CD8 naïve T cells are less well understood, these genes were also analyzed among tissues. Interestingly, *Vsir* was unchanged in plaque CD8 naïve T cells, while genes regulating memory (*Tcf7*, *Bcl2*, *Ii7r*, *Slamf6*, *Ifngr1*) and antagonizing the expression of *Klf2* (*Klf3*) and modulating TCR signaling (*Cd247*, *Lat*, *Nfkb1*, *Pdcd1*, *Cd5*, *Cd6*, *Lck*) were increased when compared to WT RLNs CD8 naïve T cells (**Fig. 3.20B**). This data supports the conclusion that activation of CD8 naïve T cells is initiated in plaques. The role of VISTA in mediating quiescence of CD8 naïve T cells remains to be fully understood calling for further studies to clarify the mechanisms to regulate CD8 naïve T cell quiescence.

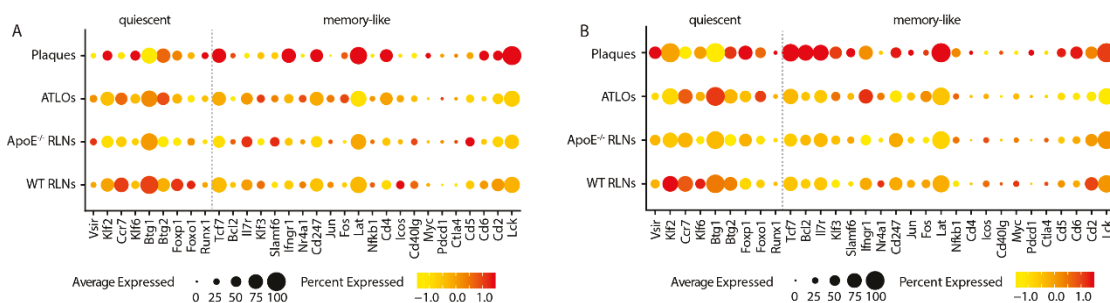


Fig. 3.20 The average expression of genes regulate the quiescent and memory-like state of naïve T cells. Dotplot display the average expression of genes regulating the quiescent and memory-like states in CD4 (A) and CD8 (B) naïve T cells.

RESULTS

3.10 Impaired immunosuppressive function of T_{reg} cells in atherosclerosis

T_{reg} cells are the major T cell population to suppress immune responses and their dysfunction result in autoimmune diseases, unhinged infection, and chronic inflammation. Above, a reduction of T_{reg} cells (eT_{reg} and cT_{reg}) (**Fig. 3.11B**) and a higher clonal expansion of CD8 T_{eff/mem} cells in atherosclerotic plaques and associated LNs were shown. These findings led us to consider another key tolerance checkpoint, i.e. the immunosuppressive capability of T_{reg} cells. Thus, the gene expression profiles of T_{reg} cells in different tissues were compared. T_{reg} cells in WT RLNs showed high expression of two canonical T_{reg} cell markers *Foxp3* and *Il2ra* (encoding CD25), along with a low expression of CD127 encoding the *Il7r* gene. Importantly, the expression of the former genes in T_{reg} cells of ApoE^{-/-} RLNs and ATLOs was the same as their expression in T_{reg} cells of WT RLNs, but we observed reduced expression of *Il2ra* in ApoE^{-/-} RLNs and increased expression of *Il7r* in cT_{reg} cells of ATLOs. In sharp contrast, cT_{reg} cells in plaques showed lower expression of *Foxp3* and *Il2ra* and higher expression of *Il7r* compared to RLNs and ATLOs (**Fig. 3.21**). Although *Foxp3* expression level in eT_{reg} cells of plaques was similar to other tissues, there was a reduction of *Il2ra*, *Stat5a* and an increase of *Il7r* in plaques compared with the eT_{reg} cells in RLNs and ATLOs (**Fig. 3.21**). The main genes in TNFRSF-NF-κB pathway reported to be involved in the development of eT_{reg} cells were also analyzed [181]. The results revealed that *Tnfrsf8*, *Tnfrsf9*, *Tnfrsf4* and *Tnfrsf1b* were significantly upregulated in eT_{reg} cells vs cT_{reg} cells, which confirmed the phenotype of cT_{reg} and eT_{reg} cells (**Fig. 3.21**). Interferon regulatory factor 4 (IRF4), i.e. a TCR-dependent transcription factor regulating eT_{reg} differentiation [183], was also found to be higher in eT_{reg} cells than that of cT_{reg} cells, but it was reduced in eT_{reg} cells in plaques (**Fig. 3.21**). These differences of phenotype and differentiation-related genes in T_{reg} cells reveal a severe dysfunction of T_{reg} cells in atherosclerotic plaques.

We next examined T_{reg} immunosuppressive function-associated genes. The expressions of *Tgfb1*, *Ctla4*, *Icos*, *Tigit*, *Il10*, and *Cd83* are important for T_{reg} cell

RESULTS

immunosuppressive activities [210, 211]. The expression of these genes was higher in activated eT_{reg} cells vs cT_{reg} cells in ApoE RLNs and ATLOs (**Fig. 3.21**). However, eT_{reg} cells in plaques had a lower expression of *Ctla4*, *Il10*, *Tigit* and *Cd83* when compared to eT_{reg} cells from other tissues. Moreover, a higher expression of *Tgfb1* was observed in plaque cT_{reg} and eT_{reg} cells, which has been documented to mediate T_{reg} cell suppressive function and drive the generation of Th₁₇ and RORγ⁺ T_{reg} cells [212, 213](**Fig. 3.21**).

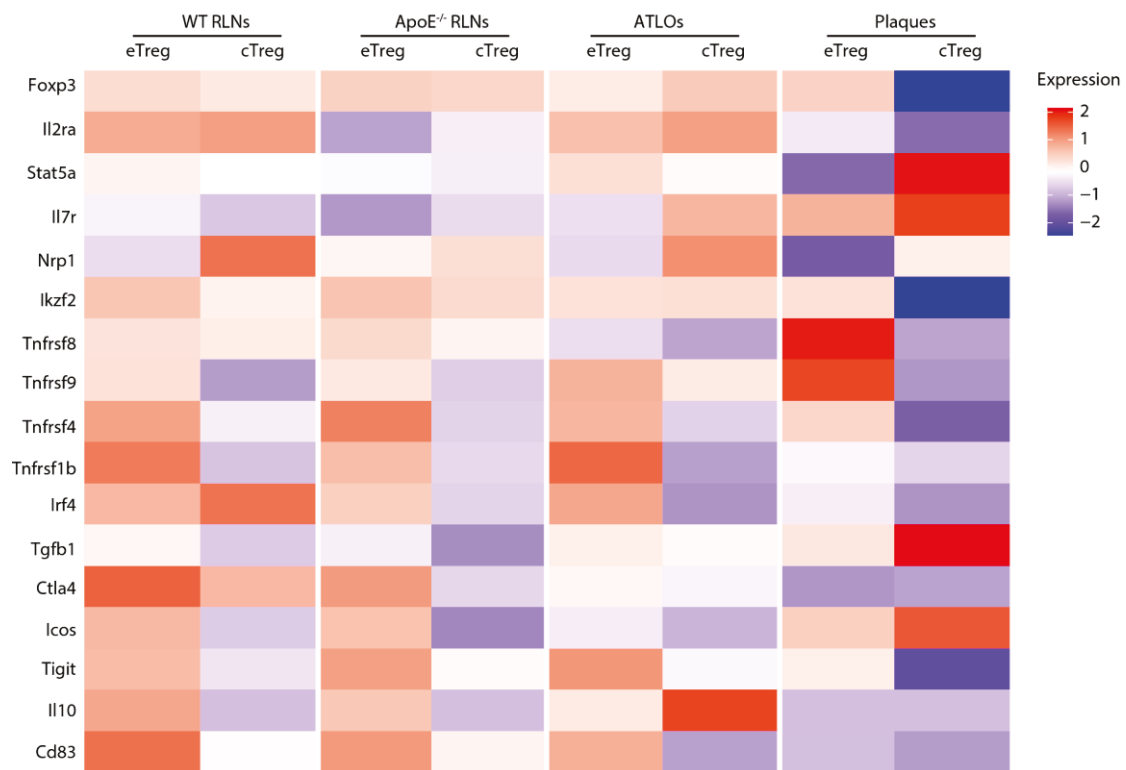


Fig. 3.21 The average expression of T_{reg} phenotype and function related genes in eT_{reg} and cT_{reg} cells of each tissue. Heatmap shows gene expression levels of selected function-associated genes in eT_{reg} and cT_{reg} cells. The red color represents high expression, while the blue color represents low expression.

The dysfunction of T_{reg} cells in atherosclerosis raises another key question, i.e. whether the T_{reg} cells differentiate into other effector Th cells, which has been documented in several atherosclerosis studies [63, 214]. Therefore, the gene expression of different Th cell markers was investigated in different tissues. Apart from a slight increase of *Cxcr3* and *Tbx21* in plaque cT_{reg} cells, the transcription factor *Tbx21* and *Bcl6* and the chemokine receptor *Cxcr3* and *Cxcr5*, which promote

RESULTS

Th₁ and T_{fh} differentiation, respectively, showed similar expression in all tissues (**Fig. 3.22**). However, the data showed eT_{reg} and cT_{reg} in all tissues had a low level of *Ifng*, the main proatherogenic cytokine of Th₁ cells (**Fig. 3.22**). Cytokine IL-4, secreted by Th₂ cells, also maintained low expression levels in all tissues (**Fig. 3.22**). However, its transcription factor *Gata3* and cell marker *Ccr4* were highly expressed in ATLO and plaque eT_{reg} and cT_{reg} cells relative to their counterparts in RLNs, with particularly pronounced expression in atherosclerotic plaques (**Fig. 3.22**). In addition, the cytokine and transcription factor associated genes of Th₁₇ cells, like *Il17a*, *Il17f*, and *Rorc* remained low in RLNs and ATLOs. In contrast, plaque eT_{reg} and cT_{reg} cells had a higher expression of *Il17a*, *Il17f*, *Rorc*, *Rora*, *Stat3*, and *Ccr6*, suggesting the differentiation of T_{reg} cells into Th₁₇-like exT_{reg} cells (or RORγt⁺ T_{reg} cells) (**Fig. 3.22**). This result led us to explore whether chronic inflammation of atherosclerosis promoted the conversion of T_{reg} cells into Th₁₇-like cells. It has been reported that T_{reg} cells convert to IL-17-producing cells in inflammatory conditions [215-217]. Using the T_{reg} cell lineage tracking mice, it has been reported that the conversion of T_{reg} cells to Th₁₇-like cells in autoimmune arthritis and atherosclerosis under high fat diet support disease progression [54, 63].

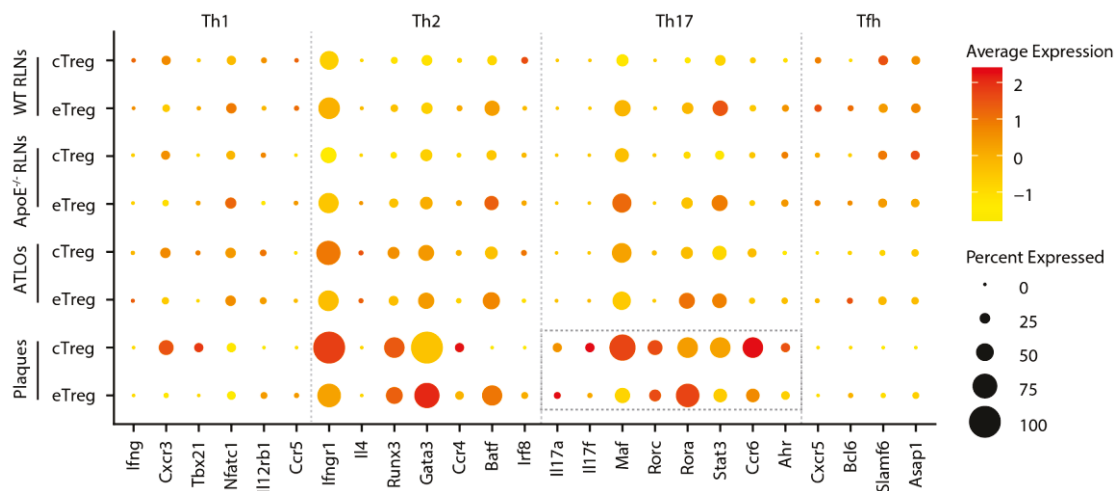


Fig. 3.22 Gene expression of Th-defining genes. Dotplot shows gene expression levels of each Th cell type-associated genes in eT_{reg} and cT_{reg} cells. The dot size represents the percentage of expressed cells. The color designates the average gene expression level.

To obtain direct evidence of T_{reg}-Th₁₇ conversion, T cells that concomitantly express

RESULTS

both T_{reg} and Th₁₇ cell markers were sought, which represent a transient state during T_{reg}-Th₁₇ conversion. A few T cells were found to co-express transcription factor *Foxp3* and *Rorc* genes. There were 2/1100 T_{reg} cells in WT RLNs, 1/1156 T_{reg} cells in ApoE^{-/-} RLNs, 2/712 T_{reg} cells in ATLOs, and 1/294 T_{reg} cells in plaques (**Fig. 3.23A**). Since T_{reg} cells lose the *Foxp3* expression in chronic inflammatory state, we also examined two further cell surface markers of T_{reg} cells, namely *Nrp1* (Neuropilin 1) and *Ii2ra* (encoding CD25). Cells double positive for *Nrp1* and *Rorc* were 0/1100 Treg cells in WT RLNs, 1/1156 T_{reg} cells in ApoE^{-/-} RLNs, 3/712 T_{reg} cells in ATLOs, and 2/294 T_{reg} cells in plaques (**Fig. 3.23A**). Cells double positive for *Ii2ra* and *Rorc* were observed 2/1100 Treg cells in WT RLNs, 0/1156 T_{reg} cells in ApoE^{-/-} RLNs, 1/712 T_{reg} cells in ATLOs, and 4/294 T_{reg} cells in plaques (**Fig. 3.23A**). In line with this hypothesis, two twin-T cells carrying the identical paired-TCRs were observed in our data. One T cell was a Foxp3⁺Rorc⁻ T_{reg} cell located in ApoE^{-/-} RLNs, while the other T cell was a Foxp3⁺Rorc⁺ T_{reg}-Th₁₇ converting cell obtained from plaques (**Fig. 3.23B**).

Since the predicted number of T_{reg} cells in the blood of aged WT and ApoE^{-/-} mice is small (less than 16 cells in WT or ApoE^{-/-} mice blood in our scRNA-seq data) according to our previous study based on flow cytometry approach (around 3.3-3.5% of blood CD45⁺ cells) [121]. In our current data, only a few cells with *Foxp3* gene expression but scattered in T cell subclusters were found. Therefore, the immunosuppressive function of peripheral T_{reg} cells between WT mice and ApoE^{-/-} mice could not be analyzed in our present data.

RESULTS

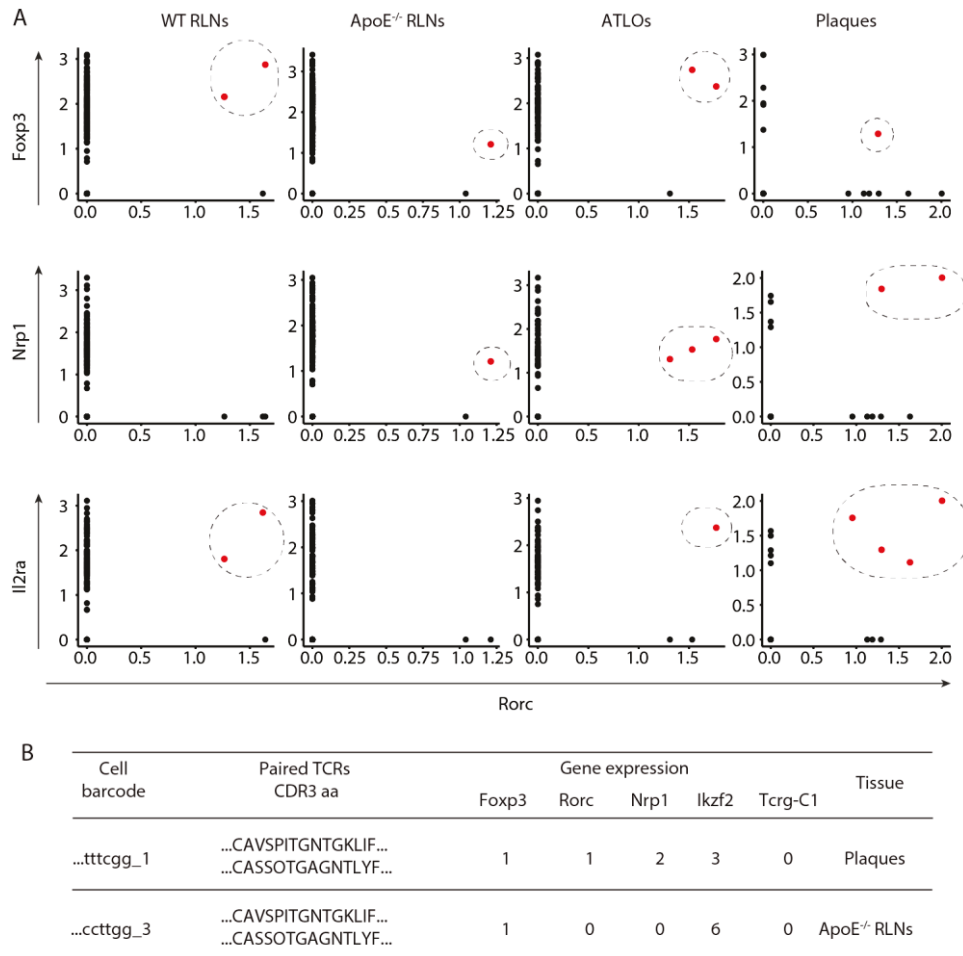


Fig. 3.23 The conversion of T_{reg} to Th₁₇-like cells in atherosclerosis. A. T_{reg} cells (including cT_{reg} and eT_{reg}) express T_{reg} marker and Th₁₇ marker simultaneously in four tissues. The dot in the dashed red circle indicates the cells are double positive for T_{reg} and Th₁₇ markers. Each dot represents one cell. **B.** Two cells with identical paired-TCR αβ chains confirm the conversion of T_{reg} cells to Th₁₇ cells.

A clinical study has shown that patients with severe coronary atherosclerosis have increased CD4⁺IL-17⁺ cells and decreased T_{reg} cells and CD4⁺IL-10⁺ T cells and the T_{reg}/Th₁₇ ratios were low [218]. More importantly, IL-17-producing T_{reg} cells have been reported to be much less effective in suppressing the activation of naïve T cells [53]. To decipher the potential mechanisms of Th₁₇ phenotype T cells derived from T_{reg} cells in atherosclerosis, pathways involved in regulating IL-17 expression were examined. Recent studies have suggested a dominant role of IL-1β over IL-6 in generating IL-17-producing T_{reg} cells [217]. IL-6, but not IL-23, exerts synergistic effects to enhance IL1R1 mRNA expression. In contrast to RLNs and ATLOs, plaque cT_{reg} cells had a high expression of IL-1R (*Il1r1*), IL-6R (*Il6ra*) and IL-23R (*Il23r*) (**Fig.**

RESULTS

3.24). The activation of IL-1R1 signaling recruits of MyD88 resulting in the activation of downstream NF- κ B and MAPK pathways to promote IL-17 expression. A higher expression of *Myd88*, AKT (*Akt1*), PI3K (*Pik3ca*), *Jun*, p50 (*Nfkb1*), *Rela* and IKK- β (*Ikbkb*), which are the main regulators in NF- κ B pathway, were observed in plaque cT_{reg} cells. The expression of p38 MAPK (*Mapk14*), ERK2 (*Mapk1*), and JNK1 (*Mapk8*), which participate in MAPK pathways were not found to be upregulated in plaque cT_{reg} cells (**Fig. 3.24**). More evidence is still needed on whether the IL-1R1 pathway promotes the T_{reg} and Th₁₇ conversion in atherosclerosis. Using the IL-1R1 knock out T_{reg} tracking mouse models should be used to address this problem.

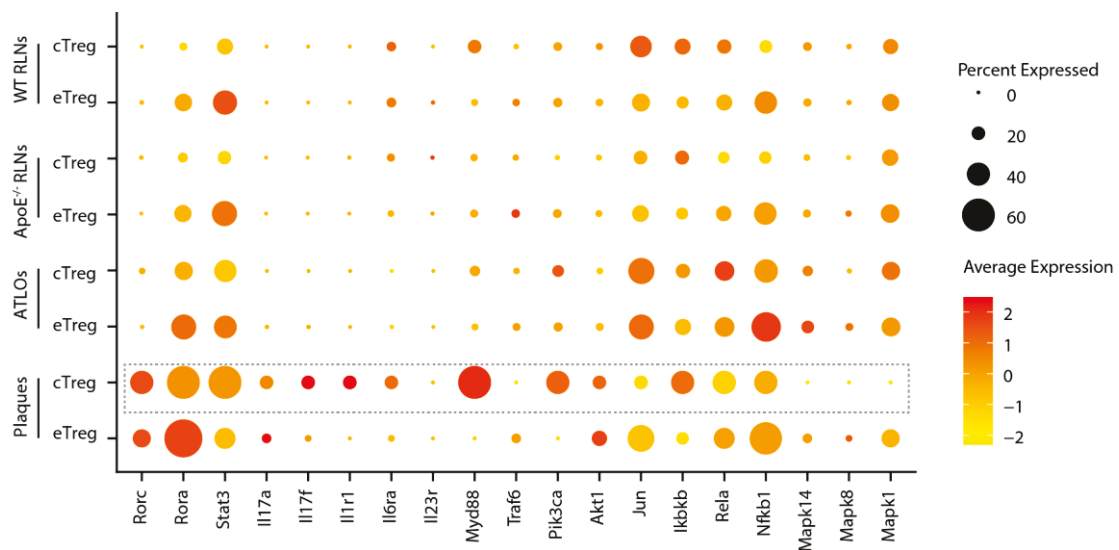


Fig. 3.24 Heatmap to show the expression of IL-1R1 pathway-associated genes in T_{reg} cells. The average expressions of IL-17 producing signaling pathway associated gene are shown in eT_{reg} and cT_{reg} cells of each tissue.

3.11 Atypical gene expression profiles of CD4 and CD8 T_{eff/mem} cells in atherosclerosis

Dysfunction of T_{reg} cells in atherosclerosis may result in the hyperreactivity of their counterpart T_{eff/mem} cells, which in turn may exacerbate the dysfunctional peripheral tolerance in atherosclerosis. Our present approach to combine the gene transcriptional profiles and the paired-TCR α/β sequences at single cell resolution, enabled us to compare transcript expression between clonally expanded T cells versus non-clonally expanded T cells in different tissues. To understand the

RESULTS

contribution of expanded and non-expanded T cells to the immune responses in atherosclerosis, the average gene expression of several gene sets reflecting the T cell biological functions were analyzed in expanded and non-expanded T cells of CD8 and CD4 T_{eff/mem} cells among tissues, namely T cell egress and residency, T cell activation and migration, T cell cytokine secretion and cytotoxicity, and T cell exhaustion. T cell homing and residency markers, i.e. *Ccr7*, *S1pr1* (Sphingosine-1-phosphate receptor 1), and *Sell* were first compared. CCR7 is a chemokine receptor that is involved in regulating T cell egress from peripheral tissue and homing to secondary lymphoid organs [219, 220]. S1PR1 and CD62L are reported to mediate T cell egress from lymphoid organs, and downregulation of these two proteins prevents T cell egress [221, 222]. These genes were found to be highly expressed in both the non-expanded CD4 and CD8 T_{eff/mem} cells versus their expanded T cell counterparts, suggesting expanded T cells were more prone to egress to peripheral tissues when compared to non-expanded T cells (**Fig. 3.25A and B, upper first panel**). More importantly, CD8 T_{eff/mem} cells in WT RLNs had higher expression of these genes in both expanded and non-expanded T cells, while a gradual reduction in these gene expressions was observed in ApoE^{-/-} RLNs, ATLOs (**Fig. 3.25A and B, upper first panel**). In particular, plaques showed even less expression of these genes, indicating the CD8 T_{eff/mem} cells in plaques predispose to residency in the atherosclerotic plaques. High expression of residency-associated genes was found in non-expanded CD4 T_{eff/mem} cells of WT RLNs, whereas lower expression of these genes was found in expanded CD4 T_{eff/mem} cells of WT RLNs and CD4 T_{eff/mem} cells (both expanded and non-expanded) in ApoE^{-/-} RLNs, ATLOs, and plaques (**Fig. 3.25A and B, upper first panel**). These results raised the possibility that atherosclerosis may promote T cell residency in the atherosclerotic plaques and atherosclerosis associated LNs.

For activation and migration-related genes, such as *Cxcr6*, *Ccr5*, *Slamf7* (Signaling lymphocytic activation molecule F7), *Adgre5* (Adhesion G Protein-Coupled Receptor E5), *S100a4* (S100 Calcium Binding Protein A4), *S100a6* (S100 Calcium Binding Protein A6), *Ctsw* and *H2-D1*, we did not find major differences between expanded

RESULTS

and non-expanded CD8 and CD4 T_{eff/mem} cells in RLNs, ATLOs and plaques (**Fig. 3.25A and B, upper second panel**). CD8 T_{eff/mem} cells in WT RLNs had low expression of activation and migration related genes. ApoE^{-/-} RLNs and ATLOs showed high expression of some of these genes. Notably, higher expression of these genes was observed in plaques compared to RLNs and ATLOs (**Fig. 3.25A upper second panel**). Similarly, CD4 T_{eff/mem} cells in WT RLNs also showed low expression of activation- and migration-related genes. Low expression of these genes was also observed ApoE^{-/-} RLNs, similar to WT RLNs (**Fig. 3.25B upper second panel**). Some of these genes were found with a relatively high expression in CD4 T_{eff/mem} cells of ATLOs (**Fig. 3.25B upper second panel**). Higher expression of activation and migration associated genes in CD4 T_{eff/mem} cells were detected in plaques (**Fig. 3.25B upper second panel**). These results suggest an activation phenotype of CD4 and CD8 T_{eff/mem} cells in atherosclerosis was more pronounced in atherosclerotic plaques.

Previous studies have shown that CD8 T cells had a high expression of cytotoxic and cytokine markers (*Cst7, Gzmb, Gzmk, Gzmm, Ifng, Nkg7, Prf1, Efhd2, Ccl5, Ccl4*) to execute cytotoxic effects on target cells. Expanded CD8 T_{eff/mem} cells expressed higher levels of cytotoxicity- and cytokine-related genes when compared to non-expanded CD8 T_{eff/mem} cells in RLNs, ATLOs and plaques (**Fig. 3.25A third panel**). Non-expanded CD8 T_{eff/mem} cells in RLNs and ATLOs expressed similar levels for most cytotoxicity- and cytokine- associated genes. However, some differences were found in expanded CD8 T_{eff/mem} cells, WT RLNs had higher expression of *Gzmm, Ifng, and Prf1*, while ApoE^{-/-} RLNs and ATLOs showed high expression of *Gzmb, Gzmk, and Ccl5*. CD8 T_{eff/mem} cells in plaques showed a relatively high expression of cytotoxicity- and cytokine-associated genes when compared to corresponding non-expanded and expanded CD8 T cells in RLNs and ATLOs (**Fig. 3.25A third panel**). These data support the concept that dysfunctional immune checkpoints promote more robust CD8 T_{eff/mem} cell reactions in atherosclerotic plaques. CD4 T helper cells can be classified into several subsets based on different transcription factors and secreted cytokines [26, 223]. Activated Th₁ cells upregulate immunostimulant-

RESULTS

associated cytokines IL-2, IFN- γ , lymphotoxin, and TNF- α , thereby inducing an inflammatory response [26, 224]. While Th₂ cells, which were considered as the counterpart of Th₁, produce IL-4, IL-5, IL-6, IL-10, and IL-13 [4]. Lymphotoxin-alpha (encoded by *Lta* gene) is secreted by Th₁ cells and considered a pro-inflammatory cytokine in systemic and local immune responses. In addition, *Lta* was found to be expressed in the atherosclerotic plaques and implicated in coronary heart disease [225]. IL-4, the major cytokine that mediates differentiation of Th₀ into Th₂ cells, is controversial with regard to its effect on atherosclerosis. Research showed IL-4^{-/-} ApoE^{-/-} double knock out mice had a 27% decrease of plaque area in aortic root compared to ApoE^{-/-} mice at 30 weeks of age, but at 45 weeks of age, there was no significant difference in aortic root in double knock out mice, but a 58% reduction was found in aortic arch [226]. Another study found no effect on atherosclerotic lesion in ApoE^{-/-} or Ldlr^{-/-} mice [227]. The expression of these genes will help us to unveil the phenotype and function of CD4 T_{eff/mem} cells in atherosclerosis. Therefore, the expression of Th cell related genes in expanded and non-expanded CD4 T_{eff/mem} cells in different tissues were compared. WT RLNs, ApoE^{-/-} RLNs and ATLOs displayed similar expression of different Th cell-associated cytokine and transcription factor genes, with high expression of the main cytokine gene *Ifng* for Th₁ and *Il4*, *Gata3* for Th₂. A relatively higher expression of Th₁-related genes *Lta* and *Tbx21* were found in plaques compared to ATLOs and RLNs, while the Th₂-related genes *Il4* and *Gata3* were expressed at a low level in plaque CD4 T_{eff/mem} cells (**Fig. 3.25B third panel**). More interestingly, Th₁₇-related genes *Rorc* and *Il17a* were notably expressed in plaque CD4 T_{eff/mem} cells relative to ATLOs and RLNs (**Fig. 3.25B third panel**). Taken together, plaque CD4 T_{eff/mem} cells were found to be more likely to express Th₁ and Th₁₇ phenotype- related genes, both of which are considered to play a pro-inflammatory effect on atherosclerosis.

RESULTS

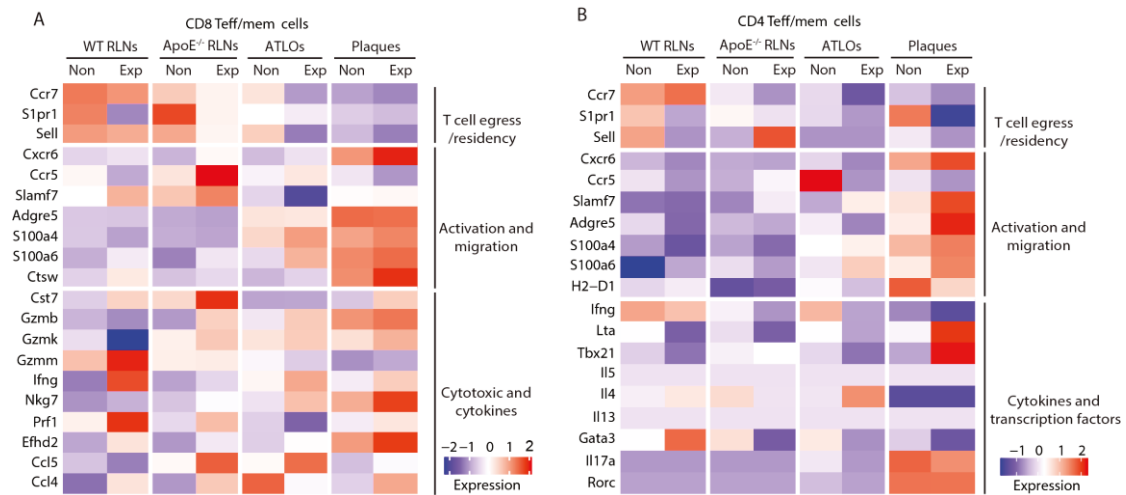


Fig. 3.25 Heatmap of average gene expression levels of selected function-associated genes in T cells (only expanded and non-expanded T cells were included for comparison). Gene expressions of T cell function-associated markers for homing, activation and migration, cytotoxicity and cytokine production in CD8 (**A**) and CD4 (**B**) $T_{eff/mem}$ non-expanded T cells versus expanded T cells from WT RLNs, ApoE^{-/-} RLNs, ATLOs, and plaques are shown. T cells with undetected TCRs were excluded from the assays.

Studies have demonstrated that exposure of T cells to chronic viral infection leads to upregulation of inhibitory PD-1 on viral-specific CD8⁺ T cells, thereby curtailing T cell proliferation and function, which is referred to as T cell exhaustion [228, 229]. PD-1 ligand-deficient *Ldlr*^{-/-} mice showed increased atherosclerotic lesions with higher numbers of CD4⁺ and CD8⁺ T cells compared to control *Ldlr*^{-/-} mice [230]. Apart from PD-1, exhausted T cells were found to co-express many other co-inhibitory molecules, like TIM3 (encoding by *Havcr2*), LAG3, CTLA4 and other transcription factors, which were found to be also implicated in T cell exhaustion [231]. Inhibiting these molecules could reverse T cell exhaustion [231-233]. Therefore, the average gene expression levels of exhaustion-related genes were compared in different tissues. Even though exhaustion signaling pathway- and transcription factor-associated genes were widely expressed in all tissues with the notable exception of CD4 $T_{eff/mem}$ cells in plaques (**Fig. 3.26A middle and lower panel**), CD8 $T_{eff/mem}$ T cells in ApoE^{-/-} mice had a relatively higher expression level of exhaustion surface receptor-related genes when compared to WT mice, which may contribute to limiting the immune responses in ApoE^{-/-} mice (**Fig. 3.26A upper panel**). Moreover,

RESULTS

expanded CD8 T cells expressed more exhaustion surface marker genes than non-expanded T cells (**Fig. 3.26A upper panel**). However, most exhaustion-related genes, such as *Pdcd1*, *Tigit*, *Lag3* and *Ctla4* were found to be extensively expressed in expanded and non-expanded CD4 T_{eff/mem} cells of RLNs and ATLOs, but not in plaques (**Fig. 3.26B upper panel**).

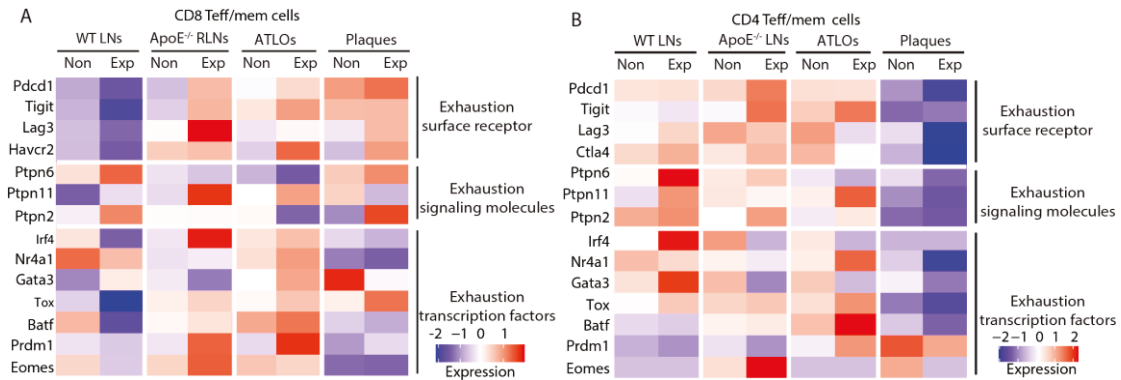


Fig. 3.26 Heatmap of average gene expression levels of T cell exhaustion-associated genes in CD8 (A) and CD4 (B) T_{eff/mem} cells (only expanded and non-expanded T cells were included for comparison. Cells with non-detected TCR were excluded for analysis). Genes contribute to the exhaustion surface receptor, signaling molecules and transcription factors are shown. T cells with undetected TCRs were excluded from the assays.

The prominent downregulation of *S1pr1*, *Sell*, *Ccr7* and upregulation of *Cxcr6*, *Pdcd1* in plaque CD8 T_{eff/mem} cells also led us to examine the presence of tissue resident memory T cells (TRMs) in plaques. TRMs have been described as the non-circulating T cell pool and are thought to permanently reside in tissues including in disease sites thereby providing long-lived local immune surveillance. They have been reported to be present in many tissues such as brain, lung, skin, and reproductive tract, and are involved in various diseases like cancer, infection, and autoimmune diseases [222, 234]. To keep TRMs resident at the peripheral disease sites, TRMs suppress the expression of CD62L, S1PR1, S1PR5, CX3CR1 and transcription factor Klf2, Klf3 to effectively block egress and promote the expression of CXCR6, CD49a (*Itga1*), CD103 (*Itgae*) to assist TRMs homing and retention [222, 235]. CD69 and PD-1 were also reported as markers for TRM identification [222, 236, 237]. To assess the presence of TRMs in plaques, gene expressions defining TRMs were analyzed in different CD8 memory T cells. CD8 T_{em} cells in plaques were

RESULTS

observed to have a prominent gene expression profile of TRM phenotypes relative to ATLOs and RLNs (**Fig. 3.27**). This data indicated that CD8 T_{em} cells in plaques have TRM phenotype.

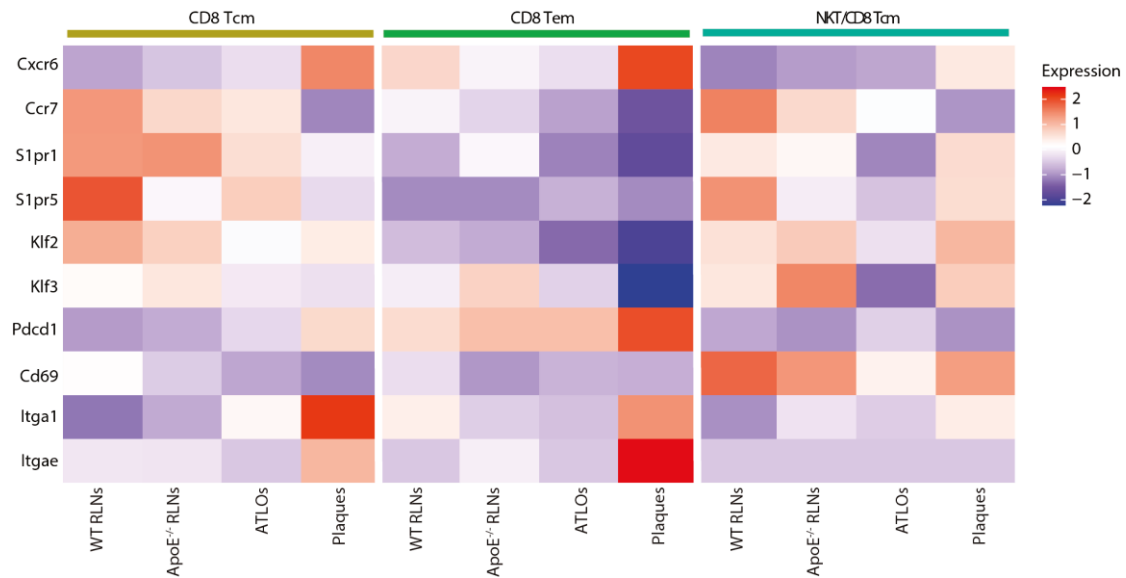


Fig. 3.27 Heatmap of average gene expression levels of TRM phenotype-related genes in different CD8 memory T cells of each tissue.

To investigate whether the compromised tolerance checkpoints alter the function of CD4 and CD8 T_{eff/mem} cells in peripheral blood, they were examined in blood of WT and ApoE^{-/-} mice. Data showed these genes had similar expression levels in WT blood and ApoE^{-/-} blood (**Fig. 3.28**) supporting our conclusion that tolerance breakdown of CD4 and CD8 T_{eff/mem} cells in atherosclerosis occurs at the level of tissues subsequent to their emigration from the circulation.

RESULTS

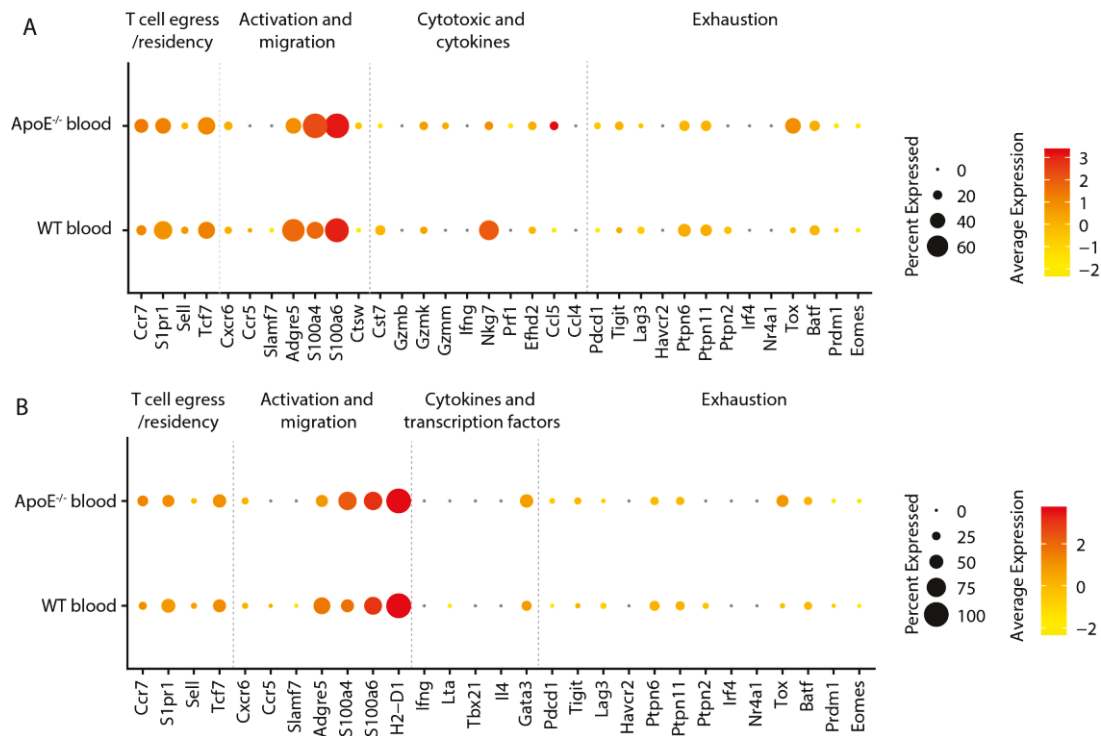


Fig. 3.28 Dotplot to display of average gene expression levels of selected function-associated genes in T cells. Gene expressions of T cell function-associated markers for T cell homing, activation and migration, cytokine production and exhaustion are shown for CD8 (A) and CD4 (B) T_{eff/mem} cells in WT blood and ApoE^{-/-} blood.

3.12 High expression of co-stimulatory and co-inhibitory molecules in myeloid cells in atherosclerosis

APCs present antigen-MHC-II/MHC-I complexes on their surface to activate CD4/CD8 T cells [238]. They also express various inhibitory molecules to induce T cell tolerance [114, 115]. We wished to explore the impact of myeloid cells on activation and exhaustion of CD8 T cells in atherosclerosis. For this purpose, we examined the expression of co-stimulatory (*Cd80*, *Cd86*, *Cd83*, *Cd40*) and co-inhibitory (*Cd274*/PD-L1, *Pdcd1lg2*/PD-L2, *Lgals3*/Galectin3, *Cd200*, *Fas*, *Icosl*) molecules on different myeloid cell populations. DCs had a relatively higher co-stimulatory gene expression relative to macrophages (Fig. 3.29A). WT RLNs showed comparable expression of co-stimulatory genes with ApoE^{-/-} RLNs in myeloid cell types (Fig. 3.29A). ATLOs showed a slight increase of *Cd83*, *Cd86* in Lyve1⁺ res-like MΦ and Trem2^{high} MΦ compared to WT RLNs (Fig. 3.29A). Compared to

RESULTS

their counterparts in RLNs, plaque myeloid cells acquired a moderate increase of co-stimulatory gene expressions in CD11c⁻ DC, Lyve1⁺ res-like MΦ, Trem2^{high} MΦ, suggesting a potential robust T cell priming effect of myeloid cells in atherosclerotic plaques (**Fig. 3.29A**). The antigen presentation score was calculated to assess the antigen presentation capacity of myeloid cells in each cluster. All the DC and macrophage clusters had potent antigen presentation capability (**Fig. 3.29B**). This result showed that WT RLNs and ApoE^{-/-} RLNs had similar antigen presentation capabilities and ATLOs showed a further increase of antigen presentation capability compared to RLNs. Yet, the highest capability of different DC and macrophage clusters to present antigen were observed in plaques compared to RLNs and ATLOs (**Fig. 3.29B**), pointing to a strong capacity of APCs in atherosclerotic plaques to induce T cell activation (**Fig. 3.29B**). Moreover, CD11c⁻ DCs obtained more inhibitory molecules expression when compared to other DC and macrophage clusters, which indicates an immunosuppressive phenotype of CD11c⁻ DCs (**Fig. 3.29A**). CD11c⁻ DCs in plaques showed further increases of *Cd247*, *Pdcd1lg2*, *Cd200*, *Fas*, and *Icosl* than their counterparts in ATLOs and RLNs (**Fig. 3.29A**). Conventional tolerogenic DCs are suggested to derive from immature DCs and semi-mature tolerance regulating DCs. They are characterized by low levels of co-stimulatory molecules, weak antigen processing and presentation, but enhanced immunosuppressive function mediated by inhibitory molecules [114, 115]. However, different from the conventional tolerogenic DCs, the immunosuppressive CD11c⁻ DCs in plaques also displayed higher co-stimulatory expression and antigen presentation capacity, which suggest an atypical profile of CD11c⁻ DCs indicative for the hypothesis that they may mediate the atypical CD8 T cell immune responses in atherosclerosis. In consideration of the dominant population of myeloid cell in plaques, the abundance of inhibitory and stimulatory molecules in each tissue was calculated by multiplying the coefficient of their cell percentage in total CD45⁺ leukocytes, which may reflect the possibility of T cell activation and suppression are induced by myeloid cells. The data showed similar values of each gene expression profile between WT RLNs and ApoE^{-/-} RLNs. ATLOs showed increase values in some of these genes, such as

RESULTS

Cd83, *Cd86*, and *Lgals3*. Whereas plaques had higher abundance of both inhibitory and stimulatory molecules relative to ATLOs and RLNs (**Fig. 3.29C**).

The cell-cell interactions of CD8 T_{em} with myeloid cells were predicted by using established computation approaches. A stronger interaction of PDCD1 with its ligands (*CD274*, *PDCD1LG2*, *FAM3C*) in plaques were detected when compared to ATLOs and RLNs, which support a potent immunosuppressive role of myeloid cells in atherosclerotic plaques (**Fig. 3.29D**).

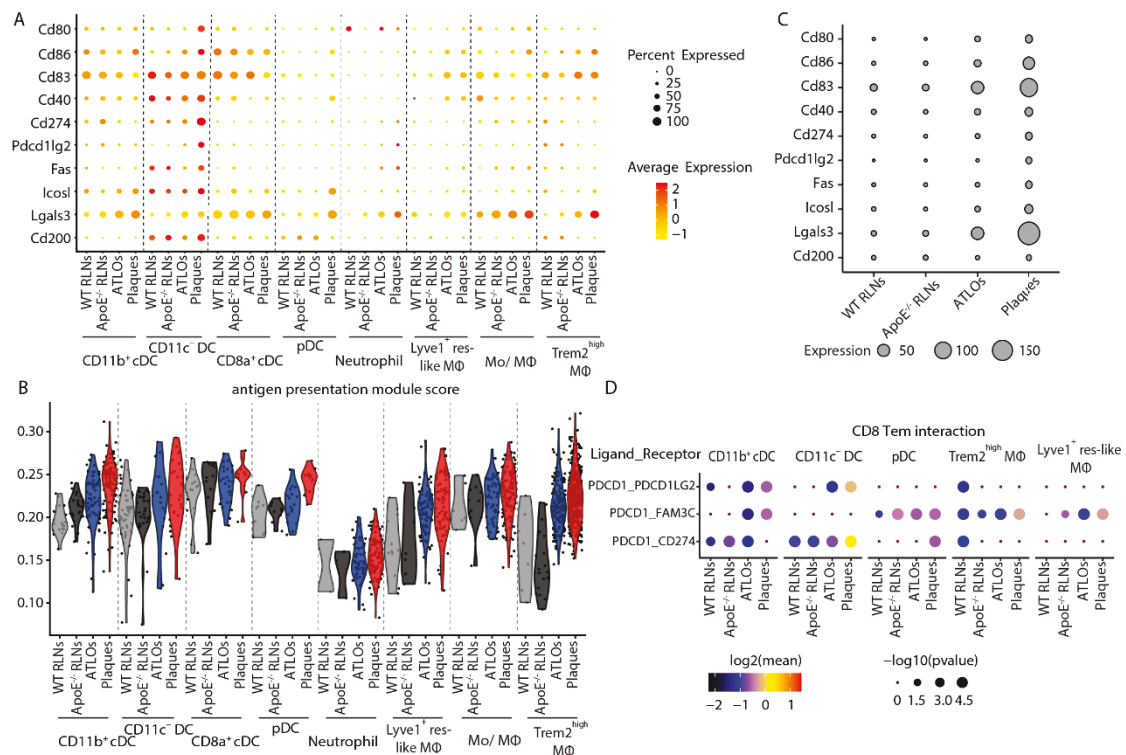


Fig. 3.29 Myeloid cells mediate immunosuppressive functions on T cells. **A.** The expression of myeloid cell-derived co-stimulatory genes (*Cd80*, *Cd86*, *Cd83*, *Cd40*) and checkpoint inhibitors (*Cd274*/*PD-L1*, *Pdcd1lg2*/*PD-L2*, *Fas*, *Icosl*, *Lgals3*, *Cd200*) in sub-clusters of myeloid cells in each tissue. The dot size represents the cell expression percentage. The color designates the average expression level. **B.** The antigen presentation module score of each myeloid cluster in each tissue. **C.** The abundance of co-stimulatory genes and checkpoint inhibitors expressed by different myeloid subsets. **D.** Predicted interactions of PDCD1 and its ligands between CD8 T_{em} cells with myeloid sub-clusters in WT RLNs, ApoE^{-/-} RLNs, ATLOs, and plaques. The color represents the ligand-receptor interaction value. The dot size indicates the interaction p value.

RESULTS

3.13 Cell-cell interactomes in atherosclerotic plaques, ATLOs, ApoE^{-/-} RLNs and WT RLNs

Using established computational approaches [171], cell-to-cell communications between different immune cells were examined. These interactions between different cell types may contribute to T cell phenotype modulation and adaptation in atherosclerotic plaques when compared to LNs (**Fig. 3.30**). The interactions of different cell types in four tissues were first analyzed. The data showed there were numerous and complex interaction networks in each tissue. WT RLNs and ApoE^{-/-} RLNs showed a similar interaction network. Increased interaction scores in ApoE^{-/-} RLNs Lyve1⁺ res-like MΦs was found relative to WT RLNs (**Fig. 3.30A**). In contrast to WT RLNs, some significantly increased interactions were observed in ATLOs and plaques such as Trem2^{high} MΦs, Lyve1⁺ res-like MΦs, neutrophils and Mo/MΦ, suggesting stronger and more complex interactions in ATLOs and plaques (**Fig. 3.30A**). Some T cell clusters such as CD8 T_{em}, CD8 T_{cm}, cT_{reg} and γδ T cells showed slightly increased interactions with other cells in ATLOs and atherosclerotic plaques compared to WT RLNs (**Fig. 3.30A**). These data provided a first blueprint of the mutual interactions within different immune cells in atherosclerosis.

Since compromised immune tolerance induced an atypical phenotype of CD8 T_{eff/mem} cells in atherosclerosis, we predicted the cell-to-cell interaction map of CD8 T_{em} with other immune cell subsets within plaques, ATLOs, and RLNs to help to get insight into the mechanisms of these interactions (**Fig. 3.30**). *SELL* encodes the T cell homing receptor CD62L. A low expression of *SELL* in T_{em} cells maintains their movement capacity. The SELL(CD62L)-SELPLG(CD162) interaction was almost undetectable supporting the veracity and significance of the algorithms employed here (**Fig. 3.30B**). The interaction map showed a distinctive feature of CD8 T_{em} in tissues (**Fig. 3.30B**). WT RLNs and ApoE^{-/-} RLNs showed similar interactions in CD8 T_{em} with other cells (**Fig. 3.30B**). PDCD1 (also known as PD-1) is a marker of T cell exhaustion and regulates T cell immunity [97]. Low interaction values of PDCD1 with their receptors, i.e., PDCD1LG2 (PD-L2), FAM3C and CD274 (also known as PD-L1) were observed in CD8 T_{em} cells of WT RLNs and ApoE^{-/-} RLNs. CD8 T_{em} cells in

RESULTS

ATLOs and plaques showed higher interaction values between PDCD1 and their receptors with other cells when compared to RLNs (**Fig. 3.30B**). Strong CXCR6-CXCL16 interactions were found to be present in CD8 T_{em} cells, CD4 T_{reg} and CD4 T_{em} cells and $\gamma\delta$ T cells of plaques when compared to RLNs (**Fig. 3.30B, other data were not shown**). CXCR6-CXCL16 interaction has been reported to be correlated with atherosclerosis by recruiting T cells and macrophages to accumulate in plaque lesions [239, 240]. CCL5 is a chemokine and is important for the maintenance of CD8 memory function [241]. Plaques and ATLOs showed extensive interactions when compared to RLNs on CCL5-CCR5, CCL5-CCR4, CCL5-CCR1 (**Fig. 3.30B**). Of note, the communication of CCL4, a chemoattractant for leukocytes recruitment, with its receptors were found in ATLOs and RLNs, but they were reduced in plaques (**Fig. 3.30B**). IFN γ can be expressed by CD8 T cells after activation. It upregulates the expression of MHC-I, which facilitates the CD8 T cells to recognize antigens [242]. The intensive interaction of IFNG-Type II IFNR was found in plaques and ATLOs CD8 T_{em} cells, while it was weak in WT RLNs and ApoE^{-/-} RLNs (**Fig. 3.30C**). All these data support to a distinct CD8 T_{em} cell-to-cell interactions in atherosclerotic plaques and atherosclerosis-associated LNs.

RESULTS

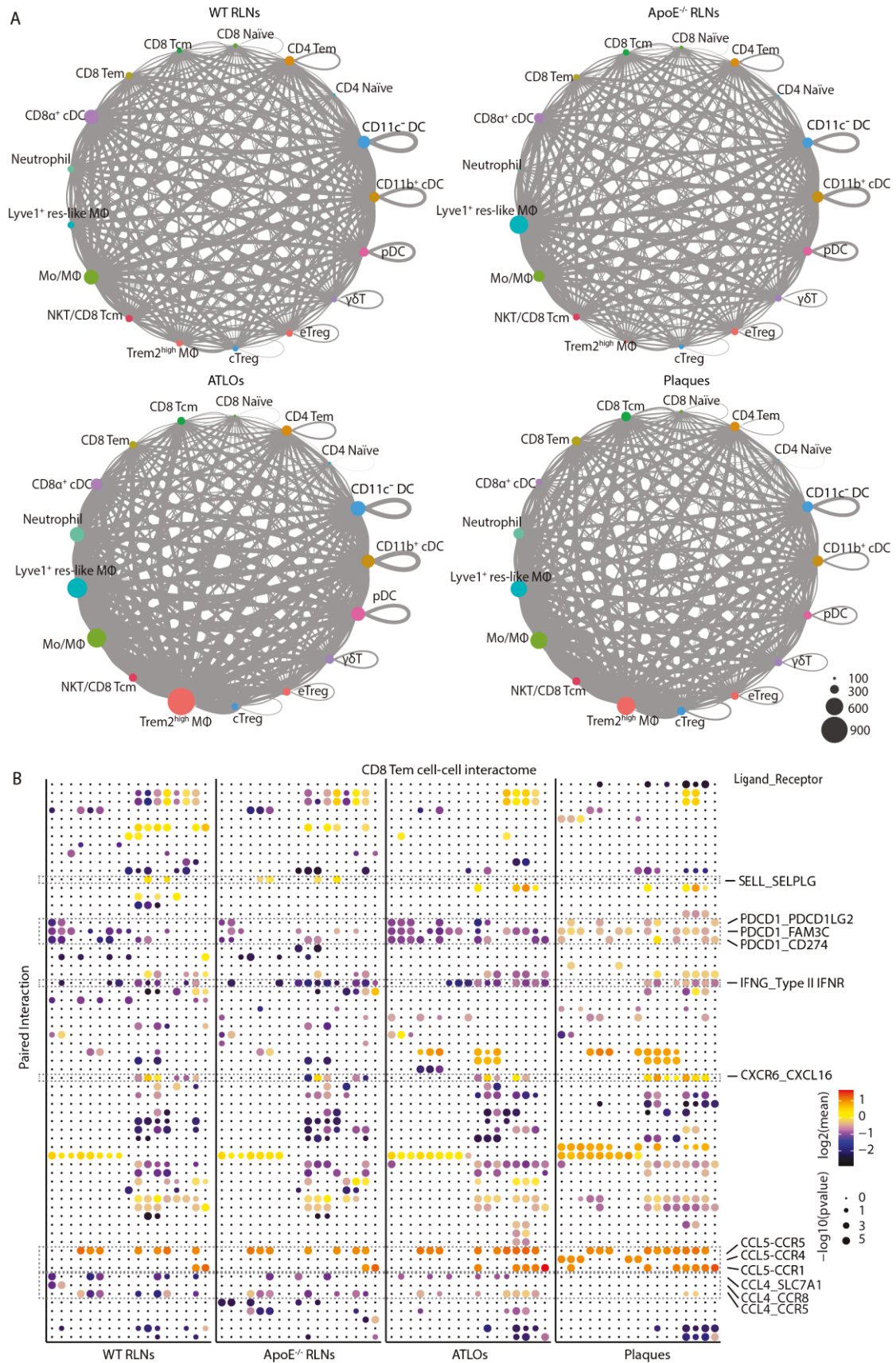


Fig. 3.30 Cell-cell interactome map predicts T cell dysfunction in plaque. A. Predicted cell-cell interactions of different cell types among four tissues represented by circular plots. The dot size

RESULTS

designates the total interaction number of each different cell type. The thickness of ribbons connecting cell types represents the interaction numbers between these two different cell types. **B.** Predicted cell-cell interactome of CD8 T_{em} cells with other immune subsets. The x axis represents the CD8 T_{em} cells interacts with all 27 immune subsets; the y axis designates the predicted paired ligand-receptor interactions according to database. Interactions contributing to T cell dysfunction in the plaque are listed on the right. The size of circles is based on $-\log_{10}$ p values; color scheme is based on log2 value.

3.14 T cell adaptation in atherosclerotic plaques

Migration and adaptation of T cells to non-lymphoid tissues is important to immune surveillance. Studies have documented different phenotypes of T_{reg} cells in non-lymphoid tissues and lymphoid tissues [181]. A recent study reported that auto-aggressive CXCR6⁺ CD8 T cells in the liver of murine nonalcoholic steatohepatitis showed different profiles of CXCR6⁻ CD8 T cells versus normal mice [243]. However, T cell adaptations in atherosclerotic lesions remain unclear. Our present scRNA-seq and scTCR-seq pairing approach can address this question by focusing on the cells with identical TCRs if we find them in different tissues. The cells used for this analysis need to meet two criteria: (i) cells with identical paired TCR; (ii) they must be located in two or more different tissues. Thus, a total of 81 CD8 T_{eff/mem} cells (28 T cells in plaques, 27 T cells in ATLOs, and 26 T cells in ApoE^{-/-} RLNs) from several T cell clones that met our criteria were included in the analysis (**Fig. 3.31A**). The DEGs of plaque T cells with their counterpart T cells in ATLOs and ApoE^{-/-} RLNs were examined. 7 upregulated genes (*Cxcr6*, *Cd8b1*, *S100a6*, *Lgals1*, *S100a4*, *H2-D1*, *Reep5*) and 3 downregulated genes (*mt-Atp8*, *mt-Co3*, *mt-Co1*) between plaque CD8 T_{eff/mem} cells and their counterparts in ATLOs, ApoE^{-/-} RLNs were detected (**Fig. 3.31B**). These transcripts showed a progressive increase or reduction in expression from ApoE^{-/-} RLNs, ATLOs to plaques (**Fig. 3.31B**). Different T cell clones were found to have similar gene expression profiles as shown in **Fig. 3.31B**, which indicates different T cell clones have less impact on our result (**Fig. 3.31C**). Of note, several of

RESULTS

these 10 DEGs were correlated with T cell activation and migration, such as *Cxcr6*, *S100a6*, *S100a4*, and *Cd8b1*. *Cxcr6* has been reported to contribute to the migration and activation of T cells during inflammation and play a proatherogenic role in atherosclerosis [239, 244]; *S100a6* and *S100a4* encode calcium-binding proteins involved in a broad range of biological functions mediating cell migration, proliferation, and differentiation [245]. They have also been reported to regulate T cell infiltration and cytotoxicity functions [246]. *Lgals1* has been demonstrated to be involved in T cell immune responses. *Lgals1*^{-/-} mice showed impaired suppressive function of T_{reg} cells, enhanced Th₁, Th₁₇ responses and are more susceptible to autoimmune diseases [247, 248]. *Lgals1*^{-/-} mice showed an increase of CD8 T cell infiltration and cytokine secretion in a contact hypersensitivity mouse model [249]. *Reep5* is involved in regulating endoplasmic reticulum organization, but its role in T cell immune responses is still elusive. *mt-Atp8*, *mt-Co3*, and *mt-Co1* are mitochondrial-related genes, which contribute to cellular energy metabolisms. Next, the expression levels of upregulated *Cxcr6*, *Lgals1*, *Reep5*, and *S100a6* in all T cell subsets were examined. This may help us to investigate whether the T cell adaptation in atherosclerotic plaques are T cell subtypes dependent (**Fig. 3.31D**). The data showed that different T cell subsets expressed different levels of *Cxcr6*, *Lgals1*, *Reep5* and *S100a6* in RLNs, ATLOs, and plaques. For example, *Cxcr6* was predominantly expressed by CD8 T_{eff/mem} cells. *Lgals1* and *S100a6* were highly expressed by CD8 T_{eff/mem} cells, CD4 T_{reg} cells, and CD4 T_{eff/mem} cells, while *Reep5* was expressed by all T cell subsets (**Fig. 3.31D**). However, all these genes showed higher expression levels in plaques when compared to ATLOs and RLNs (**Fig. 3.31D**). Our present results reveal that the T cell adaption in atherosclerosis may be modulated by regulating T cell function-associated genes. Our data propose a new paradigm of T cell regulation and tolerance in atherosclerosis.

RESULTS

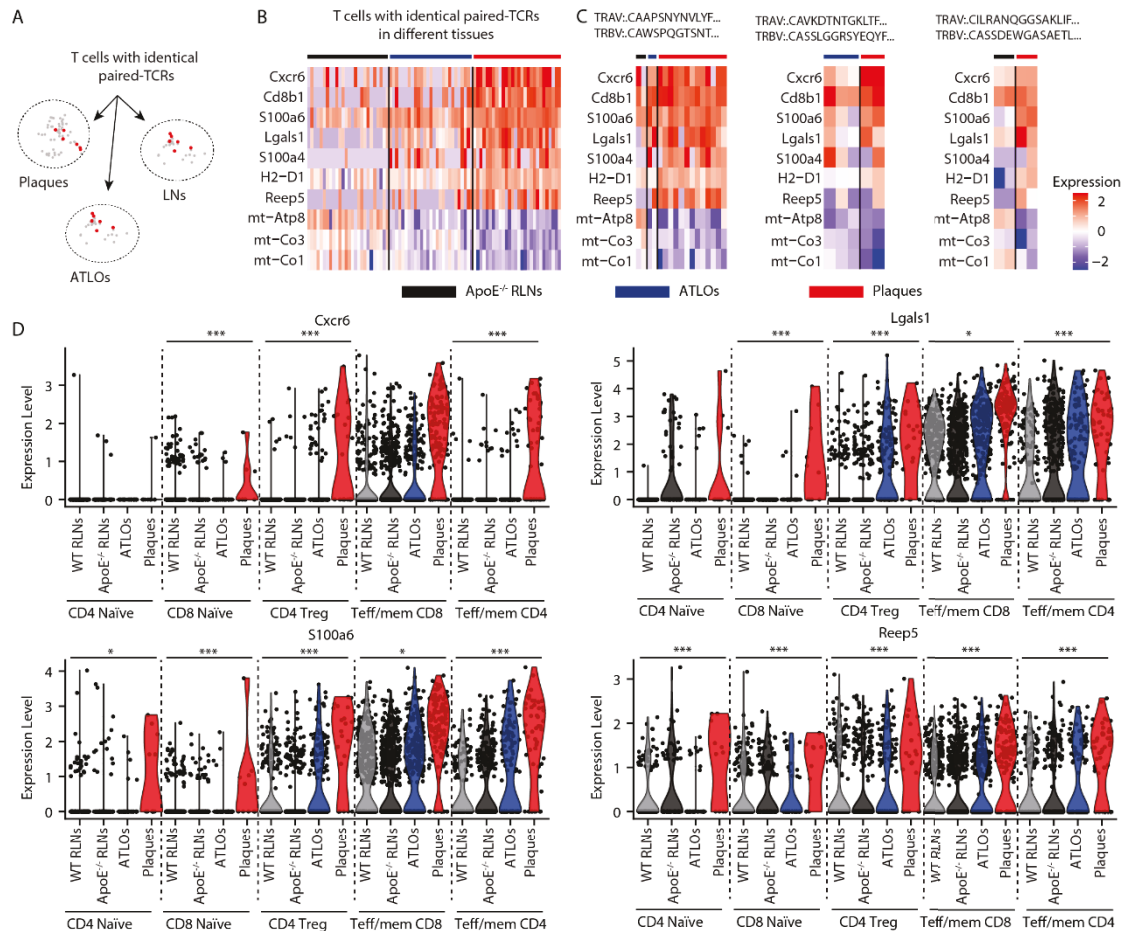


Fig. 3.31 Delineation of plaque microenvironment-induced T cell adaption. **A.** Schematic view of the design of the experiment. **B.** Heatmap of DEGs of pooled T cells carrying the identical paired-TCRs in different tissues. Each row represents one individual T cell. $n = 28$ individual T cells in plaques, 27 individual T cells in ATLOs, and 26 individual T cells in ApoE^{-/-} RLNs. DEGs were detected by Wilcoxon Rank Sum test with adjusted P value < 0.05 in Seurat package. **C.** Heatmap of plaque-induced genes in three T cell clones. T cells with the identical paired-TCR sequences from different tissues are compared. The CDR3 aa sequences of the paired TCR α/β chains are listed at the top of the heatmap. **D.** Violin plots showed *Cxcr6*, *Lgals1*, *Reep5* and *S100a6* gene expression by different T cell subsets. Each dot represents one cell. The comparison of gene expression levels of different T cell subtypes in tissues were performed by the Kruskal-Wallis rank sum test. The differences between two different tissues were compared by Kruskal–Wallis test with Dunn's non-parametric all-pairs comparison test. The p values were adjusted by Benjamini Hochberg method. * designates $p < 0.05$, ** designates $p < 0.01$, *** designates $p < 0.001$. Only significant differences in four tissues were shown.

3.15 Atherosclerotic plaques are home to IL-17-producing $\gamma\delta$ T cells

We showed above that $\gamma\delta$ T cells increase in ATLOs and plaques accounting for

RESULTS

around one fourth of T cells in plaques (**Fig. 3.11F**). However, its effect on atherosclerosis remains elusive [49]. Thus, the pathway enrichment analysis was used to search for biological functions of $\gamma\delta$ T cells. Many pathways involved in inflammation and immune responses were identified, including Th₁₇ cell differentiation, regulation of T cell activation, neutrophil degranulation, interferon-gamma production, and inflammatory responses (**Fig. 3.32**). This may provide clues for us to study the functions of $\gamma\delta$ T cells.

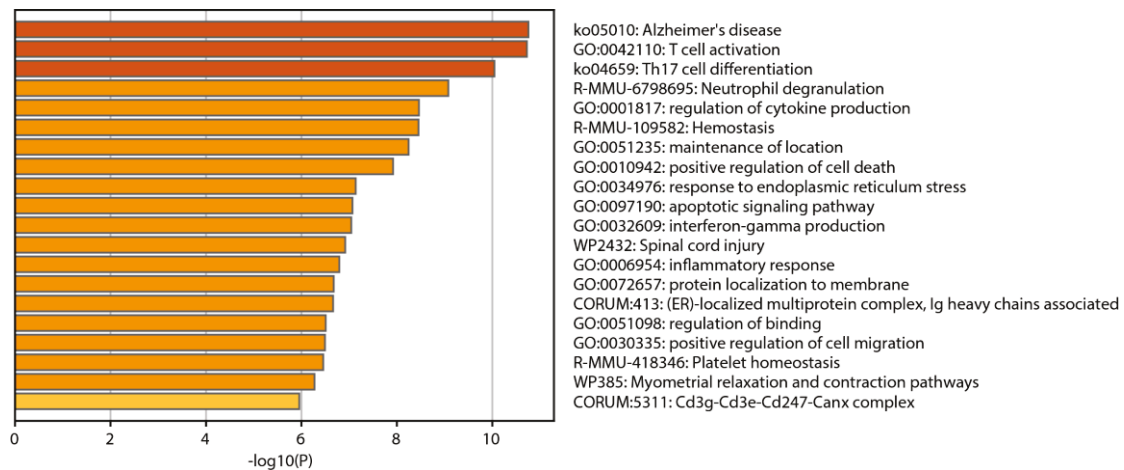


Fig. 3.32 Pathway enrichment to analyze $\gamma\delta$ T cells. DEGs of $\gamma\delta$ T cells against other T cells were used for pathway enrichment analysis.

To find differences of the $\gamma\delta$ T cells in atherosclerosis, DEGs between $\gamma\delta$ T cells in ApoE^{-/-} RLNs, ATLOs, plaques and their counterparts in WT RLNs were examined, respectively. Major differences were found in plaques compared to WT RLNs, while only a few DEGs were found to be upregulated in ATLOs (*Tagln2*, *S100a6*, *Ckb*, *Fxyd5*, *Vim*, *Anxa2*, *Crip1*) and ApoE^{-/-} RLNs (*mt-Atp8*) compared to $\gamma\delta$ T cells in WT RLNs. Volcano plots were used to visualize the differences of $\gamma\delta$ T cells between plaques and WT RLNs (**Fig. 3.33A**). The data showed that *Cd163/1* (*Scart1*), *Blk*, *S100a6*, *Cxcr6*, *Tmem176a*, *Tmem176b* were significantly upregulated in plaque lesions (**Fig. 3.33A and B**). $\gamma\delta$ T cells commit to IFN γ -producing or IL-17-producing $\gamma\delta$ T cells during intra-thymic maturation [250]. CD27 and NK1.1 (encoded by *Klrb1c*) were demonstrated to distinguish IFN γ -producing and IL-17-producing $\gamma\delta$ T cells, respectively [251]. CD27⁻ $\gamma\delta$ T cells had a high production of IL-17 after activation

RESULTS

with phorbol 12-myristate 13-acetate (PMA) *in vitro*, whereas CD27⁺ $\gamma\delta$ T cells showed significant IFN γ and TNF secretion. Studies documented that the transcription factor SRY-Box Transcription Factor 13 (*Sox13*) and *Rorc* were required for the development of IL-17-producing $\gamma\delta$ T cells. Apart from the above-described markers to separate these two populations, IL-17-producing $\gamma\delta$ T cells were reported with higher levels of CCR6, IL-23R, IL-1R1, and IL-7Ra, while IFN γ -producing $\gamma\delta$ T cells had a higher expression of CD122 (*Il2rb*) [250]. Next, to explore different $\gamma\delta$ T cells in atherosclerosis, gene expressions of these two phenotypes of $\gamma\delta$ T cells in different tissues were compared. Of note, the data displayed IL-17-producing $\gamma\delta$ T cells associated genes were highly expressed in RLNs, ATLOs and plaques when compared to IFN γ -producing $\gamma\delta$ T cells associated genes (**Fig. 3.33B**). Further, $\gamma\delta$ T cell in plaques acquired higher expression of IL-17-producing $\gamma\delta$ T cell-related genes compared to their counterparts in SLOs and ATLOs (**Fig. 3.33B**).

$\gamma\delta$ T cells recognize antigens without MHC presentation, and recent studies demonstrated they could recognize phosphorylated prenyl metabolites and lipids in complex with cluster of differentiation 1 molecules [46]. Even though we do not know the exact role of $\gamma\delta$ T cells (or IL-17-producing $\gamma\delta$ T cells) in atherosclerosis progression, further studies are needed by considering the important role of $\gamma\delta$ T cells present lipid antigens in triggering atherosclerosis and the different phenotypes of $\gamma\delta$ T cells in ApoE^{-/-}, WT mice.

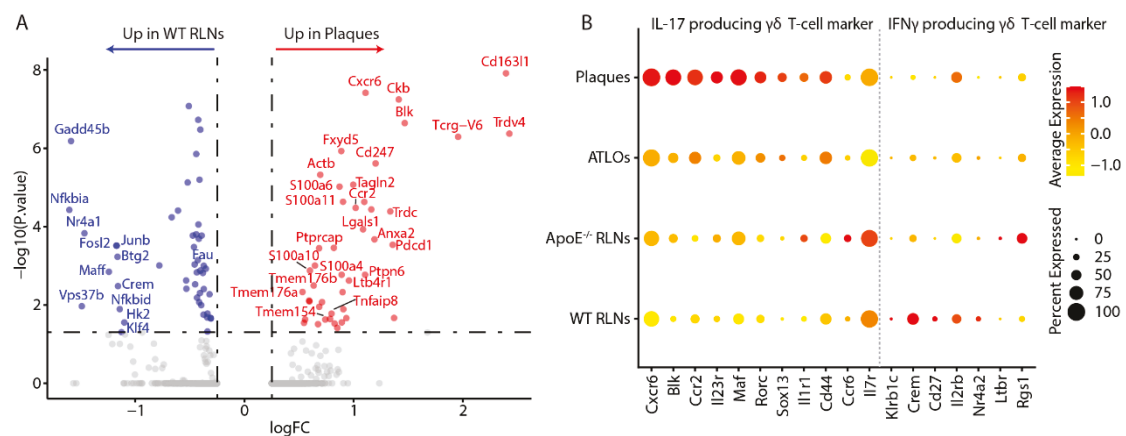


Fig. 3.33 The IL-17-producing $\gamma\delta$ T cells in atherosclerotic plaques. **A.** Volcano plots show the differential expression genes of $\gamma\delta$ T cells between atherosclerotic plaques and WT RLNs. The red

RESULTS

dots represent significantly upregulated genes in atherosclerotic plaques, the blue dots indicate significantly downregulated genes. **B.** Dot plots display gene expression associated with IFN γ -producing and IL-17-producing $\gamma\delta$ T cells in plaques, ATLOs, ApoE^{-/-} RLNs and WT RLNs.

3.16 Integrative analysis of murine and human plaques

3.16.1 scRNA-seq integration analysis reveals similar CD8 T cell tolerance dysfunction in human and mouse atherosclerotic plaques

To get a better understanding of the T cell subsets in human and murine atherosclerotic plaques and the possibility of tolerance dysfunction, we attempted to integrate published human versus our mouse scRNA-seq data. The integration method in the Seurat package enabled us to identify the shared cell types across different samples [252]. After integration analysis, all datasets were integrated, indicating that the method had largely removed batch effects caused by different experimental conditions, ages, and species (**Fig. 3.34A**). A total of 6368 cells were separated into 15 clusters (**Fig. 3.34B**). Based on DEGs and canonical gene markers for different cell types, each cluster was named as follows: cluster 1: CD8 T_{em}-1, cluster 2: $\gamma\delta$ T-1, cluster 3: CD8 T_{em}-2, cluster 4: $\gamma\delta$ T-2, cluster 5: CD8 T_{cm}-1, cluster 6: CD4/CD8 Naïve-1, cluster 7: eT_{reg}, cluster 8: CD4 T_{em}-1, cluster 9: CD4 T_{em}-2, cluster 10: NKT/CD8 T_{cm}, cluster 11: cT_{reg}, cluster 12: CD4/CD8 Naïve-2, cluster 13: CD8 T_{cm}-2, cluster 14: CD8 T_{em}-3, cluster 15: $\gamma\delta$ T-3 (**Fig. 3.34C**). The cell distribution of the original mouse clusters data was highlighted for visualization. All cluster cells in our data were found to match to the integration clusters (**Fig. 3.34D**). In the absence of lymph node and ATLO data in human patients with atherosclerosis, our data had to be limited to plaques of human coronary arteries and carotid arteries. Published data sets from another genetic mouse model, i.e. the Ldlr-deficient mouse fed a Western-type diet were also used.

RESULTS

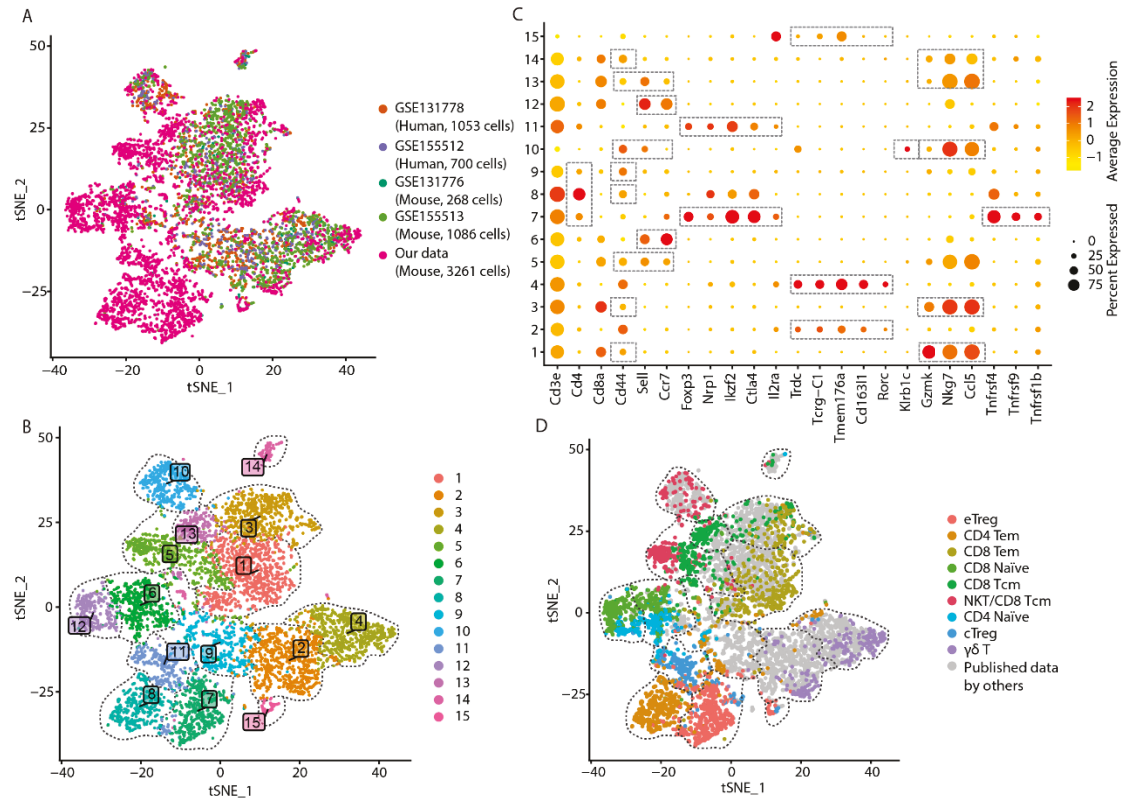


Fig. 3.34 Integrating analysis to investigate the T cell compositions in human and mouse atherosclerotic plaques. tSNE plot shows the T cells of each dataset (A) and related clusters (B). GSE131778: human coronary artery, n=4, total 1053 cells; GSE155512: human carotid artery, n=3, total 700 cells; GSE131776: ApoE^{-/-} mice fed with HFD, total 268 cells; GSE155513: ApoE^{-/-} and Ldlr^{-/-} mice fed with HFD, total 1086 cells. C. Dotplot displays expression of canonical lineage markers and DEGs. Dot size represents percentage of one gene in each cluster. Dot color designates gene average expression. D. Highlight of the distribution of original clusters of our own data relative to data in the integrative analysis. The grey color designates cells from other human and mouse datasets. The other colors represent clusters of our data.

These clusters were then further grouped into 5 groups, namely CD4 T_{eff/mem} cells (I, cluster 8, 9), CD4 T_{reg} cells (II, cluster 7, 11), CD8 T_{eff/mem} cells (III, cluster 1, 3, 5, 10, 13, 14), naïve T cells (IV, including CD4 and CD8 naïve T cells, cluster 6, 12), $\gamma\delta$ T cells (V, cluster 2, 4, 15) (Fig. 3.35A). Of note, CD4 T_{eff/mem} cells showed a significant incongruency of human versus mouse plaques. The proportion of CD4 T_{eff/mem} cells was higher in human coronary and carotid plaques (9%-23%) than mouse plaques (0%-10%) (Fig. 3.35B).

Similar to our mouse data, both human and HFD mouse plaques showed less T_{reg}

RESULTS

cells and naïve T cells. Importantly, T_{reg} cells as the main population to regulate peripheral tolerance were undetectable in most of human and mouse samples (**Fig. 3.35C**). Naïve T cells in human and mouse plaques also displayed significant variability, even among different human samples, with human patients having more than 3.8% of naïve T cells, while in the mouse plaques, naïve T cells made up less than 3.4% of total T cell population (**Fig. 3.35E**). However, the composition of CD8 T_{eff/mem} cells was consistent in different murine and human samples, which also showed similar percentages with our scRNA-seq results (**Fig. 3.35D**). Moreover, $\gamma\delta$ T cells accounted for around 30% of T cells in mice and human plaques (**Fig. 3.35F**). CD8 T_{eff/mem} cells and $\gamma\delta$ T cells accounted for the main population of mouse plaques after 8 weeks of HFD, possibly suggesting a critical role of CD8 T_{eff/mem} and $\gamma\delta$ T cells in mouse atherosclerosis progression. The higher percentage of CD8 T_{eff/mem} cells with less T_{reg} cells and naïve T cells were found to represent a common feature in both human and murine (HFD/ND) atherosclerotic plaques. These data support the conclusion that critical mouse data are translatable to human CD8 T cell immune tolerance dysfunction. However, considerably more work is needed to analyze other immune tolerance checkpoints affecting CD4 and T_{reg} cells once such data will become available in the future. Finally, there is an urgent need to analyze human LNs of patients with and without atherosclerosis and compare different age groups and possible gender-related differences as well as taking complex risk factor profiles into consideration. These important issues will require a considerable extension of human data and tissues for future research into the similarities and dissimilarities of mouse versus human atherosclerosis.

RESULTS

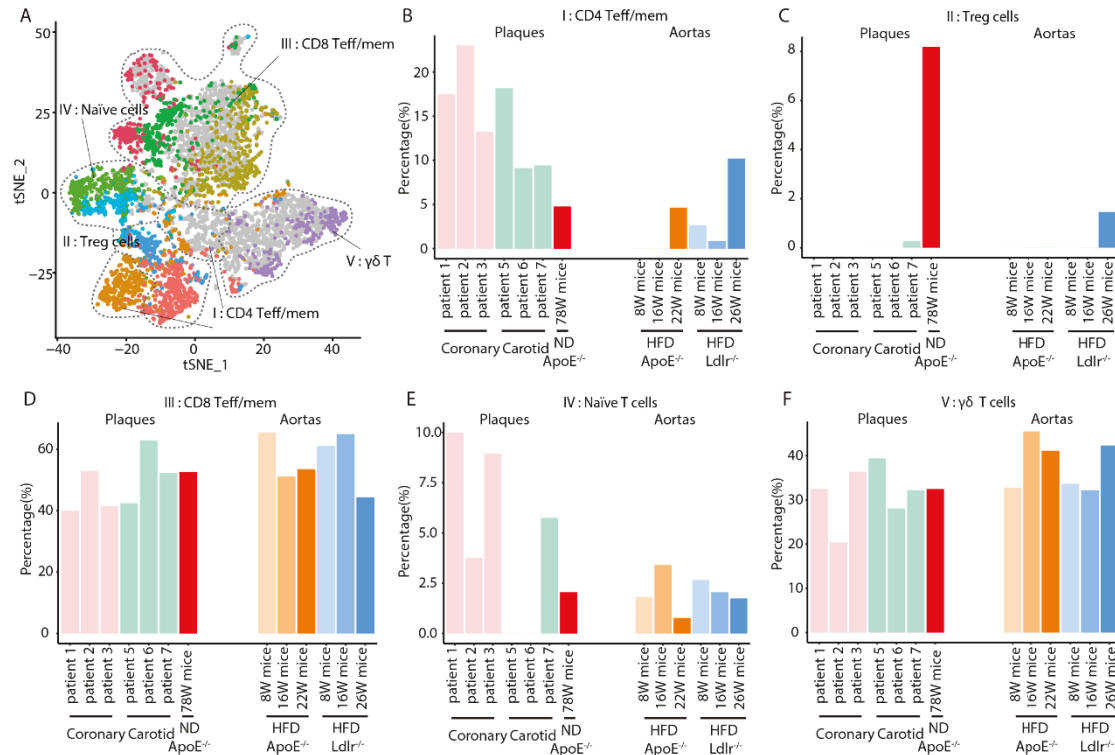


Fig. 3.35 T cell subset percentages in human and mouse atherosclerotic plaques. A. T cell subsets were grouped according to the cells' phenotype and function. I: CD4 $T_{eff/mem}$ (cluster 8, 9); II: CD4 T_{reg} cells (e T_{reg} and c T_{reg} , cluster 7, 11); III: CD8 $T_{eff/mem}$ (CD8 T_{em} , NKT/CD8 T_{cm} , CD8 T_{cm} , cluster 1, 3, 5, 10, 13, 14); IV: Naïve T cells (CD4 and CD8 naïve T cells, cluster 6, 12); V: $\gamma\delta$ T (cluster 2, 4, 15) Each T cell subset percentage among human and mouse atherosclerotic plaques (**B-F**). The T cell subset percentages of GSE131776 and the fourth patient in GSE131778 study were not shown due to the smaller number of T cells. Patient 1-3 were from GSE131778; patient 5-7 were from GSE15512. HFD: high fat diet; ND: normal diet; Ldlr: low density lipoprotein receptor.

3.16.2 Gene expression analysis reveals shared profiles of CD8 $T_{eff/mem}$ cells in murine and human atherosclerotic plaques

To examine whether compromised tolerance in murine atherosclerotic plaques is also present in human atherosclerotic plaques, gene expression profiles of murine and human T cells were examined. Human CD8 $T_{eff/mem}$ cells showed high a high degree of similarity with murine CD8 $T_{eff/mem}$ cells versus other T cell subsets (**Fig. 3.36**). Among different T cell subsets, CD8 $T_{eff/mem}$ cells between mouse and human had the highest correlation values (**Fig. 3.36**). By combining the T cell compositions in atherosclerosis, these data show a similar gene expression profile of CD8 $T_{eff/mem}$ cells in murine and human atherosclerosis.

RESULTS

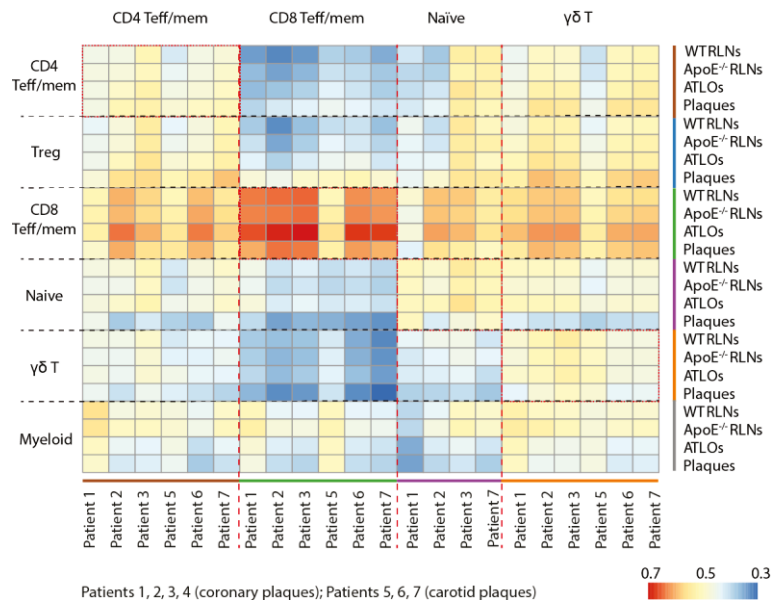


Fig. 3.36 The similarity of different T cell subsets between murine and human atherosclerotic plaques. Each square represents the similarity of T cells between murine and human studies. The color of each square indicates the degree of Spearman correlation coefficient value.

Considering the role of CD8 T_{eff/mem} cells in murine and human atherosclerosis, next, the expression of CD8 T_{eff/mem} cell function-associated genes as described above were investigated in different murine and human studies. Data showed lower levels of *Ccr7*, *S1pr1*, and *Sell* in CD8 T_{eff/mem} cells in murine and human atherosclerotic plaques (**Fig. 3.37**). Both murine and human samples had a higher expression of cytotoxicity and cytokine-related genes, even though more *Gzmb* was expressed in murine plaques while *Gzmm* was expressed in human plaques (**Fig. 3.37**). *Cxcr6* expression in murine plaque CD8 T_{eff/mem} cells were higher than its counterpart in human plaques, especially in aged ApoE^{-/-} mice. Other T cell activation-related genes had similar expression levels between murine and human atherosclerotic plaques (**Fig. 3.37**). Exhaustion-related transcripts also found a broad expression in murine and human atherosclerotic plaques compared to WT RLNs. *Pdcd1* and *Tigit* showed markedly higher expression in CD8 T_{eff/mem} cells of aged ApoE^{-/-} mice plaques when compared to CD8 T_{eff/mem} cells of HFD-treated ApoE^{-/-}, *Ldlr*^{-/-} mice and human plaques (**Fig. 3.37**).

RESULTS

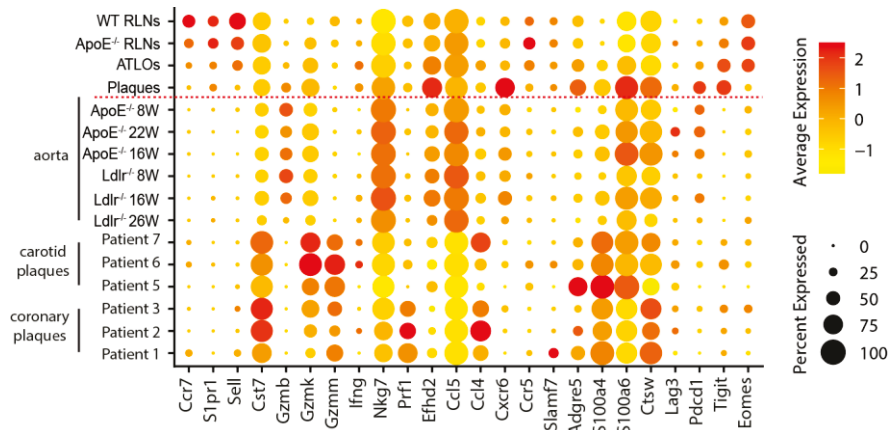


Fig. 3.37 Heatmap of average gene expression levels of selected function-associated genes in CD8 T_{eff/mem} cells in murine versus human atherosclerotic plaques.

3.16.3 Human and mouse scRNA-seq integration analysis indicates similar myeloid cell compositions in atherosclerotic plaques

As with T cell integration analysis, myeloid cell integration analysis to compare the murine and human myeloid cell profiles were performed. A total of 16574 cells were included and cells were separated into 19 clusters (**Fig. 3.38A and B**). Based on differentially expressed genes and canonical gene expression markers for different cell types, each cluster was named as follows: cluster 1: Trem2^{high} MΦ -1, cluster 2: Trem2^{high} MΦ -2, cluster 3: Trem2^{high} MΦ -3, cluster 4: Trem2^{high} MΦ -4, cluster 5: Mo/MΦ-1, cluster 6: CD11b⁺ cDC, cluster 7: Lyve1⁺ res-like MΦ-1, cluster 8: Lyve1⁺ res-like MΦ-2, cluster 9: Mo/MΦ-2, cluster 10: Granulocytes-1, cluster 11: proliferating Trem2^{high} MΦ, cluster 12: Trem2^{high} MΦ -5, cluster 13: CD11c⁻ DC, cluster 14: CD8a⁺ cDC, cluster 15: Granulocytes-2 (mast cell), cluster 16: Granulocytes-3, cluster 17: SMC-derived intermediate (SEM) cells, cluster 18: pDC (**Fig. 3.38C**). Moreover, the cell distribution of original clusters in our mouse data were highlighted and all cluster cells in our data were found to match to the integration clusters (**Fig. 3.38D**).

RESULTS

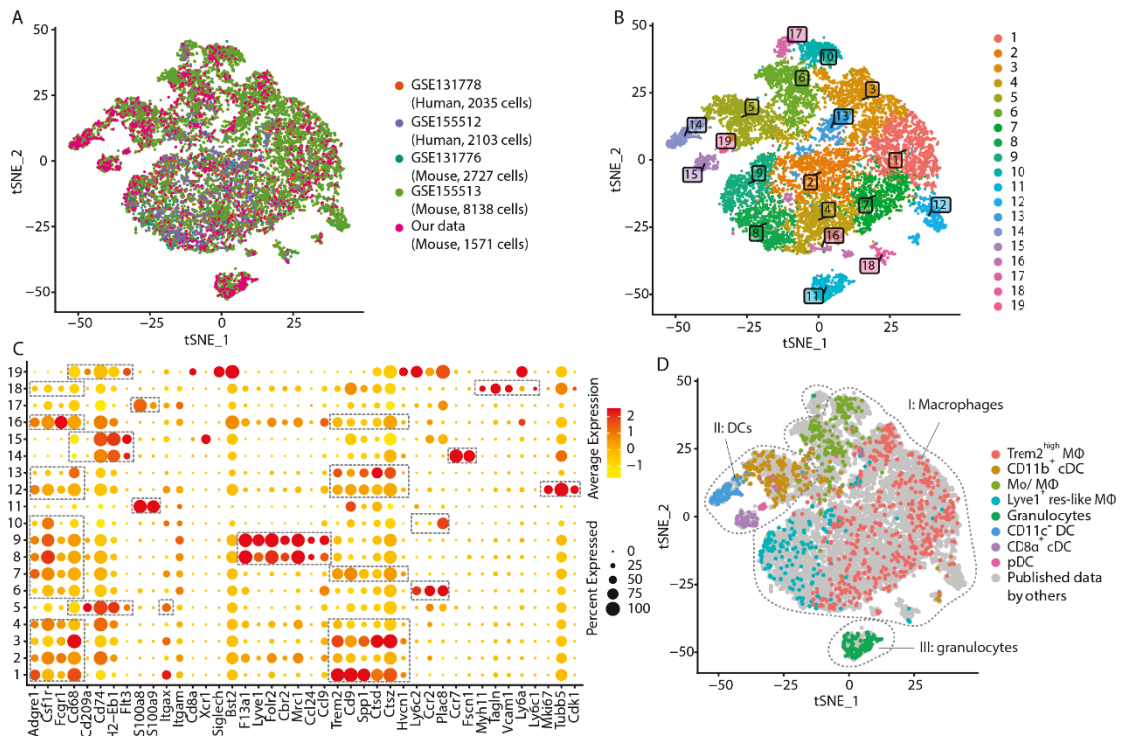


Fig. 3.38 Integration analysis of the myeloid cell compositions in human and murine atherosclerotic plaques. tSNE plots show the myeloid cells of each dataset (**A**) and related clusters (**B**). GSE131778: human coronary artery, n=4, total 2035 cells; GSE155512: human carotid artery, n=3, total 2103 cells; GSE131776: ApoE^{-/-} mice fed with HFD, total 2727 cells; GSE155513: ApoE^{-/-} and Ldlr^{-/-} mice fed with HFD, total 8138 cells. **C**. Dotplots display expression of canonical lineage markers and differential gene expression. Dot sizes represent percentages of one gene in each cluster. Dot colors designate average gene expression. **D**. Highlight the distribution of original clusters of our data relative to those of the integrative analysis. The gray color designates cells from other human and mouse datasets. The other colors represent clusters of our data.

The percentage of each myeloid cell subset was then calculated. Macrophages were found to be dominant in human plaques with very comparable percentage in mouse plaques (**Fig. 3.39A**). DCs and granulocytes had a low level in human plaques, but this data was highly variable among different human samples (**Fig. 3.39B and C**). The different sub-populations of macrophages and DCs were examined. Human plaques showed a similar composition compared to mouse plaques, and Trem2^{high} MΦs were the largest population of macrophages, followed by Lyve1⁺ res-like MΦs (**Fig. 3.39D**). A small population of SMC-derived intermediate phenotype cells were found in both human and mouse plaques. These cells had been reported to be capable of differentiating into macrophage-like cells in mice [174]. For DCs, CD11b⁺

RESULTS

cDCs made up ~ 90% per total DCs. Yet, in patient 4 and patient 6 there is a caveat of very few DCs (less than 6 cells) (**Fig. 3.39E**). CD11c⁻ DCs displaying migratory and inhibitory phenotypes, were only detected in mouse plaques.

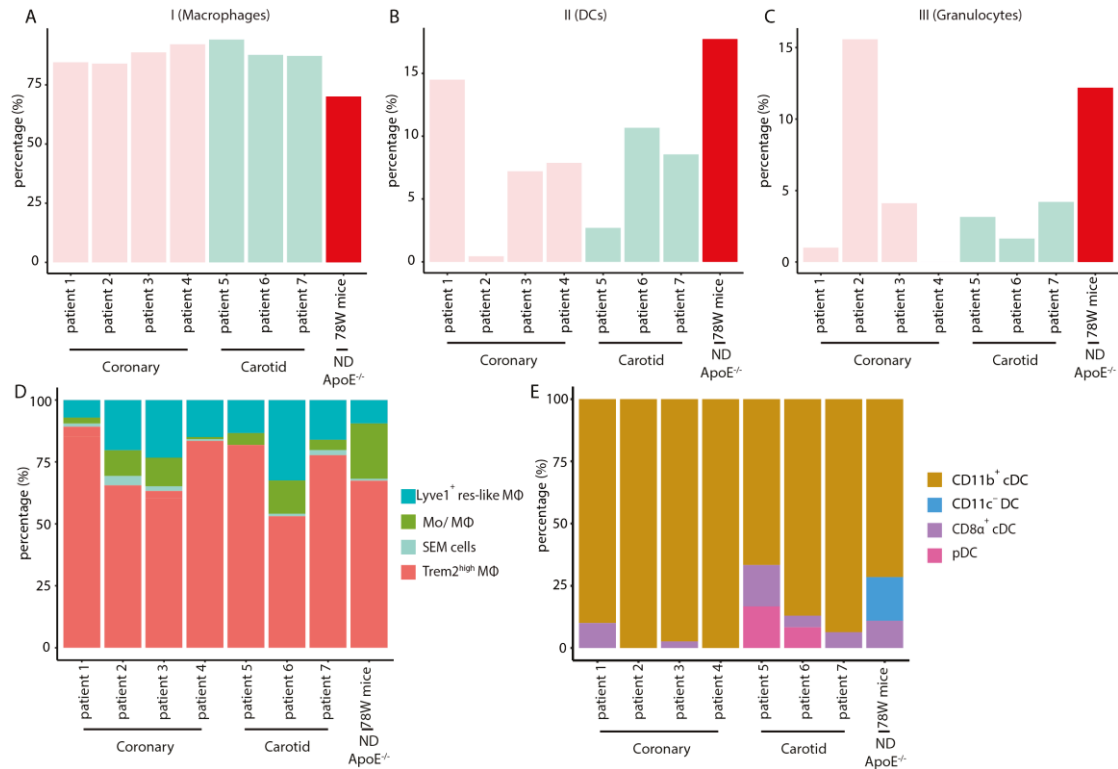


Fig. 3.39 Myeloid cell subset percentages in human and mouse atherosclerotic plaques. The percentage of macrophages (**A**), DCs (**B**) and granulocytes (**C**) in human and mouse atherosclerotic plaques. The sub-population of macrophages (**D**) and DCs (**E**) among different samples. Due to the experiment design, the myeloid cell subset percentages of GSE131776 and GSE155513 study were not shown. Patient 1-4 were from GSE131778; patient 5-7 were from GSE155512. ND: normal diet.

3.16.4 Gene expression analysis reveals similarities of APCs in murine versus human plaques

To investigate the effect of APCs in modulating potential T cell functions in human plaques, the expression of mRNAs coding for co-inhibitory and co-stimulatory in macrophages and DCs between mouse and human atherosclerotic plaques were compared. A broad expression of co-stimulatory genes was found in human plaque macrophages. Apart from *Lgals3*, most of the co-inhibitory transcripts were expressed at low levels in both mouse and human plaques. Macrophages in aged ApoE^{-/-} mice plaque showed a relatively higher expression of *Lgals3*, *Icosl*, *Fas*, and *Cd274* when compared to their counterparts in human plaques (**Fig. 3.40A**). As

RESULTS

professional APCs, DCs also displayed expression of co-stimulatory genes between mouse and human plaques. The migratory and inhibitory CD11c⁺ DCs were only detected in murine plaques (Fig. 3.39E). Other DC cell types displayed low expression of co-inhibitory genes in both mouse and human plaques (Fig. 3.40B).

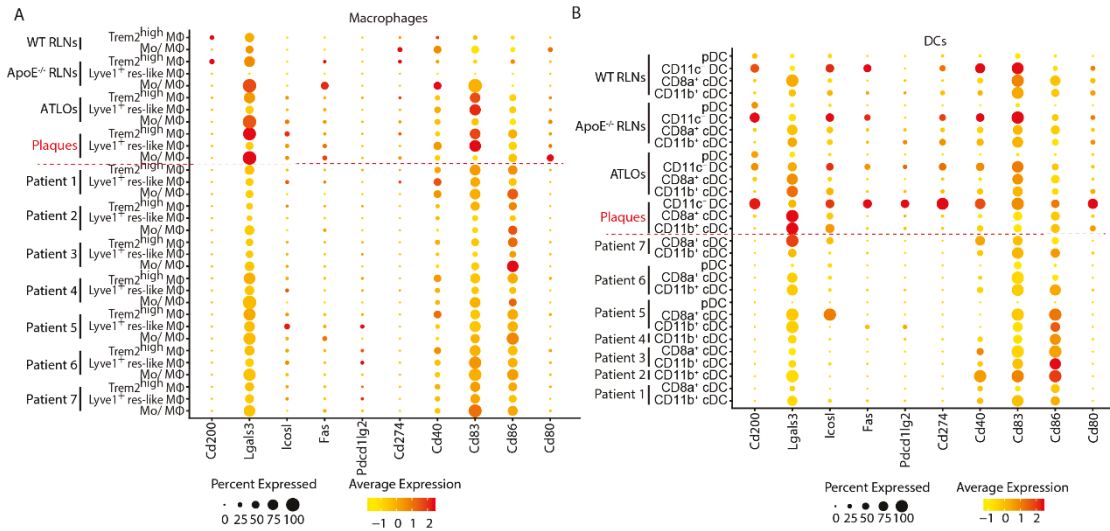


Fig. 3.40 Average expression of co-stimulatory and co-inhibitory genes in mouse and human atherosclerotic plaque myeloid cells. The expression of co-stimulatory and co-inhibitory genes in different subtypes of macrophages (A) and DCs (B). Patients 1-4 were from GSE131778; patients 5-7 were from GSE155512.

4. DISCUSSION

Data reported here support several major conclusions: a multifaceted peripheral T cell tolerance dysfunction emerges in aged ApoE^{-/-} mice burdened with advanced atherosclerosis (**Fig. 4**). Tolerance dysfunction is apparent in three major types of T cells, i.e. CD4, CD8 and T_{reg} cells. It is highly tissue-specific with pronounced in ApoE^{-/-} RLNs, further developed in ATLOs and most evident in atherosclerotic plaques compared to WT RLNs. Its multifaceted nature is indicated by partial activation within the naïve T cell pool; the involvement of key functionally important aspects of T cells including movement, activation, exhaustion, and clonal expansion; dysregulation of costimulation and inhibition of checkpoints mediated by APCs; a significant decline of the T_{reg} pool; apparent T_{reg}-Th₁₇ conversion; and plaque environment-induced T cell function-related genes. Finally, tolerance breakdown is most evident in T_{eff/mem} cells of clonally expanded CD4, CD8 and T_{reg} cells. When taken together, our data reveal widespread T cell dysfunction in advanced atherosclerosis during ageing providing a comprehensive blueprint for further studies to characterize atherosclerosis as a bona fide T cell-associated autoimmune disease. Moreover, we propose that the body of evidence outlined in this thesis provide numerous and unprecedented opportunities to develop T cell therapies of atherosclerosis including the development of therapies to reconstitute tolerance dysfunction [253-257], interfere with T cell costimulation, activation, migration and exhaustion [258] and address immune senescence [259].

The unbiased approach to pair scRNA-seq analyses with scTCR-seq profiling at a single cell level in four major tissues involved in atherosclerosis immune responses, i.e. the circulation, RLNs, ATLOs and plaques allowed us to uncover a series of unexpected mechanisms of tolerance breakdown amounting to not less than considerable and previously unknown mechanistic insights into atherosclerosis T cell immunity. The data supports and considerably extends our previous hypothesis that atherosclerosis may be a disease with T cell-associated autoimmune responses [121, 123, 124].

DISCUSSION

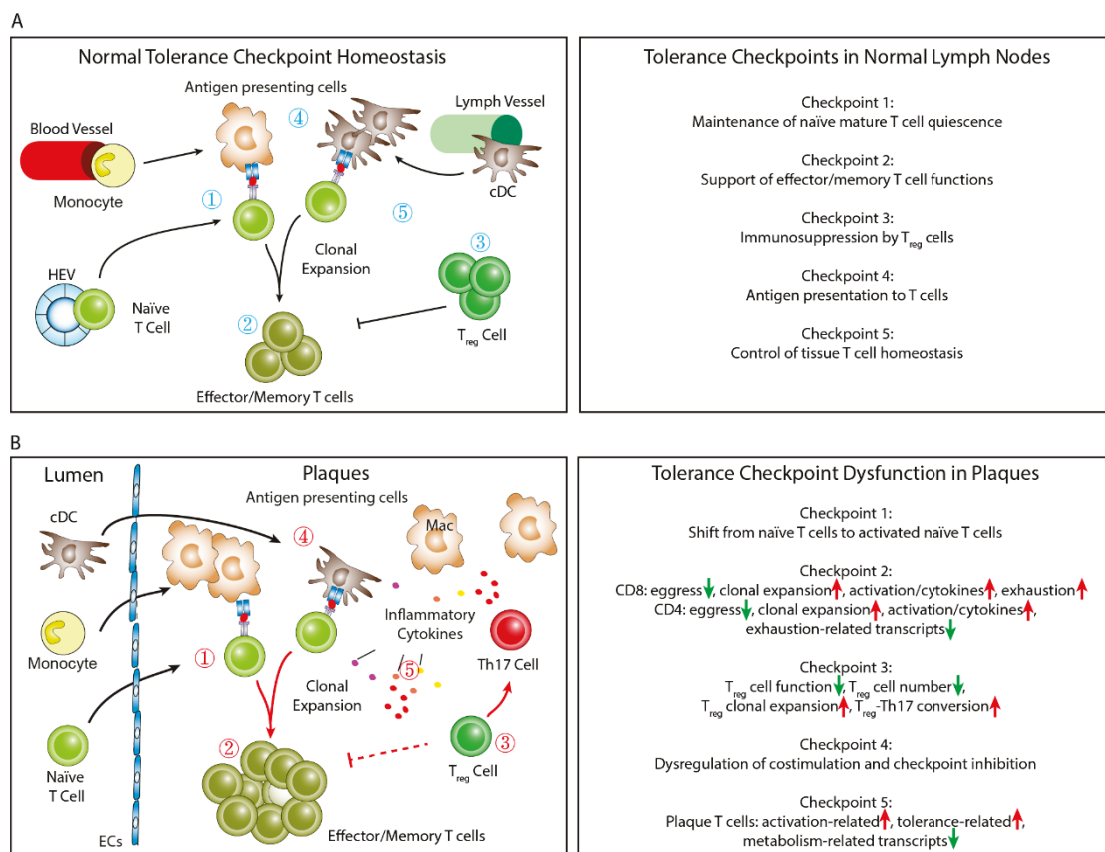


Fig. 4: Landscape of T cell and myeloid cell tolerance breakdown in atherosclerosis. A. The immune system developed checkpoints (upper left panel 1 - 5 marked as blue for normal tolerance homeostasis) to maintain immune tolerance in LNs to avoid autoimmune injury of self while maintaining effective protection against foreign invaders. 1. maintenance of quiescence of naïve T cells; 2. support of effector/memory T cell functions; 3. immunosuppression by T_{reg} cells; 4. antigen presentation to T cells; 5. control of tissue T cell homeostasis. **B.** Multiple checkpoints are compromised (1 - 5, marked as red) in a tissue-specific manner in murine advanced atherosclerosis as follows: ApoE^{-/-} RLNs are compromised at checkpoint 2; ATLOs show aberrant features at checkpoints 2, 3, 4; plaques are compromised at all 5 checkpoints.

4.1. T_{reg} cell plasticity, tolerance and clonal expansion in atherosclerosis and caveats

T_{reg} cells are the major immunosuppressive T cell population playing key roles in the maintenance of peripheral tolerance [83]. The reduction of T_{reg} cell numbers in murine atherosclerosis documented here raises by itself the possibility of a weakened immunosuppressive activity in peripheral tissues. Moreover, the gene transcriptome of plaque T_{reg} cells provides ample evidence for a loss of function of

DISCUSSION

T_{reg} cells by identifying candidate genes that are crucial to their loss of function. Apart from the apparent phenotype- and function-associated transcripts, the higher expression of Th₁₇-related genes such as *Rora*, *Rorc* and *Il17a* in plaque T_{reg} cells indicate that T_{reg} cells convert from an atheroprotective to a proatherogenic phenotype [63]. T_{reg} cells are known to switch sides from immunosuppression to proinflammatory phenotypes in other diseases, such as autoimmune arthritis [54], periodontitis [55] and diabetes [56], which speaks to the enormous plasticity of T_{reg} cells in disease conditions. In addition, T_{reg} cell conversion in atherosclerosis is a phenomenon that should be a reason for concern when a broad approach to increase T_{reg} cells is considered to treat patients with atherosclerosis. They should be taken as a potential detrimental consequence unless T_{reg} cell immune responses are better defined. Th₁-like IFN γ ⁺CCR5⁺ T_{reg} cells were found by Li et al. and Butcher et al. in atherosclerotic plaques [260, 261]. These cells showed little immunosuppressive power and, more importantly, adoptive transfer of these cells significantly aggravates atherosclerosis [260, 261]. Recently, ApoB antigen-specific T_{reg} cells were found to lose Foxp3 and gained atherogenic Th₁₇ or Th₁-like marker ROR γ t or T-bet. Remarkably, after 12 weeks of Western diet, more than half of ApoB antigen-specific T_{reg} cells in ApoE^{-/-} mice lost Foxp3 and CD25 expression and failed to restrain atherosclerosis development [63]. In sharp contrast of the expected outcome, these ApoB antigen-specific T_{reg} cells in atherosclerosis were demonstrated to aggravate atherosclerosis [64]. However, the mechanisms mediating the conversion of T_{reg} to other effector/memory phenotype Th cells remain unclear. A full elucidation of these mechanisms will help to refine and design new strategies that avoid the flaws of treatment strategies encountered in clinical trials of atherosclerosis [262-264]. In view of these caveats, it will be instrumental to identify potential arterial wall-derived autoantigens and their antigen-specific B cell receptors and/or antigen-specific T cell receptors similar to approaches to effective treatment regimens conducted in patients with B cell lymphomas using chimeric antigen receptor engineering approaches including the CRISPR-CAS9 gene editing [265]. This approach could lead to both vaccination strategies, antibody treatment

DISCUSSION

strategies and T cell therapies by engineering T cell receptors that specifically recognize beneficial or detrimental peptide sequences in bona fide atherosclerosis-specific autoantigens. T_{reg} cells generated in the thymus are thought to have a strong binding affinity with self-peptide-MHC complexes [69]. Clonal expansion of T_{reg} cells in atherosclerosis may indicate a putative autoantigen-induced T cell immune response. The identification of ApoB-specific T_{reg} cells in mouse atherosclerosis supports the idea of autoreactive T_{reg} cells in atherosclerosis [63]. Thus, restoring the Th₁₇/T_{reg} balance and identifying T_{reg}-specific antigens may be a promising - and in our view the only - way to rescue T_{reg} cell tolerance dysfunction and attenuate the development of atherosclerosis.

4.2. CD4 and CD8 T_{eff/mem} cells tolerance and clonal expansion in atherosclerosis

CD4 Th and CD8 T cells are the main effector cells directed at foreign antigens by producing a variety of cytokines and cytotoxic molecules, respectively. To avoid self-injury, multiple mechanisms are being employed by the immune system. Expression of genes encoding for exhaustion, immunosuppression mediated by APCs and immunosuppression by T_{reg} cells form an intricate balance that must be continuously monitored and readjusted [83]. Clonal expansion of CD4 Th and CD8 T cells described here involve effector and memory T cells, suggesting that they qualify to discover their autoantigen-specificity. The transcriptomes of T_{eff/mem} CD4 Th and CD8 T cells in plaques showed distinct phenotypes involving T cell residence, activation, cytokine production, and exhaustion compared with their counterparts in WT RLNs, indicating a malfunction of their immune tolerance. The high expression of genes associated with T cell activation and cytokine production may be caused by the continuous stimulation of antigens in atherosclerotic plaques, which would explain their exhaustion-related transcript profiles. In line with previous studies [94, 95], we observed significant exhaustion-associated gene expression in CD8 T_{eff/mem} cells of atherosclerotic plaques. In contrast, CD4 T_{eff/mem} cells showed lower expression of

DISCUSSION

these genes, although the impact of exhaustion of CD4 T cells remains to be determined for atherosclerosis. The prevalence of APCs in atherosclerotic plaques with high expression levels of co-inhibitory transcripts may contribute to exhaustion of CD8 T_{eff/mem} cells whereas the lack of similar profiles of CD4 T_{eff/mem} cells in atherosclerotic plaques remains to be fully understood. Different CD4 Th subtypes can be defined by transcription factors and cytokines associated with each subtype in FACS. However, the low gene expression of Th subtype-associated transcription factors and cytokines at the single cell level limits the precise designation of Th cell subtypes by scRNA-seq [266]. Even though the different Th subtypes were not fully defined in our study, our data still showed higher expression of proatherogenic Th₁ and Th₁₇-related genes in atherosclerotic plaques compared to WT RLNs, indicating a pro-inflammatory profile of CD4 Th cells in plaques reflected by the expression of Th₁ and Th₁₇-related genes. CD8 T_{eff/mem} cells in atherosclerotic plaques exhibited a complex phenotype with both activation, cytokine production, and exhaustion-related gene expressions, which play different facets on CD8 T cell function. Although the protective effect of PD1 in atherosclerosis has been reported in PD1 and PD-L1 knockout mice [96], cautious interpretation is still needed when treating atherosclerosis by targeting PD1 or other exhaustion-related genes on CD8 T_{eff/mem} cells. Recent studies in non-alcoholic steatohepatitis-triggered hepatocellular carcinoma in mice showed progressive accumulation of activated CD8⁺PD1⁺CXCR6⁺ T cells in affected livers. Thus, unexpectedly, anti-PD1 treatment led to the exacerbation of tumor progression [267]. Importantly, clonal expansion of CD4 and CD8 cells was also observed in human coronary plaques by others though no pairing approach was used limiting these findings regarding transcript profiles and subtype delineation [155]. However, these data show significant similarities of CD8 T cells in human and mouse atherosclerosis. Further aspects of antigen-specific CD4/CD8 T cell immune responses in atherosclerosis will be discussed below.

DISCUSSION

4.3. T cell clonal expansion of major T cell subtypes indicate plaque antigen-specific T cell immune responses in atherosclerosis

T cell clonal expansion of three major T cell subtypes in aged ApoE^{-/-} mice is among the most prominent finding of this thesis building on previous work to characterize T cell immunity in atherosclerosis [121]. When specific antigenic peptides presented by MHC molecules on APCs are encountered by cognate TCRs, T cells will undergo activation and proliferation. In our study, clonal expansion of CD4, CD8 and T_{reg} cells suggested a robust T cell (auto)antigen-specific immune response in atherosclerosis. Furthermore, the broad overlap of CDR3 in expanded CD8 T_{eff/mem} cells across plaques, ATLOs and ApoE^{-/-} RLNs, but not in WT RLNs, strongly suggests a disease-specific atherosclerosis-specific autoantigen-induced T cell immune response. T cell clonal expansion in atherosclerosis has been reported both in murine and human studies [95, 155, 195]. As mentioned above, one study showed CD8⁺ T cells with an activated phenotype (CD69⁺CCR5⁺PD1^{int}CD127⁻) were clonally expanded in human coronary plaques [95]. Recently, by using a single cell TCR cloning approach, both CD4 and CD8 T cells were found clonally expanded in human coronary plaques, and clonal expansion in CD8 T cells were more pronounced compared to CD4 T cells [155]. Both studies are consistent with our current results in mouse atherosclerosis and support our findings, but the studies of human coronary arteries did not report clonal expansion of T_{reg} cells from total CD4 T cells probably due to the limitations of the authors single cell TCR cloning approach and the scarcity of these cells in plaques. Unlike this previous report that did not use a pairing approach, we were able to characterize the clonally expanded T cells and identify their transcriptome profiles.

Clonal expansion of T cells in atherosclerosis raises another question, namely, whether antigen-specific T cells in atherosclerosis are involved in the pathogenesis of atherosclerosis. Previous studies exploring T cell antigen responses in atherosclerosis employed a vaccination approach by using oxLDL or MDA-LDL versus native LDL [10]. These studies by their nature were unable to resolve the issues of clonal expansion and autoimmunity and regarded as the first attempt to

DISCUSSION

approach the issue of autoimmunity. However, this work was of interest as it demonstrated a high degree of native LDL antigenicity versus a low degree of antigenicity of oxLDL. Subsequently, scientists adopted an alternative - though biased - strategy to examine atherosclerosis-specific antigens by focusing on ApoB peptide sequences [63, 135]. By matching TCR sequences to available databases of TCRs with known antigens, Chowdhury and her colleagues found that TCRs in plaques recognized epitopes of influenza, cytomegalovirus, and other viruses. More importantly, they elucidated cross-reactivity of these viruses-specific TCRs with human antigens on SMCs, endothelial cells, and cardiomyocytes [155]. This study indicated the possibility of TCR clonal expansion and that cross-reactivity of virus antigens with atherosclerosis-promoting epitopes building on a similar hypothesis that has been voiced for many years in the past [268]. Although our current data did not show the corresponding antigens of TCRs, the clonal expansion of T cell subtypes detected in plaques and other tissues indicate that atherosclerosis-specific antigen-induced T cell immune responses may either be initiated in plaques or that the clonally expanded T cells have a preference for homing in plaques. We conclude that an unbiased approach, similar to the one used here, is the best and methodologically most advanced approach to resolve the mystery and indeed enigma surrounding the issue of autoimmune T cells in atherosclerosis. It provides a comprehensive blueprint to identify the autoantigens as well as the T cell subtypes involved and thus will advance our long-term goal to characterize atherosclerosis as a bona fide autoimmune T cell-associated disease.

4.4. Immune tolerance in cancer and autoimmune diseases

The peripheral tolerance mechanisms described above have been studied in cancer and autoimmune diseases including multiple sclerosis and rheumatoid arthritis, manifested by T cell anergy, T_{reg} cell plasticity, APCs to suppress T cell activation, and T cell exhaustion [9, 54, 269-272]. All these studies - similar to the atherosclerosis model used here - revealed multiple compromised tolerance

DISCUSSION

checkpoints in cancer and autoimmune diseases. Although the pathologies and their underlying molecular and cellular origins of atherosclerosis versus other autoimmune diseases are distinct, it is of major importance that they seem to share similar mechanisms of T cell peripheral tolerance dysfunction. Thus, comprehensive comparisons between cancer and autoimmune diseases versus atherosclerosis will yield important insights into the complex network of T cell immune tolerance in multiple disease conditions which we believe is one important prerequisite to develop treatment of both diseases and understand potential side effects of treating either.

Our available data focused on T cell peripheral tolerance of atherosclerosis. However, the role of central tolerance in multiple diseases other than atherosclerosis has been delineated [273]. Therefore, the role of central tolerance in atherosclerosis deserves further studies.

4.5. How can tolerance checkpoint dysfunction in autoimmune diseases be translated to develop new targets for atherosclerosis treatments?

Anti-inflammatory strategies as the alternative way to treat atherosclerosis have been widely studied [8]. However, in the CANTON trial that received widespread recognition as a proof-of-concept clinical trial for the potential effectiveness of anti-inflammatory therapies, the systemic and non-specific anti-inflammatory treatment with canakinumab, an IL-1 β antibody, was associated with a higher incidence of severe clinical infections versus placebo patients [274]. Moreover, it has been pointed out that some disease endpoints showed to be effective for patient subgroups in this trial, the overall mortality rate remained unchanged while the risk of infection increased [263]. Therefore, the CANTON trial may be taken as evidence that anti-inflammatory antigen-independent strategies will fail, and it casts doubt on the viability of similar approaches targeting other broad inflammation pathways. In relation to the current work detailed above, rescue strategies to reconstitute tolerance in the treatment of atherosclerosis need to be carefully considered. Indeed, several strategies to induce antigen-specific immune tolerance have been reported,

DISCUSSION

such as treatment with antigen-specific tolerogenic DCs, antigen-specific T_{reg} treatment and vaccination with disease-specific antigens [253]. Studies have been performed by using these strategies to treat multiple autoimmune diseases, such as arthritis, type I diabetes and multiple sclerosis [254-257, 275, 276].

The atheroprotective effects of T_{reg} cells have been reported by different studies including depleting T_{reg} cells with anti-CD25 antibody or expansion T_{reg} cells with IL2/anti-IL2 antibody complexes in mice [33, 277]. Immunization strategies have been broadly studied by using hypothetical autoantigens in atherosclerosis with or without different adjuvants in mice [136-138, 278, 279]. The atheroprotective effect of peptide vaccination approaches on atherosclerosis were reported mediated by regulating T_{reg} cell expansion and by reducing DCs through cytolytic CD8 T cells [280, 281]. Although most immunization studies have reported promising results in reducing atherosclerosis [136, 138, 278, 279], proatherogenic effects have also been observed [137]. The conventional approach to identify of well-defined disease-specific TCRs/antigens has greatly limited the study and application of immune tolerance in atherosclerosis. Therefore, we suggest that our unbiased approach using the pairing approach is superior to conventional approaches because they open the way to identify the bona fide autoantigens in atherosclerosis and the resultant autoantigens will provide unprecedented opportunities to test antigen-specific B cell and T cell therapies in atherosclerosis.

4.6. Lessons from experimental mice for human atherosclerosis

Our integrated scRNA-seq data revealed a similar T cell subset composition and some aspects of compromised T cell immune tolerance in atherosclerosis in mice and humans. Along with our mouse data, published human studies showed a significant CD8 T cell clonal expansion in atherosclerosis, and a stronger clonal expansion of CD8 T cells versus CD4 T cells [95, 155].

Apart from the similar transcript profiles of CD8 T cells in human and mouse atherosclerosis, our integration data also showed reduction of naïve and T_{reg} cells in

DISCUSSION

human and mouse atherosclerosis. In addition, the conversion of T_{reg} into effector/memory-like phenotype Th cells was also observed in human patients [62, 64]. All these data provide strong evidence that the T cell immune responses in mouse models and human atherosclerosis may be similar. Due to the limitations of clinical samples available so far, mouse studies provide a more comprehensive perspective for understanding T cell immune responses in human plaques. However, compromised T cell immune tolerance in aorta-associated LNs remains unknown due to limitations of cell numbers and lack of human samples, further studies are needed to better understand T cell tolerance breakdown in humans. Moreover, similarities of macrophage phenotypes were also found between mouse and human atherosclerosis. The resemblance of two major immune cell components in atherosclerosis will encourage scientists to explore similarities of other cell types between mouse and human atherosclerosis.

4.7. Outlook

In our present study, we integrated scRNA-seq and scTCR-seq to investigate the T cell immune response in atherosclerotic plaques, ATLOs and SLOs. Our body of data lays a solid foundation for further studying atherosclerosis prevention and treatment strategies, such as approaches to reverse T_{reg} cell contraction and conversion, to modulate CD8 T cells, and to induce immune tolerance by tolerogenic DCs. Identification plaque-specific antigens will provide opportunities for the development an entirely new class of therapies given the comprehensive blueprint of T cell autoimmunity reported above. Although the identification of T cell antigens remains a challenge, several platforms have been developed recently to identify disease-specific T cell antigens [130, 160, 282-285]. The vision to treat atherosclerosis with engineered T cells similar to some types of cancer may come true earlier than previously thought.

REFERENCES

REFERENCES

1. Lozano, R., et al., Global and regional mortality from 235 causes of death for 20 age groups in 1990 and 2010: a systematic analysis for the Global Burden of Disease Study 2010. *Lancet*, 2012. 380(9859): p. 2095-128.
2. Tabas, I., K.J. Williams, and J. Boren, Subendothelial lipoprotein retention as the initiating process in atherosclerosis: update and therapeutic implications. *Circulation*, 2007. 116(16): p. 1832-44.
3. Hansson, G.K. and A. Hermansson, The immune system in atherosclerosis. *Nat Immunol*, 2011. 12(3): p. 204-12.
4. Saigusa, R., H. Winkels, and K. Ley, T cell subsets and functions in atherosclerosis. *Nat Rev Cardiol*, 2020. 17(7): p. 387-401.
5. Tabas, I., Macrophage death and defective inflammation resolution in atherosclerosis. *Nat Rev Immunol*, 2010. 10(1): p. 36-46.
6. Mayerl, C., et al., Atherosclerosis research from past to present--on the track of two pathologists with opposing views, Carl von Rokitansky and Rudolf Virchow. *Virchows Arch*, 2006. 449(1): p. 96-103.
7. Hansson, G.K., A.K. Robertson, and C. Soderberg-Naucler, Inflammation and atherosclerosis. *Annu Rev Pathol*, 2006. 1: p. 297-329.
8. Soehnlein, O. and P. Libby, Targeting inflammation in atherosclerosis - from experimental insights to the clinic. *Nat Rev Drug Discov*, 2021. 20(8): p. 589-610.
9. Waldman, A.D., J.M. Fritz, and M.J. Lenardo, A guide to cancer immunotherapy: from T cell basic science to clinical practice. *Nat Rev Immunol*, 2020. 20(11): p. 651-668.
10. Nilsson, J. and G.K. Hansson, Vaccination Strategies and Immune Modulation of Atherosclerosis. *Circ Res*, 2020. 126(9): p. 1281-1296.
11. Zhou., X., S. Stemme., and G.K. Hansson., <evidence for a local immune response in atherosclerosis.pdf>. *Am J Pathol*, 1996.
12. Gronberg, C., J. Nilsson, and M. Wigren, Recent advances on CD4(+) T cells in atherosclerosis and its implications for therapy. *Eur J Pharmacol*, 2017. 816: p. 58-66.
13. Nakanishi, K., et al., Interleukin-18 regulates both Th1 and Th2 responses. *Annu Rev Immunol*, 2001. 19: p. 423-74.
14. Voloshyna, I., M.J. Littlefield, and A.B. Reiss, Atherosclerosis and interferon-gamma: new insights and therapeutic targets. *Trends Cardiovasc Med*, 2014. 24(1): p. 45-51.
15. Whitman, S.C., et al., Exogenous interferon-gamma enhances atherosclerosis in apolipoprotein E-/- mice. *Am J Pathol*, 2000. 157(6): p. 1819-24.
16. Gupta, S., et al., IFN-gamma potentiates atherosclerosis in ApoE knock-out mice. *J Clin Invest*, 1997. 99(11): p. 2752-61.
17. Buono, C., et al., Influence of interferon-gamma on the extent and phenotype of diet-induced atherosclerosis in the LDLR-deficient mouse. *Arterioscler*

REFERENCES

- Thromb Vasc Biol, 2003. 23(3): p. 454-60.
18. Ashkenazi, A. and V.M. Dixit, Death receptors: signaling and modulation. *Science*, 1998. 281(5381): p. 1305-8.
 19. Mackay, F., et al., Tumor necrosis factor alpha (TNF-alpha)-induced cell adhesion to human endothelial cells is under dominant control of one TNF receptor type, TNF-R55. *J Exp Med*, 1993. 177(5): p. 1277-86.
 20. Tartaglia, L.A., et al., A novel domain within the 55 kd TNF receptor signals cell death. *Cell*, 1993. 74(5): p. 845-53.
 21. Tartaglia, L.A., et al., Stimulation of human T-cell proliferation by specific activation of the 75-kDa tumor necrosis factor receptor. *J Immunol*, 1993. 151(9): p. 4637-41.
 22. Branen, L., et al., Inhibition of tumor necrosis factor-alpha reduces atherosclerosis in apolipoprotein E knockout mice. *Arterioscler Thromb Vasc Biol*, 2004. 24(11): p. 2137-42.
 23. Lee, T.S., et al., The role of interleukin 12 in the development of atherosclerosis in ApoE-deficient mice. *Arterioscler Thromb Vasc Biol*, 1999. 19(3): p. 734-42.
 24. Whitman, S.C., P. Ravisankar, and A. Daugherty, Interleukin-18 enhances atherosclerosis in apolipoprotein E(-/-) mice through release of interferon-gamma. *Circ Res*, 2002. 90(2): p. E34-8.
 25. Laurat, E., et al., In vivo downregulation of T helper cell 1 immune responses reduces atherogenesis in apolipoprotein E-knockout mice. *Circulation*, 2001. 104(2): p. 197-202.
 26. Wolf, D. and K. Ley, Immunity and Inflammation in Atherosclerosis. *Circ Res*, 2019. 124(2): p. 315-327.
 27. Nakae, S., et al., IL-17 production from activated T cells is required for the spontaneous development of destructive arthritis in mice deficient in IL-1 receptor antagonist. *Proc Natl Acad Sci U S A*, 2003. 100(10): p. 5986-90.
 28. Fujino, S., et al., Increased expression of interleukin 17 in inflammatory bowel disease. *Gut*, 2003. 52(1): p. 65-70.
 29. Smith, E., et al., Blockade of interleukin-17A results in reduced atherosclerosis in apolipoprotein E-deficient mice. *Circulation*, 2010. 121(15): p. 1746-55.
 30. Usui, F., et al., Interleukin-17 deficiency reduced vascular inflammation and development of atherosclerosis in Western diet-induced apoE-deficient mice. *Biochem Biophys Res Commun*, 2012. 420(1): p. 72-7.
 31. Danzaki, K., et al., Interleukin-17A deficiency accelerates unstable atherosclerotic plaque formation in apolipoprotein E-deficient mice. *Arterioscler Thromb Vasc Biol*, 2012. 32(2): p. 273-80.
 32. Madhur, M.S., et al., Role of interleukin 17 in inflammation, atherosclerosis, and vascular function in apolipoprotein e-deficient mice. *Arterioscler Thromb Vasc Biol*, 2011. 31(7): p. 1565-72.
 33. Ait-Oufella, H., et al., Natural regulatory T cells control the development of atherosclerosis in mice. *Nat Med*, 2006. 12(2): p. 178-80.

REFERENCES

34. Klingenberg, R., et al., Depletion of FOXP3⁺ regulatory T cells promotes hypercholesterolemia and atherosclerosis. *J Clin Invest*, 2013. 123(3): p. 1323-34.
35. Sakaguchi, S., et al., Regulatory T cells and immune tolerance. *Cell*, 2008. 133(5): p. 775-87.
36. Schmitt, E.G. and C.B. Williams, Generation and function of induced regulatory T cells. *Front Immunol*, 2013. 4: p. 152.
37. Sakaguchi, S., et al., The plasticity and stability of regulatory T cells. *Nat Rev Immunol*, 2013. 13(6): p. 461-7.
38. Mor, A., et al., Altered status of CD4(+)CD25(+) regulatory T cells in patients with acute coronary syndromes. *Eur Heart J*, 2006. 27(21): p. 2530-7.
39. George, J., et al., Regulatory T cells and IL-10 levels are reduced in patients with vulnerable coronary plaques. *Atherosclerosis*, 2012. 222(2): p. 519-23.
40. Fernandez, D.M., et al., Single-cell immune landscape of human atherosclerotic plaques. *Nat Med*, 2019. 25(10): p. 1576-1588.
41. Elhage, R., et al., Deleting TCR alpha beta⁺ or CD4⁺ T lymphocytes leads to opposite effects on site-specific atherosclerosis in female apolipoprotein E-deficient mice. *Am J Pathol*, 2004. 165(6): p. 2013-8.
42. Kyaw, T., et al., Cytotoxic and proinflammatory CD8⁺ T lymphocytes promote development of vulnerable atherosclerotic plaques in apoE-deficient mice. *Circulation*, 2013. 127(9): p. 1028-39.
43. Ludewig, B., et al., Linking immune-mediated arterial inflammation and cholesterol-induced atherosclerosis in a transgenic mouse model. *Proc Natl Acad Sci U S A*, 2000. 97(23): p. 12752-7.
44. Clement, M., et al., Control of the T follicular helper-germinal center B-cell axis by CD8(+) regulatory T cells limits atherosclerosis and tertiary lymphoid organ development. *Circulation*, 2015. 131(6): p. 560-70.
45. Cheng, H.Y., R. Wu, and C.C. Hedrick, Gammadelta (gammadelta) T lymphocytes do not impact the development of early atherosclerosis. *Atherosclerosis*, 2014. 234(2): p. 265-9.
46. Legut, M., D.K. Cole, and A.K. Sewell, The promise of gammadelta T cells and the gammadelta T cell receptor for cancer immunotherapy. *Cell Mol Immunol*, 2015. 12(6): p. 656-68.
47. Millonig, G., G.T. Malcom, and G. Wick, Early inflammatory-immunological lesions in juvenile atherosclerosis from the Pathobiological Determinants of Atherosclerosis in Youth (PDAY)-study. *Atherosclerosis*, 2002. 160(2): p. 441-8.
48. Kleindienst, R., et al., Immunology of atherosclerosis. Demonstration of heat shock protein 60 expression and T lymphocytes bearing alpha/beta or gamma/delta receptor in human atherosclerotic lesions. *Am J Pathol*, 1993. 142(6): p. 1927-37.
49. Vu, D.M., et al., gammadeltaT cells are prevalent in the proximal aorta and drive nascent atherosclerotic lesion progression and neutrophilia in hypercholesterolemic mice. *PLoS One*, 2014. 9(10): p. e109416.

REFERENCES

50. Marks, B.R., et al., Thymic self-reactivity selects natural interleukin 17-producing T cells that can regulate peripheral inflammation. *Nat Immunol*, 2009. 10(10): p. 1125-32.
51. Taleb, S., A. Tedgui, and Z. Mallat, IL-17 and Th17 cells in atherosclerosis: subtle and contextual roles. *Arterioscler Thromb Vasc Biol*, 2015. 35(2): p. 258-64.
52. Potekhina, A.V., et al., Treg/Th17 balance in stable CAD patients with different stages of coronary atherosclerosis. *Atherosclerosis*, 2015. 238(1): p. 17-21.
53. Yang, X.O., et al., Molecular antagonism and plasticity of regulatory and inflammatory T cell programs. *Immunity*, 2008. 29(1): p. 44-56.
54. Komatsu, N., et al., Pathogenic conversion of Foxp3+ T cells into TH17 cells in autoimmune arthritis. *Nat Med*, 2014. 20(1): p. 62-8.
55. Tsukasaki, M., et al., Host defense against oral microbiota by bone-damaging T cells. *Nat Commun*, 2018. 9(1): p. 701.
56. Zhou, X., et al., Instability of the transcription factor Foxp3 leads to the generation of pathogenic memory T cells in vivo. *Nat Immunol*, 2009. 10(9): p. 1000-7.
57. Bovenschen, H.J., et al., Foxp3+ regulatory T cells of psoriasis patients easily differentiate into IL-17A-producing cells and are found in lesional skin. *J Invest Dermatol*, 2011. 131(9): p. 1853-60.
58. Sanchez Rodriguez, R., et al., Memory regulatory T cells reside in human skin. *J Clin Invest*, 2014. 124(3): p. 1027-36.
59. Zhang, L., et al., Increased Th17 cells are accompanied by FoxP3(+) Treg cell accumulation and correlated with psoriasis disease severity. *Clin Immunol*, 2010. 135(1): p. 108-17.
60. Kryczek, I., et al., IL-17+ regulatory T cells in the microenvironments of chronic inflammation and cancer. *J Immunol*, 2011. 186(7): p. 4388-95.
61. Beriou, G., et al., IL-17-producing human peripheral regulatory T cells retain suppressive function. *Blood*, 2009. 113(18): p. 4240-9.
62. Kimura, T., et al., Regulatory CD4(+) T Cells Recognize Major Histocompatibility Complex Class II Molecule-Restricted Peptide Epitopes of Apolipoprotein B. *Circulation*, 2018. 138(11): p. 1130-1143.
63. Wolf, D., et al., Pathogenic Autoimmunity in Atherosclerosis Evolves From Initially Protective Apolipoprotein B100-Reactive CD4(+) T-Regulatory Cells. *Circulation*, 2020. 142(13): p. 1279-1293.
64. Saigusa, R., et al., Single cell transcriptomics and TCR reconstruction reveal CD4 T cell response to MHC-II-restricted APOB epitope in human cardiovascular disease. *Nature Cardiovascular Research*, 2022. 1(5): p. 462-475.
65. Love, P.E. and A. Bhandoola, Signal integration and crosstalk during thymocyte migration and emigration. *Nat Rev Immunol*, 2011. 11(7): p. 469-77.
66. Takahama, Y., Journey through the thymus: stromal guides for T-cell development and selection. *Nat Rev Immunol*, 2006. 6(2): p. 127-35.

REFERENCES

67. Starr, T.K., S.C. Jameson, and K.A. Hogquist, Positive and negative selection of T cells. *Annu Rev Immunol*, 2003. 21: p. 139-76.
68. Germain, R.N., T-cell development and the CD4-CD8 lineage decision. *Nat Rev Immunol*, 2002. 2(5): p. 309-22.
69. Xing, Y. and K.A. Hogquist, T-cell tolerance: central and peripheral. *Cold Spring Harb Perspect Biol*, 2012. 4(6).
70. Capalbo, D., et al., Autoimmune polyendocrinopathy candidiasis ectodermal dystrophy: insights into genotype-phenotype correlation. *Int J Endocrinol*, 2012. 2012: p. 353250.
71. Ramsey, C., et al., Aire deficient mice develop multiple features of APECED phenotype and show altered immune response. *Hum Mol Genet*, 2002. 11(4): p. 397-409.
72. Derbinski, J., et al., Promiscuous gene expression in medullary thymic epithelial cells mirrors the peripheral self. *Nat Immunol*, 2001. 2(11): p. 1032-9.
73. Gotter, J., et al., Medullary epithelial cells of the human thymus express a highly diverse selection of tissue-specific genes colocalized in chromosomal clusters. *J Exp Med*, 2004. 199(2): p. 155-66.
74. Wu, L. and K. Shortman, Heterogeneity of thymic dendritic cells. *Semin Immunol*, 2005. 17(4): p. 304-12.
75. Proietto, A.I., et al., Dendritic cells in the thymus contribute to T-regulatory cell induction. *Proc Natl Acad Sci U S A*, 2008. 105(50): p. 19869-74.
76. Hadeiba, H., et al., Plasmacytoid dendritic cells transport peripheral antigens to the thymus to promote central tolerance. *Immunity*, 2012. 36(3): p. 438-50.
77. Anderson, M.S., et al., Projection of an immunological self shadow within the thymus by the aire protein. *Science*, 2002. 298(5597): p. 1395-401.
78. Hsieh, C.S., H.M. Lee, and C.W. Lio, Selection of regulatory T cells in the thymus. *Nat Rev Immunol*, 2012. 12(3): p. 157-67.
79. Moran, A.E., et al., T cell receptor signal strength in Treg and iNKT cell development demonstrated by a novel fluorescent reporter mouse. *J Exp Med*, 2011. 208(6): p. 1279-89.
80. Jordan, M.S., et al., Thymic selection of CD4+CD25+ regulatory T cells induced by an agonist self-peptide. *Nat Immunol*, 2001. 2(4): p. 301-6.
81. Moran, A.E. and K.A. Hogquist, T-cell receptor affinity in thymic development. *Immunology*, 2012. 135(4): p. 261-7.
82. Kurd, N. and E.A. Robey, T-cell selection in the thymus: a spatial and temporal perspective. *Immunol Rev*, 2016. 271(1): p. 114-26.
83. ElTanbouly, M.A. and R.J. Noelle, Rethinking peripheral T cell tolerance: checkpoints across a T cell's journey. *Nat Rev Immunol*, 2021. 21(4): p. 257-267.
84. Hwang, S.S., et al., mRNA destabilization by BTG1 and BTG2 maintains T cell quiescence. *Science*, 2020. 367(6483): p. 1255-1260.
85. Buckley, A.F., C.T. Kuo, and J.M. Leiden, Transcription factor LKLF is sufficient to program T cell quiescence via a c-Myc-dependent pathway. *Nat*

REFERENCES

- Immunol, 2001. 2(8): p. 698-704.
86. Ouyang, W., et al., An essential role of the Forkhead-box transcription factor Foxo1 in control of T cell homeostasis and tolerance. *Immunity*, 2009. 30(3): p. 358-71.
 87. Wong, W.F., et al., Runx1 deficiency in CD4+ T cells causes fatal autoimmune inflammatory lung disease due to spontaneous hyperactivation of cells. *J Immunol*, 2012. 188(11): p. 5408-20.
 88. ElTanbouly, M.A., et al., VISTA is a checkpoint regulator for naive T cell quiescence and peripheral tolerance. *Science*, 2020. 367(6475).
 89. Fathman, C.G. and N.B. Lineberry, Molecular mechanisms of CD4+ T-cell anergy. *Nat Rev Immunol*, 2007. 7(8): p. 599-609.
 90. Kalekar, L.A., et al., CD4(+) T cell anergy prevents autoimmunity and generates regulatory T cell precursors. *Nat Immunol*, 2016. 17(3): p. 304-14.
 91. Greenwald, R.J., et al., CTLA-4 regulates induction of anergy in vivo. *Immunity*, 2001. 14(2): p. 145-55.
 92. Deaglio, S., et al., Adenosine generation catalyzed by CD39 and CD73 expressed on regulatory T cells mediates immune suppression. *J Exp Med*, 2007. 204(6): p. 1257-65.
 93. Robert, C., A decade of immune-checkpoint inhibitors in cancer therapy. *Nat Commun*, 2020. 11(1): p. 3801.
 94. McKinney, E.F., et al., T-cell exhaustion, co-stimulation and clinical outcome in autoimmunity and infection. *Nature*, 2015. 523(7562): p. 612-6.
 95. Fernandez, D.M., et al., Single-cell immune landscape of human atherosclerotic plaques. *Nature Medicine*, 2019. 25(10): p. 1576-1588.
 96. Bu, D.X., et al., Impairment of the programmed cell death-1 pathway increases atherosclerotic lesion development and inflammation. *Arterioscler Thromb Vasc Biol*, 2011. 31(5): p. 1100-7.
 97. Sharpe, A.H. and K.E. Pauken, The diverse functions of the PD1 inhibitory pathway. *Nat Rev Immunol*, 2018. 18(3): p. 153-167.
 98. Nagai, K., Co-inhibitory Receptor Signaling in T-Cell-Mediated Autoimmune Glomerulonephritis. *Front Med (Lausanne)*, 2020. 7: p. 584382.
 99. Zhao, Y., Q. Shao, and G. Peng, Exhaustion and senescence: two crucial dysfunctional states of T cells in the tumor microenvironment. *Cell Mol Immunol*, 2020. 17(1): p. 27-35.
 100. Sakaguchi, S., K. Wing, and T. Yamaguchi, Dynamics of peripheral tolerance and immune regulation mediated by Treg. *Eur J Immunol*, 2009. 39(9): p. 2331-6.
 101. Salomon, B., et al., B7/CD28 costimulation is essential for the homeostasis of the CD4+CD25+ immunoregulatory T cells that control autoimmune diabetes. *Immunity*, 2000. 12(4): p. 431-40.
 102. Read, S., V. Malmstrom, and F. Powrie, Cytotoxic T lymphocyte-associated antigen 4 plays an essential role in the function of CD25(+)CD4(+) regulatory cells that control intestinal inflammation. *J Exp Med*, 2000. 192(2): p. 295-302.
 103. Miyara, M., et al., Functional delineation and differentiation dynamics of

REFERENCES

- human CD4⁺ T cells expressing the FoxP3 transcription factor. *Immunity*, 2009. 30(6): p. 899-911.
104. Tivol, E.A., et al., Loss of CTLA-4 leads to massive lymphoproliferation and fatal multiorgan tissue destruction, revealing a critical negative regulatory role of CTLA-4. *Immunity*, 1995. 3(5): p. 541-7.
 105. Takahashi, T., et al., Immunologic self-tolerance maintained by CD25(+)CD4(+) regulatory T cells constitutively expressing cytotoxic T lymphocyte-associated antigen 4. *J Exp Med*, 2000. 192(2): p. 303-10.
 106. Schildknecht, A., et al., FoxP3⁺ regulatory T cells essentially contribute to peripheral CD8⁺ T-cell tolerance induced by steady-state dendritic cells. *Proc Natl Acad Sci U S A*, 2010. 107(1): p. 199-203.
 107. Ovcinnikovs, V., et al., CTLA-4-mediated transendocytosis of costimulatory molecules primarily targets migratory dendritic cells. *Sci Immunol*, 2019. 4(35).
 108. Kornete, M. and C.A. Piccirillo, Functional crosstalk between dendritic cells and Foxp3(+) regulatory T cells in the maintenance of immune tolerance. *Front Immunol*, 2012. 3: p. 165.
 109. Rubtsov, Y.P., et al., Regulatory T cell-derived interleukin-10 limits inflammation at environmental interfaces. *Immunity*, 2008. 28(4): p. 546-58.
 110. Maynard, C.L., et al., Regulatory T cells expressing interleukin 10 develop from Foxp3⁺ and Foxp3⁻ precursor cells in the absence of interleukin 10. *Nat Immunol*, 2007. 8(9): p. 931-41.
 111. Domogalla, M.P., et al., Tolerance through Education: How Tolerogenic Dendritic Cells Shape Immunity. *Front Immunol*, 2017. 8: p. 1764.
 112. Iwasaki, A. and R. Medzhitov, Control of adaptive immunity by the innate immune system. *Nat Immunol*, 2015. 16(4): p. 343-53.
 113. Sporri, R. and C. Reis e Sousa, Inflammatory mediators are insufficient for full dendritic cell activation and promote expansion of CD4⁺ T cell populations lacking helper function. *Nat Immunol*, 2005. 6(2): p. 163-70.
 114. Probst, H.C., et al., Inducible transgenic mice reveal resting dendritic cells as potent inducers of CD8⁺ T cell tolerance. *Immunity*, 2003. 18(5): p. 713-20.
 115. Hasegawa, H. and T. Matsumoto, Mechanisms of Tolerance Induction by Dendritic Cells In Vivo. *Front Immunol*, 2018. 9: p. 350.
 116. Lee, J.H., et al., Tolerogenic dendritic cells are efficiently generated using minocycline and dexamethasone. *Sci Rep*, 2017. 7(1): p. 15087.
 117. Cifuentes-Rius, A., et al., Inducing immune tolerance with dendritic cell-targeting nanomedicines. *Nat Nanotechnol*, 2021. 16(1): p. 37-46.
 118. Stern, J.N., et al., Promoting tolerance to proteolipid protein-induced experimental autoimmune encephalomyelitis through targeting dendritic cells. *Proc Natl Acad Sci U S A*, 2010. 107(40): p. 17280-5.
 119. Moos, M.P., et al., The lamina adventitia is the major site of immune cell accumulation in standard chow-fed apolipoprotein E-deficient mice. *Arterioscler Thromb Vasc Biol*, 2005. 25(11): p. 2386-91.
 120. Grabner, R., et al., Lymphotoxin beta receptor signaling promotes tertiary

REFERENCES

- lymphoid organogenesis in the aorta adventitia of aged ApoE^{-/-} mice. *J Exp Med*, 2009. 206(1): p. 233-48.
121. Hu, D., et al., Artery Tertiary Lymphoid Organs Control Aorta Immunity and Protect against Atherosclerosis via Vascular Smooth Muscle Cell Lymphotoxin beta Receptors. *Immunity*, 2015. 42(6): p. 1100-15.
 122. Srikakulapu, P., et al., Artery Tertiary Lymphoid Organs Control Multilayered Territorialized Atherosclerosis B-Cell Responses in Aged ApoE^{-/-} Mice. *Arterioscler Thromb Vasc Biol*, 2016. 36(6): p. 1174-85.
 123. Yin, C., et al., Artery Tertiary Lymphoid Organs: Powerhouses of Atherosclerosis Immunity. *Front Immunol*, 2016. 7: p. 387.
 124. Mohanta, S.K., et al., Artery tertiary lymphoid organs contribute to innate and adaptive immune responses in advanced mouse atherosclerosis. *Circ Res*, 2014. 114(11): p. 1772-87.
 125. Sallusto, F., J. Geginat, and A. Lanzavecchia, Central memory and effector memory T cell subsets: function, generation, and maintenance. *Annu Rev Immunol*, 2004. 22: p. 745-63.
 126. Woodland, D.L. and J.E. Kohlmeier, Migration, maintenance and recall of memory T cells in peripheral tissues. *Nat Rev Immunol*, 2009. 9(3): p. 153-61.
 127. Witebsky, E., et al., Chronic thyroiditis and autoimmunization. *J Am Med Assoc*, 1957. 164(13): p. 1439-47.
 128. Olsson, T., et al., Autoreactive T lymphocytes in multiple sclerosis determined by antigen-induced secretion of interferon-gamma. *J Clin Invest*, 1990. 86(3): p. 981-5.
 129. Goodnow, C.C., Multistep pathogenesis of autoimmune disease. *Cell*, 2007. 130(1): p. 25-35.
 130. Siewert, K., et al., Unbiased identification of target antigens of CD8⁺ T cells with combinatorial libraries coding for short peptides. *Nat Med*, 2012. 18(5): p. 824-8.
 131. Ruhl, G., et al., Multiple sclerosis: Molecular mimicry of an antimyelin HLA class I restricted T-cell receptor. *Neurol Neuroimmunol Neuroinflamm*, 2016. 3(4): p. e241.
 132. Lee, J.W., et al., Peripheral antigen display by lymph node stroma promotes T cell tolerance to intestinal self. *Nat Immunol*, 2007. 8(2): p. 181-90.
 133. Coppieters, K.T., et al., Demonstration of islet-autoreactive CD8 T cells in insulitic lesions from recent onset and long-term type 1 diabetes patients. *J Exp Med*, 2012. 209(1): p. 51-60.
 134. Hermansson, A., et al., Inhibition of T cell response to native low-density lipoprotein reduces atherosclerosis. *J Exp Med*, 2010. 207(5): p. 1081-93.
 135. Fredrikson, G.N., et al., Identification of immune responses against aldehyde-modified peptide sequences in apoB associated with cardiovascular disease. *Arterioscler Thromb Vasc Biol*, 2003. 23(5): p. 872-8.
 136. Fredrikson, G.N., et al., Inhibition of atherosclerosis in apoE-null mice by immunization with apoB-100 peptide sequences. *Arterioscler Thromb Vasc Biol*, 2003. 23(5): p. 879-84.

REFERENCES

137. Shaw, M.K., et al., T-Cells Specific for a Self-Peptide of ApoB-100 Exacerbate Aortic Atheroma in Murine Atherosclerosis. *Front Immunol*, 2017. 8: p. 95.
138. Tse, K., et al., Atheroprotective Vaccination with MHC-II Restricted Peptides from ApoB-100. *Front Immunol*, 2013. 4: p. 493.
139. Nikolich-Zugich, J., M.K. Slifka, and I. Messaoudi, The many important facets of T-cell repertoire diversity. *Nat Rev Immunol*, 2004. 4(2): p. 123-32.
140. Glanville, J., et al., Identifying specificity groups in the T cell receptor repertoire. *Nature*, 2017. 547(7661): p. 94-98.
141. Attaf, M., E. Huseby, and A.K. Sewell, alphabeta T cell receptors as predictors of health and disease. *Cell Mol Immunol*, 2015. 12(4): p. 391-9.
142. Rosati, E., et al., Overview of methodologies for T-cell receptor repertoire analysis. *BMC Biotechnol*, 2017. 17(1): p. 61.
143. Paulsson, G., et al., Oligoclonal T cell expansions in atherosclerotic lesions of apolipoprotein E-deficient mice. *Arterioscler Thromb Vasc Biol*, 2000. 20(1): p. 10-7.
144. Mason, D., A very high level of crossreactivity is an essential feature of the T-cell receptor. *Immunol Today*, 1998. 19(9): p. 395-404.
145. Sewell, A.K., Why must T cells be cross-reactive? *Nat Rev Immunol*, 2012. 12(9): p. 669-77.
146. Yin, Y. and R.A. Mariuzza, The multiple mechanisms of T cell receptor cross-reactivity. *Immunity*, 2009. 31(6): p. 849-51.
147. Cunningham, M.W., T cell mimicry in inflammatory heart disease. *Mol Immunol*, 2004. 40(14-15): p. 1121-7.
148. Liu, X.S. and E.R. Mardis, Applications of Immunogenomics to Cancer. *Cell*, 2017. 168(4): p. 600-612.
149. Tang, F., et al., mRNA-Seq whole-transcriptome analysis of a single cell. *Nat Methods*, 2009. 6(5): p. 377-82.
150. Hwang, B., J.H. Lee, and D. Bang, Single-cell RNA sequencing technologies and bioinformatics pipelines. *Exp Mol Med*, 2018. 50(8): p. 96.
151. Winkels, H., et al., Atlas of the Immune Cell Repertoire in Mouse Atherosclerosis Defined by Single-Cell RNA-Sequencing and Mass Cytometry. *Circ Res*, 2018. 122(12): p. 1675-1688.
152. Cochain, C., et al., Single-Cell RNA-Seq Reveals the Transcriptional Landscape and Heterogeneity of Aortic Macrophages in Murine Atherosclerosis. *Circ Res*, 2018. 122(12): p. 1661-1674.
153. Krasemann, S., et al., The TREM2-APOE Pathway Drives the Transcriptional Phenotype of Dysfunctional Microglia in Neurodegenerative Diseases. *Immunity*, 2017. 47(3): p. 566-581.e9.
154. Jaitin, D.A., et al., Lipid-Associated Macrophages Control Metabolic Homeostasis in a Trem2-Dependent Manner. *Cell*, 2019. 178(3): p. 686-698.e14.
155. Chowdhury, R.R., et al., Human Coronary Plaque T Cells Are Clonal and Cross-React to Virus and Self. *Circ Res*, 2022. 130(10): p. 1510-1530.
156. Baekkeskov, S., et al., Identification of the 64K autoantigen in insulin-

REFERENCES

- dependent diabetes as the GABA-synthesizing enzyme glutamic acid decarboxylase. *Nature*, 1990. 347(6289): p. 151-6.
157. Wenzlau, J.M., et al., The cation efflux transporter ZnT8 (Slc30A8) is a major autoantigen in human type 1 diabetes. *Proc Natl Acad Sci U S A*, 2007. 104(43): p. 17040-5.
 158. Bernard, C.C., et al., Myelin oligodendrocyte glycoprotein: a novel candidate autoantigen in multiple sclerosis. *J Mol Med (Berl)*, 1997. 75(2): p. 77-88.
 159. Seitz, S., et al., Reconstitution of paired T cell receptor alpha- and beta-chains from microdissected single cells of human inflammatory tissues. *Proc Natl Acad Sci U S A*, 2006. 103(32): p. 12057-62.
 160. Arakawa, A., et al., Melanocyte antigen triggers autoimmunity in human psoriasis. *J Exp Med*, 2015. 212(13): p. 2203-12.
 161. Codina-Busqueta, E., et al., TCR bias of in vivo expanded T cells in pancreatic islets and spleen at the onset in human type 1 diabetes. *J Immunol*, 2011. 186(6): p. 3787-97.
 162. Gorski, J., et al., Circulating T cell repertoire complexity in normal individuals and bone marrow recipients analyzed by CDR3 size spectratyping. Correlation with immune status. *J Immunol*, 1994. 152(10): p. 5109-19.
 163. Dash, P., et al., Paired analysis of TCRalpha and TCRbeta chains at the single-cell level in mice. *J Clin Invest*, 2011. 121(1): p. 288-95.
 164. Baker, F.J., et al., Restricted islet-cell reactive T cell repertoire of early pancreatic islet infiltrates in NOD mice. *Proc Natl Acad Sci U S A*, 2002. 99(14): p. 9374-9.
 165. Ozawa, T., et al., Comprehensive analysis of the functional TCR repertoire at the single-cell level. *Biochem Biophys Res Commun*, 2008. 367(4): p. 820-5.
 166. Huang, H., et al., Select sequencing of clonally expanded CD8(+) T cells reveals limits to clonal expansion. *Proc Natl Acad Sci U S A*, 2019. 116(18): p. 8995-9001.
 167. Hu, D., et al., Preparation of Single Cell Suspensions from Mouse Aorta. *Bio Protoc*, 2016. 6(11).
 168. Wang, Z., et al., Combined Single-Cell RNA and Single-Cell alpha/beta T Cell Receptor Sequencing of the Arterial Wall in Atherosclerosis. *Methods Mol Biol*, 2022. 2419: p. 727-746.
 169. Zhou, Y., et al., Metascape provides a biologist-oriented resource for the analysis of systems-level datasets. *Nat Commun*, 2019. 10(1): p. 1523.
 170. Liu, Y., et al., Tumour heterogeneity and intercellular networks of nasopharyngeal carcinoma at single cell resolution. *Nat Commun*, 2021. 12(1): p. 741.
 171. Vento-Tormo, R., et al., Single-cell reconstruction of the early maternal-fetal interface in humans. *Nature*, 2018. 563(7731): p. 347-353.
 172. Subramanian, A., et al., Gene set enrichment analysis: a knowledge-based approach for interpreting genome-wide expression profiles. *Proc Natl Acad Sci U S A*, 2005. 102(43): p. 15545-50.
 173. Yu, G., et al., clusterProfiler: an R package for comparing biological themes

REFERENCES

- among gene clusters. *Omics*, 2012. 16(5): p. 284-7.
174. Pan, H., et al., Single-Cell Genomics Reveals a Novel Cell State During Smooth Muscle Cell Phenotypic Switching and Potential Therapeutic Targets for Atherosclerosis in Mouse and Human. *Circulation*, 2020. 142(21): p. 2060-2075.
 175. Wirka, R.C., et al., Atheroprotective roles of smooth muscle cell phenotypic modulation and the TCF21 disease gene as revealed by single-cell analysis. *Nat Med*, 2019. 25(8): p. 1280-1289.
 176. Huang, S., et al., Lymph nodes are innervated by a unique population of sensory neurons with immunomodulatory potential. *Cell*, 2021. 184(2): p. 441-459 e25.
 177. Grieshaber-Bouyer, R., et al., The neutrotime transcriptional signature defines a single continuum of neutrophils across biological compartments. *Nat Commun*, 2021. 12(1): p. 2856.
 178. Saeki, K., et al., Mammary cell gene expression atlas links epithelial cell remodeling events to breast carcinogenesis. *Commun Biol*, 2021. 4(1): p. 660.
 179. Barsheshet, Y., et al., CCR8(+)FOXP3(+) Treg cells as master drivers of immune regulation. *Proc Natl Acad Sci U S A*, 2017. 114(23): p. 6086-6091.
 180. Vasanthakumar, A., et al., The TNF Receptor Superfamily-NF-kappaB Axis Is Critical to Maintain Effector Regulatory T Cells in Lymphoid and Non-lymphoid Tissues. *Cell Rep*, 2017. 20(12): p. 2906-2920.
 181. Miragaia, R.J., et al., Single-Cell Transcriptomics of Regulatory T Cells Reveals Trajectories of Tissue Adaptation. *Immunity*, 2019. 50(2): p. 493-504.e7.
 182. Tan, L., et al., Single-Cell Transcriptomics Identifies the Adaptation of Scart1(+) Vgamma6(+) T Cells to Skin Residency as Activated Effector Cells. *Cell Rep*, 2019. 27(12): p. 3657-3671.e4.
 183. Koizumi, S.I. and H. Ishikawa, Transcriptional Regulation of Differentiation and Functions of Effector T Regulatory Cells. *Cells*, 2019. 8(8).
 184. Lanzavecchia, A. and F. Sallusto, Regulation of T cell immunity by dendritic cells. *Cell*, 2001. 106(3): p. 263-6.
 185. Dick, S.A., et al., Self-renewing resident cardiac macrophages limit adverse remodeling following myocardial infarction. *Nat Immunol*, 2019. 20(1): p. 29-39.
 186. Waskow, C., et al., The receptor tyrosine kinase Flt3 is required for dendritic cell development in peripheral lymphoid tissues. *Nat Immunol*, 2008. 9(6): p. 676-83.
 187. Baratin, M., et al., Homeostatic NF-kappaB Signaling in Steady-State Migratory Dendritic Cells Regulates Immune Homeostasis and Tolerance. *Immunity*, 2015. 42(4): p. 627-39.
 188. Bedoui, S., et al., Cross-presentation of viral and self antigens by skin-derived CD103+ dendritic cells. *Nat Immunol*, 2009. 10(5): p. 488-95.
 189. Henri, S., et al., CD207+ CD103+ dermal dendritic cells cross-present keratinocyte-derived antigens irrespective of the presence of Langerhans

REFERENCES

- cells. *J Exp Med*, 2010. 207(1): p. 189-206.
190. Worbs, T., S.I. Hammerschmidt, and R. Forster, Dendritic cell migration in health and disease. *Nat Rev Immunol*, 2017. 17(1): p. 30-48.
 191. Ohi, L., et al., CCR7 governs skin dendritic cell migration under inflammatory and steady-state conditions. *Immunity*, 2004. 21(2): p. 279-88.
 192. Yamakita, Y., et al., Fascin1 promotes cell migration of mature dendritic cells. *J Immunol*, 2011. 186(5): p. 2850-9.
 193. Kou, Z.C., et al., T-Cell receptor Vbeta repertoire CDR3 length diversity differs within CD45RA and CD45RO T-cell subsets in healthy and human immunodeficiency virus-infected children. *Clin Diagn Lab Immunol*, 2000. 7(6): p. 953-9.
 194. Yang, H.Q., et al., Single-Cell TCR Sequencing Reveals the Dynamics of T Cell Repertoire Profiling During Pneumocystis Infection. *Front Microbiol*, 2021. 12: p. 637500.
 195. Lin, Z., et al., Deep sequencing of the T cell receptor beta repertoire reveals signature patterns and clonal drift in atherosclerotic plaques and patients. *Oncotarget*, 2017. 8(59): p. 99312-99322.
 196. Oksenberg, J.R., et al., Analysis of the T-cell receptor repertoire in human atherosclerosis. *Cardiovasc Res*, 1997. 36(2): p. 256-67.
 197. Lee, M., et al., Single-cell RNA sequencing identifies shared differentiation paths of mouse thymic innate T cells. *Nat Commun*, 2020. 11(1): p. 4367.
 198. Chaudhary, N. and D.R. Wesemann, Analyzing Immunoglobulin Repertoires. *Front Immunol*, 2018. 9: p. 462.
 199. Aversa, I., et al., Molecular T-Cell Repertoire Analysis as Source of Prognostic and Predictive Biomarkers for Checkpoint Blockade Immunotherapy. *Int J Mol Sci*, 2020. 21(7).
 200. Gkazi, A.S., et al., Clinical T Cell Receptor Repertoire Deep Sequencing and Analysis: An Application to Monitor Immune Reconstitution Following Cord Blood Transplantation. *Front Immunol*, 2018. 9: p. 2547.
 201. Oakes, T., et al., Quantitative Characterization of the T Cell Receptor Repertoire of Naive and Memory Subsets Using an Integrated Experimental and Computational Pipeline Which Is Robust, Economical, and Versatile. *Front Immunol*, 2017. 8: p. 1267.
 202. Yang, X., et al., Long Noncoding RNA AW112010 Promotes the Differentiation of Inflammatory T Cells by Suppressing IL-10 Expression through Histone Demethylation. *J Immunol*, 2020. 205(4): p. 987-993.
 203. Thomson, D.W., et al., Aberrant RAG-mediated recombination contributes to multiple structural rearrangements in lymphoid blast crisis of chronic myeloid leukemia. *Leukemia*, 2020. 34(8): p. 2051-2063.
 204. Grawunder, U., et al., DNA ligase IV is essential for V(D)J recombination and DNA double-strand break repair in human precursor lymphocytes. *Mol Cell*, 1998. 2(4): p. 477-84.
 205. Woehrle, T., et al., Pannexin-1 hemichannel-mediated ATP release together with P2X1 and P2X4 receptors regulate T-cell activation at the immune

REFERENCES

- synapse. *Blood*, 2010. 116(18): p. 3475-84.
206. Apostolopoulos, J., I.F. McKenzie, and M.S. Sandrin, Ly6d-L, a cell surface ligand for mouse Ly6d. *Immunity*, 2000. 12(2): p. 223-32.
 207. Koizumi, S.I., et al., JunB regulates homeostasis and suppressive functions of effector regulatory T cells. *Nat Commun*, 2018. 9(1): p. 5344.
 208. Bezman, N.A., et al., Molecular definition of the identity and activation of natural killer cells. *Nat Immunol*, 2012. 13(10): p. 1000-9.
 209. Zemmour, D., et al., Single-cell gene expression reveals a landscape of regulatory T cell phenotypes shaped by the TCR. *Nat Immunol*, 2018. 19(3): p. 291-301.
 210. Shevryev, D. and V. Tereshchenko, Treg Heterogeneity, Function, and Homeostasis. *Front Immunol*, 2019. 10: p. 3100.
 211. Grosche, L., et al., The CD83 Molecule - An Important Immune Checkpoint. *Front Immunol*, 2020. 11: p. 721.
 212. Bommireddy, R. and T. Doetschman, TGFbeta1 and Treg cells: alliance for tolerance. *Trends Mol Med*, 2007. 13(11): p. 492-501.
 213. Turner, J.A., et al., Regulatory T Cell-Derived TGF-beta1 Controls Multiple Checkpoints Governing Allergy and Autoimmunity. *Immunity*, 2020. 53(6): p. 1202-1214 e6.
 214. Gaddis, D.E., et al., Apolipoprotein AI prevents regulatory to follicular helper T cell switching during atherosclerosis. *Nat Commun*, 2018. 9(1): p. 1095.
 215. Li, L., J. Kim, and V.A. Boussiotis, IL-1beta-mediated signals preferentially drive conversion of regulatory T cells but not conventional T cells into IL-17-producing cells. *J Immunol*, 2010. 185(7): p. 4148-53.
 216. Engelbertsen, D., et al., IL-1R and MyD88 signalling in CD4+ T cells promote Th17 immunity and atherosclerosis. *Cardiovasc Res*, 2018. 114(1): p. 180-187.
 217. Chung, Y., et al., Critical regulation of early Th17 cell differentiation by interleukin-1 signaling. *Immunity*, 2009. 30(4): p. 576-87.
 218. Liu, Z.D., et al., Increased Th17 cell frequency concomitant with decreased Foxp3+ Treg cell frequency in the peripheral circulation of patients with carotid artery plaques. *Inflamm Res*, 2012. 61(10): p. 1155-65.
 219. Debes, G.F., et al., Chemokine receptor CCR7 required for T lymphocyte exit from peripheral tissues. *Nat Immunol*, 2005. 6(9): p. 889-94.
 220. Martens, R., et al., Efficient homing of T cells via afferent lymphatics requires mechanical arrest and integrin-supported chemokine guidance. *Nat Commun*, 2020. 11(1): p. 1114.
 221. Matloubian, M., et al., Lymphocyte egress from thymus and peripheral lymphoid organs is dependent on S1P receptor 1. *Nature*, 2004. 427(6972): p. 355-60.
 222. Kumar, B.V., et al., Human Tissue-Resident Memory T Cells Are Defined by Core Transcriptional and Functional Signatures in Lymphoid and Mucosal Sites. *Cell Rep*, 2017. 20(12): p. 2921-2934.
 223. Nurieva, R.I. and Y. Chung, Understanding the development and function of T

REFERENCES

- follicular helper cells. *Cell Mol Immunol*, 2010. 7(3): p. 190-7.
224. Robertson, A.K. and G.K. Hansson, T cells in atherogenesis: for better or for worse? *Arterioscler Thromb Vasc Biol*, 2006. 26(11): p. 2421-32.
225. Schreyer, S.A., C.M. Vick, and R.C. LeBoeuf, Loss of lymphotoxin-alpha but not tumor necrosis factor-alpha reduces atherosclerosis in mice. *J Biol Chem*, 2002. 277(14): p. 12364-8.
226. Davenport, P. and P.G. Tipping, The role of interleukin-4 and interleukin-12 in the progression of atherosclerosis in apolipoprotein E-deficient mice. *Am J Pathol*, 2003. 163(3): p. 1117-25.
227. King, V.L., L.A. Cassis, and A. Daugherty, Interleukin-4 does not influence development of hypercholesterolemia or angiotensin II-induced atherosclerotic lesions in mice. *Am J Pathol*, 2007. 171(6): p. 2040-7.
228. Day, C.L., et al., PD-1 expression on HIV-specific T cells is associated with T-cell exhaustion and disease progression. *Nature*, 2006. 443(7109): p. 350-4.
229. Barber, D.L., et al., Restoring function in exhausted CD8 T cells during chronic viral infection. *Nature*, 2006. 439(7077): p. 682-7.
230. Gotsman, I., et al., Proatherogenic immune responses are regulated by the PD-1/PD-L pathway in mice. *J Clin Invest*, 2007. 117(10): p. 2974-82.
231. Blackburn, S.D., et al., Coregulation of CD8+ T cell exhaustion by multiple inhibitory receptors during chronic viral infection. *Nat Immunol*, 2009. 10(1): p. 29-37.
232. Butler, N.S., et al., Therapeutic blockade of PD-L1 and LAG-3 rapidly clears established blood-stage Plasmodium infection. *Nat Immunol*, 2011. 13(2): p. 188-95.
233. Kaufmann, D.E., et al., Upregulation of CTLA-4 by HIV-specific CD4+ T cells correlates with disease progression and defines a reversible immune dysfunction. *Nat Immunol*, 2007. 8(11): p. 1246-54.
234. Molodtsov, A. and M.J. Turk, Tissue Resident CD8 Memory T Cell Responses in Cancer and Autoimmunity. *Front Immunol*, 2018. 9: p. 2810.
235. Mueller, S.N. and L.K. Mackay, Tissue-resident memory T cells: local specialists in immune defence. *Nat Rev Immunol*, 2016. 16(2): p. 79-89.
236. Hombrink, P., et al., Programs for the persistence, vigilance and control of human CD8(+) lung-resident memory T cells. *Nat Immunol*, 2016. 17(12): p. 1467-1478.
237. Malik, B.T., et al., Resident memory T cells in the skin mediate durable immunity to melanoma. *Sci Immunol*, 2017. 2(10).
238. Wieczorek, M., et al., Major Histocompatibility Complex (MHC) Class I and MHC Class II Proteins: Conformational Plasticity in Antigen Presentation. *Front Immunol*, 2017. 8: p. 292.
239. Galkina, E., et al., CXCR6 promotes atherosclerosis by supporting T-cell homing, interferon-gamma production, and macrophage accumulation in the aortic wall. *Circulation*, 2007. 116(16): p. 1801-11.
240. Butcher, M.J., et al., CXCR6 regulates the recruitment of pro-inflammatory IL-17A-producing T cells into atherosclerotic aortas. *Int Immunol*, 2016. 28(5): p.

REFERENCES

- 255-61.
241. Marçais, A., et al., Cell-Autonomous CCL5 Transcription by Memory CD8 T Cells Is Regulated by IL-4. *The Journal of Immunology*, 2006. 177(7): p. 4451-4457.
 242. Raval, A., et al., Cytokine regulation of expression of class I MHC antigens. *Exp Mol Med*, 1998. 30(1): p. 1-13.
 243. Dudek, M., et al., Auto-aggressive CXCR6(+) CD8 T cells cause liver immune pathology in NASH. *Nature*, 2021. 592(7854): p. 444-449.
 244. Latta, M., K. Mohan, and T.B. Issekutz, CXCR6 is expressed on T cells in both T helper type 1 (Th1) inflammation and allergen-induced Th2 lung inflammation but is only a weak mediator of chemotaxis. *Immunology*, 2007. 121(4): p. 555-64.
 245. Xia, C., et al., S100 Proteins As an Important Regulator of Macrophage Inflammation. *Front Immunol*, 2017. 8: p. 1908.
 246. Dukhanina, E.A., et al., The role of S100A4 protein in anticancer cytotoxicity: its presence is required on the surface of CD(4+)CD(25+)PGRPs(+)S100A4(+) lymphocyte and undesirable on the surface of target cells. *Cell Cycle*, 2018. 17(4): p. 479-485.
 247. Garin, M.I., et al., Galectin-1: a key effector of regulation mediated by CD4+CD25+ T cells. *Blood*, 2007. 109(5): p. 2058-65.
 248. Toscano, M.A., et al., Differential glycosylation of TH1, TH2 and TH-17 effector cells selectively regulates susceptibility to cell death. *Nat Immunol*, 2007. 8(8): p. 825-34.
 249. Castillo-Gonzalez, R., et al., Galectin-1 Expression in CD8(+) T Lymphocytes Controls Inflammation in Contact Hypersensitivity. *J Invest Dermatol*, 2020.
 250. Papotto, P.H., J.C. Ribot, and B. Silva-Santos, IL-17(+) gammadelta T cells as kick-starters of inflammation. *Nat Immunol*, 2017. 18(6): p. 604-611.
 251. Ribot, J.C., et al., CD27 is a thymic determinant of the balance between interferon-gamma- and interleukin 17-producing gammadelta T cell subsets. *Nat Immunol*, 2009. 10(4): p. 427-36.
 252. Stuart, T., et al., Comprehensive Integration of Single-Cell Data. *Cell*, 2019. 177(7): p. 1888-1902 e21.
 253. Passerini, L. and S. Gregori, Induction of Antigen-Specific Tolerance in T Cell Mediated Diseases. *Front Immunol*, 2020. 11: p. 2194.
 254. Selck, C. and M. Dominguez-Villar, Antigen-Specific Regulatory T Cell Therapy in Autoimmune Diseases and Transplantation. *Front Immunol*, 2021. 12: p. 661875.
 255. Jansen, M.A.A., et al., Matured Tolerogenic Dendritic Cells Effectively Inhibit Autoantigen Specific CD4(+) T Cells in a Murine Arthritis Model. *Front Immunol*, 2019. 10: p. 2068.
 256. Ferreira, G.B., et al., 1,25-Dihydroxyvitamin D3 promotes tolerogenic dendritic cells with functional migratory properties in NOD mice. *J Immunol*, 2014. 192(9): p. 4210-20.
 257. Florez-Grau, G., et al., Tolerogenic Dendritic Cells as a Promising Antigen-

REFERENCES

- Specific Therapy in the Treatment of Multiple Sclerosis and Neuromyelitis Optica From Preclinical to Clinical Trials. *Front Immunol*, 2018. 9: p. 1169.
258. Bluestone, J.A. and H. Bour-Jordan, Current and future immunomodulation strategies to restore tolerance in autoimmune diseases. *Cold Spring Harb Perspect Biol*, 2012. 4(11).
259. Zhang, J., et al., Senescent T cells: a potential biomarker and target for cancer therapy. *EBioMedicine*, 2021. 68: p. 103409.
260. Butcher, M.J., et al., Atherosclerosis-Driven Treg Plasticity Results in Formation of a Dysfunctional Subset of Plastic IFN γ ⁺ Th1/Tregs. *Circ Res*, 2016. 119(11): p. 1190-1203.
261. Li, J., et al., CCR5+T-bet+FoxP3⁺ Effector CD4 T Cells Drive Atherosclerosis. *Circ Res*, 2016. 118(10): p. 1540-52.
262. Libby, P. and B.M. Everett, Novel Antiatherosclerotic Therapies. *Arterioscler Thromb Vasc Biol*, 2019. 39(4): p. 538-545.
263. Lutgens, E., et al., Immunotherapy for cardiovascular disease. *Eur Heart J*, 2019. 40(48): p. 3937-3946.
264. Williams, J.W., L.H. Huang, and G.J. Randolph, Cytokine Circuits in Cardiovascular Disease. *Immunity*, 2019. 50(4): p. 941-954.
265. Ferreira, L.M.R., et al., Next-generation regulatory T cell therapy. *Nat Rev Drug Discov*, 2019. 18(10): p. 749-769.
266. Zernecke, A., et al., Meta-Analysis of Leukocyte Diversity in Atherosclerotic Mouse Aortas. *Circ Res*, 2020. 127(3): p. 402-426.
267. Pfister, D., et al., NASH limits anti-tumour surveillance in immunotherapy-treated HCC. *Nature*, 2021. 592(7854): p. 450-456.
268. Binder, C.J., et al., Pneumococcal vaccination decreases atherosclerotic lesion formation: molecular mimicry between *Streptococcus pneumoniae* and oxidized LDL. *Nat Med*, 2003. 9(6): p. 736-43.
269. Weyand, C.M. and J.J. Goronzy, The immunology of rheumatoid arthritis. *Nat Immunol*, 2021. 22(1): p. 10-18.
270. Wang, T., et al., Regulatory T cells in rheumatoid arthritis showed increased plasticity toward Th17 but retained suppressive function in peripheral blood. *Ann Rheum Dis*, 2015. 74(6): p. 1293-301.
271. Brabb, T., et al., In situ tolerance within the central nervous system as a mechanism for preventing autoimmunity. *J Exp Med*, 2000. 192(6): p. 871-80.
272. Hori, S., et al., Specificity requirements for selection and effector functions of CD25⁺4⁺ regulatory T cells in anti-myelin basic protein T cell receptor transgenic mice. *Proc Natl Acad Sci U S A*, 2002. 99(12): p. 8213-8.
273. Westerberg, L.S., C. Klein, and S.B. Snapper, Breakdown of T cell tolerance and autoimmunity in primary immunodeficiency--lessons learned from monogenic disorders in mice and men. *Curr Opin Immunol*, 2008. 20(6): p. 646-54.
274. Ridker, P.M., et al., Antiinflammatory Therapy with Canakinumab for Atherosclerotic Disease. *N Engl J Med*, 2017. 377(12): p. 1119-1131.
275. Morante-Palacios, O., et al., Tolerogenic Dendritic Cells in Autoimmunity and

REFERENCES

- Inflammatory Diseases. *Trends Immunol*, 2021. 42(1): p. 59-75.
276. Alhadj Ali, M., et al., Metabolic and immune effects of immunotherapy with proinsulin peptide in human new-onset type 1 diabetes. *Sci Transl Med*, 2017. 9(402).
277. Dinh, T.N., et al., Cytokine therapy with interleukin-2/anti-interleukin-2 monoclonal antibody complexes expands CD4+CD25+Foxp3+ regulatory T cells and attenuates development and progression of atherosclerosis. *Circulation*, 2012. 126(10): p. 1256-66.
278. van Puijvelde, G.H., et al., Induction of oral tolerance to oxidized low-density lipoprotein ameliorates atherosclerosis. *Circulation*, 2006. 114(18): p. 1968-76.
279. Fredrikson, G.N., et al., Treatment with apo B peptide vaccines inhibits atherosclerosis in human apo B-100 transgenic mice without inducing an increase in peptide-specific antibodies. *J Intern Med*, 2008. 264(6): p. 563-70.
280. Wigren, M., et al., Evidence for a role of regulatory T cells in mediating the atheroprotective effect of apolipoprotein B peptide vaccine. *J Intern Med*, 2011. 269(5): p. 546-56.
281. Chyu, K.Y., et al., CD8+ T cells mediate the athero-protective effect of immunization with an ApoB-100 peptide. *PLoS One*, 2012. 7(2): p. e30780.
282. Gee, M.H., et al., Antigen Identification for Orphan T Cell Receptors Expressed on Tumor-Infiltrating Lymphocytes. *Cell*, 2018. 172(3): p. 549-563 e16.
283. Kisielow, J., F.J. Obermair, and M. Kopf, Deciphering CD4(+) T cell specificity using novel MHC-TCR chimeric receptors. *Nat Immunol*, 2019. 20(5): p. 652-662.
284. Joglekar, A.V., et al., T cell antigen discovery via signaling and antigen-presenting bifunctional receptors. *Nat Methods*, 2019. 16(2): p. 191-198.
285. Li, G., et al., T cell antigen discovery via trogocytosis. *Nature Methods*, 2019. 16(2): p. 183-190.

APPENDIX

APPENDIX

Table 1. The DEGs of different immune cells between ApoE^{-/-} blood and WT blood. Data were calculated by the FindMarkers function in Seurat package; only the significant DEGs are shown (avg_logFC > 0.25 or avg_logFC < -0.25 and p_adj_val < 0.05). The positive avg_logFC designates genes upregulated in ApoE^{-/-} blood. The negative avg_logFC represents genes downregulated in ApoE^{-/-} blood. p_val: p value; avg_logFC: log fold-change of the average expression between the two groups; pct.1: the percentage of cells where the feature is detected in the first group; pct.2: the percentage of cells where the feature is detected in the second group; p_val_adj: adjusted p value.

128

Cell type	Gene symbol	Gene name	p_val	avg_logFC	pct.1	pct.2	p_val_adj
CD8 Naïve	Slc1a5	solute carrier family 1 (neutral amino acid transporter), member 5	3,39E-12	-0,52374	0,027	0,311	4,41E-08
CD8 effector/memory	Pglyrp1	peptidoglycan recognition protein 1	6,86E-08	-0,46974	0,325	0,603	0,000892
	Hbb-bs	hemoglobin, beta adult s chain	1,40E-07	-0,39134	0,06	0,258	0,001827
	Gnai2	G protein subunit alpha I2	1,98E-07	0,339278	0,795	0,67	0,002581
	Zmat2	zinc finger matrin-type 2	3,98E-07	-0,36693	0,19	0,416	0,00518
	Gpr183	G protein-coupled receptor 183	1,47E-06	-0,37341	0,355	0,627	0,019129
	Slc1a5	solute carrier family 1 (neutral amino acid transporter), member 5	2,51E-06	-0,34485	0,09	0,278	0,032672
Monocytes	ApoE	apolipoprotein E	1,48E-61	-2,54821	0,075	0,886	1,93E-57
	Pglyrp1	peptidoglycan recognition protein 1	3,75E-14	0,82211	0,801	0,418	4,87E-10
	Hbb-bs	hemoglobin, beta adult s chain	1,11E-12	1,20876	0,041	0,291	1,44E-08
	Apoc1	apolipoprotein C-I	2,18E-07	-0,26768	0,045	0,209	0,002841
	Taf10	TATA-box binding protein associated factor 10	2,63E-07	0,499347	0,609	0,392	0,003425
	Plin2	perilipin 2	3,49E-07	-0,3444	0,444	0,671	0,004544

APPENDIX

	Mfap3	microfibril associated protein 3	2,11E-06	-0,29859	0,12	0,304	0,027395
B cells	Apoe	apolipoprotein E	2,28E-50	-0,70061	0,022	0,158	2,97E-46
	Serinc3	serine incorporator 3	1,16E-31	-0,33073	0,476	0,656	1,50E-27
	Slc1a5	solute carrier family 1 (neutral amino acid transporter), member 5	5,98E-28	-0,3737	0,071	0,189	7,77E-24
	H2-T23	histocompatibility 2, T region locus 23	7,02E-25	-0,33015	0,309	0,473	9,14E-21
	Pltp	phospholipid transfer protein	4,65E-18	-0,31721	0,088	0,184	6,05E-14
	Tsc22d3	TSC22 domain family, member 3	5,16E-17	-0,27841	0,515	0,641	6,71E-13
	Pitpna	phosphatidylinositol transfer protein, alpha	1,93E-11	0,269901	0,325	0,25	2,51E-07
	Gm42031	/	8,59E-11	0,258736	0,337	0,255	1,12E-06
Neutrophils	Pglyrp1	peptidoglycan recognition protein 1	1,85E-17	0,348919	0,867	0,79	2,41E-13
	Hbb-bs	hemoglobin, beta adult s chain	6,27E-14	-1,12371	0,063	0,183	8,16E-10
	H2-D1	histocompatibility 2, D region locus 1	4,14E-13	-0,30715	0,833	0,886	5,38E-09
	Junb	jun B proto-oncogene	5,03E-13	-0,36247	0,773	0,86	6,55E-09
	Lrg1	leucine-rich alpha-2-glycoprotein 1	1,38E-11	-0,49315	0,328	0,481	1,79E-07
	Plaur	plasminogen activator, urokinase receptor	9,39E-10	0,496037	0,215	0,1	1,22E-05
	Socs3	suppressor of cytokine signaling 3	6,69E-09	-0,56038	0,107	0,21	8,71E-05
	Fos	FBJ osteosarcoma oncogene	1,82E-08	-0,48909	0,302	0,439	0,000236
	Hp	haptoglobin	3,72E-07	-0,25203	0,643	0,732	0,00484
	Arhgdib	Rho, GDP dissociation inhibitor (GDI) beta	2,71E-06	0,273667	0,595	0,505	0,035313
	Tnfaip2	tumor necrosis factor, alpha-induced protein 2	3,73E-06	-0,26843	0,475	0,59	0,048522

APPENDIX

Table 2. The top 20 DEGs of different T cell clusters. Data were calculated by the FindAllMarkers function in the Seurat package, only the top 20 significant DEGs are shown (avg_logFC > 0.25 or avg_logFC < -0.25 and p_adj_val < 0.05). p_val: p value; avg_logFC: log fold-change of the average expression between the two groups; pct.1: the percentage of cells where the feature is detected in the first group; pct.2: the percentage of cells where the feature is detected in the second group; p_val_adj: adjusted p value.

Cell type	Gene symbol	Gene name	avg_logFC	pct.1	pct.2	p_val_adj
eT _{reg}	Tnfrsf4	tumor necrosis factor receptor superfamily, member 4	1,51036	0,743	0,181	1,32E-171
	Foxp3	forkhead box P3	1,197495	0,495	0,052	3,17E-171
	Ikzf2	IKAROS family zinc finger 2	1,428962	0,781	0,245	3,91E-163
	Areg	amphiregulin	1,806199	0,556	0,09	1,96E-156
	Cd83	CD83 antigen	1,507889	0,49	0,081	2,31E-135
	Ccr8	chemokine (C-C motif) receptor 8	1,207215	0,366	0,033	1,63E-134
	Ctla4	cytotoxic T-lymphocyte-associated protein 4	1,263941	0,688	0,219	7,61E-121
	Cd81	CD81 antigen	1,196349	0,459	0,078	1,12E-119
	Itgav	integrin alpha V	1,265542	0,587	0,161	9,34E-117
	Izumo1r	IZUMO1 receptor, JUNO	1,078894	0,766	0,281	2,53E-108
	Tnfrsf9	tumor necrosis factor receptor superfamily, member 9	1,344482	0,436	0,082	3,49E-107
	Samsn1	SAM domain, SH3 domain and nuclear localization signals, 1	1,140786	0,686	0,283	3,65E-96
	Junb	jun B proto-oncogene	0,886491	0,977	0,78	7,10E-88
	Arhgap31	Rho GTPase activating protein 31	0,999573	0,642	0,289	1,65E-75
	Fth1	ferritin heavy polypeptide 1	0,691875	0,989	0,987	5,85E-73
Tnfrsf18	tumor necrosis factor receptor superfamily,	0,964061	0,697	0,369	7,70E-73	

APPENDIX

		member 18				
	Il1r2	interleukin 1 receptor, type II	0,928507	0,213	0,02	1,05E-71
	Cebpb	CCAAT/enhancer binding protein (C/EBP), beta	0,945789	0,644	0,311	4,65E-66
	Ifrd1	interferon-related developmental regulator 1	1,135106	0,69	0,395	1,61E-65
	Zfp36l1	zinc finger protein 36, C3H type-like 1	0,916622	0,81	0,557	1,60E-63
CD4 T _{em}	Gpm6b	glycoprotein m6b	1,287653	0,569	0,043	1,09E-234
	Sostdc1	sclerostin domain containing 1	2,171258	0,385	0,02	1,61E-174
	Tnfsf8	tumor necrosis factor (ligand) superfamily, member 8	1,544859	0,649	0,151	5,47E-157
	Cd4	CD4 antigen	1,067793	0,715	0,17	2,52E-151
	Tbc1d4	TBC1 domain family, member 4	1,130457	0,569	0,111	4,44E-137
	Cd200	CD200 antigen	0,96078	0,373	0,04	1,63E-124
	Cd40lg	CD40 ligand	0,970187	0,505	0,101	1,73E-110
	Eea1	early endosome antigen 1	1,003544	0,519	0,114	1,24E-107
	Hif1a	hypoxia inducible factor 1, alpha subunit	1,15891	0,689	0,258	1,02E-105
	Izumo1r	IZUMO1 receptor, JUNO	0,93562	0,768	0,284	4,55E-99
	Angptl2	angiopoietin-like 2	0,592618	0,206	0,008	1,96E-94
	Smco4	single-pass membrane protein with coiled-coil domains 4	0,828143	0,565	0,172	1,74E-86
	Slamf6	SLAM family member 6	1,032243	0,553	0,179	8,33E-85
	Lag3	lymphocyte-activation gene 3	0,992224	0,415	0,089	3,23E-83
	Ly6a	lymphocyte antigen 6 complex, locus A	1,002519	0,794	0,411	1,61E-80
	Spp1	secreted phosphoprotein 1	1,661427	0,174	0,007	6,00E-80
	Ptms	parathyrosin	0,887309	0,503	0,15	5,71E-77
	Spry1	sprouty RTK signaling antagonist 1	0,681294	0,251	0,03	3,46E-73
	Gm14718	predicted gene 14718	0,45379	0,168	0,011	7,87E-66
	Tnfrsf4	tumor necrosis factor receptor superfamily, member 4	0,674225	0,615	0,209	1,46E-65

APPENDIX

CD8 T _{em}	Gzmk	granzyme K	2,143833	0,826	0,051	0
	Nkg7	natural killer cell group 7 sequence	1,507327	0,944	0,379	2,04E-168
	Ccl5	chemokine (C-C motif) ligand 5	1,758704	0,926	0,308	8,08E-163
	Eomes	eomesodermin	1,136958	0,521	0,108	2,06E-116
	Ccr5	chemokine (C-C motif) receptor 5	1,053404	0,416	0,076	6,50E-96
	Ctla2a	cytotoxic T lymphocyte-associated protein 2 alpha	1,057659	0,633	0,231	2,61E-82
	Lmo1	LIM domain only 1	0,450562	0,136	0,002	3,13E-73
	Nr4a2	nuclear receptor subfamily 4, group A, member 2	1,190893	0,548	0,182	1,41E-72
	Ccl4	chemokine (C-C motif) ligand 4	1,623686	0,333	0,062	3,68E-71
	Xcl1	chemokine (C motif) ligand 1	0,930494	0,432	0,13	1,35E-56
	Hcst	hematopoietic cell signal transducer	0,612324	0,94	0,778	1,07E-52
	Esm1	endothelial cell-specific molecule 1	0,468811	0,114	0,005	9,51E-48
	Il10ra	interleukin 10 receptor, alpha	0,652962	0,34	0,091	1,74E-47
	Itga4	integrin alpha 4	0,596825	0,62	0,287	2,55E-43
	Ms4a4b	membrane-spanning 4-domains, subfamily A, member 4B	0,586937	0,913	0,682	6,68E-40
	Ccl3	chemokine (C-C motif) ligand 3	0,90804	0,128	0,013	3,51E-37
	Epha3	Eph receptor A3	0,259762	0,101	0,006	4,35E-37
	Fasl	Fas ligand (TNF superfamily, member 6)	0,665809	0,353	0,126	5,44E-35
	Runx3	runt related transcription factor 3	0,604167	0,568	0,306	1,52E-34
	Rgs1	regulator of G-protein signaling 1	0,76116	0,617	0,342	8,08E-33
CD8 Naïve	Igfbp4	insulin-like growth factor binding protein 4	1,016436	0,6	0,054	1,07E-202
	Dapl1	death associated protein-like 1	1,18998	0,559	0,063	3,19E-175
	Cd8b1	CD8 antigen, beta chain 1	1,181446	0,905	0,261	2,53E-152
	Rps20	ribosomal protein S20	0,570923	1	0,993	4,70E-129
	Cd8a	CD8 antigen, alpha chain	0,93041	0,785	0,216	2,61E-127

APPENDIX

133

	Rplp0	ribosomal protein, large, P0	0,554262	1	0,991	4,07E-127
	Rps24	ribosomal protein S24	0,406821	1	0,997	5,34E-106
	Rps19	ribosomal protein S19	0,512333	0,998	0,985	2,39E-101
	Rpl35	ribosomal protein L35	0,457298	0,998	0,983	7,06E-100
	Rps27a	ribosomal protein S27A	0,383949	1	0,995	2,03E-99
	Rps8	ribosomal protein S8	0,406653	1	0,995	4,78E-99
	Rpl35a	ribosomal protein L35A	0,379166	1	0,994	7,00E-98
	Lef1	lymphoid enhancer binding factor 1	0,814584	0,798	0,291	3,69E-97
	Rplp1	ribosomal protein, large, P1	0,401854	1	0,995	1,52E-96
	Rps28	ribosomal protein S28	0,427218	1	0,991	2,01E-95
	Rpl23	ribosomal protein L23	0,392918	1	0,995	1,19E-93
	Rpl8	ribosomal protein L8	0,407206	0,998	0,991	8,05E-93
	Rps4x	ribosomal protein S4, X-linked	0,404113	1	0,994	5,74E-92
	Rps7	ribosomal protein S7	0,405488	0,998	0,994	2,11E-90
	Ccr7	chemokine (C-C motif) receptor 7	0,803909	0,771	0,258	9,22E-89
CD8 T _{cm}	Ly6c2	lymphocyte antigen 6 complex, locus C2	1,736965	0,886	0,148	3,92E-230
	Fcgrt	Fc receptor, IgG, alpha chain transporter	0,679	0,424	0,037	2,89E-142
	Ccl5	chemokine (C-C motif) ligand 5	1,098164	0,989	0,317	2,67E-139
	Nkg7	natural killer cell group 7 sequence	0,887669	0,989	0,388	2,50E-108
	Gzmm	granzyme M (lymphocyte met-ase 1)	0,784032	0,334	0,032	5,21E-104
	Cd8b1	CD8 antigen, beta chain 1	0,952421	0,851	0,277	1,03E-100
	Klrd1	killer cell lectin-like receptor, subfamily D, member 1	0,73011	0,671	0,166	3,74E-95
	Ifitm10	interferon induced transmembrane protein 10	0,637937	0,571	0,123	3,52E-91
	Ctsw	cathepsin W	0,854371	0,902	0,363	3,87E-91
	Klrk1	killer cell lectin-like receptor subfamily K, member 1	0,893833	0,495	0,107	1,61E-80
	Klrc1	killer cell lectin-like receptor subfamily C,	0,688872	0,429	0,085	1,24E-72

APPENDIX

		member 1					
	1700025G04 Rik	RIKEN cDNA 1700025G04 gene	0,476811	0,391	0,071	6,63E-72	
	Cd7	CD7 antigen	0,652463	0,628	0,186	3,11E-69	
	Cd8a	CD8 antigen, alpha chain	0,58131	0,707	0,234	1,65E-59	
	Sidt1	SID1 transmembrane family, member 1	0,565809	0,579	0,178	2,63E-59	
	Ctla2a	cytotoxic T lymphocyte-associated protein 2 alpha	0,448299	0,707	0,232	7,05E-58	
	Ms4a4c	membrane-spanning 4-domains, subfamily A, member 4C	0,516673	0,424	0,104	1,04E-56	
	Rps12	ribosomal protein S12	0,431511	1	0,982	1,08E-50	
	Samd3	sterile alpha motif domain containing 3	0,376894	0,302	0,059	7,23E-49	
	Ms4a4b	membrane-spanning 4-domains, subfamily A, member 4B	0,579488	0,976	0,681	7,60E-47	
134	NKT/CD8 T _{cm}	Fcεr1g	Fc receptor, IgE, high affinity I, gamma polypeptide	1,921767	0,473	0,015	2,16E-227
		Klrb1c	killer cell lectin-like receptor subfamily B member 1C	1,101745	0,36	0,006	1,33E-197
		Klre1	killer cell lectin-like receptor family E member 1	1,077947	0,516	0,042	3,14E-164
		Klra7	killer cell lectin-like receptor, subfamily A, member 7	1,025516	0,392	0,022	2,05E-150
		Klrk1	killer cell lectin-like receptor subfamily K, member 1	1,289448	0,678	0,1	6,30E-149
		Tyrobp	TYRO protein tyrosine kinase binding protein	2,035886	0,322	0,011	3,40E-148
		Klrc1	killer cell lectin-like receptor subfamily C, member 1	1,080998	0,558	0,082	6,15E-118
		Klrc2	killer cell lectin-like receptor subfamily C, member 2	0,710372	0,304	0,017	5,06E-115
		Ly6c2	lymphocyte antigen 6 complex, locus C2	1,342582	0,767	0,18	1,25E-113

APPENDIX

	Ncr1	natural cytotoxicity triggering receptor 1	1,031533	0,177	0,001	8,26E-109
	Cd7	CD7 antigen	1,232769	0,753	0,187	8,37E-106
	Ccl5	chemokine (C-C motif) ligand 5	1,006294	0,996	0,335	2,47E-105
	Sytl3	synaptotagmin-like 3	0,824629	0,59	0,116	8,52E-95
	Klrd1	killer cell lectin-like receptor, subfamily D, member 1	0,957493	0,71	0,177	1,50E-92
	Xcl1	chemokine (C motif) ligand 1	1,038656	0,597	0,131	4,86E-85
	1700025G04 Rik	RIKEN cDNA 1700025G04 gene	0,662685	0,456	0,074	6,41E-84
	Nfkbiz	nuclear factor of kappa light polypeptide gene enhancer in B cells inhibitor, zeta	1,122874	0,731	0,249	1,27E-75
	Nkg7	natural killer cell group 7 sequence	0,741238	0,986	0,406	7,41E-70
	Klra8	killer cell lectin-like receptor, subfamily A, member 8	0,651474	0,12	0,001	6,04E-69
	Klri2	killer cell lectin-like receptor family I member 2	0,485771	0,131	0,002	1,77E-67
CD4 Naïve	Ly6c1	lymphocyte antigen 6 complex, locus C1	0,930549	0,254	0,019	6,00E-78
	Igfbp4	insulin-like growth factor binding protein 4	1,482762	0,466	0,093	1,57E-74
	Lef1	lymphoid enhancer binding factor 1	0,925214	0,701	0,325	2,69E-46
	Rpl21	ribosomal protein L21	0,288104	0,996	0,997	6,92E-35
	Rps3a1	ribosomal protein S3A1	0,287607	0,992	0,998	1,33E-33
	Rpl8	ribosomal protein L8	0,331183	0,981	0,992	3,27E-33
	Rps24	ribosomal protein S24	0,291268	0,996	0,997	3,95E-33
	Rpl35a	ribosomal protein L35A	0,290196	0,985	0,996	4,50E-31
	Rps4x	ribosomal protein S4, X-linked	0,299331	0,985	0,996	7,35E-30
	Rps29	ribosomal protein S29	0,289378	0,985	0,996	8,24E-30
	Rps19	ribosomal protein S19	0,352971	0,985	0,987	3,50E-29
	Rps27a	ribosomal protein S27A	0,28873	0,992	0,996	4,43E-29
	Ccr7	chemokine (C-C motif) receptor 7	0,703526	0,625	0,296	5,45E-29
	Rps8	ribosomal protein S8	0,311726	0,981	0,997	6,50E-29

APPENDIX

	Rps7	ribosomal protein S7	0,310607	0,992	0,995	7,32E-28
	Rplp0	ribosomal protein, large, P0	0,33272	0,981	0,993	1,17E-27
	Rps20	ribosomal protein S20	0,334037	0,981	0,995	3,47E-27
	Rps16	ribosomal protein S16	0,250597	0,981	0,997	1,01E-25
	Actn1	actinin, alpha 1	0,549623	0,371	0,133	9,76E-24
	Rpl7	ribosomal protein L7	0,312125	0,966	0,982	5,18E-23
cT _{reg}	Foxp3	forkhead box P3	0,996138	0,448	0,097	8,66E-55
	Izumo1r	IZUMO1 receptor, JUNO	0,81357	0,734	0,329	4,33E-37
	Ikzf2	IKAROS family zinc finger 2	0,899308	0,672	0,304	7,88E-36
	Shisa5	shisa family member 5	0,559839	0,975	0,959	6,33E-33
	AW112010	expressed sequence AW112010	0,657327	0,925	0,865	3,53E-27
	Cd81	CD81 antigen	0,70434	0,382	0,12	1,57E-26
	Ighm	immunoglobulin heavy constant mu	0,764423	0,701	0,505	6,38E-22
	Malat1	metastasis associated lung adenocarcinoma transcript 1 (non-coding RNA)	0,456763	0,992	0,998	4,49E-19
	Iifi27l2a	interferon, alpha-inducible protein 27 like 2A	0,670432	0,772	0,518	2,97E-18
	H2-K1	histocompatibility 2, K1, K region	0,328056	0,979	0,987	2,01E-16
	Samhd1	SAM domain and HD domain, 1	0,699012	0,631	0,476	1,24E-15
	Cd74	CD74 antigen (invariant polypeptide of major histocompatibility complex, class II antigen-associated)	0,862302	0,502	0,282	4,46E-15
	Ltb	lymphotoxin B	0,615749	0,822	0,794	1,46E-14
	Il2ra	interleukin 2 receptor, alpha chain	0,625202	0,282	0,105	1,72E-13
	Gimap3	GTPase, IMAP family member 3	0,448306	0,855	0,842	1,78E-13
	Tspan32	tetraspanin 32	0,645663	0,502	0,293	2,71E-12
	Capg	capping protein (actin filament), gelsolin-like	0,61331	0,523	0,3	1,02E-11
	Inpp4b	inositol polyphosphate-4-phosphatase, type II	0,608012	0,577	0,398	3,07E-11
	Itgae	integrin alpha E, epithelial-associated	0,552343	0,187	0,058	3,99E-11

APPENDIX

	H2-D1	histocompatibility 2, D region locus 1	0,293531	0,971	0,983	6,18E-11
γδ T	Tmem176b	transmembrane protein 176B	2,510663	0,964	0,055	0
	Tmem176a	transmembrane protein 176A	2,469548	0,973	0,044	0
	Tcrγ-C1	T cell receptor gamma constant 1	1,712282	0,664	0,018	0
	Actn2	actinin alpha 2	1,662009	0,834	0,038	0
	Blk	B lymphoid kinase	1,653624	0,561	0,003	0
	Serpinb1a	serine (or cysteine) peptidase inhibitor, clade B, member 1a	1,506228	0,659	0,013	0
	Pxdc1	PX domain containing 1	1,455658	0,596	0,011	0
	Ly6g5b	lymphocyte antigen 6 complex, locus G5B	1,384824	0,583	0,005	0
	Kcnk1	potassium channel, subfamily K, member 1	1,17256	0,534	0,001	0
	Tcrγ-V6	T cell receptor gamma, variable 6	1,965349	0,457	0,002	2,18E-291
	Cd163l1	CD163 molecule-like 1	2,22155	0,498	0,006	5,75E-291
	Ckb	creatine kinase, brain	2,123388	0,839	0,061	5,93E-290
	Trdv4	T cell receptor delta variable 4	2,954665	0,475	0,007	6,47E-264
	Ltb4r1	leukotriene B4 receptor 1	1,34608	0,592	0,023	4,37E-248
	Rorc	RAR-related orphan receptor gamma	1,063946	0,48	0,011	4,67E-238
	Il23r	interleukin 23 receptor	0,972881	0,395	0,003	2,85E-235
	Il17re	interleukin 17 receptor E	0,972136	0,439	0,008	7,10E-230
	Trdc	T cell receptor delta constant	1,739761	0,516	0,019	6,55E-225
	Zbtb16	zinc finger and BTB domain containing 16	0,834809	0,336	0,004	3,30E-190
Rbpms2	RNA binding protein with multiple splicing 2	0,681888	0,287	0,001	1,05E-181	

APPENDIX

Table 3. The top 20 DEGs of different myeloid cell clusters. Data were calculated by the FindAllMarkers function in the Seurat package, only the top 20 significant DEGs are shown (avg_logFC > 0.25 or avg_logFC < -0.25 and p_adj_val < 0.05). p_val: p value; avg_logFC: log fold-change of the average expression between the two groups; pct.1: the percentage of cells where the feature is detected in the first group; pct.2: the percentage of cells where the feature is detected in the second group; p_val_adj: adjusted p value.

138

Cell type	Gene symbol	Gene name	avg_logFC	pct.1	pct.2	p_val_adj
CD11c ⁻ DC	Ccr7	chemokine (C-C motif) receptor 7	2,885895	1	0,871	6,23E-70
	Fscn1	fascin actin-bundling protein 1	3,31479	0,984	0,7	5,59E-68
	Socs2	suppressor of cytokine signaling 2	2,165473	0,967	0,563	2,31E-64
	Cacnb3	calcium channel, voltage-dependent, beta 3 subunit	1,858324	0,959	0,469	2,23E-62
	Tmem123	transmembrane protein 123	2,623222	0,975	0,777	3,14E-62
	Ccl5	chemokine (C-C motif) ligand 5	4,329179	0,967	0,641	4,69E-62
	Cxcl16	chemokine (C-X-C motif) ligand 16	1,857401	0,959	0,519	3,29E-59
	Tbc1d4	TBC1 domain family, member 4	1,845622	1	0,655	1,57E-58
	Tmem176a	transmembrane protein 176A	1,951575	0,975	0,638	1,79E-58
	Tspan3	tetraspanin 3	1,998682	0,959	0,661	9,02E-57
	Marcks1	MARCKS-like 1	1,880634	0,967	0,791	1,98E-51
	Il4i1	interleukin 4 induced 1	1,938963	0,975	0,843	1,67E-50
	Apol7c	apolipoprotein L 7c	2,576779	0,877	0,244	8,85E-48
	Serpinb6b	serine (or cysteine) peptidase inhibitor, clade B, member 6b	2,188534	0,918	0,778	9,32E-47
	Crip1	cysteine-rich protein 1 (intestinal)	1,871186	0,967	0,927	1,48E-43
Epsti1	epithelial stromal interaction 1 (breast)	2,459475	0,934	0,911	3,46E-38	

APPENDIX

	Fabp5	fatty acid binding protein 5, epidermal	2,055613	0,934	0,765	8,25E-37
	Ccl22	chemokine (C-C motif) ligand 22	2,067212	0,754	0,419	3,96E-28
	AW112010	expressed sequence AW112010	1,929234	0,91	0,914	3,59E-26
	Zmynd15	zinc finger, MYND-type containing 15	1,82703	0,73	0,3	1,68E-21
CD11b ⁺ cDC	Ppp1r14a	protein phosphatase 1, regulatory inhibitor subunit 14A	0,980839	0,973	0,875	1,48E-104
	Ccnd1	cyclin D1	1,531684	0,991	0,773	2,89E-83
	Avpi1	arginine vasopressin-induced 1	1,123443	0,995	0,726	1,60E-82
	Cd7	CD7 antigen	1,499596	0,946	0,833	7,45E-82
	H2-DMb2	histocompatibility 2, class II, locus Mb2	1,445429	0,991	0,918	1,14E-81
	Cd74	CD74 antigen (invariant polypeptide of major histocompatibility complex, class II antigen-associated)	1,178419	1	0,957	2,11E-78
	H2-Oa	histocompatibility 2, O region alpha locus	1,126288	0,968	0,941	9,38E-69
	Haus8	4HAUS augmin-like complex, subunit 8	0,945392	0,964	0,626	1,10E-66
	Gsn	gelsolin	0,924604	0,959	0,559	5,73E-65
	Klrd1	killer cell lectin-like receptor, subfamily D, member 1	1,142366	0,887	0,773	4,08E-64
	Tbc1d4	TBC1 domain family, member 4	0,905759	0,964	0,636	4,73E-64
	Napsa	napsin A aspartic peptidase	0,910988	0,977	0,783	7,36E-64
	H2-Eb1	histocompatibility 2, class II antigen E beta	1,016606	0,995	0,911	1,48E-63
	Cfp	complement factor properdin	1,133066	0,977	0,67	2,39E-61
	Gng10	guanine nucleotide binding protein (G protein), gamma 10	0,884832	0,977	0,816	7,81E-59
	H2-Aa	histocompatibility 2, class II antigen A, alpha	0,906597	1	0,936	8,31E-58
	H2-Ab1	histocompatibility 2, class II antigen A, beta 1	0,926928	1	0,857	1,11E-55
	S100a4	S100 calcium binding protein A4	0,792089	0,964	0,508	2,89E-51
	Gm2a	GM2 ganglioside activator protein	0,804115	0,968	0,805	8,78E-51
	Ffar2	free fatty acid receptor 2	0,813111	0,783	0,621	2,65E-35

APPENDIX

140

CD8a ⁺ cDC	Xcr1	chemokine (C motif) receptor 1	1,531536	1	0,156	1,61E-43
	Ppt1	palmitoyl-protein thioesterase 1	2,065057	1	0,733	5,10E-42
	Cst3	cystatin C	2,534819	1	0,967	8,34E-42
	A530099J19Rik	NA	1,137563	0,972	0,237	4,47E-41
	Ifi205	interferon activated gene 205	1,520139	1	0,782	2,91E-40
	Plbd1	phospholipase B domain containing 1	1,735714	1	0,772	1,13E-39
	Atpif1	ATPase inhibitory factor 1	1,444247	1	0,799	1,51E-38
	Irf8	interferon regulatory factor 8	1,62248	1	0,871	7,05E-38
	Naaa	N-acylethanolamine acid amidase	1,725117	0,972	0,461	1,94E-36
	Wdfy4	WD repeat and FYVE domain containing 4	1,396248	1	0,589	2,76E-36
	Clec9a	C-type lectin domain family 9, member a	1,364805	0,958	0,431	1,91E-34
	Rab7b	RAB7B, member RAS oncogene family	1,19834	0,972	0,449	2,31E-34
	H2-Ab1	histocompatibility 2, class II antigen A, beta 1	1,342984	1	0,871	1,42E-33
	Ckb	creatine kinase, brain	1,55658	0,986	0,663	3,01E-33
	Atox1	antioxidant 1 copper chaperone	1,146357	1	0,911	5,07E-33
	Psap	prosaposin	1,204952	1	0,946	3,48E-32
	Id2	inhibitor of DNA binding 2	1,237402	1	0,567	7,91E-29
	Gm2a	GM2 ganglioside activator protein	1,056479	1	0,82	3,05E-27
	H2-Eb1	histocompatibility 2, class II antigen E beta	1,055341	1	0,92	2,85E-26
	H2-DMb1	histocompatibility 2, class II, locus Mb1	1,084821	0,972	0,766	7,84E-26
pDC	Cd8b1	CD8 antigen, beta chain 1	3,036901	1	0,775	1,78E-29
	Ccr9	chemokine (C-C motif) receptor 9	2,27159	1	0,655	1,96E-29
	Siglech	sialic acid binding Ig-like lectin H	2,92791	1	0,767	2,65E-29
	Atp1b1	ATPase, Na ⁺ /K ⁺ transporting, beta 1 polypeptide	2,108957	1	0,725	3,49E-29
	Bst2	bone marrow stromal cell antigen 2	2,839159	1	0,875	1,47E-28
	Dnajc7	DnaJ heat shock protein family (Hsp40) member C7	2,070017	1	0,784	1,71E-28

APPENDIX

141

	Tcf4	transcription factor 4	1,992675	1	0,737	4,36E-28
	Ly6c2	lymphocyte antigen 6 complex, locus C2	2,584884	1	0,662	1,35E-27
	Ly6a	lymphocyte antigen 6 complex, locus A	2,573798	1	0,849	4,59E-27
	Lgals1	lectin, galactose binding, soluble 1	1,866787	1	0,732	6,83E-27
	Iglc3	immunoglobulin lambda constant 3	2,835025	0,98	0,805	7,11E-27
	Cyb561a3	cytochrome b561 family, member A3	1,607105	0,98	0,645	9,17E-27
	Ctsl	cathepsin L	2,12464	0,98	0,54	1,03E-26
	Ly6d	lymphocyte antigen 6 complex, locus D	3,079712	0,98	0,83	1,20E-26
	Irf8	interferon regulatory factor 8	2,066521	1	0,873	1,44E-26
	Rnase6	ribonuclease, RNase A family, 6	1,845995	1	0,857	1,48E-26
	Cox6a2	cytochrome c oxidase subunit 6A2	2,64953	0,939	0,479	2,11E-24
	Grn	granulin	1,580974	1	0,82	2,68E-23
	Cd209d	CD209d antigen	1,845591	0,939	0,613	3,77E-23
	Pltp	phospholipid transfer protein	1,743557	1	0,679	5,65E-22
Trem2 ^{high} MΦ	Fcgr	Fc fragment of IgM receptor	0,703587	0,963	0,852	8,94E-132
	Iglc2	immunoglobulin lambda constant 2	0,492791	0,957	0,761	1,46E-125
	Gimap6	GTPase, IMAP family member 6	0,470469	0,957	0,77	4,12E-114
	Cd79a	CD79A antigen (immunoglobulin-associated alpha)	1,20535	0,955	0,776	6,05E-114
	Lyz1	lysozyme 1	1,133423	0,933	0,649	1,01E-111
	Pla2g2d	phospholipase A2, group IID	0,666949	0,983	0,709	3,71E-110
	Ebf1	early B cell factor 1	0,861672	0,963	0,741	8,36E-108
	Ptpn22	protein tyrosine phosphatase, receptor type, C polypeptide-associated protein	0,591585	0,967	0,887	1,74E-107
	Ptpn22	protein tyrosine phosphatase, receptor type, C polypeptide-associated protein	0,591585	0,967	0,887	1,74E-107
	Ms4a1	membrane-spanning 4-domains, subfamily A, member 1	0,738388	0,957	0,798	6,39E-102
	Cst7	cystatin F (leukocystatin)	0,453657	0,946	0,802	1,10E-97

APPENDIX

	Igkc	immunoglobulin kappa constant	0,538821	0,97	0,864	1,01E-83
	Cd79b	CD79B antigen	0,682932	0,957	0,862	3,25E-73
	Acp5	acid phosphatase 5, tartrate resistant	0,658211	0,937	0,768	1,66E-50
	Cd81	CD81 antigen	0,434043	0,913	0,517	8,29E-50
	Myc	myelocytomatosis oncogene	0,608029	0,833	0,651	5,87E-46
	Cd72	CD72 antigen	0,630006	0,757	0,56	1,24E-32
	Hebp1	heme binding protein 1	0,555054	0,777	0,698	8,49E-25
	Ctsd	cathepsin D	0,647024	0,881	0,707	1,19E-21
	Phlda1	pleckstrin homology like domain, family A, member 1	0,551584	0,618	0,404	4,84E-17
	Ccl12	chemokine (C-C motif) ligand 12	0,488489	0,429	0,45	0,086342
Mo/MΦ	Ly6i	lymphocyte antigen 6 complex, locus I	2,02134	0,97	0,701	1,35E-97
	Ace	angiotensin I converting enzyme (peptidyl-dipeptidase A) 1	1,132179	0,945	0,656	1,33E-89
	Plac8	placenta-specific 8	2,341632	0,99	0,869	1,88E-85
	Ifitm3	interferon induced transmembrane protein 3	1,879943	0,985	0,774	1,63E-83
	Csf1r	colony stimulating factor 1 receptor	1,361162	0,975	0,586	9,11E-77
	Fcer1g	Fc receptor, IgE, high affinity I, gamma polypeptide	1,281284	1	0,934	2,89E-76
	Clec4a3	C-type lectin domain family 4, member a3	1,349865	0,96	0,525	2,29E-73
	Cybb	cytochrome b-245, beta polypeptide	1,611856	0,985	0,797	1,10E-71
	Lst1	leukocyte specific transcript 1	1,193138	1	0,765	5,95E-71
	Ms4a6c	membrane-spanning 4-domains, subfamily A, member 6C	1,286944	0,98	0,837	3,00E-66
	Fgr	FGR proto-oncogene, Src family tyrosine kinase	1,179205	0,965	0,657	2,82E-63
	Clec4a1	C-type lectin domain family 4, member a1	1,174011	0,915	0,506	2,25E-59
	Ms4a4c	membrane-spanning 4-domains, subfamily A, member 4C	1,139164	0,965	0,884	7,05E-58
	Lyz2	lysozyme 2	1,145723	0,995	0,734	2,65E-57

APPENDIX

143

	Cyp4f18	cytochrome P450, family 4, subfamily f, polypeptide 18	1,243863	0,9	0,472	1,86E-56
	Cebpb	CCAAT/enhancer binding protein (C/EBP), beta	1,327828	0,975	0,675	2,71E-56
	Gngt2	guanine nucleotide binding protein (G protein), gamma transducing activity polypeptide 2	1,151495	0,975	0,805	1,10E-48
	Itgal	integrin alpha L	1,223638	0,92	0,775	9,19E-44
	Ifi27l2a	interferon, alpha-inducible protein 27 like 2A	1,122966	0,945	0,757	4,71E-38
	Hp	haptoglobin	1,0721	0,786	0,498	1,65E-30
Lyve1 ⁺ res-like MΦ	Selenop	selenoprotein P	2,554917	0,972	0,585	2,21E-77
	Cd5l	CD5 antigen-like	1,044064	0,943	0,566	2,03E-75
	C1qc	complement component 1, q subcomponent, C chain	2,130659	0,943	0,472	3,57E-75
	Fcna	ficolin A	1,742985	0,943	0,634	1,51E-72
	C1qb	complement component 1, q subcomponent, beta polypeptide	1,903135	0,932	0,484	4,08E-68
	C1qa	complement component 1, q subcomponent, alpha polypeptide	1,67405	0,938	0,518	1,47E-65
	Timd4	T cell immunoglobulin and mucin domain containing 4	1,246616	0,96	0,862	3,24E-57
	Cpq	carboxypeptidase Q	0,920585	0,943	0,635	2,65E-55
	Pla2g2d	phospholipase A2, group IID	1,051163	0,96	0,785	4,39E-49
	Timp2	tissue inhibitor of metalloproteinase 2	0,964126	0,972	0,594	2,76E-47
	Sdc3	syndecan 3	1,283749	0,915	0,703	1,59E-39
	Ctsd	cathepsin D	0,940284	0,977	0,741	8,13E-38
	Ctsb	cathepsin B	1,129074	0,989	0,938	2,12E-36
	Igf1	insulin-like growth factor 1	1,166825	0,852	0,692	7,96E-34
	Mafb	v-maf musculoaponeurotic fibrosarcoma oncogene family, protein B (avian)	1,05279	0,847	0,423	2,60E-33

APPENDIX

	Lyz2	lysozyme 2	0,932199	0,943	0,746	3,01E-33
	Igfbp7	insulin-like growth factor binding protein 7	1,207866	0,886	0,484	3,35E-32
	Fxyd2	FXVD domain-containing ion transport regulator 2	0,963777	0,858	0,788	1,21E-27
	Igfbp4	insulin-like growth factor binding protein 4	1,030076	0,761	0,388	1,64E-21
	Ccl8	chemokine (C-C motif) ligand 8	1,82512	0,688	0,426	3,64E-13
Neutrophils	Asprv1	aspartic peptidase, retroviral-like 1	1,877191	0,938	0,695	7,52E-60
	Msrb1	methionine sulfoxide reductase B1	1,644444	0,957	0,722	1,28E-51
	Dusp1	dual specificity phosphatase 1	1,842786	0,969	0,743	4,60E-51
	Isg15	ISG15 ubiquitin-like modifier	1,940832	0,981	0,823	2,52E-44
	Csf3r	colony stimulating factor 3 receptor (granulocyte)	2,10222	0,852	0,331	7,60E-44
	Pglyrp1	peptidoglycan recognition protein 1	2,114803	0,889	0,816	2,77E-39
	Slc7a11	solute carrier family 7 (cationic amino acid transporter, y+ system), member 11	1,64865	0,796	0,34	3,48E-30
	Klf2	Kruppel-like factor 2 (lung)	1,428409	0,907	0,817	2,29E-27
	Egr1	early growth response 1	1,487691	0,809	0,551	7,70E-26
	Il1rn	interleukin 1 receptor antagonist	1,834537	0,765	0,593	4,50E-21
	Hcar2	hydroxycarboxylic acid receptor 2	1,387943	0,735	0,228	5,82E-20
	Slpi	secretory leukocyte peptidase inhibitor	2,363698	0,741	0,517	5,14E-19
	Cxcr2	chemokine (C-X-C motif) receptor 2	1,71746	0,716	0,577	4,09E-16
	Mmp9	matrix metalloproteinase 9	1,662026	0,704	0,538	1,19E-14
	Slfn1	schlafen 1	1,491774	0,71	0,656	7,31E-12
	Ccl2	chemokine (C-C motif) receptor-like 2	1,525488	0,673	0,545	5,30E-08
	Ccl6	chemokine (C-C motif) ligand 6	1,673223	0,63	0,585	6,21E-07
	Wfdc17	WAP four-disulfide core domain 17	1,451409	0,63	0,657	0,005012
	Acod1	aconitate decarboxylase 1	1,76464	0,586	0,152	0,034372
	Ccl3	chemokine (C-C motif) ligand 3	1,543832	0,537	0,437	0,229421

ACKNOWLEDGEMENTS

ACKNOWLEDGEMENTS

Time flies, five years have passed, and my doctoral studies have come to an end. But I still remembered the day I first arrived in Germany in the winter of 2017. It was my first time in a completely new environment, with both worries and excitement. Many thanks to all the people who helped me get through the difficult times to complete my project.

First and foremost, I would like to thank my supervisor Prof. Andreas Habenicht, who gave me the opportunity to join this excellent group to explore the immune system and atherosclerosis. His scientific advice and rigorous attitude to each question really helped me to complete my research. His innovative ideas and extensive academic knowledge in atherosclerosis will be a role model for me to learn from in my future life and work.

I would also like to sincerely thank Dr. Changjun Yin for his kind help in all my research. His help in discussing each result and suggestions for improvement when encountering problems strongly supported me in advancing my project.

Many thanks to PD Dr. Klaus Dornmair for being a member of my thesis advisory committee. His advice helped me to figure out the analysis and interpretation of TCR repertoires. His expertise in T cell research has given me more inspiration for future research.

I would like to express my gratitude to Dr. Sarajo Mohanta for his help in my project. I'm very grateful to Dr. Donato Santovito for his help in statistical analysis and to Dr. Michael Hristov for his help in single cell sorting. Also, Many thanks to Prof. Klaus Ley for his valuable comments on specific issues of my project. In addition, I would like to thank my colleagues, Dr. Yuanfang Li, Dr. Zhe Ma, Dr. Chuankai Zhang, Xi Zhang, Ting Sun, Shu Lu, Yutao Li, Rui Su, Mingyang Hong, Xinyi Deng, and Mohammad Rafiee Monjezi whose assistance and suggestion in my daily life helped me to overcome every problem and made my life colorful. I really appreciate helps from other people of IPEK, Rundan Duan, Dr. Xavier Blanchet, Chang Pan, Dr. Virginia Egea, Catherine Gunczi, Emanuel Putz, Iliriana Vatovci, Damaris Bindl,

ACKNOWLEDGEMENTS

Thomas Pitsch, whose help in studies and personal matters made it easy for me to integrate into an unfamiliar environment.

I also really appreciate the financial support from Oversea Study Program of Guangzhou Elite Project. Without their support, I would not have been able to complete my doctoral studies.

Last but not least, I would like to express my love to my parents, my elder brother and his wife, my nephew and my niece. The care and understanding of my parents encouraged me to finish my studies. Great thanks to my elder brother and sister-in-law, who have helped me take care of my parents for the past five years. Also, thanks to my young nephew and niece, who have brought so much joy to my daily life.

AFFIDAVIT

AFFIDAVIT

	LUDWIG- MAXIMILIANS- UNIVERSITÄT MÜNCHEN	Promotionsbüro Medizinische Fakultät		
Affidavit				

Wang Zhihua

Surname, first name

Street

Zip code, town, country

I hereby declare, that the submitted thesis entitled:

Pairing of Single Cell RNA Sequencing and Single Cell T Cell Receptor Profiling Reveals Tolerance Breakdown of T Cells in Atherosclerosis

.....

is my own work. I have only used the sources indicated and have not made unauthorised use of services of a third party. Where the work of others has been quoted or reproduced, the source is always given.

I further declare that the submitted thesis or parts thereof have not been presented as part of an examination degree to any other university.

Munich, 13.12.2022

place, date

Zhihua Wang

Signature doctoral candidate

CONFIRMATION OF CONGRUENCY

CONFIRMATION OF CONGRUENCY



Confirmation of congruency between printed and electronic version of the doctoral thesis

Wang Zhihua

Surname, first name

Street

Zip code, town, country

I hereby declare, that the submitted thesis entitled:

Pairing of Single Cell RNA Sequencing and Single Cell T Cell Receptor Profiling Reveals Tolerance Breakdown of T Cells in Atherosclerosis

.....

is congruent with the printed version both in content and format.

Munich, 13.12.2022

place, date

Zhihua Wang

Signature doctoral candidate

LIST OF PUBLICATIONS

LIST OF PUBLICATIONS

Zhihua Wang, Xi Zhang, Shu Lu, Chuankai Zhang, Zhe Ma, Rui Su, Yuanfang Li, Ting Sun, Yutao Li, Mingyang Hong, Xingyi Deng, Rafiee Monjezi Mohammad, Michael Hristov, Sabine Steffens, Donato Santovito, Sarajo Mohanta, Klaus Dornmair, Klaus Ley, Christian Weber, Andreas Habenicht, Changjun Yin. Pairing of single-cell RNA analysis and T-cell receptor profiling indicates breakdown of T-cell tolerance checkpoints in atherosclerosis. **Nat Cardiovasc Res**. (in revision) 2022

Livia Habenicht, **Zhihua Wang**, Xi Zhang, Yuanfang Li, Carolin Mogler, Julia Slotta Huspenina, Roland M. Schmid, Christian Weber, Sarajo Mohanta, Zhe Ma, Changjun Yin. The C1q-ApoE Complex: A New Hallmark Pathology of Virus Hepatitis and Nonalcoholic Fatty Liver Disease. **Front. Immunol.** 2022 Oct 6;13:970938. doi: 10.3389/fimmu.2022.970938. PMID: 36304458.

Zhihua Wang, Xi Zhang, Chuankai Zhang, Yutao Li, Shu Lu, Sarajo Mohanta, Christian Weber, Andreas Habenicht, Changjun Yin. Combined Single cell RNA and Single cell α/β T Cell Receptor Sequencing of the Arterial Wall in Atherosclerosis. **Methods Mol Biol.** 2022;2419:727-746. doi: 10.1007/978-1-0716-1924-7_44. PMID: 35237998.

Xi Zhang, **Zhihua Wang**, Chuankai Zhang, Yutao Li, Shu Lu, Sabine Steffens, Sarajo Mohanta, Christian Weber, Andreas Habenicht, Changjun Yin. Laser Capture Microdissection-Based mRNA Expression Microarrays and Single cell RNA Sequencing in Atherosclerosis Research. **Methods Mol Biol.** 2022;2419:715-726. doi: 10.1007/978-1-0716-1924-7_43. PMID: 35237997.